



Universität der Künste Berlin



A Small Scale Solar Electric Powered Air Cooling System for Apartments in the MENA Region

Dissertation zur Erlangung des akademischen Grades
Doktor / Doktorin der Ingenieurwissenschaften (Dr.-Ing.)
an der Fakultät Gestaltung
der Universität der Künste Berlin

vorgelegt von
Christoph T. I. Banhardt, M.Sc.

Januar 2021



"A Small Scale Solar Electric Powered Air Cooling System for Apartments
in the MENA Region"

**Dissertation zur Erlangung des akademischen Grades
Doktor / Doktorin der Ingenieurwissenschaften (Dr.-Ing.)
an der Fakultät Gestaltung
der Universität der Künste Berlin**

vorgelegt von

Christoph Banhardt, M.Sc.

Januar 2021

Gutachter: Prof. Dr.-Ing. Christoph Nytsch-Geusen, UdK Berlin

Gutachter: Prof. Dr.-Ing. Felix Ziegler, TU Berlin

Tag der Disputation: 12. November 2021

Diese Publikation wird unter der Lizenz [CC BY 4.0](https://creativecommons.org/licenses/by/4.0/) veröffentlicht.
Abbildungen mit anderen Nachweisen sind ausgenommen.

Eidesstattliche Versicherung

Ich, Christoph T. I. Banhardt, versichere an Eides statt durch meine eigenhändige Unterschrift, dass ich die vorgelegte Dissertation mit dem Thema: *A Solar Powered Air Conditioning System for the MENA Region* selbstständig und ohne nicht offengelegte Hilfe Dritter verfasst und keine anderen als die angegebenen Quellen und Hilfsmittel genutzt habe.

Alle Stellen, die wörtlich oder dem Sinne nach auf Publikationen oder Vorträgen anderer Autoren beruhen, sind als solche in korrekter Zitierung (siehe „Uniform Requirements for Manuscripts (URM)“ des ICMJE - www.icmje.org) kenntlich gemacht. Die Abschnitte zu Methodik (insbesondere praktische Arbeiten, Laborbestimmungen, statistische Aufarbeitung) und Resultaten (insbesondere Abbildungen, Graphiken und Tabellen) entsprechen den URM (s.o) und werden von mir verantwortet. Meine Anteile an etwaigen Publikationen zu dieser Dissertation entsprechen denen, die in der untenstehenden gemeinsamen Erklärung mit dem Betreuer, angegeben sind. Sämtliche Publikationen, die aus dieser Dissertation hervorgegangen sind und bei denen ich Autor bin, entsprechen den URM (s.o) und werden von mir verantwortet.

Die Bedeutung dieser eidesstattlichen Versicherung und die strafrechtlichen Folgen einer unwahren eidesstattlichen Versicherung (§156, 161 des Strafgesetzbuches) sind mir bekannt und bewusst.

Datum und Unterschrift

Anteilerklärung an etwaigen erfolgten Publikationen

Christoph Banhardt hatte folgenden Anteil an den folgenden Publikationen:

Publikation 1: Christoph Banhardt und Christoph Nytsch-Geusen, Analysis of Electric Peak Load Reduction by Solar Electric Powered Room Air Cooling for Apartment Housings in the MENA-Region, Proceedings of IPSA Building Simulation Conference 2015 in Hyderabad, Indien, 2016

Beitrag im Einzelnen: Durchführung der Simulationen und Messungen im vorgestellten Fallstudien-apartment. Die Betrachtungen wurden im Rahmen dieser Dissertation mit dem Co-autor, Christoph Nytsch-Geusen besprochen und ausgewertet.

Publikation 2: Christoph Banhardt und Grigori Grozman und Christoph Nytsch-Geusen, Simulation and Validation of Thermal Air Stratification in Living Spaces, Proceedings of BauSim Conference 2016 in Dresden, Deutschland, 2016

Beitrag im Einzelnen: Die Nutzung und die Validierung eines neuen Simulationsalgorithmus für die Software *IDA-ICE* wurde in enger Zusammenarbeit mit dem Programmierer G. Grozman durchgeführt. Dieser hat in dem Paper die mathematischen und physikalischen Grundlagen vorgestellt. Diese Leistungsfähigkeit wurde vom Autor dieser Dissertation untersucht und dazu das vorgestellte Apartment simuliert. Die Ergebnisse wurden mit dem betreuenden Professor, Christoph Nytsch-Geusen besprochen, ausgewertet und zusammengefasst.

Publikation 3: Christoph Banhardt und Christoph Nytsch-Geusen und Daniel Wolf, Simplifying the Parametrization of the Extended Kinetic Battery Model to Calculate Voltage, Current, and a Variable Load Dependent Capacity, Proceedings of IPSA Building Simulation Conference 2019 in Rome, Italy, 2020

Beitrag im Einzelnen: Das erweiterte Batteriemodell wurde vom Autor dieser Arbeit auf Grundlage eines stark vereinfachten Batteriemodells in der *BuildingSystems*-Bibliothek des Co-autors Christoph Nytsch-Geusen entwickelt und programmiert. Dazu wurden Grundlagen aus einer Vorlesung von Daniel Wolf herangezogen. Mit diesem wurden die Ergebnisse des Modells validiert.

Publikation 4: Christoph Banhardt und Timo Blumberg, Identification and Analysis of Demand-Side Management Potentials within Touristic Resorts, Applied Energy, Special Issue for SDEWES conference 2019 in Dubrovnik, Croatia, Handed in January 2020

Beitrag im Einzelnen: Für das Paper wurden die Temperaturkurven, die aus einer Wetterstation in El Gouna stammen, aus dieser Arbeit verwendet. Weiterhin wurde dort die Methodik angewendet, die im Rahmen dieser Dissertation entwickelt wurde. Dabei handelt es sich um ein neuartiges Standardlastprofil, das nicht nur auf der Anzahl an Einwohnern beruht, sondern auch von der Außentemperatur abhängig ist.

Unterschrift, Datum und Stempel des betreuenden Hochschullehrers/der betreuenden Hochschullehrerin

Unterschrift des Doktoranden

Zusammenfassung

Diese Arbeit fokussiert sich auf kleinskalige Wohnraumklimatisierung mit weitverbreiteten Einzelraumkühlsystemen in der Region des Mittleren Osten und Nordafrika. Das Vorhandensein dieser Einzelraum- oder Wohnungskühlsysteme wird bewertet und ihre Auswirkungen in der gesamten Region beurteilt. Sie haben einen enormen Einfluss auf die Stromversorgung in Ländern wie Saudi-Arabien, wo die meisten Haushalte bereits über ein Klimagerät verfügen. Die Auswirkungen in anderen Ländern mit relativ wenig installierten Systemen, wie in Ägypten, sind bereits entscheidend und führen zu regelmäßigen Stromunterbrechungen. Die Stabilität der Netze dieser Länder wird mit einer höheren Durchdringungsrate von elektrischen Klimaanlagen weiter abnehmen.

Die derzeitige Technologieentwicklung zielt darauf ab, den Energiebedarf für die Gebäudekühlung zu reduzieren, die Leistungszahl zu erhöhen oder den Kühlmechanismus durch einen anderen Ansatz wie z.B. Sorptionskühlsysteme zu ersetzen. Diese Systeme erfordern jedoch eine kosten- und zeitintensive Änderung der Gebäudestruktur oder einen Austausch des bestehenden Kühlsystems. Aus diesen Gründen konzentriert sich die vorliegende Arbeit auf die zusätzliche Installation eines kleinen PV-Systems, einschließlich einer Batterie und der Anwendung fortschrittlicher Regelungsstrategien zur Nutzung der thermischen Speicherkapazität der Gebäudemassen.

Daher wird ein Raumkühlsystem als Referenzsystem modelliert, wie es in der gesamten Region vorhanden sein könnte. Dieses System besteht aus einem Raummodell einer typischen Apartmentstruktur welches kreuzvalidiert wurde. Zwei Nutzungsszenarien wurden untersucht: ein Schlafzimmer und ein Wohnzimmer. Darüber hinaus enthält es ein Modell des solaren elektrischen Systems, das ebenfalls auf regionale Werte parametrisiert ist. Neu werden ein Kleinkälteanlagenmodell und ein erweitertes Modell der kinetischen Batterie aufgestellt. Die einzelnen Modelle werden zu einer Gesamtsystems simulation kombiniert. Anschliessend werden die Hauptparameter in Partikelschwarm-Optimierungsläufen variiert, um die Einflüsse verschiedener Randbedingungen wie Strompreis und Einspeisetarife, Batterie- und thermische Speicherkapazitäten, oder die Solarkollektorfeldgrösse, zu bestimmen. Die Simulationsergebnisse werden hinsichtlich der nivellierten Kosten für die Kühlung, der solaren Deckungsrate und der solaren Kühlungsautonomie verglichen.

Die Ergebnisse werden in einer Fallstudie untersucht. Diese Studie beleuchtet die Ergebnisse des Stadtbezirks *El Gouna* von *Hurghada, Ägypten*. Dort wurden, wo möglich, persönliche Beobachtungen und eine eingehende Analyse der Ergebnisse vorgenommen. An diesem Standort sinken die nivellierten Stromkosten für ein PV-Kleinanlagensystem mit $1kW_{peak}$ auf $0.18USD/kWh$ bei einer kurzen Investitionsdauer von 5 Jahren. Bei einer Investitionsdauer von 15 oder 25 Jahren sinken sie sogar auf 0.08 bzw. $0.05USD/kWh$. Mit diesen Werten werden verschiedene nivellierte Kosten der Kühlung als Parameterfeld der Partikelschwarmoptimierung simuliert. Die Ergebnisse zeigen, dass die Kühlkosten in den meisten Fällen schon bei relativ kurzen Investitionszeiträumen negativ werden.

Innerhalb eines Schlafzimmers kann mit einem kleinen PV-System mit gewichteten Kosten von nur $677USD$ eine solare Deckungsrate von 0.9 erreicht werden. In Bezug auf die Autonomie der solaren Kühlung hat das kosteneffizienteste System gewichtete Kosten von $1,036USD$, was zu einem Deckungsgrad von 0.71 führt. Das Wohnzimmer-Klimasystem kann die besten gewichteten Kosten von $1,459USD$ für eine Kühlungsautonomie von 0.86 erreichen.

Weiterhin wird die Anwendung eines PV-elektrischen Kühlsystems in kleinem Maßstab durch den Autor am Standort der Fallstudie bewertet. Die Grenzen des theoretischen Systemdesigns werden vorgestellt und diskutiert. Teil der Analyse ist der Einfluss der thermische Schichtung in gewölbten Apartmentstrukturen auf die Abweichung zwischen simuliertem und gemessenem Kühlbedarf.

Conclusion

This thesis focuses on small scale residential cooling application with unitary air conditioning units as they are wide spread in the so called *Middle East North African* region. The presence of these single room or single apartment cooling systems is evaluated and their impact throughout the region assessed. They have a tremendous impact on the electric supply in countries like Saudi Arabia where most of the households already have an AC-unit. The impact in other countries with relatively less installed systems, like in Egypt, is already crucial and leads to regular power cuts. However, the stability of the grids of these countries will decrease further with a higher penetration rate of electric air conditioning systems.

Current technology development aims to reduce the buildings cooling energy demand, increase the coefficient of performance, or to substitute the cooling mechanism with a different approach such as sorptive cooling systems. However, these systems require a costly and time intensive change of the building structure or an exchange of the existing cooling system. Due to this reasons, this thesis focuses on the additional installation of a small scale PV electric system, including a battery and applying advanced control strategies to utilize the thermal storage capacity of the building masses.

Therefore, the present room cooling system is modeled as a reference system as it could be present throughout the entire region. This system consists of a room model of a typical apartment structure and is cross validated. Two use cases are applied: a bed room and a living room. Further, it includes a model of the solar electric system which is as well parametrized to regional values. Newly, a split unit model and an extended Kinetic Battery model are set up. The single models are combined to an entire system simulation. Afterwards, the main parameters are varied in particle swarm optimization runs to determine the impact of various boundary conditions, such as the electricity price and feed in tariffs, battery and thermal storage capacities, and solar collector field size. The simulation results are compared in terms of levelized costs of cooling, solar coverage rate and the solar cooling autonomy.

The findings are compared in a case study. This study highlights the results of the *Hurghada, Egypt* city district of *El Gouna*. There, personal observations of the results where possible and an in depth analysis of the results was undertaken. In this location, the levelized costs of electricity for a small scale PV system with $1kW_{peak}$ drop there to $0.18USD/kWh$ with a short investment period of 5 years. They even drop to 0.08 and $0.05USD/kWh$ when taking an investment period of 15 or 25 years into consideration. With this values, various levelized costs of cooling are simulated as a parameter field of the particle swarm optimization. The findings show, that in most cases, the cooling costs become negative, even with relatively short investment periods.

Within a bed room, a solar coverage rate of 0.9 can be achieved with a small scale PV system with weighted costs of only $677USD$. In terms of solar cooling autonomy, the most cost efficient system has weighted costs of $1,036USD$, resulting in a coverage rate of 0.71. The living room air conditioning system can achieve best weighted costs of $1,459USD$ for a cooling autonomy of 0.86.

Further, the practical application of a small scale PV electric solar cooling system was evaluated by the author in the case study location itself. The limitations of the theoretic system design are presented and discussed. Part of this analysis is the thermal stratification in typical vaulted apartment structures as they have a huge impact on the deviation between simulated and measured room air cooling demand.

Contents

1	Introduction	1
1.1	Structure of this thesis	2
1.2	Classification within the UN development goals	4
1.3	Background	4
1.3.1	Energy usage in the MENA region	4
1.3.2	Room air conditioners in the MENA region	5
1.3.3	Impact of energy demand of air conditioning systems	9
1.3.4	Necessity of new technologies	12
1.4	Research hypothesis and aim of thesis	12
1.5	Fields of application	12
1.5.1	Apartments as predominant usage type	12
1.5.2	Hotel rooms as predominant usage type	13
2	Methodology	15
2.1	Previous work and overview	15
2.1.1	Air conditioners in the MENA region	16
2.1.2	Approaches for solar powered room air conditioners	17
2.1.3	Simulation environments	18
2.2	Columns of research	20
2.3	Simulation model	22
2.3.1	Overview of system components	22
2.3.2	System setup for room air cooling	23
2.3.3	Room air energy balance	27
2.3.4	HVAC component models	33
2.3.5	Electrical models	39
3	System Design	47
3.1	Climate condition bandwidth	48
3.2	User behavior bandwidth	49
3.3	Apartment design bandwidth	50
3.4	System design spectrum	51
3.4.1	Reference system	51
3.4.2	Electric energy exchange systems	52
3.4.3	Thermal energy storage systems	53
3.5	Feasible system variants	56
3.5.1	Grid stability	57
3.5.2	Maximum solar coverage rate and solar autonomy	58
3.5.3	Minimum investment costs	59
3.5.4	Minimum life cycle costs	60

3.5.5	Minimum environmental impact	61
3.5.6	Thermal comfort bandwidth	62
3.5.7	Optimization boundaries	62
4	System Modeling	65
4.1	In- and outputs	65
4.2	System template	66
4.3	Weather data and radiation transformation	67
4.3.1	In- and outputs of the weather data models	67
4.4	Demand models	71
4.4.1	In- and outputs of the building demand model	71
4.4.2	Set points - boundaries of indoor comfort	72
4.4.3	User presence	74
4.4.4	Building properties in the MENA region	77
4.5	Electricity supply system	79
4.5.1	Photovoltaic system model	80
4.5.2	Battery systems	82
4.5.3	Grid connection and SLP	90
4.6	Thermal supply system	97
4.6.1	Overview	97
4.6.2	Split-unit A/C system	98
4.6.3	Water cooling system	100
4.6.4	Cold water storage	101
4.6.5	Thermal storage in building masses	102
4.6.6	Optimization modelling	103
5	Simulations and results	105
5.1	Reference system	106
5.1.1	Performance of reference model	106
5.2	System performance	113
5.2.1	Reference system - performance in the MENA region	114
5.2.2	Performance with minimized investment costs	125
5.2.3	Performance of a water cooling system	127
5.2.4	Evaluation of the LCOE and LCOC	130
5.2.5	Evaluation of the SCR and SCA	133
5.3	System Conclusion	135
6	Case study El Gouna, Egypt	137
6.1	Boundary condition of El Gouna	138
6.1.1	Apartment building H12	138
6.1.2	Modeling of Apartment 214	139
6.1.3	Reference system of Apartment H12-214	140
6.1.4	Simulation results of case study location	141
6.1.5	Supply system performance of case study system	144
6.1.6	Validation of simulation results	145
6.2	Measured Performance of the Case Study Apartment	153
6.2.1	Thermal simulation of case study apartment	154
6.2.2	Modelling of comparative system variants	155
6.2.3	Comparison of performance results	156

Contents

6.2.4	Comparison of thermal stratification	157
6.2.5	Comparison of simulation models	159
6.3	Discussion on case study	160
7	Conclusion and Outlook	161
7.1	Applicability of findings	161
7.1.1	Extractable findings	161
7.1.2	Socio-cultural applicability of the work	162
7.2	Methodology review	163
7.2.1	Conclusion of the simulation method	163
7.2.2	Review of the simulated environment	163
7.2.3	Conclusion on the case study	164
7.3	Further investigation fields	164
7.3.1	New control strategies: sensible heat storage in walls	164
7.3.2	Standard load profiles	166
7.3.3	Degradation of PV modules in desert environments	166
7.3.4	Maintenance	169
7.4	Contribution to the UN development goals	170
A	List of Abbreviations and Subscripts	XIX
B	List of Symbols and Units	XXIII
C	List of parameters and variables	XXV
D	Additional information	XXVII
E	<i>Modelica</i> code sources	XXXV
	Bibliography	XXXVII

List of Figures

1.1	Countries of the MENA Region, base map by DanPMK (2011) [1]	1
1.2	Graphical representation of thesis structure	3
1.3	Directly affected UN sustainable development goals of this research [2].	4
1.4	Inputs and outputs in megatons of oil equivalent, <i>Mtoe</i> , to and from the electricity generation in the MENA region, based on IEA data for 2016 [3].	5
1.5	Example floor plan and building scheme for a traditionally constructed house in New Gouna, Egypt [4, p. 275].	6
1.6	Satellite image showing an area in the 8th District, Cairo, Egypt (left) [5] and two typical building typologies (right) [6, pp. 5–6]	7
1.7	Top left: Outdoor units of split-units on a rooftop in Hyderabad, India. Lower left: Packaged systems on an apartment building in El Gouna, Egypt. Right: Outdoor units on balconies of a residential building in Kaohsiung, Taiwan.	8
1.8	Increasing number of used unitary air conditioners of all countries of the MENA region, except Iraq, based on data by the Green Cooling Initiative [7].	8
1.9	Increasing electric energy demand of the Middle East (blue) and share of residential used electricity (red) and subshare of electricity used for residential cooling (green). Data extracted from World Energy Outlook 2018 [8] and based on assumptions for share of cooling energy demands [9].	9
1.10	Increasing peak load (left axis) over number of used unitary air conditioners (right axis) in Egypt. Data extracted from annual reports of the Egyptian Ministry of Electricity and Renewable Energies (2010-2017)	10
1.11	Share of peak electricity demand of air conditioners in 2016 (triangles) and in 2050 (squares) over the total share of annual residential final energy demand in 2016 (blue) and in 2050 (red), data based on IEA study "The Future of Cooling" [10, p. 63f.]	10
1.12	Measured load duration profile on the peak load day in 2014 of the Red Sea coast resort town El Gouna from 15 to 22 MW, data provided by El Gouna Electrics [11].	11
2.1	Average electricity prices in selected countries in 2018 [12]. Associated MENA states are highlighted in dark blue, sometimes associated nations are highlighted in bright blue. The LCOE for small scale PV in Egypt is highlighted in yellow [13].	18
2.2	Columns of research.	21
2.3	Table of system components and their functionality. Yellow are electrical components, blue are components working with a cooled fluid, and red are thermal storage systems.	22
2.4	Most common UAC system used to cool room air world wide.	24
2.5	System setup of a solar and grid powered cooling system.	25
2.6	System setup of a water based cooling system.	26
2.7	System setup of a solely solar powered cooling system.	27
2.8	Global climate regions according to Köppen-Geiger-Pohl [14].	29

List of Figures

2.9	Example process of an R22 compression chiller in the T-S-Diagram, modified from [15] with chiller data from [16]. Cut out x-axis intervals from $\vartheta = -40^{\circ}C$ to $\vartheta = 0^{\circ}C$ and from $\vartheta = 100^{\circ}C$ to $\vartheta = 200^{\circ}C$	35
2.10	Working scheme of an air cooled compression chiller which is supplying a connected cold water loop, based on [17, p. 6].	37
2.11	Implementation of cold water network with a water storage tank as buffer.	38
2.12	I-V curve model for PV modules [18, p. 74], one and two diode cell model [19, p. 211] and three diode cell model [20, p. 107] for the modeling of photovoltaic systems.	39
2.13	Applied kinetic battery model, based on Manwell (1993) [21, p. 400].	42
2.14	General performance curve of an electric direct current to alternating current transformer, based on [22, p. 48].	46
3.1	System fields and interconnections, graphic based on vectorized images [23].	48
3.2	Daily average weather temperature, measured from 2012 to 2018, data provided by KBC El Gouna [24].	49
3.3	Floor plans of building typology 1 and 2 and their urban context according to Attia et al. (2012), p. 274f.	51
3.4	Reference cooling supply system of a typical apartment in the MENA-region.	52
3.5	Cooling system with a PV and battery system and a grid connection.	53
3.6	Charging of building mass during day time and no occupancy.	54
3.7	Use of building mass as thermal sink during occupancy and after peak demand time.	54
3.8	Extended system with a sub-cooling control algorithm to thermally activate the building mass.	55
3.9	Extended system with a water chiller, cold water storage, cooling coil and thermally activated building mass.	56
3.10	Average load duration [11] and total horizontal irradiation profile from June to September in El Gouna [25].	58
4.1	In- and outputs to and from used modeling and simulation software.	66
4.2	Modelica simulation template for parametric code generation and optimization, shown in Dymola with new and existing components from the BuildingSystems library [26].	67
4.3	In- and outputs to and from the ambient and the SolarRadiationTransformation model within Modelica.	68
4.4	Climatic boundary condition of each city and WMO weather station code. Radiation data generated with Meteonorm [25], CDD with BizEE [27].	69
4.5	Cooling and heating degree days per year and city, based on weather data of each weather station, calculated with BizEE [27]	70
4.6	Monthly average outdoor air temperature (red dots), its standard deviation (blue bars) and monthly maxima values (blue dots) over monthly incoming total horizontal radiation (orange bars), data generated with Meteonorm [25].	71
4.7	In- and outputs to and from the building demand model within Modelica.	72
4.8	Occupancy of a bedroom in a typical Egyptian flat [6, p. 278].	75
4.9	Occupancy of a living room in a typical Egyptian flat [6, p. 278].	75
4.10	Lighting of a bedroom in a typical Egyptian flat [6, p. 278].	76
4.11	Lighting of a living room in a typical Egyptian flat [6, p. 278].	76
4.12	Residential buildings in Giza (Abd El Latif Street on 25 April 2015).	78
4.13	In- and outputs to and from the entire electrical system models and graphical representation in Modelica.	80

4.14	In- and outputs to and from the <code>PVmodule</code> system component and graphical representation in <i>Modelica</i>	81
4.15	Graphical representation of the electric <code>battery</code> component in <i>Modelica</i>	83
4.16	Terminal voltage of two different batteries over time at various discharging currents, <i>C20</i> -rate in red, resulting slope parameter in blue	84
4.17	Terminal voltage of simulation vs. data sheet during 1C, C10, and C20 discharging of Long WP7.2-12 battery	86
4.18	Terminal voltage of simulation vs. data sheet during 1C, C10, and C20 discharging of Chloride CLH12-200 battery	87
4.19	Comparison of RMSDs for both batteries and for a depth of discharge of 100% and 80%.	87
4.20	Transformer efficiency at the corresponding fraction of the applied load	89
4.21	Power output of and power input to the transformer at the corresponding fraction of the applied load	89
4.22	Annual electric, occupancy and temperature profile for the highlighted seasons winter (blue background), summer (red background) and Ramadan (green background), according to Attia et al. (2012).	91
4.23	Electric load and temperature profiles for all three seasons, based on the electricity demand curve and outdoor air temperature of El Gouna in 2014.	92
4.24	Standardized load profile per capita and Kelvin for all three seasons, based on data for El Gouna in 2014.	93
4.25	Comparison of the monthly electricity demand between the measured values (green) and the demand, which is scaled to the occupancy (blue) and additionally to the outdoor air temperature (red).	94
4.26	Comparison of different load profiles of a week during Ramadan.	95
4.27	Comparison of different load profiles of a week during Season 1.	96
4.28	Comparison of different load profiles of a week during Season 2.	96
4.29	Comparison of peak load profiles [28] and outdoor air temperatures [29] for 6 August 2013 (dashed lines) and 12 August 2014 (solid lines).	97
4.30	In- and outputs of the thermal supply model components	98
4.31	In- and outputs of the <code>splitUnit</code> component in <i>Modelica</i>	99
4.32	Outdoor and indoor unit of a unitary air conditioner (left) [30] and examples of a split system [31] and a packaged system [16].	99
4.33	In- and outputs of the <code>waterCooler</code> component, graphical representation in <i>Modelica</i>	101
4.34	In- and outputs of the <code>fluidStorage</code> component, graphical representation in <i>Modelica</i>	102
4.35	In- and outputs of the <code>coolingSurface</code> component, graphical representation in <i>Modelica</i>	103
5.1	IDA ICE simulation model of a typical apartment building with zone names (left), and example results for Hurghada, Egypt of the ideal heating and cooling loads (top right) and monthly room air energy balance (bottom left).	107
5.2	IDA ICE simulation results of annual heating (red bars) and cooling energy demand (blue bars) of all 26 locations and their corresponding needed ideal heating (green triangles) and cooling (purple squares) loads.	108
5.3	Western side of standard floor in reference building from typology 2 and rooms in the south eastern apartment (right) and comparison of room energy balance for the bed room (top left) and the living room (bottom left) for an example week in the transition period (22 to 28 May).	110
5.4	<i>Modelica</i> set up for the comparative simulation between IDA ICE and <i>Modelica</i> for the bed room (top) and the living room (bottom).	111

List of Figures

5.5	Comparison of simulated cooling energy demand for the bed room between the reference model of IDA ICE (green) and the system which will be used for optimizations with Modelica (blue).	112
5.6	Comparison of simulated cooling energy demand for the living room between the reference model of IDA ICE (green) and the system which will be used for optimizations with Modelica (blue).	113
5.7	Comparison of the annual cooling energy demands for a bed room (blue) and the corresponding annual electrical power demand for the split-unit air conditioner (red).	114
5.8	Comparison of monthly cooling energy demands for a bed room (blue) and the corresponding monthly electrical power demand for the split-unit air conditioner (red).	115
5.9	Comparison of the annual cooling energy demands for a living room (blue) and the corresponding annual electrical power demand for the split-unit air conditioner (red) for all 26 locations.	116
5.10	Comparison of monthly cooling energy demands for a living room (blue) and the corresponding monthly electrical power demand for the split-unit air conditioner (red) in Hurghada, Egypt.	117
5.11	Annual costs for cooling (left y-axis) for all 26 selected locations for a bedroom (blue bars) and a living room (red bars), based on electricity prices from 2018 [12] (except locations marked with an asterisk) and annual carbon emissions (right y-axis) for a bedroom (green squares) and a living room (purple triangles), based on El Khoury (2009)[32] (except Iran and Israel, their emissions are the regions average). The orange line marks the annual carbon equivalent emissions budget per person to reduce global warming to $2K$ [33].	118
5.12	Average share of the electricity demand for air cooling during peak load hours (5 to 9pm) in the total daily electricity demand for air cooling of a bed room (blue) and a living room (red) in all 26 locations.	119
5.13	Annual number of on/off switching cycles of the reference A/C in a bed room (blue) and a living room (red) in all 26 locations.	119
5.14	Average daily electric demand profile for an air cooling in a typical bed room in Hurghada, Egypt during summer (season 1, highlighted in red), during winter (season 2, outlined in blue), and during Ramadan (season 3, indicated in green).	120
5.15	Average daily electric demand profile for an air conditioner in a typical living room in Hurghada, Egypt during summer (season 1, highlighted in red), during winter (season 2, outlined in blue), and during Ramadan (season 3, indicated in green).	121
5.16	Monthly (left y-axis) and annual (right y-axis) number of on/off switching cycles of the reference A/C in a bed room (blue) and a living room (red) in Hurghada, Egypt.	122
5.17	Absolute annual (right y-axis) hourly accumulated degrees difference between room air temperature and the outer wall surface temperature of a bed room (blue) and a living room (red) of all locations. Only the hours where the wall surface temperature is above $28^{\circ} C$ are accounted.	122
5.18	Absolute monthly (left y-axis) and annual (right y-axis) hourly accumulated degrees difference between room air temperature and the outer wall surface temperature of a bed room (blue) and a living room (red) in Hurghada, Egypt. Only the hours where the wall surface temperature is above $28^{\circ} C$ are accounted.	123
5.19	Annual amount of roundtrip energy stored in the internal thermal masses of a bed room (blue) and a living room (red) in all 26 locations.	124
5.20	Monthly (left y-axis) and annual (right y-axis) amount of roundtrip energy stored in the thermal masses of a bed room (blue) and a living room (red) in Hurghada, Egypt.	125

5.21	Modelica set up for any location for the bed or living room (naming example for the bed room) with a small scale photovoltaic and battery system.	125
5.22	Bed room - annual solar coverage rate (red) and solar autonomy rate (blue) for a bed room with a minimum sized solar electric power system in all 26 locations.	126
5.23	Living room - annual solar coverage rate (red) and solar autonomy rate (blue) for a living room with a minimum sized solar electric power system in all 26 locations.	127
5.24	Modelica set up for any location for the bed or living room (naming example for the bed room) with a small scale photovoltaic, battery and water cooling system which consists of a water cooler, a cold water storage and a room transfer unit.	127
5.25	Results for a bed room: change in annual energy demands for the chiller (blue), the annual amount of energy being sold to the grid (red), and the annual amount being purchased from the grid (green) for all 26 locations.	129
5.26	Results for a living room: change in annual energy demands for the chiller (blue), the annual amount of energy being sold to the grid (red), and the annual amount being purchased from the grid (green) for all 26 locations.	129
5.27	Difference in number of on/off cycles between the water and the air cooling system for a bed room (blue) and a living room (red).	130
5.28	Levelized cost of electricity for an increasing peak capacity of the pv field in Hurghada, Egypt for an investment period of 5 (green), 15 (red), and 25 (blue) years.	131
5.29	Variability of the differences in the levelized costs of cooling for an investment period of 25 (blue and red) and 5 years. The first four box plots indicate a small scale PV system with a battery storage, while the last two indicate a chilled water system. Blue, green and yellow are used for an analyzing a bed room in Hurghada, Egypt. Red, purple and azure are used for a living room.	132
5.30	Variability of the weighted solar coverage rate and solar cooling autonomy. The box plots indicate the variability of a small scale PV system with a battery and a cold water storage. The electricity price is fixed at $cst_{elect} = 0.30 \text{ \$/kWh}$ and the investment period is set to 5 years. Blue and red indicate the SCR of the system when installed to a bed resp. a living room. The SCA is indicated in green for a bed room and purple for a living room.	134
6.1	Location of the case study location El Gouna at the Red Sea Coast of Egypt, 30km north of Hurghada (top left) and official development plan.	137
6.2	Urban context of simulated apartment in El Gouna, Egypt and IDA-ICE simulation model of the building (top right corner).	138
6.3	Floor plan (left) of the building H12 in Downtown El Gouna, its appearance (top right) and a 3D simulation model of the building (lower right).	140
6.4	Photovoltaic panels on apartment H12-214 during the erection (left side) and the final set-up on top of the apartment (right side).	140
6.5	Comparison of simulated monthly cooling energy demands in the living room of apartment H12-214 in El Gouna (red) and a typical Egyptian apartment with the same shape under the climatic conditions of Hurghada.	142
6.6	Simulated monthly numbers of on and off switches of the living room split-unit in apartment H12-214 (red) and a comparable living room in Hurghada (blue).	142
6.7	Absolute monthly (left y-axis) and annual (right y-axis) hourly accumulated degrees difference between room air temperature and the outer wall surface temperature of the living room of H12-214. Only the hours where the wall surface temperature is above $28^\circ C$ are accounted.	143

List of Figures

6.8	Monthly (left y-axis) and annual (right y-axis) amount of roundtrip energy stored in the thermal masses of the living room in H12-214 (red) and as a typical apartment in Hurghada (blue)	144
6.9	Temperature sensors on both side of the walls and data point names for the living room of the case study apartment H12-214.	146
6.10	Temperature sensors on both side of the walls and data point names for the living room of the case study apartment H12-214.	146
6.11	Free floating indoor temperature in the apex of the vault (blue) and close to the floor (pink) with the measurements on the westward facing wall (solid lines) and on the eastward facing wall (dashed lines) over the environmental temperature (yellow). . . .	147
6.12	Interior surface temperatures in a the case study apartment while the air below is free floating.	148
6.13	Indoor temperature in all heights on the westward facing wall over the environmental temperature (yellow). The color and height of each sensor is indicated in the picture to the right of the graph.	149
6.14	cylindrical heating devices ($\vartheta > 30^{\circ}C$) with smaller sources of coldness ($\vartheta < 15^{\circ}C$) at the beginning of the experiment.	151
6.15	Air temperatures in the room before, during and after the experiment in the top of the vault (red), near the ground (blue) and the outside temperature (yellow). Additionally, the sound pressure level is indicated in grey and on the right y-axis.	152
6.16	Thermographic pictures during the time from 12:30 to 2 am, showing the variety of different performance states of the internal heat sources.	153
6.17	Measured electricity profile of the apartment for the period of one year in El Gouna. The period was assembled from the time span of March 2015 to March 2016.	154
6.18	Shape boundaries of and simulation model in IDA-ICE 5.0 alpha.	155
6.19	Simplification of the complex shape of the living room in IDA-ICE 5.0 alpha.	156
6.20	Comparison of cooling energy demand (blue bars) and simulation time (red lines). . .	157
6.21	Comparison of operative (blue) and mean air temperature (red) in the reference simulation model of the apartment.	157
6.22	Layer temperatures with single modeled layers with standard simulation algorithm. . .	158
6.23	Layer temperatures with new model and flow elements de-activated on 24 June 2016. .	159
6.24	Layer temperatures with new model and flow elements activated on 24 June 2016. . . .	159
7.1	Cooling process of apartment H12-214 in El Gouna, Egypt on 11 July 2016 with the average indoor temperature (blue), the outdoor temperature (orange) and the sound pressure level (grey).	165
7.2	Test to sub cool the apartment H12-214 in El Gouna, Egypt on 12 July 2016 with the average indoor temperature (blue), the outdoor temperature (orange) and the sound pressure level (grey).	165
7.3	System set up of the real small scale PV plant (left) and the numbering of the recorded I-V-curves with the HT Solar I-V measurement system (right).	167
7.4	Results of the measured I-V-curves (left y-axis) and I-P-curves (right y-axis). The nominal curves are shown in blue and red. The measured curve fall drastically below this lines.	168
7.5	Thermal image of all used PV modules (left), single pictures of each module (middle) and a clearly visible thermal crack in a single cell (right).	169
7.6	Outdoor unit of a multi-split-unit at the road crossing of Ismail Mohamed and Yousif Kamel street on Zamalek, Cairo, Egypt, taken by the author on 10 November 2017. . .	170

List of Tables

3.1	Overview of additional system components with minimum investment costs.	60
3.2	Parameters and variables for LCOE cost calculation as presented by Hussein et al. (2016)[13] for small scale residential applications of photovoltaic systems on Egypt's Red Sea cost	61
3.3	Design parameters for optimization.	63
4.1	Physical properties of common used building material.	77
4.2	Layers and U-values of construction components.	78
4.3	Window properties for a typical building [34, p. 170]	79
4.4	Given and determined parameters for two different PV module types.	81
4.5	Parameters in data record for two newly introduced lead acid batteries	85
4.6	Parameters from data sheet from comparable A/C split-unit [16][35].	100
4.7	Design parameters for particle swarm optimization.	104
5.1	Resulting building parameter	106
6.1	Properties of construction material being used in El Gouna, Egypt.	139
6.2	Properties of construction material being used in El Gouna, Egypt.	145
7.1	Measured data points of the previously shown PV panels in El Gouna, Egypt	167
A.1	List of abbreviations and subscripts in alphabetical order	XIX
B.1	List of symbols and units	XXIII
C.1	List of parameters and variables	XXV
D.8	Energy balances for the bed and the living room for all 26 locations and the calculated solar coverage rate and solar autonomy rate.	XXVII
D.1	Overview of simulation results of <i>IDA-ICE</i> for the specific heating and cooling energy demands and capacities	XXIX
D.2	<i>IDA-ICE</i> simulation results of ideal calculated annual cooling energy demands	XXX
D.3	Specific costs for electricity and greenhouse gas emissions for a kWh of electricity	XXXI
D.4	Impact on grid stability: share of electricity demand for peak load hours in total cooling energy and number of on/off switches	XXXII
D.5	Thermal comfort and Latent energy storage throughput in bed and living rooms	XXXIII
D.6	Monthly cooling and electric energy demands in kWh of the reference location of Hurghada, Egypt.	XXXIII
D.7	Simulation results for the reference location Hurghada, Egypt for the number of on/off switching cycles for the air conditioner system, the cooling degree hours and the energy throughput to and from the internal walls in a bed and a living room.	XXXIV

1. Introduction

The text in hand describes a method to reduce the economic and ecologic impact of unitary air conditioners. At first, this introduction classifies the presented research under the United Nations sustainable development goals. Afterwards, it describes the selected target region for the research, the Middle East and North African region and their current structure of fossil resources based electricity supply and their energy intense methods for room air cooling and conditioning. This region is highlighted in the following map in Figure 1.1 [1]. Countries, which are normally associated with this region, are highlighted in dark blue. Additionally, countries, which are sometimes associated with the MENA region are highlighted in bright blue.

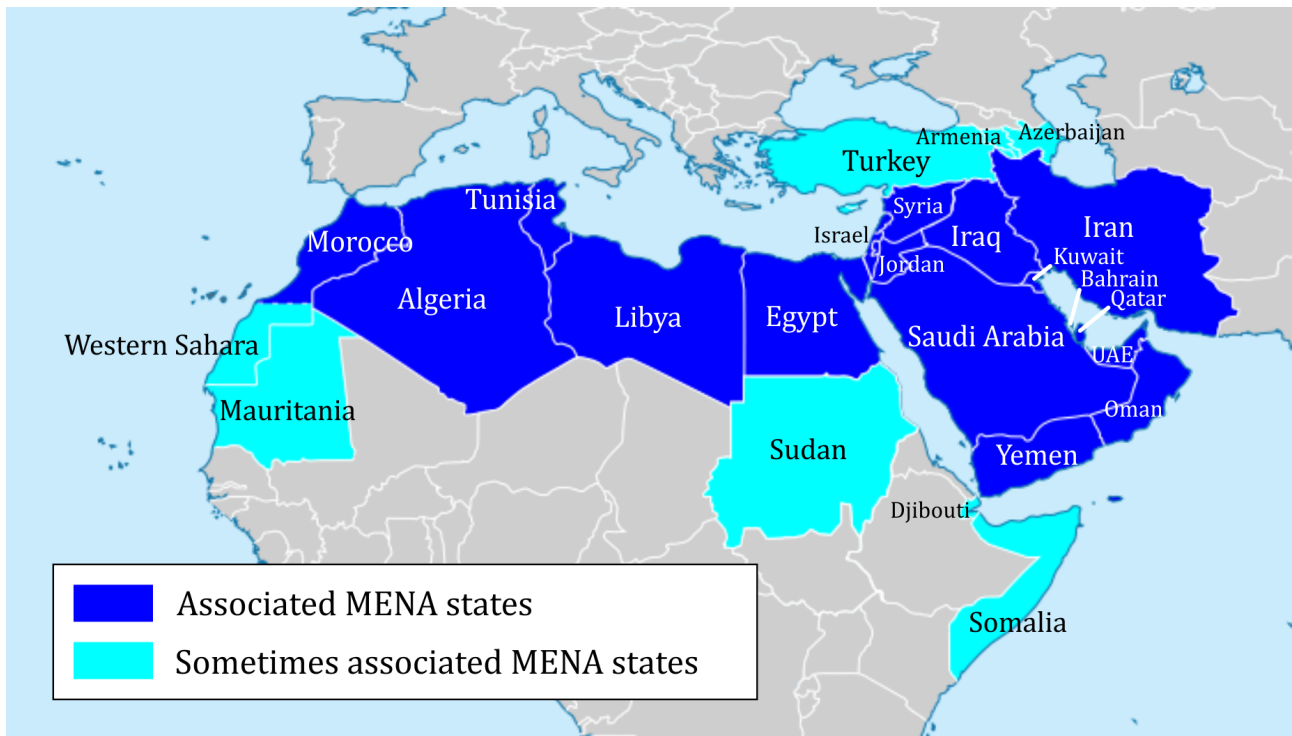


Figure 1.1.: *Countries of the MENA Region, base map by Dan.PMK (2011) [1]*

The region is selected, because the author of this dissertation was based for the duration of his research in El Gouna, Egypt. Throughout his stay, he gained a deep insight into the socio-cultural similarities and differences was gathered and the increasing problem of electric operated and already installed air cooling systems identified. The introduction describes the path from the local traditional architecture, with passive cooling techniques, to the extensive use of air conditioners, A/C's, in high density urban areas and their impact on the electricity grid. These systems are mainly operated with grid electricity, which causes immense problems on the supply security, besides economic burdens for the operators and a continuous ecologic impact. Solar powered alternatives offer an attractive solution as the overall incoming radiation offers tremendous potential throughout the region. The decision, to focus on solar electric powered air cooling is mainly because of the only few investigations in this area. Current research mainly focuses on solar thermal powered air conditioners.

1. Introduction

A common and wide spread A/C system is defined together with its main control variable. This system can be found in millions of households. Further, an extended system with a photovoltaic, PV, system and a battery storage, a water based cooling system, and a grid independent system, are introduced. The shapes, properties and physical behavior of each system component are described and their dependencies highlighted. All system components that are needed are evaluated and the needed background and their structural base to set them up are presented.

The overall system is divided into four subcategories of different energy qualities. The different subsystems of these categories are presented and the expected bandwidth within this research is evaluated. This includes the climatic boundaries, the user behavior and common building designs. It is done in particular for the reference system. A common control strategy is presented for this system. The possibilities for optimization in terms of boundary conditions and design goals are weighted according to their feasibility.

The resulting possible system set ups are concluded in a matrix which can be used to find a best feasible system set up to increase the performance of existing or newly planned single room air cooling systems with feasible measures.

1.1. Structure of this thesis

The content of this research can be divided into three parts. This structure can be found as a graphical representation in Figure 1.2. The first is the general introduction to the topic and the current efforts and rising problems of the electricity supply within the MENA region. The scope and fields of application of this thesis are defined besides the aim and goals in Chapter 1.

The second part begins with Chapter 2. There, the previous done research and possible modelling and simulation environments are evaluated. The findings are used to define a common reference system and to identify needed system components. Chapter 3 combines these components to define different setups and the parameter bandwidth for the inputs. Possible systems are concluded. The performance of each single system component is modeled in Chapter 4. First, the overall data flow from the user and between programs is presented. Afterwards, the subcategories are presented as a model template. The inputs of the user to define the properties and performance of the systems are stated besides the data that is exchanged between the components and the subcategories. Each single component is described in detail within this chapter. For example, the in- and outputs from the weather data model to the solar radiation transformer are highlighted.

Newly developed or newly derived conclusions from previous research is presented in more detail. This includes the development of a standardized load profile, SLP, for the electricity consumption in residential applications in the MENA region. Also, the extension of an existing battery model is shown in great detail and the performance of this new model is evaluated. The modelling of other components, like the split-unit, is based on previous created models of an existing library for building simulations.

The third part starts with the presentation of the simulation results in Chapter 5. The performance of the previous presented system components and variants is evaluated. Chapter 6 is the undertaken case study for a solar powered air cooling system which proofs the outcomes of the simulation matrix. Here, the outputs of an existing possible setup is compared with the theoretical performance of a digital twin of the system. This part is concluded with Chapter 7 where the findings of the simulation results are discussed. The thesis is also closed with an outlook as part of this chapter. There, all relevant findings are brought together and further research options are suggested.

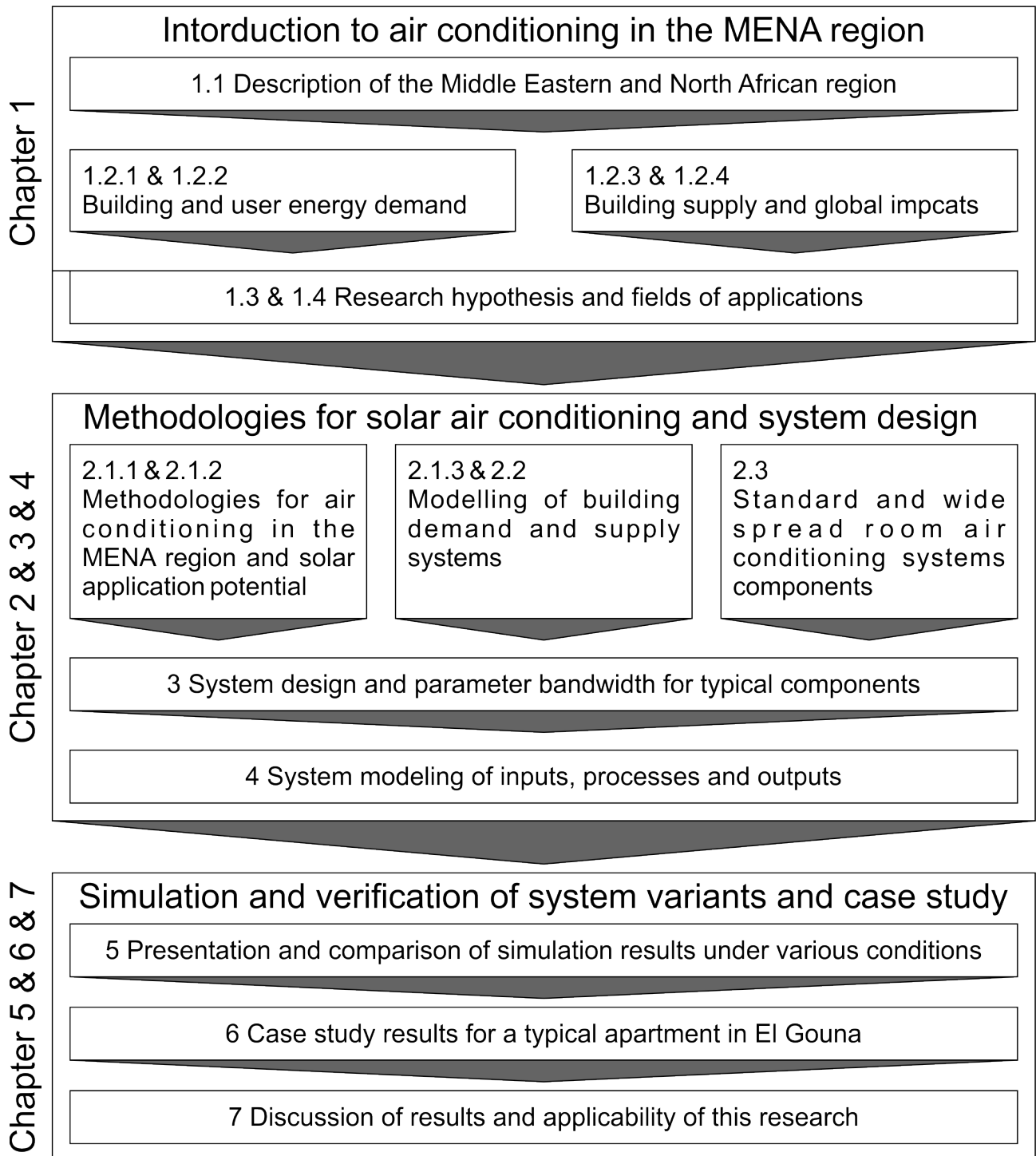


Figure 1.2.: Graphical representation of thesis structure

1. Introduction

1.2. Classification within the UN development goals

All United Nation Member states agreed in 2015 on an agenda, the so called Sustainable Development Goals. This agenda comprises 17 topic and corresponding goals which should be achieved in a joint effort until 2030. This research is classified according to these topics to take part in fostering this development. This directly includes Goal 7 "affordable and clean energy", Goal 11 "sustainable cities and communities", and Goal 12 "responsible consumption and production" [2]. They are represented in the picture in Figure 1.3. Applying this research on a greater scale will help to ensure the access to affordable reliable energy as the costs for cooling are reduced and the electricity grid stabilized. Further, room air cooling is needed to ensure adequate housing in the continuously growing and urbanizing MENA region. The single user applicability of this thesis enables each user to reduce their environmental impact and achieve a higher living standard with a lowered recourse demand for room air cooling.



Figure 1.3.: Directly affected UN sustainable development goals of this research [2].

1.3. Background

This section describes the general energy use in the entire MENA region with a special emphasis on residential energy consumption. The impact of room air conditioner is investigated and the resulting power demand, the connected carbon emissions and impact on the grid stability concluded. Based on this findings, the necessity of new technologies is derived.

1.3.1. Energy usage in the MENA region

The energy demands of the MENA region are mainly satisfied by the use of fossil fuels. Most of the associated MENA states have their own gas and/or oil fields and enough refinery capacities to partly or totally satisfy the local demand. Even besides the transportation sector, the region almost fully relies on oil and gas. This is true as well for the entire electricity production market. Its energy inputs and outputs are presented in the *Sankey*-diagram in Figure 1.4. The energy use is shown for the year 2016 and the data was gathered through the statistical country data from the International Energy Agency IEA [3] and is given in *mega tons of oil equivalent*. Natural gas is, with a share of 54%, the biggest energy source for the electricity generation with a primary energy input of 316 *Mtoe* (\equiv 3661 *TWh*). The second biggest source are oil and gas products (25%). Thereafter, 17% are produced by renewable electricity sources solar, tide and wind plus an additional 1% from hydro power. Coal accounts for only 3% and is only used in Israel and Morocco in power plants. Nuclear, biofuels and waste incinerations are almost not present in the region.

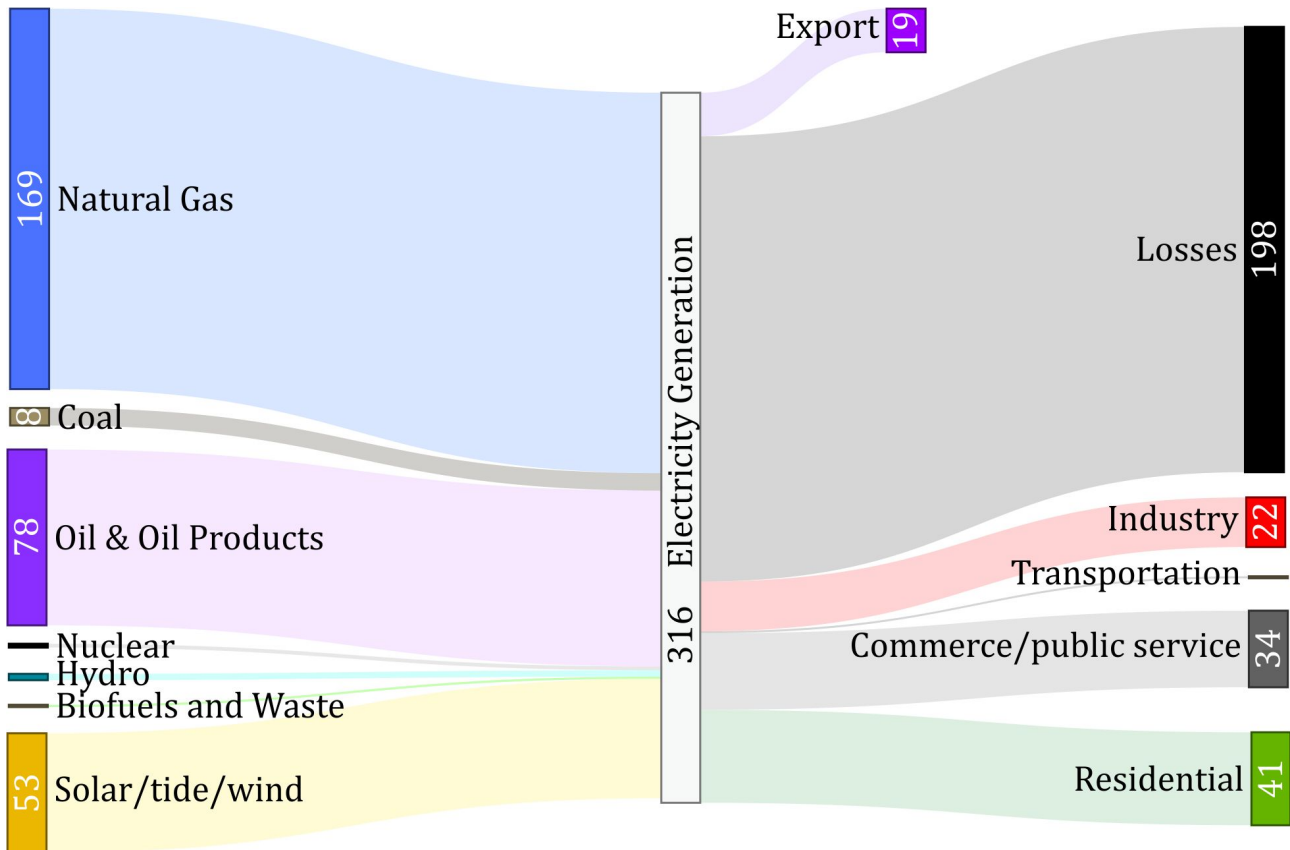


Figure 1.4.: Inputs and outputs in megatons of oil equivalent, *Mtoe*, to and from the electricity generation in the MENA region, based on IEA data for 2016 [3].

A gross of 198 *Mtoe* (63%) of the outputs are losses due to energy conversions and transmissions. The entire region is a net electricity exporter and supplies the surrounding countries with 19 *Mtoe* (6%). The residential sector has the highest electricity demand with 41 *Mtoe* (13%), followed by a demand of 34 *Mtoe* for commercial and public services (11%). At least 22 *Mtoe* (7%) are needed by the industry. The electricity demand for transportation is only 2 *Mtoe* (<1%).

Khoury concluded, at least for 2009, the average prime energy factors to calculate the carbon emissions for almost all countries of the MENA region (except Iran and Israel) [32]. The weighted average carbon emissions of electricity usage are $em_{avg} = 658$ grams of carbon equivalent emissions per used kilowatt hour of electricity ($gCO_{2,equiv}/kWh$). This cumulates into annual emissions of $Em = 3,305 GtCO_{2,equiv}/a$ for the entire electricity generation of the entire MENA region. 211 $GtCO_{2,equiv}/a$ are the direct result of the residential electricity demand. The global budget, which is left to keep global warming below a rise of 2 K is 697,074 $GtCO_{2,equiv}$ [36]. Major reductions have to be achieved in all fields of applications as soon as possible and the residential sector of the MENA region offers tremendous potential, especially for room air cooling. This will be illustrated in the following sections.

1.3.2. Room air conditioners in the MENA region

The traditional architecture of the region is designed to keep low indoor air temperatures inside even without sophisticated technological approaches. Simple techniques are narrow street paths that provide intershading of buildings and courtyards with greenery and water bodies to cause evaporative cooling

1. Introduction

effects [37]. Vaults and domes increase the radiation surface to exchange radiation with the much cooler night sky [38]. Small and shaded window openings are placed on southern facades, while northward facing walls include ventilation openings to allow the air to enter on the shaded colder side of the building. More advanced concepts include a windcatcher. This construction causes a fresh air stream which can also be cooled by evaporation effects on water or wet areas. The application of this technique can be still observed in the city of Yazd, Iran, where it was extensively applied to buildings [39]. Further, massive constructions with mud clay bricks allow a high humidity transfer from the inside to the outside wall and, thereby, cooling through evaporation on the outdoor wall surfaces. However, the inside wall needs to be exposed to moisture for this to work properly [40]. The most prominent recent architect to promote this type of construction is Hassan Fathy who created a manual to design buildings which do not need any additional cooling technologies but can maintain an acceptable indoor temperature by means of their architectural and structural conception [4]. An example of his building style is shown in the scheme in Figure 1.5. There, an outside view of one building side is illustrated above its floor plan. Clearly visible are the roots to the traditional architectural styles of the region.

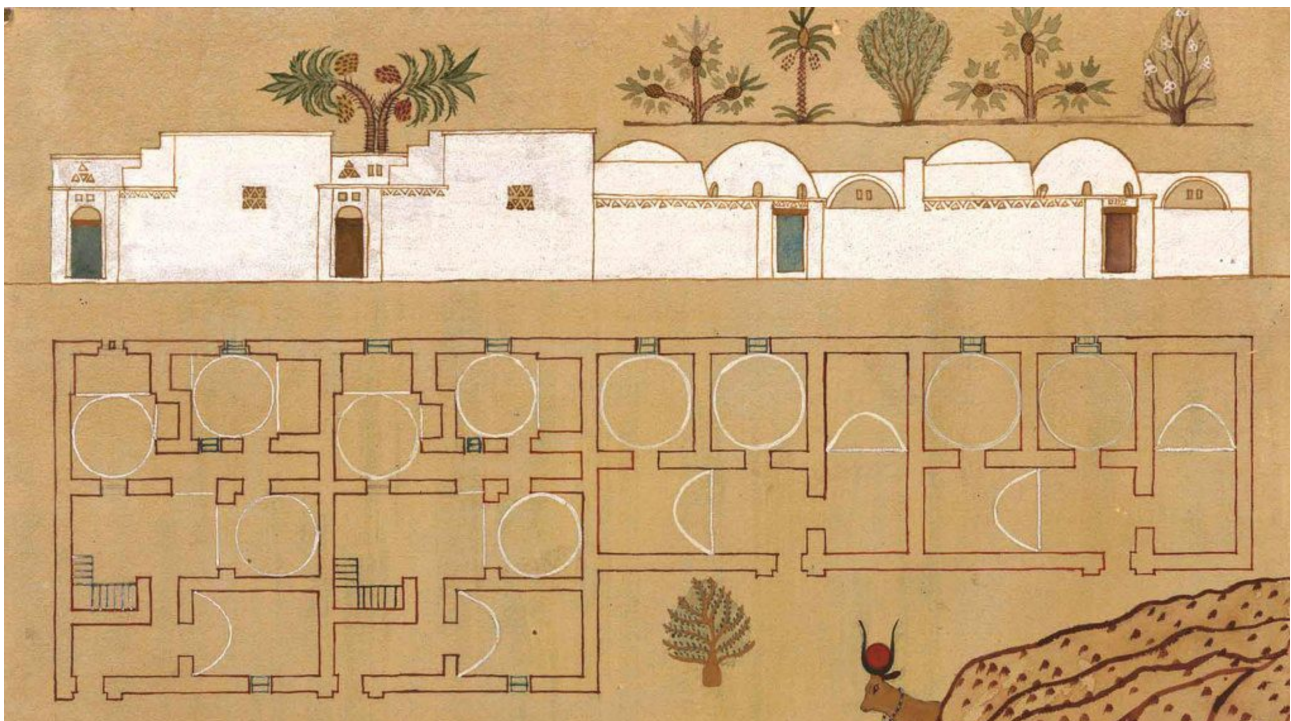


Figure 1.5.: *Example floor plan and building scheme for a traditionally constructed house in New Gourna, Egypt [4, p. 275].*

The newly planned city of Masdar, Abu Dhabi, aims to become a totally carbon neutral city and therefore applies many of these strategies to avoid energy consumption through building air conditioners [41]. However, these techniques require space for construction and are not applicable in high density city areas. The massive population growth of the last decades has caused a high demand for living space. Current common construction methods aim to supply large numbers of apartments within the shortest possible time. This results in quickly-built high rise buildings in skeleton construction with a poor thermal quality and a lack of energy reducing planning. S. Attia et al. (2012) analyzed the existing building stock to identify "... middle class neighbourhoods [...] with high penetration values of air-conditioning units. [...] The site observations showed that those residential neighbourhoods have buildings with minimalist and replicated modular architecture. Apartment blocks and concrete walk-up

buildings are dominant." [6, p. 2]. A typical side like this is shown in the following satellite image on the left of Figure 1.6. It shows the repetitive architecture of the Nasr City 8th District in Cairo which was developed in the 1960s. The two representative typologies are presented on the right side of Figure 1.6 [6, p. 5f.]. There, they are shown in a high density urban context as they are built all around the entire MENA region, e.g. in the new planned capital of the Egypt. They are by far the most dominant architectural type throughout those countries.

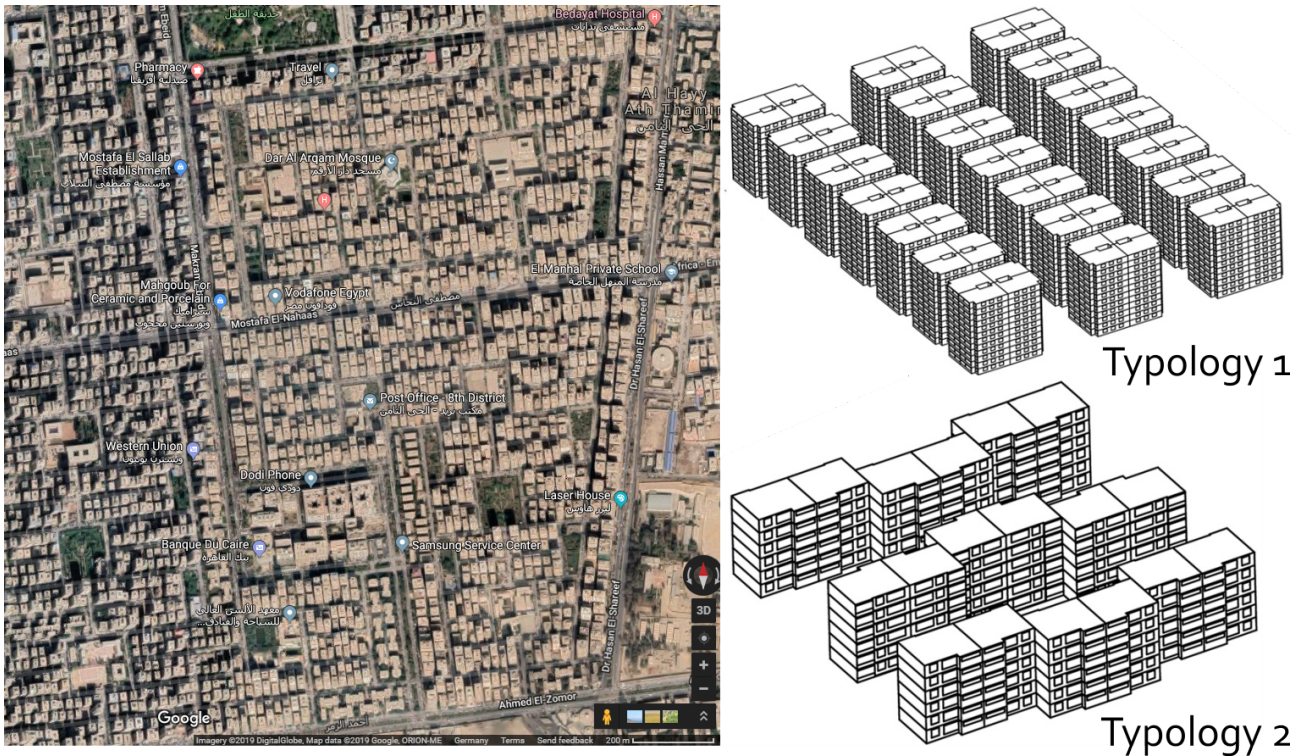


Figure 1.6.: Satellite image showing an area in the 8th District, Cairo, Egypt (left) [5] and two typical building typologies (right) [6, pp. 5–6]

Once an apartment is occupied, the thermal comfort inside is achieved with a standard air cooling system (author's own observations in Egypt, 2012-2019). The most commonly used system world wide is the so-called unitary air conditioner, also known as a UAC. The Green Cooling Initiative by the GIZ (2019) stated a total number of 833 million UACs in 2016, accounting for 0.112 units per human world wide [7]. This number is expected to rise to a total number of 3.7 billion units in 2050. This can result in a share of 0.379 UACs per human if the current slope of population growth is assumed [42]. Currently, 80% of these systems are so called split-unit systems [43]. These are a subcategory of unitary air conditioners. They are the cheapest in terms of investment costs and installation effort. The following three pictures in Figure 1.7 were taken to illustrate the massive use of split-unit systems around the world. The systems are marked with red circles in each photograph.

The following graph in Figure 1.8 shows the rising number of operated UACs in all countries of the MENA region, except Iraq, from 2000 to 2018. Each color represents a nation of the region. The data for Morocco includes the areas of the Western Sahara. The number of AC units in Israel excludes the number of UACs used in the West Bank and Gaza. No information was available for these areas. The overall statistical data was provided by the Green Cooling Initiative (2019) [7].

1. Introduction



Figure 1.7.: Top left: Outdoor units of split-units on a rooftop in Hyderabad, India. Lower left: Packaged systems on an apartment building in El Gouna, Egypt. Right: Outdoor units on balconies of a residential building in Kaohsiung, Taiwan.

Currently, there are 26.04 million units used within the region (status 2018). This number is expected to rise exponentially until 2030 and continuously afterwards until at least 2050, cumulating in an overall number 81.43 million units in operation. Today, the dominant users are Saudi Arabia (5.16 million) and Egypt (4.76 million). Currently, only 5% of Egypt's population have a UAC system, but almost 16% of Saudi Arabia's people. The expected growth of the gross domestic product will enable more and more parts of the Egyptian society to afford air conditioners which will cause the expected exponential growth of sold UACs. In 2050, Egypt will have the most UACs in operation (16.8 million) in the entire MENA region, followed by Saudi Arabia (13.5 million). The effects on the electric supply grid are tremendous.

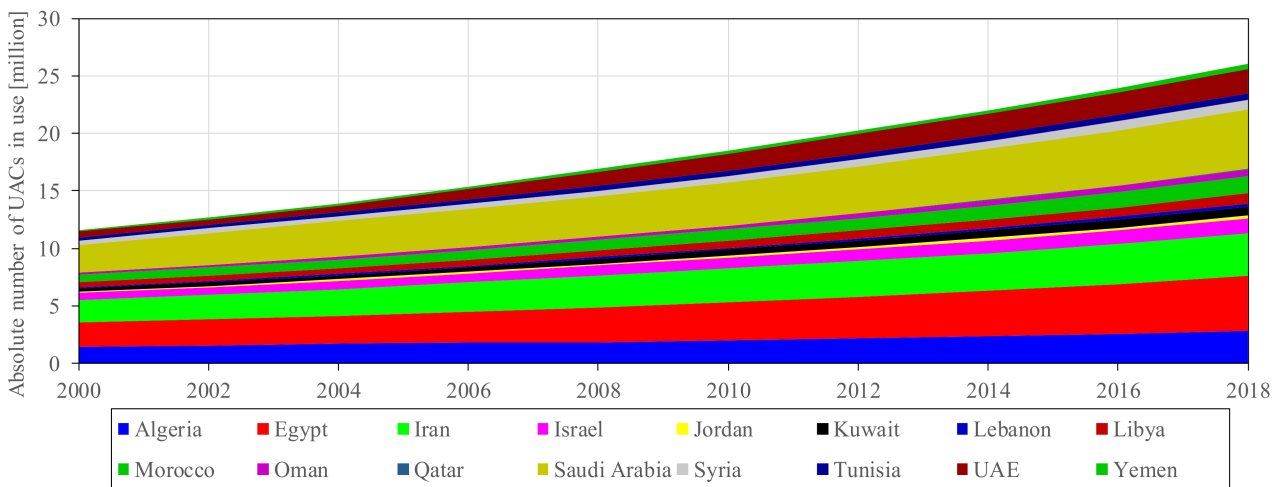


Figure 1.8.: Increasing number of used unitary air conditioners of all countries of the MENA region, except Iraq, based on data by the Green Cooling Initiative [7].

1.3.3. Impact of energy demand of air conditioning systems

The overall demand for electrical energy is currently growing exponentially with the growing population of almost every country of the region. The International Energy Agency, IEA, provides the energy consumption statistics for almost all countries in the world and provides a single combined data set for the Middle East. The entire residential sector of this region consumed 32.1 *Mtoe/a* of 74.7 *Mtoe/a* of the produced electricity. That makes up 43.3% of the entire electricity production in 2016. This share has been almost constant since the middle of the 80s. However, the overall annual demand has risen exponentially from 15.5 *Mtoe/a* in 1990 [8]. The room air conditioning takes up to 50% of this electricity demand in the Middle East [9]. The rise of the demands are shown in the following graph. The overall annual electricity supply is highlighted in blue in Figure 1.9. Red indicates the share of residential usage of this supply. Green shows the share of the electric demand to satisfy the cooling energy demand of this residential supply.

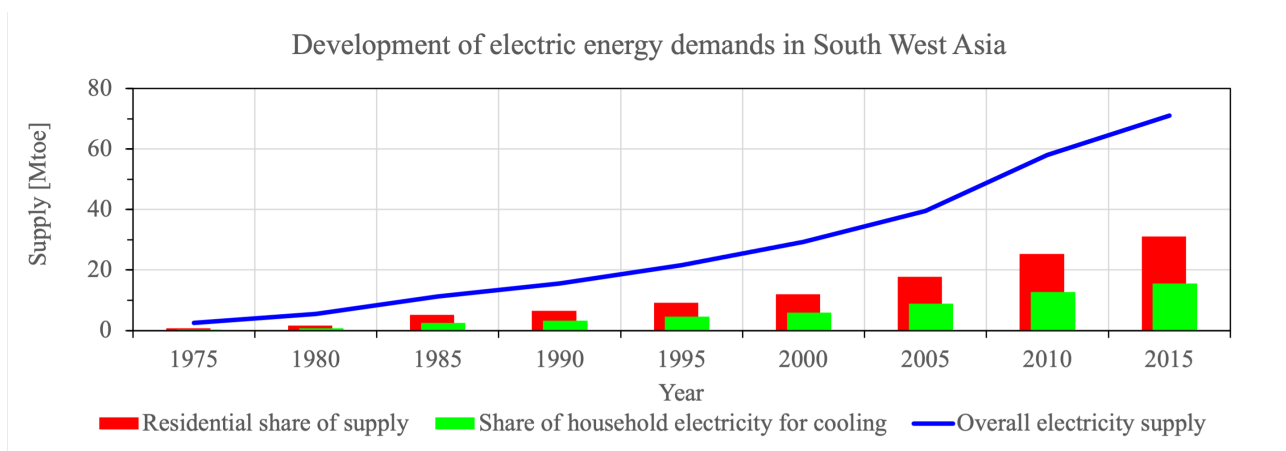


Figure 1.9.: Increasing electric energy demand of the Middle East (blue) and share of residential used electricity (red) and subshare of electricity used for residential cooling (green). Data extracted from *World Energy Outlook 2018* [8] and based on assumptions for share of cooling energy demands [9].

The rise in residential electricity demand is mainly driven by the still growing population. For example, the fertility rate of Egypt was 5.38 babies per women in 1985 but decreased to a stable value around 3.2 (± 0.15) since 2000 [44]. However, the number of installed air cooling systems is constantly rising due to increasing wealth and dropping prices of UACs. The massive installation of electric air conditioners, such as split-units, is a tremendous burden on any electricity grid. For example, S. Padmanaban, Senior Energy Advisor for USA/India's bilateral program, mentioned during his keynote speech at the IBPSA 2015 conference in Hyderabad, India: "We [India] have a peak load problem [...] and it's caused by the ACs" [45]. The same situation was observed in other developing countries like Egypt. "As consumers try to switch on fans and air conditioning units across the vast metropolis, supply has routinely failed to meet demand in the summer, forcing authorities to impose rolling power cuts neighbourhood by neighbourhood", as reported by A. Ibrahim on East Eye News [46]. The rise in peak load demand is exemplarily shown for the Arab Republic of Egypt from 2008 to 2016 in Figure 1.10. In each year, the peak load occurred during the summer and main cooling season (cf. [47], [48], [49], [50], [51], [28] and [52]). The peak load capacity was even increasing during the politically unstable times after the so-called "Arab Spring" (2011 to 2014 in Egypt), except for a slight decrease from 2012 to 2013. However, the number of unitary air conditioners continuously rose throughout the whole presented time period. The total number of units used is presented in red and on the right y-axis.

1. Introduction

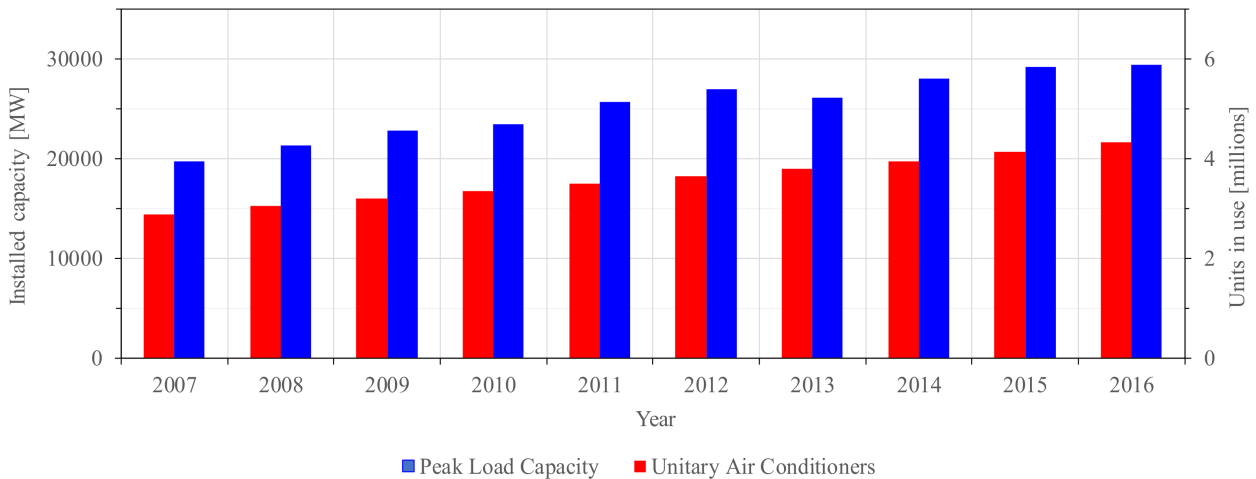


Figure 1.10.: Increasing peak load (left axis) over number of used unitary air conditioners (right axis) in Egypt. Data extracted from annual reports of the Egyptian Ministry of Electricity and Renewable Energies (2010-2017)

While the increasing overall residential electricity demand has multiple reasons, like growing population and increasing wealth, the increasing numbers of UACs mainly causes a rise in peak demand during the early evening hours, as is the case for most countries of the MENA region. This peak can be up to 25% of the total installed capacity, if the consumption is dominated by residential applications. This trend is visible throughout the world as it is concluded in the "Future of Cooling" report by the International Energy Agency IEA. The current and future share of the peak and overall residential electricity demand of air conditioners in different regions of the world is highlighted in the following graph in Figure 1.11.

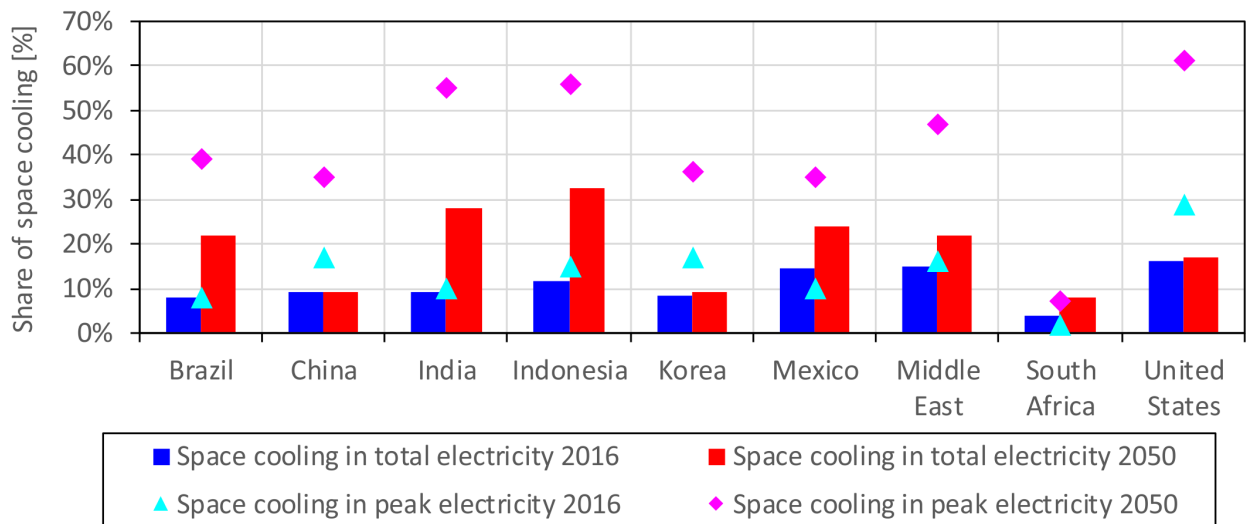


Figure 1.11.: Share of peak electricity demand of air conditioners in 2016 (triangles) and in 2050 (squares) over the total share of annual residential final energy demand in 2016 (blue) and in 2050 (red), data based on IEA study "The Future of Cooling" [10, p. 63f.]

Here, the growing share of the peak load demand for air conditioning is shown for the year 2016 and as an estimate for 2050. Further, the overall share of the residential final energy demand is indicated for 2016 and 2050. The forecasts for 2050 are based on the current increased rate of A/C ownership. This baseline scenario estimates that around 65% of households own at least one air conditioner [10]. In the Middle East, the share of electric energy demand for cooling was only 15% in 2016 and is expected to grow to 50% in 2050. Countries like Egypt or Saudi Arabia have shares of more than 50% yet alone. The electricity grid always must be capable to supply the exact amount of needed electricity directly when it is needed. A peak demand of 125% means that a quarter of the installed capacity (aka power plants or backup reserve) is only needed for a short period during the day. *"Building, maintaining and operating electricity capacity to meet peak demand is particularly costly – often between two and four times the cost per kWh of baseload electricity supply and sometimes higher – because the generation and network capacity dedicated to meeting peak load is used only for limited periods"* as the IEA concluded in 2018 [10, p. 27].

A peak of more than 3MW can be observed around 8pm in the load duration profile of the resort town El Gouna, Egypt. This is shown in the following graph in Figure 1.12. The load duration profile of the peak load day in 2014 is highlighted there. This 3MW are an increase of more than 10% compared to the day time base load supply of about 19MW. Further, the curve shows that the load decreased during the night hours to slightly above 16 MW. During the morning hours the demand rose to more than 19 MW from 7am to 10am. It stayed almost constant until a sharp rise around 7pm to more than 21 MW. This is a rise of more than 30% of the base load demand.

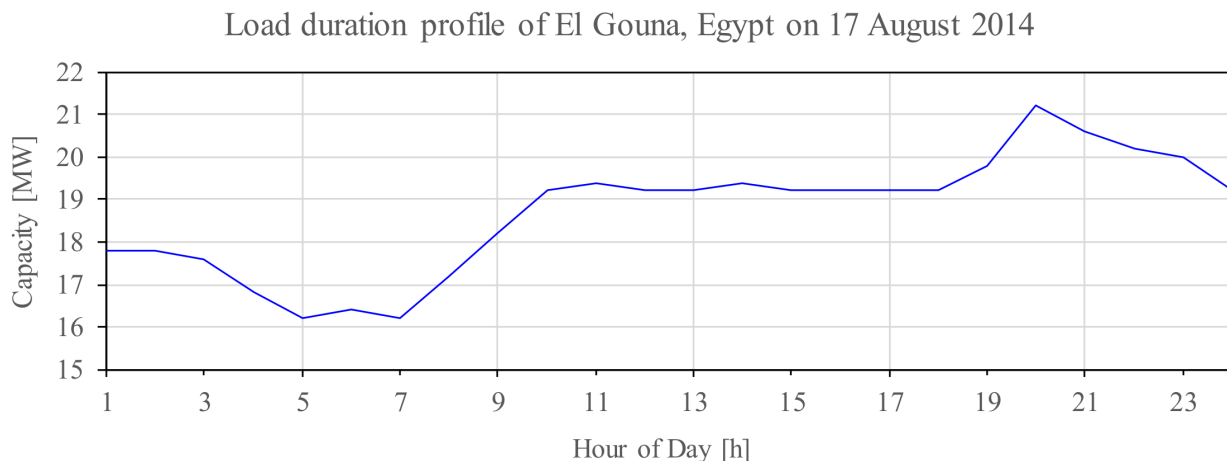


Figure 1.12.: Measured load duration profile on the peak load day in 2014 of the Red Sea coast resort town El Gouna from 15 to 22 MW, data provided by El Gouna Electrics [11].

A similar peak can be observed in the load profile of the entire country of Egypt. It also occurs in the early evening hours during August within the same week as the peak load day of El Gouna. This is as well the hottest period of the year in the country. In both cases, the peak occurs due to high demands of AC units during this time. The peak of cooling energy demand also occurs around 7pm, due to the thermal delay brought about by the heat capacity and transmittance of the apartment walls. However, the overall peak, with less than 10% of the load in the hours before, is slightly smaller as in the holiday town of El Gouna. This is due to other electricity consumers, e.g. commercial or industrial consumers, increase the overall demand curve with more constant load.

1. Introduction

1.3.4. Necessity of new technologies

Resulting from the previous discussion, new ways for room air cooling need to be found, due to the steadily increasing number of air cooling and conditioning systems in the MENA region and their impact on the electricity grid and additional carbon emissions. This accounts especially for the huge number of already present systems and their massive electricity demand which causes high peak loads on the overall grid and massive carbon emissions.

New available systems have a much better coefficient of performance, COP, and need much less electricity. Alternatively, ab- or adsorptive cooling technologies as well as open sorptive systems profit from a rising user awareness for the topic. However, the carbon footprint for all alternatives should be compared with the overall lifetime emissions of a product: from production, installation and operation to recycling.

1.4. Research hypothesis and aim of thesis

It is assumed that all air conditioning and cooling systems can be designed to decrease the electricity peak demands with none or minor impact to the thermal comfort, while having an additional further economic benefit for the operator and an ecologic benefit for the society. This has to be true for states in arid and dry climates, especially in the Middle Eastern and North African Region. The additional components must be easy to install to existing systems, while they reduce its impact on the connected grid, reduce operation costs and further reduce the ecological impact. Therefore, an optimal balance of present and additional storage technologies exists. Goal of this thesis is to find a method to determine a flexible solution for various boundary conditions in different fields of applications. Therefore, the energy storage technologies of a battery storage, cold water storage, thermal capacity of building walls, or through selling and buying from the grid will be considered as available technologies to match offer, demand, and surplus. This solution must be dependent on the boundary conditions of an analyzed system.

1.5. Fields of application

Within the MENA region, all rooms have to apply strategies to provide a thermal comfortable (or less exhausting) situation compared to the outside environment, especially during summer. Currently, traditional passive strategies are abandoned and substituted with electricity based compression chilling. Electric A/Cs are present in all scales and all kinds of environments. They cool the cabins of cars, trucks and trains. They can supply single rooms, or multiple apartments as well as entire facilities. This thesis will limit the field of application to small scale residential and holiday applications, as larger systems require as well the planning demand for the coldness distribution inside the building and/or facility. However, a broad range of outdoor climates of the region is considered to account for the vast variability of outside conditions in the MENA region.

1.5.1. Apartments as predominant usage type

The residential sector is the biggest consumer of electric energy in the MENA region, as it was shown in the Sankey diagram in Figure 1.4 on page 5. Further, close to zero planning and system sizing was done for the existing systems. The size of a system is often directly determined by the budget of the apartment owner. Long term investments and amortization calculations are seldom. However, system owners and user are often the same which makes an additional installation to operate the A/C cost neutral attractive. Rising electricity prices due to reduced and cut subsidies will increase the attractiveness of such system expansions.

1.5.2. Hotel rooms as predominant usage type

Often, holiday apartments have a similar usage profile. The requirements for the thermal comfort are normally higher or more strict. Therefore, the cooling systems are often oversized to make sure that a guest always feels comfortable. The rooms are smaller than in an apartment and the A/Cs have a bigger cooling capacity. Holiday apartments and hotel rooms are categorized into the *commercial and public service sector* by the International Energy Agency, IEA, as they are built and operated by revenue oriented entities like private companies. However, their energy demand and impact onto a local electricity grid can be enormous. Especially in touristic areas, like the Red Sea region, hotels are the main electric consumer. For example, the city of Hurghada operates an own peak load power plant to support the electric grid during the highest demand times in summer evenings. In many countries of the MENA region, the power plants are often operated by national entities.

Further, hotels need extensive licensing and their operation must be granted by local authorities. This could be an easy lever to reduce their impact on the grid. Therefore, a feasible possibility to reduce their peak load demand must be available. Hotel operators could be lawfully forced to help to stabilize the grid by reducing their peak load demand or otherwise face rolling power cuts for the disadvantage of their guests.

2. Methodology

This chapter concludes the possibilities through previous efforts to reduce the impact of unitary air conditioners economically and ecologically. Therefore, a broad analysis of available technologies and techniques, especially in the MENA region, is undertaken. Boundary conditions and input parameters are investigated and presented besides the possible system components. Here, the focus lies on the extension and/or modification of existing A/C systems.

The realization that air conditioners are a burden to the electrical grid and are the cause of an unreliable electricity supply (cf. Section 1.3.3, p. 9) leads to the need for new technologies and techniques to supply cooling energy or to reduce the electric peak demand on the grid. Various systems for room air conditioning, which can be found in the MENA region, are finally presented and are based on the previous findings.

2.1. Previous work and overview

M. Abdalla (2015) created a decision making matrix to select suitable measures to reduce the primary energy demand for cooling of a building. The insulation of the building with a thin layer (2 cm) can be the most cost effective measure to reduce the cooling energy demand. However, the entire building should be considered in his case and not only single rooms or apartments [53].

Alternative cooling technologies, like ad- or absorption, open desiccative cooling or direct evaporative cooling systems can reduce the electricity demand as they are thermally driven and need a constant heat supply instead. Ghaffer et al. concluded the first three thermal cooling systems and their range of applications in 2015 [54]. Their investigations show a good usability with solar thermal systems for residential application and especially in combination with a domestic hot water production.

Direct evaporative air conditioning systems, are used massively in Iran and Iraq. There, fresh water is sprayed directly into the incoming outdoor air which is cooled by the evaporation of this water. Further, this method is applied in hot and arid climates for local space cooling in outdoor environments of bars and restaurants. Indirect systems are possible as well. They include a heat exchanger so that the humidity of the chilled air is not raised. The market is expected to grow worldwide dramatically until 2024 [55] as these systems require much less electricity. However, they are only effective in regions with a low outdoor humidity. Further, fresh water needs to be available and water stagnation in the system must be prevented.

Currently, manufacturers offer complete solutions for new air cooling and conditioning systems which are grid independent or produce at least a big share of their needed electricity themselves. There, newly developed direct current chillers are used to satisfy the cooling demand. They can be operated directly with solar generated direct current electricity or with alternating current from the grid [56]. Their overall coefficient of performance is increased as there are no losses due to current transformations. Other manufacturers offer grid independent air cooling systems, including an electrical battery for household applications [57].

Hsu (2015) investigated on the potential to reduce the energy demand by combining decentralized air conditioners to a central unit and supplying multiple rooms/apartments with one chiller. There, high annual savings can be achieved when the chiller has a good part load behavior [58].

All previously described systems require the user to install a complete new air conditioning system and in some cases as well an air supply duct system. This is associated with high investment costs, if the

2. Methodology

systems are not directly installed within a new constructions or as an exchange for a malfunctioning system. Also, the availability to purchase one of the systems is not given in many countries of the MENA region, as the author of this research observed. Therefore, the focus of this thesis is on the applicability and compatibility with the most used air cooling system, the so called split-unit A/C. They are by far the widest spread room air cooling system (cf. Section 1.3.2, p. 5).

One other method to reduce the ecological impact would be, to switch the power supply to renewable sources. This was investigated by Wellmann et al. (2016) for an entire city in the MENA region. However, the high peak demands of air conditioners in the evening hours must still be satisfied [59]. The installed capacity still has to match the peak power demand. Hence, they are no solution to stabilize the electricity supply.

2.1.1. Air conditioners in the MENA region

Unitary air conditioners are sold world wide by retailers directly to the end user. Normally, no further planning is involved. Own observations showed that the selected cooling capacity of an air conditioner is normally a matter of the financial capabilities of a customer. Often, oversized cooling systems are installed to make sure that the customer is always satisfied and won't complain about too high room air temperatures. However, oversized systems could be beneficial, if they have an increased coefficient of performance in part load behavior. Unfortunately, most of the available and installed systems in the MENA region are hermetically sealed reciprocating compressors with an *ac* motor. Those motors are relatively maintenance free and can be easily exchanged [60]. On the downside, their *COP* as the ratio of the output cooling capacity over the input electricity decreases drastically in very hot environments as the [61].

The exact sizing of a system can reduce the investment and operational costs tremendously. In Germany, the cooling demand calculation is done in accordance with the *VDI* standard 2078. There, the capacity of a cooling system is calculated. It is not calculated as a worst case scenario with a high outdoor temperature, high radiation, and the maximum internal gains as this would lead to really big systems which probably would never run under full load conditions. Therefore, the needed capacity is based on simultaneously factors for internal and external gains and a delay function which considers the thermal capacity of the constructive boundaries of a room [62].

This example shows that the right selection of a fitting air conditioner is a matter of planning and not the size of a customers wallet. The German standard is obligatory for planned buildings and the heat protection in summer must be proven by the building service planner.

Almost all countries of the MENA region have an institution for standardizations but most of them focus with their regulation on potential hazards or compliance with the local market. For example, the only Egyptian standards, related to air conditioners, are about the rating of the performance and the energy efficiency labeling [63]. These standards are based on international technical norms, the *ISO* standards in particular. This is as well the case for most countries of the region. However, no technical planning is obligatory for residential air conditioner sizing and installation.

Calculating the needed cooling capacity is internationally accepted by the calculation methods suggested by the American Society of Heating, Refrigerating and Air-Conditioning Engineers, Inc. (ASHRAE) and their *Load Calculation Applications Manual*. There, also the fundamentals of heat transfer and thermodynamics in building physics are concluded together with thermal comfort, psychrometric processes and internal and external gains [64]. The described processes and underlying physics are the base for most energy demand calculation software. These programs are used in the context of the MENA region as well and are widely spread through engineering education. Hence, they form the base for this thesis as well.

2.1.2. Approaches for solar powered room air conditioners

In a keynote lecture at the *Solar Heating and Cooling Program* in 2017, D. Mugnier highlighted that "... *it is time for solar cooling!*" [65, p. 27]. There, he expects a big market growth in the MENA region within the next decade and compares the levelized costs of cooling energy between a reference compression chiller, with additional photovoltaic (PV), and with a solar thermal and absorption system. Especially, when subsidies are excluded, the use of PV in combination with a compression chiller has lower cooling energy costs almost everywhere. Also, most solar thermal cooling applications fall below the levelized costs of cooling energy of the reference system [65, p. 17].

Y. Badran compared in his research the performance of solar thermal and photovoltaic powered air cooling systems for the cities of Aswan, Egypt and Aqaba, Jordan. He concludes in his analytical studies that "... *the performance of daily direct cooling compensation by the PV air-conditioning scenario is more efficient than in the thermal air-conditioning scenario.*" [66, p. 5]. Further, his investigations showed that a PV powered air cooling system can work with a smaller storage as the main savings are achieved through direct use of energy for cooling purposes.

Despite these findings, many investigations focus on the use of solar thermal energy for air conditioning purposes. Back in 2007, H.-M. Henning gives an overview of most available technologies to use the solar radiation for cooling purposes. In his study, he states that the only possible way to use an electric driven air cooling process in combination with solar energy is the vapor compression cycle. This is how most air conditioners are operated. However, he focuses on the variety of possible solar thermal applications as "... *the conversion of electricity by photovoltaics and the subsequent use of [...] electricity in a classical motor driven vapour compression chiller is a technically feasible concept, it is not further considered here. Reason is, that in industrialised countries, which have a well-developed electricity grid, the maximum use of photovoltaics is achieved by feeding the produced electricity into the public grid.*" [67, p. 1735]. Nowadays, also the well-developed electricity grids have problems with high shares of renewable electricity in the grid and most researchers and engineers wouldn't assume the grid as ideal storage. For example, the German annual electric demand was already covered by 43% renewable sources in 2018. The solar generated electricity contributed 8.7% alone [68, p. 6]. High incoming solar electricity, especially during noon and times of low loads can lead to distribution problems within the grid. The times, when the connected electrical grid could be seen as "*ideal storage*" are long gone. The direct consumption of solar electricity is preferred by the grid operators and regulation authorities which support residential photovoltaic operators with cheap loans to invest into battery storage systems and increase their solar coverage rate [69]. Also, a lowered feed-in tariff increases the necessity for a higher self consumption for economically feasible solar systems [70]. The German feed-in tariff is a role model for many similar designed feed-in tariffs in the MENA region. Egypt introduced a scheme for a feed-in tariff according to German paragon in 2014 [71]. Unfortunately, most authorities currently prefer large scale applications for solely electricity production which limits the residential PV use to net-metering or self consumption. In these cases, the economic feasibility for any solar powered application is not given, as the subsidized electricity price is by far lower than the levelized costs of electricity, LCOE. These costs are the resulting price per kWh over the lifetime of a system and its acquisition costs. The countries of the MENA region have the highest average subsidization rates of at least 50 % [72, p. 110]. The average electricity prices in 2018 are presented in the graph in Figure 2.1. For example, Egypt (highlighted with the left red rectangle) had almost the lowest average electricity price in the world with only 0.02 USD/kWh, followed by Iran, Iraq, Kuwait and Qatar, each with an electricity price of 0.03 USD/kWh. Germany, for comparison highlighted with the right red rectangle, had the second highest electricity price with 0.33 USD/kWh [12]. Additionally, the estimated LCOE for small scale PV applications in 2016 are presented as the yellow area between 0.11 – 0.15 USD/kWh [13].

2. Methodology

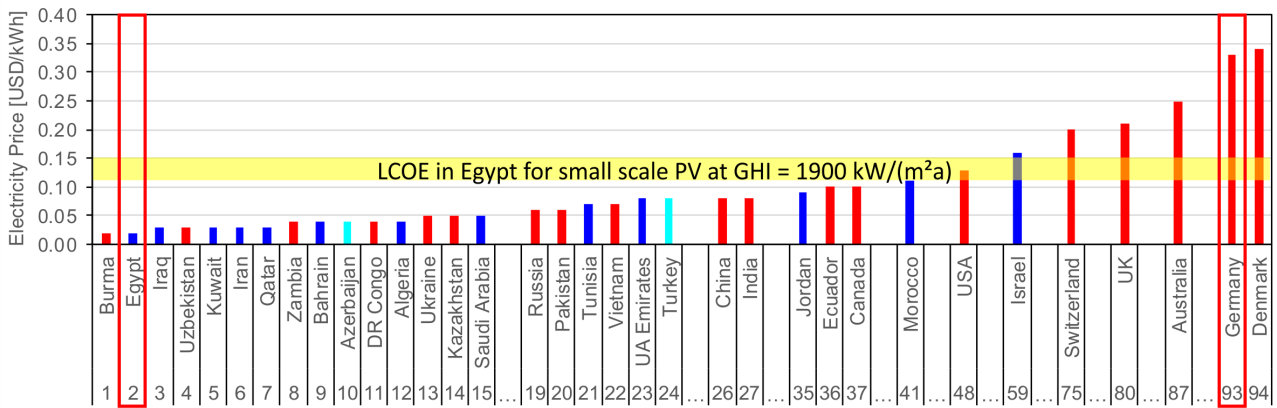


Figure 2.1.: Average electricity prices in selected countries in 2018 [12]. Associated MENA states are highlighted in dark blue, sometimes associated nations are highlighted in bright blue. The LCOE for small scale PV in Egypt is highlighted in yellow [13].

The same study expects the LCOE to become price competitive after 2020 in the region [13]. Further, the electricity prices are expected to rise, as most countries fade out their energy subsidies within the next years as the associated costs for the societies are too high [73]. Hence, it is no surprise that the World Bank reported in 2018 that "... almost all MENA countries have moved to reduce or eliminate energy subsidies..." [74]. This development opens the road for solar electric driven applications and increases the need to develop strategies to foster and steer this trend. "The projections made show that solar electric cooling will require the lowest capital investment in 2030 due to the high COPs of vapor compression refrigeration and strong cost reduction targets for PV technology" [75, p. 1287].

Finally, the latest study on "The Future of Cooling" by the International Energy Agency IEA concludes as an opportunity for energy-efficient air conditioning that "the profile of electricity demand for space cooling generally matches to some degree that of solar PV output, which can help to lower the cost of meeting peak load" [10, p. 29]. This means, that the solar energy has to be shifted only by some hours in comparison to the provided chart of load duration curve on the peak load day (see Figure 1.12 on page 11). The peak of incoming solar radiation occurs at noon. The provided energy has to be stored for some hours only to satisfy or partly support the evening peak in electric energy demand.

2.1.3. Simulation environments

The following two subsections investigate state of the art computing solutions for the building demand model and the building supply model which are investigated in this research. The first is needed to create a model of the cooling energy demand of a room. The latter is used to simulate an energy conversion system to extract the hot room air.

Building energy demand model

There are various simulation programs to calculate the building energy demand. The main difference are static and dynamic calculations. Static environments try to find the maximum cooling energy demand based on the sum of possible worst conditions and evaluate the performance at single different time stamps. For example, the cooling load is evaluated at the highest outdoor temperature and evaluated again at the highest radiation gains. Thermal masses and storage processes are accounted by time shifting factors. However, modern simulation programs, combined with current computational power, enable transient annual simulations. There are as well many tools that can perform dynamic building energy demand simulations. The *Building Energy Software Tools* directory list more than 200

simulation programs for building and climate calculations. 67 of them are capable to perform whole building energy simulations [76]. J. Sousa compared the most common tools *Energy Plus*, *ESP-r*, *IDA ICE*, *IES* and *TRNSYS* regarding their functionality. She concludes that these are "... *the most complete simulation software tools...*" [77, p. 9]. Also, B. Fassbender evaluates the quality and features of various building energy software. For example, he describes *DesignBuilder* to have "... *a sleek design, impressive appearance, and [to be] fast [...] [but that] the downside is the cost depending on your options and number of licenses.*". The integrated calculation engine is *EnergyPlus*. This engine can be used as well with a sleek *IDF Editor* where an exceptional knowledge of the program is needed to operate it with its full capacity. The classic simulation program *TRACE 700* has the disadvantage that it takes a long time in multi-zonal building simulations and that the underlying algorithm "... *is a bit of a black box*". On *IDA ICE* he concludes that it can handle "... *even wicked design conditions [...] [and that it has an] excellent performance, with an emphasis on keeping the operator comfortable*". In his opinion, a further advantage is that the algorithm of the underlying engine is fully visible and can be understood by the user [78].

In this research, *IDA ICE* is chosen for the building energy demand calculation as it offers a variety of indoor climate performance analysis and its algorithms are fully reviewable [79]. Further, previous investigations have been undertaken with this software to analyze the room performance of apartments with vaulted ceilings as they are typical in the region [38]. Also, the resulting annual load duration curves can be easily exported to be used in other simulation software. For example, these curves can be used easily by custom made building simulation environments like the *BuildingSystems* library for the modeling language *Modelica* [26].

HVAC and supply model

Most of the building simulation software includes the simulation of building supply systems as well. However, it is not possible to find a simulation solution that is capable 1. to design HVAC Systems, 2. to run parametric and optimizations, and 3. to work on the building automation and control algorithms [76]. One of the most powerful but complex programs which could be used in the context of building supply systems is *TRNSYS*. Another powerful solution would be the use of a system simulation library, which is written in the modeling language *Modelica*. There, the user has the maximum freedom to extend, manipulate and control the entire model and the underlying equations. Kim et al. (2013) compared the performance of both solutions in 2013 with an emphasis on the control system. They conclude that "... *TRNSYS will show its strength to design and test a supervisory level control algorithm where many simulations are required. However the validity judgment must be made considering the fixed time step length, time lagging of control signals, the lack of pressure-driven flow distribution and the lack of interaction of control loops through the duct static pressure. On the other hand, Modelica's adaptive time step length and event detection allows it to be used for the design and analysis of both supervisory and local level controllers. The developed control algorithms can be directly applied to a real building control system due to the consistency of inputs and outputs with actual control systems.*" [80, p. 3274]. Especially, the direct comparability of the *Modelica* model is a great advantage to implement later findings directly.

Various research groups already developed *Modelica* libraries to simulate buildings and their systems and to develop in depth control strategies. One of these libraries was introduced by Nytsch-Geusen et. al in 2013. They developed a library for object-oriented modeling and simulation of complex energetic building systems [81]. The so-called *BuildingSystems* library is one of four libraries which is based on the *Modelica IBPSA* libraries [82] and was first introduced in 2013 and is since then under ongoing development [26]. The library is capable to simulate building supply systems on a room, a building and even city quarter level. The previous work and the extensive and detailed modification possibilities are the reason to use the language *Modelica* in this thesis.

2.2. Columns of research

Based on the previous discussion, this research is set on 3 main pillars. They are given as an overview in the following Table 2.2 on page 21. The first column is dedicated to the simulation models which are derived from the previous discussions about the various simulation programs. This part is divided into the room energy balance simulation in *IDA ICE* and the object-oriented modeling language *Modelica*. *IDA ICE* is used to create 1D single zone simulations for pre-studies and a first analysis of the room behavior. The detailed 3D zone model, which has a much higher computation time, is used to create detailed load profiles, evaluate the thermal indoor comfort and to study the flow patterns and thermal stratification in a room. Further, it is used to evaluate the thermal capacity of a rooms surrounding surfaces and calculate their storage capacities. The *Modelica* language is used to simulate the entire system and enable a modular construction of simulation scenarios, which are based on varying boundary conditions. Further, parameter optimization are done to find a feasible system for a desired scenario. On the one side, this model includes the electric models for the PV system, the battery storage, the electrical transformation, the air conditioner itself, the own consumption and the trading with a connected grid. On the other side, the language is also used to describe the use of electricity to satisfy a cooling load with a compression chiller, to store "coldness" in a water tank or in a thermal building mass.

The second column represents the analysis of an actual apartment in the target region. This apartment is used to measure and analyze operational parameters of an air conditioned room and to form a case study for PV electric air cooling. Therefore, the free floating temperatures, room air temperatures during the operation of an air conditioner, surface temperatures of the vaulted ceiling, carbon dioxide and sound pressure levels are measured inside the apartment. A small scale rooftop installation of a PV system, including a battery system, is used to evaluate a possible operation of the connected air conditioner. The operation parameters, like the PV generated output, the battery status and the consumption of the air conditioner are measured.

The case study apartment is as well modeled in the simulation environment of *IDA ICE* and with the *BuildingSystems* library to first evaluate, calibrate and validate their results. Second, to create possible and feasible scenarios to reduce the impact of the electricity demand of the existing apartment and to develop control strategies to achieve these goals. Third and finally, the so called digital twin can be used to analyze the flow patterns and thermal stratification inside a room with very high ceilings.

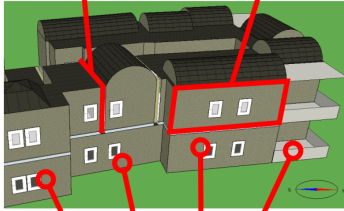
Last but not least, the third column expands the view to the city level. The apartment's surroundings define the input parameters, such as the weather conditions of different locations, the local energy prices and properties of a potentially connected electric grid. The annual load profile of a representative town in the region is used to develop a standardized load profile for the residential electricity demand. Further, typical construction techniques are evaluated to accurately model the building physics of the construction. Finally, the city scale is needed to evaluate the impact of this research in a greater context and to estimate positive and negative effects which a developed system could have.

Simulation Models

Room model in *IDA ICE*

Building mass
- heat transfer
- energy storage
- thermal capacity

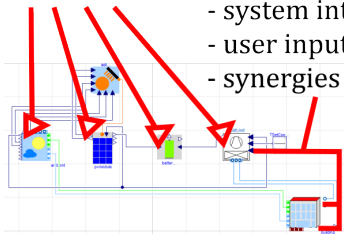
3D Zone model
- detailed analysis
- complex geometries
- load profiles



1D Zone model
- typical apartment
- entire buildings/districts
- fast computation

Electric and thermal models
- generation
- distribution
- conversion

Control algorithms
- system integration
- user input
- synergies



Optimization
parameter based optimization
regarding input boundaries
and limits

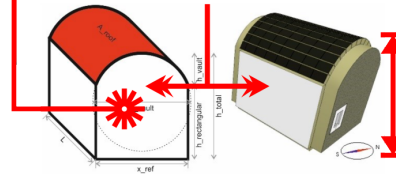
System simulation in *Modelica*

Room & System Analysis

Simulation of typical apartment

Thermal indoor air
- simulation of indoor parameter
- expected thermal comfort
- variation of in- and outputs

Indoor environment
- measurements in 7 heights
- dome surface temperatures
- humidity, CO₂, noise



Air stratification
air patterns and movement

Measurements in typical apartment

Room energy balances and A/C operation
- heat losses and gains
- annual balances



Small scale PV
performance
monitoring



System operation
- application of control strategies
- verification of theoretic results

City Analysis

Definition of global boundaries

Outdoor environment
measurements of outside weather
conditions



© tripadvisor.com - aerial-view-of-el-gouna.jpg

Building boundaries
typical material
and constructions
Load profiles
development of standardized profiles

Global impact of research

Feasibility
socio-cultural applicability in
the MENA region



© DanPMK (2011)

Impact
- ecologics and economics
- for single users or entire entities
- grid loads and grid stability

Figure 2.2.: Columns of research.



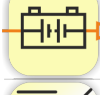




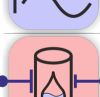
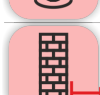
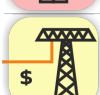


2.3. Simulation model

The overall simulation model is introduced by giving an overview of all system components and their needed functionality. These components are arranged in a general system setup for A/C's. They include models for the room air energy balance, the thermal models and the electric models.

2.3.1. Overview of system components

This section gives a detailed description of possible system setups. All systems consist of various components, which can be coupled together and be used under varying boundary conditions. The single components, which are modelled and simulated are shown within the table in Figure 2.3.

Figure 2.3.: *Table of system components and their functionality. Yellow are electrical components, blue are components working with a cooled fluid, and red are thermal storage systems.*

Symbol	Name	Input	Process	Output
	Photovoltaic module 2 Diode Model	Local boundary conditions Module type(s) and wiring Specific costs per W	Converts incoming radiation to electricity. Dependent on temperature, orientation and module parameter	Electric power (DC) in W
	Grid connection Electricity supply	Grid capacity in W Electric price per Wh	Feeds electricity from the grid to the system if no solar power or stored electricity is available. Can be limited by grid capacity.	Electric power (AC) in W specific costs
	Battery Kinetic Battery Model	Electric power (DC) in W Battery parameter Specific costs, storage size	Current is fed to system or stored in battery if no load is applied. Self-discharging over time. Only charged with access energy.	Electric power (DC) in W
	Electric transformer DC/AC converter	Electric power (AC) Transformer parameter Specific costs per W	Transforms direct current to alternating current with a limited capacity and varying efficiency.	Electric power (DC) in W
	Air conditioner Direct room air cooling system	Electric power Air conditioner type Specific costs per W	Electro-mechanical compression and evaporation to cool down recirculating air inside a building/room and transport the heat to the environment.	Air cooling capacity in W
	Water cooler Compression or other water cooling system	Electric power Air conditioner type Specific costs per W	Uses electric driven mechanical compression and evaporation to cool down a secondary cold water loop. The heat is transported to the environment.	Water cooling capacity in W
	Air outlet Room unit of A/C system	Cooling capacity in W	Wall opening for air supply of cooled recirculating air.	Convective heat transport to room air in W
	Room surface e.g. cooling ceiling or wall	Cooling capacity in W Thermal capacity of connected construction	Heat exchanger with the room air (mainly radiation), can be cooled by additional subsurface pipes or be in heat exchange with the building mass.	Heat transport to/from room air in W
	Cold water storage	Cooling capacity in W Boundary conditions Specific costs per Wh	Cooled water tank as heat sink for room air conditions. Discharges over time. Will only be charged with access energy.	Cooling capacity in W
	Building mass Usable thermal building mass	Cooling capacity Thermal capacity Specific costs per Wh	Room surrounding thermal masses that are in heat exchange with the room surrounding surfaces. Stores and releases heat in a daily cycle.	Capacity in Wh
	Grid connection Feed in	Grid capacity in W Feed-in tariff per kWh	Access alternating current can be sold at specific feed in rates to the grid.	Revenue of electricity production
	House connection Self consumption of electricity	Load profile in W	AC electricity demand of all building/apartment consumers.	Solar coverage rate of electric consumption

In the first row, the table contains the graphical representation, which is used to construct the following system schemes in the upcoming sections. Further, the components' names are given in the second column. The third row states the needed input data which is needed for the calculations inside each component. A short conclusion how it is processed is stated in column four. Finally, the resulting outputs are given in the last column.

Models, which mainly focus on electricity generation or transformation are highlighted in yellow. These are the photovoltaic modules (direct current, DC), the electric grid (alternating current, AC), an electrical battery storage (DC), an electrical transformer (DC/AC), and the household electricity load (AC). Components highlighted in blue mainly function as part of the cooling system, like the air outlet of the room air or a cooled room surface. Red is used as the background color for thermal storage systems: a cold water storage tank or the use of the building mass. The air conditioner and the water cooler use electricity to cool a medium and are therefore colored yellow and blue. The main type of an air conditioner is the so-called split-unit, where the air is cooled directly by an evaporation process in a cooling coil inside the air stream. Within most water coolers, a compression chiller cools a cold water loop, which extracts energy to the target media by heat exchangers.

Information is transferred from left (input) to right (output).

These components are linked together to assemble different possible system configurations. Energy flows can only happen between the same colored connectors which are used to illustrate the information flow between each component. The energy sources are the photovoltaic modules and the electric grid. The energy sinks are the grid, to which electricity can be sold, the household electricity consumption and the cooling energy demand which is represented in the energy demand of the air outlet or the room surfaces.

2.3.2. System setup for room air cooling

On the following pages, the layout of the reference system will be presented and extended. Therefore, the previously described components will be used to assemble 4 different room air cooling systems. The first will be the base system which will only consist of a room air cooling unit which is connected to a local grid. Second, this system is set up as reference small scale photovoltaic cooling system. Third, the capabilities of this system are expanded by introducing an air to water chiller. Finally, this system is made grid independent.

The reference system represents the world wide most common used method to cool the room air. The so called split-unit system is a unitary air cooling system to cool single rooms, apartments or a small cluster of multiple indoor units and one outdoor unit.

This system can be easily extended to work as a solar powered, but still grid connected system. This is described in the subsection following the reference system. Further, a small scale electrical battery storage system is presented to account for load shifting potentials. Besides this, the thermal mass of the room surrounding surfaces is introduced as well.

The performance of this design could be increased by introducing a water based cooling system which is done in the subsequent section. Therefore, a similar air-water cooling system is introduced in combination with a cold water storage tank. The chilled water can supply the cooling coil of an indoor recirculating air (RCU) unit or inside a cooling surface, like an active cooling ceiling.

Finally, a special case, the grid independent solar powered air cooling system is introduced. There, no electric energy should be needed from the grid. Thereby, remote applications in rural areas are possible.

2. Methodology

Base system

The split-unit is, with a share of more than 80%, by far the most common unitary air conditioning system in the world and is therefore used here as the reference system [43]. This is built with the previously described components and is shown in Figure 2.4. An electric grid is connected as source to a sink which is represented by the house and supplies there the load of a consumer, for example a standard load profile of an apartment. The electricity is also used to supply an alternating current driven air conditioner, the split-unit. It directly cools the indoor air of a room by recirculating it. They measure the temperature of the indoor air T_{air} . This connection is illustrated with the dotted purple line. The air conditioner is switched on as soon as the temperature reaches a user-defined upper limit. Afterwards, the air is cooled until the temperature falls under a lower limit. The hysteresis between switching the A/C on and off again is normally around $\Delta T 4 K$ and can vary between different systems and applications. The air temperature is measured at the air inlet. Theoretically, the building mass could be activated by sub cooling of the room. However, this control strategy is not applied so far and therefore only presented in faded tones.

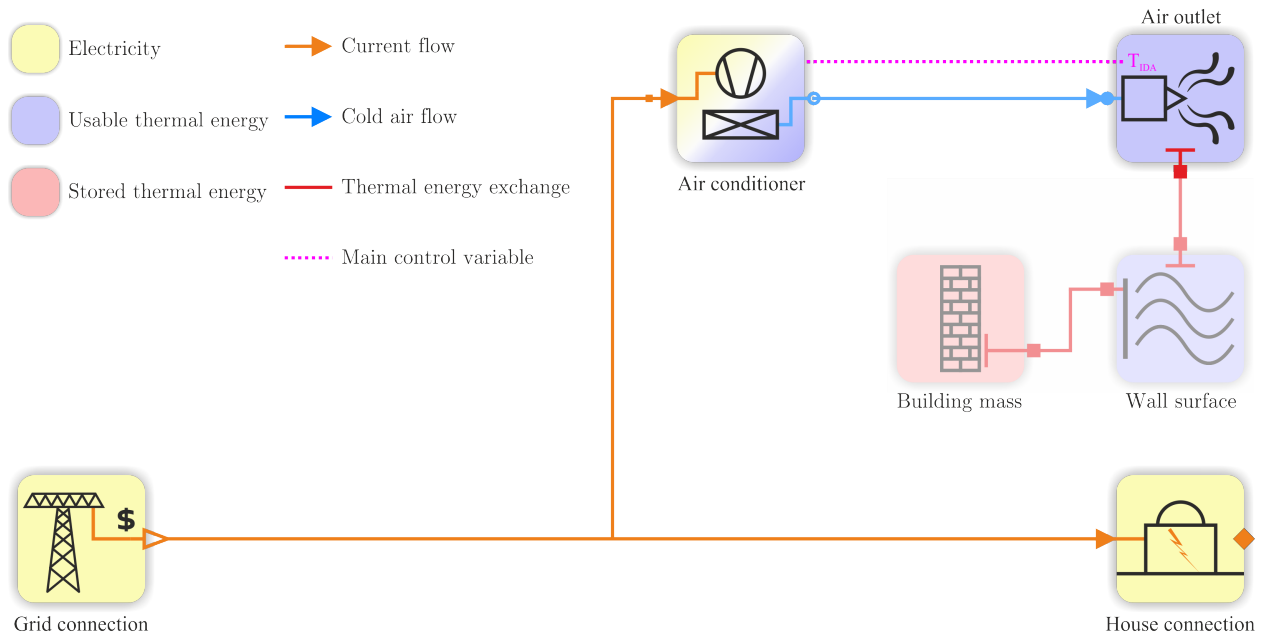


Figure 2.4.: *Most common UAC system used to cool room air world wide.*

In most cases, this system is already installed for room cooling purposes. Single rooms are normally cooled by parapet systems. Multiple rooms or entire houses can be cooled by a unit which can be placed on the roof of the building. This system has the lowest investment costs. A broad range of available cooling capacities reduces planning efforts to a minimum. Operation costs are mainly driven by the electricity costs. Maintenance costs are often limited to the cleaning of air filters and occasional refilling of the refrigerant due to leakages.

Grid connected solar powered air cooling system

The reference system is extended to work with solar electricity, the smallest feasible battery storage and an optimized control strategy to use the present building mass as thermal short term storage. To achieve a minimum effort in terms of investment costs, but a good potential to save operation costs it is necessary to design this system to work with most existing reference systems. Further, this strategy could implement the possibility to use the building mass as a heat sink for peak load times in the early evening hours. Additionally, this control strategy can lower the impact on an electric grid by reducing the electric peak demand through these two storage systems.

Below, the extended system is presented. The previous shown base system is expanded with a photovoltaic system, a battery and an electric transformer. The PV system supplies electricity, which can be stored in a battery or transferred directly to a DC/AC transformer. The air conditioner is supplied with this electricity or from a connected electric grid. The state of charge, SOC , of the connected battery determines which electricity source is selected. The air conditioner directly cools the room air. Weather or not a cooling load is present in the room is determined by the indoor room air temperature T_{IDA} . This information is transferred as information from the room as indicated by the purple dotted line.

Further, the room can be sub-cooled, when the battery is fully charged and access electricity is available. This event occurs during a rise in cooling demand, when load is expected at times with no or low incoming solar irradiance. This event is typically observable at evening peak times, since the highest demand is expected shortly after sunset due to the time the heat of the day takes to be thermally transported through the building surfaces.

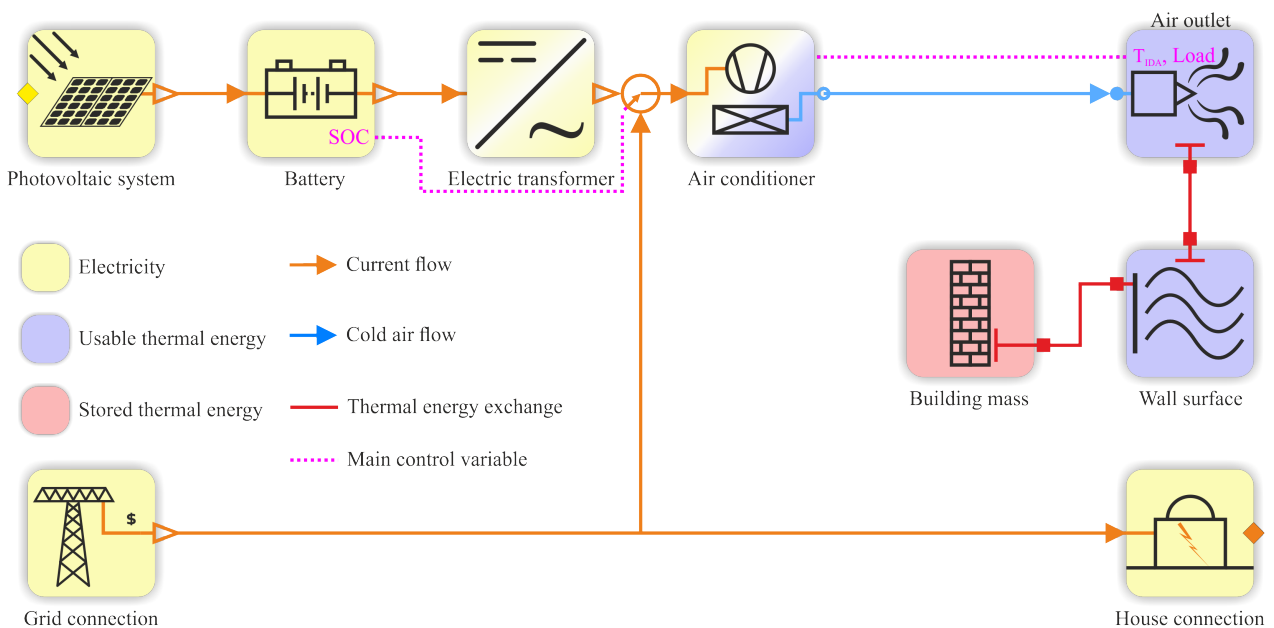


Figure 2.5.: System setup of a solar and grid powered cooling system.

2. Methodology

Water based cooling system

The air conditioner of the previously introduced setups can be substituted by a water based cooling system. This system uses an electricity driven compression chiller to cool water. Typical applications are cooling systems, which are detached from a house and supply multiple rooms. Exchanging an existing direct air conditioner with a water based system is often cost intensive due to its high planning and installation efforts. However, the operation costs can be much lower as a centralized coldness production can work more efficiently. Hence, it is recommended to install a water based cooling system when planning a completely new installation. Also, this system can be designed as grid connected or independent system.

The chilled water is distributed through a connected piping network and can charge a cold water storage tank. This is the third introduced energy storage component which can be used within the proposed setups. From there, cooled water can supply a cooling coil within an air stream, for example of a recirculating fan within a room or within a main supply air stream of a building HVAC system. Chilled water can also be used within a surface cooling system like a cooling ceiling or a thermally activated building mass. As before, the existing building mass can be sub-cooled, when the battery is fully charged and additionally the cold water storage as well. The battery size could be reduced to a minimum capacity to only supply a constant power output to the transformer while the sun is shining. The main storage capacity would be the much more cost efficient and long term stable cold water storage.

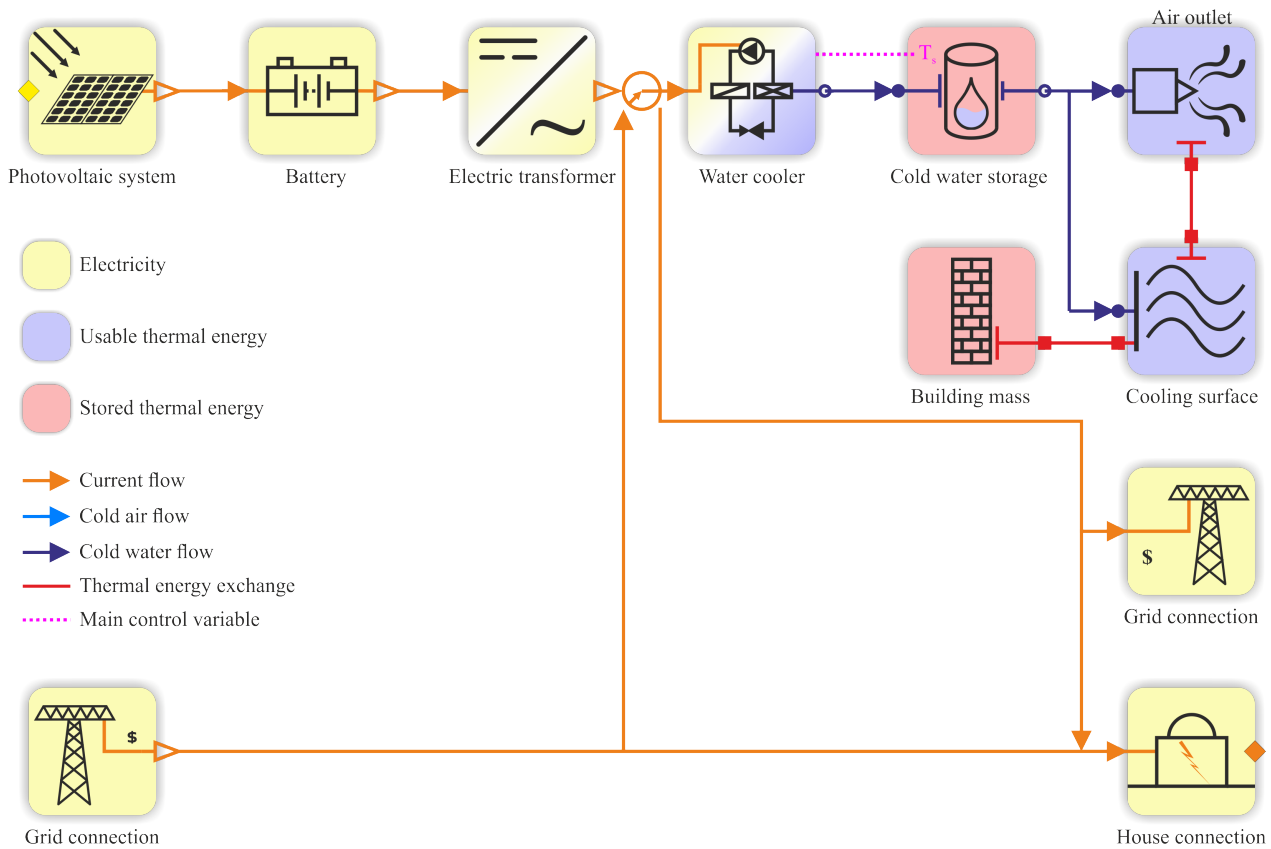


Figure 2.6.: System setup of a water based cooling system.

Grid independent solar powered air cooling system

A special case is a total grid independent room air cooling system. This system would serve as cold air supply in remote areas to avoid lethal temperatures, for example in rural hospital applications. It could also serve as electricity supply system and only use access energy for air cooling purposes. The grid connection of the reference system has been neglected in the system in Figure 2.7 to create an independent system for air cooling purposes. In those cases, the photovoltaic and battery storage system could directly serve a decentralized direct current grid. Hence, the electrical transformer and its losses can be avoided. In this case, newly available direct current driven air conditioners must be used [83].

The A/C is operated to satisfy the energy demand for cooling. However, it can be switched off if household applications are prioritized. The overall system should be designed at least to prevent unhealthy high indoor temperatures. The battery capacity could be designed to mainly supply enough electricity for the connected appliances and only support air cooling during times with access electricity by the solar modules.

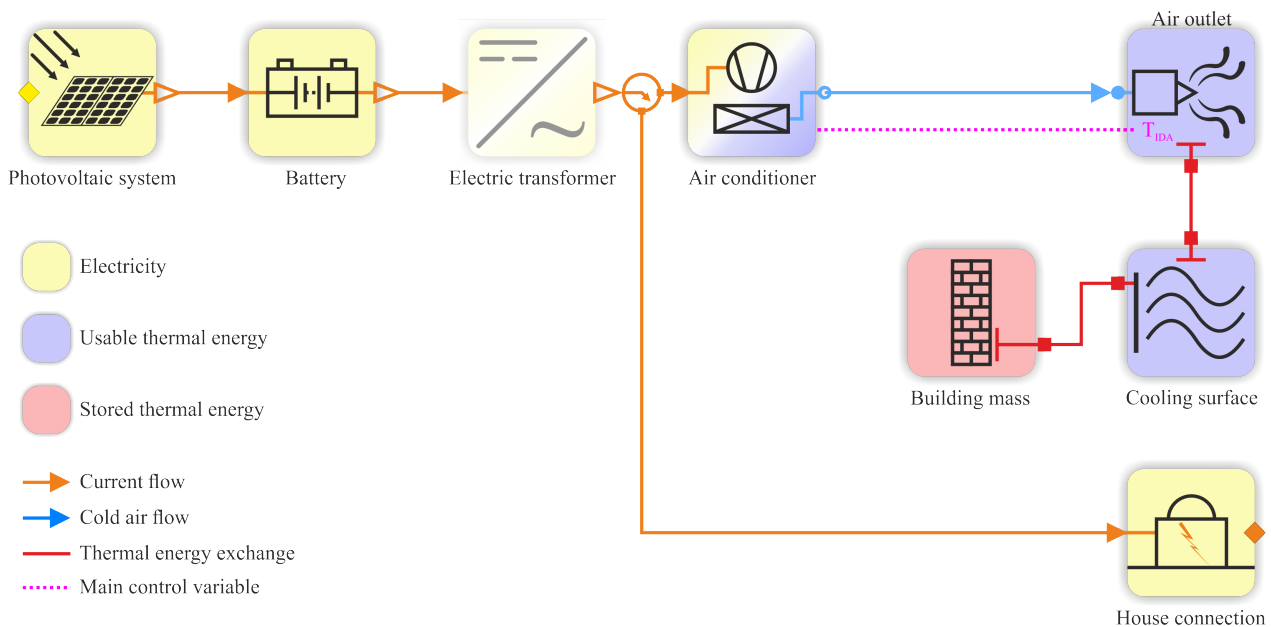


Figure 2.7.: System setup of a solely solar powered cooling system.

2.3.3. Room air energy balance

Two cases must be considered for the room energy balance calculation: the peak capacity demands, which determines the size of the needed supply systems, and the annual energy demands, which determine the annually needed amount of energy from various sources. The peak capacity has to be calculated for the worst but still possible situation to guarantee user comfort under disadvantaged conditions. For example, this is done in Europe with the standard *EN 12831*. Calculating the needed cooling capacity can be done with the *VDI 2078*. The main difference to a heating load calculation is the recognition of external, \dot{Q}_{ext} , and internal gains \dot{Q}_{int} . The sum of both is the overall needed cooling capacity \dot{Q}_{cool} (see Equation 2.1). The needed installed capacity of an air conditioner $\dot{Q}_{A/C}$ is the peak of \dot{Q}_{cool} and occurs when the sum of external and internal cooling load is the biggest. Due to the storage capacities of the building surfaces, the whole calculation process becomes highly dynamic. Heat is not only transferred through a surface, but as well stored or released. This is represented by the

2. Methodology

term \dot{Q}_{mass} which is the heat flux into or from the thermal capacity of a wall. In the manual abridged calculation process, which is presented by various standards like the *VDI 2078*, the transient behavior through building masses is accounted through time shifting factors on all following gains. However, current dynamic simulation tools calculate this behavior in detail.

The external cooling load \dot{Q}_{ext} is the result of the sum of three terms at a certain point in time of the year. Equation 2.3 concludes all three parts. First, the incoming transmission through the outside surfaces \dot{Q}_{trans} , like walls, windows, the ceiling or the floor. Second, the resulting cooling load by an enthalpy stream from the hot outside air \dot{H}_{vent} must be considered. This includes heat gains through desired ventilation and by infiltration through gaps and openings in the building enclosure. Third, the heat gains through radiation \dot{Q}_{irr} are considered. The peak of external cooling load could be during a time point with relative high outdoor temperature, causing high transmission and ventilation gains, or at a time with a high amount of incoming solar radiation. All three don't have to peak necessarily at the same time.

The other reason for cooling demand are the internal gains \dot{Q}_{int} . Its terms are presented in Equation 2.4. The first internal cooling load are the heat emissions by people \dot{Q}_{pers} . It is dependent on the activity and clothing. The heat emissions through lightbulbs \dot{Q}_{bulb} was reduced in the last decade by the propagation of energy saving bulbs and more recently the spreading of LED lighting. However, the author observed a still wide prevalence of classic incandescent light bulbs in the MENA region. Their impact on the cooling load is much higher. Additionally, machines like a computer or a fridge emit heat. Their heat emission \dot{Q}_{mach} can be estimated through their rated power and working principle, or looked up in tables. In case of factories or kitchens, hot material could enter the room. The resulting heat emission can be found in the term for \dot{Q}_{mat} . Heat can be transmitted as well through the walls of neighboring rooms \dot{Q}_{room} , like a warmer bathroom. All other, not listed, heat sources can be concluded in the term for \dot{Q}_{misc} .

$$\dot{Q}_{cool} = (\dot{Q}_{ext} + \dot{Q}_{int})_{max} \quad (2.1)$$

$$\dot{Q}_{A/C} = \dot{Q}_{cool} - \dot{Q}_{mass} \quad (2.2)$$

$$\dot{Q}_{ext} = \dot{Q}_{irr} + \dot{Q}_{trans} + \dot{H}_{vent} \quad (2.3)$$

$$\dot{Q}_{int} = \dot{Q}_{pers} + \dot{Q}_{bulbs} + \dot{Q}_{mach} + \dot{Q}_{mat} + \dot{Q}_{room} + \dot{Q}_{misc} \quad (2.4)$$

The method to calculate the annual energy demands for heating and cooling is based on the thermal losses or gains from the environment and the internal gains. It is presented in detail in the German standard *DIN V 18599* [84]. The used description of the building physics and the resulting heat transfer equations are used in most building simulation tools. It is the result of the integration of the cooling capacity \dot{Q}_{cool} of each moment of a year. Additional boundary conditions can be added. For example, the integration of the cooling demand could be stopped or the cooling set point increased during times of no occupancy or varying activities. Hence, the user profile plays an increasing role in energy demand calculations.

External heat gains \dot{Q}_{ext}

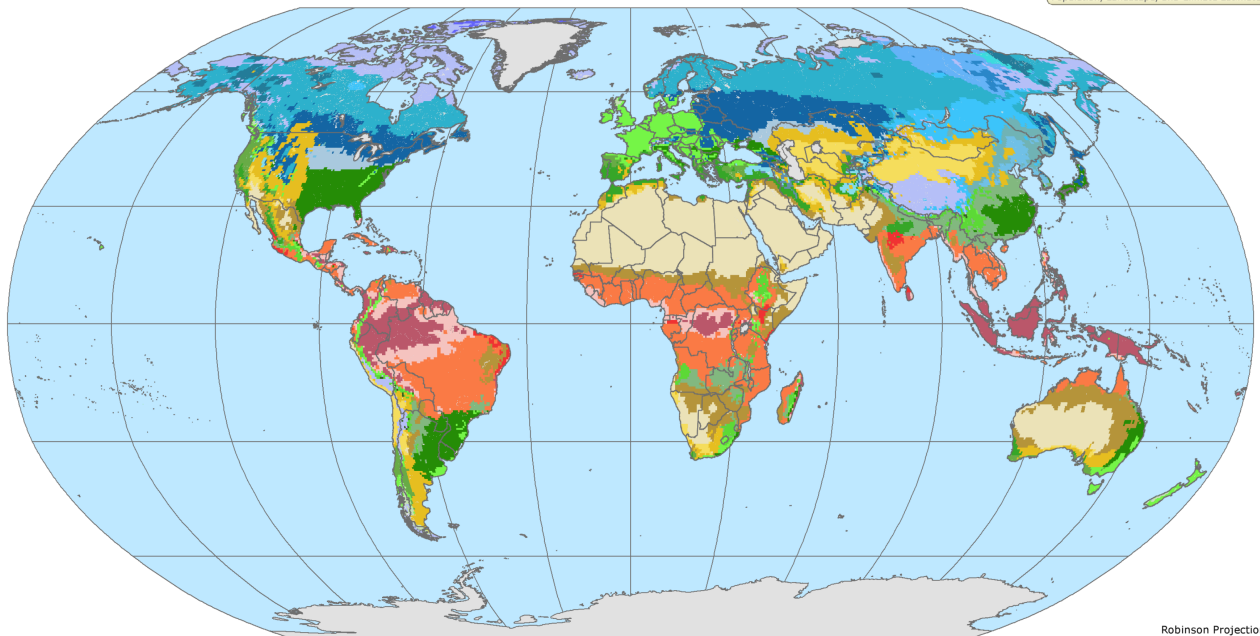
In the following two paragraphs the external heat gains are described. They are totally dependent on the local climate conditions in which a building is situated. Hence, the global weather conditions are described and narrowed down to the common climate parameters of the MENA region. Afterwards, the various external heat sources, the radiation gains \dot{Q}_{Irr} , the transmission gains \dot{Q}_{trans} , and the ventilation gains \dot{Q}_{vent} are presented.

Global weather conditions

For calculating the external gains and losses, a deep understanding of the outer climate is needed. It is the main influencing factor on the thermal building performance and has to be considered carefully and accurately. Consequently, the weather conditions are one of the main boundary conditions. The Figure 2.8 below shows the world climate zones, based on the observed climate data from 1975 to 2000 and shows the *Köppen-Geiger-Pohl* climate classification [14]. *Tropical* climates are indicated in red color tones, *dry* climates in yellow tones. Highlighted in green tones are *temperate* climates. *Cold* and *Polar* climates are marked in blue to purple tones. Often, regions with similar climatic boundaries are combined to greater areas. For example, compared with the map of countries of the MENA region in Figure 1.1 on page 1, all countries fulfill the definition of a *hot, desert* climate with its boundaries between the Atlantic and Indian Ocean, the Mediterranean and Arabic Sea, and the mountains of the Caucasus in the north and the edges of the Sahara in the south.

**Population, Landscape, and Climate Estimates, v3:
Climate Zones, Observed Climate Data 1975 - 2000, Global**

National Aggregates of Geospatial Data Collection



The Köppen-Geiger Climate Classification system is based on annual and monthly averages of temperature and precipitation ranges. These maps illustrate observed data using the TYN SC 2.03 (Mitchell et al., 2004) data set. Data was averaged over a period of 25 years. Map data were received by CIESIN as 30 arc-minute grids, in Geographic projection and resampled, using a nearest neighbor algorithm, to match the extent and resolution of GPW v3 of 2.5 arc-minutes.

A: Tropical	BWh - hot, desert	Cwb - winter dry, warm summer	Dsc - summer dry and cool
Aw - winter dry	Cc - fully humid, cool summer	Cwc - winter dry, cool summer	Dwa - winter dry, hot summer
Am - monsoonal	Cfb - fully humid, warm summer	Dwb - winter dry, warm summer	Dfa - fully humid, hot summer
Af - fully humid	Csb - summer dry and warm	Ddb - winter dry, cool summer	Dwb - winter dry, extremely continental
As - summer dry	Csc - summer dry and cool	Dfb - fully humid, warm summer	Dfd - fully humid, extremely continental
B: Dry	Cfa - fully humid, hot summer	Dfc - fully humid, cool summer	Dsd - summer dry, extremely continental
BSk - cold, steppe	Cwa - winter dry, hot summer	Dsa - summer dry and hot	E: Polar
BWk - cold, desert	Csa - summer dry and hot	Dsb - summer dry and warm	EF - frost
BSh - hot, steppe			ET - tundra

Figure 2.8.: Global climate regions according to Köppen-Geiger-Pohl [14].

The area is dominated by an equal historic architecture and building style, as it is described in Section 1.3.2 on page 5. This mainly results from the specific needs of a building structure to separate the user from the environment and its climatic boundaries to achieve the best possible indoor state. Often, socio-cultural moral values are similar as well as spread technologies, systems and techniques to tackle challenges like achieving thermal comfort inside a room.

Vast parts of the MENA region, especially around the deserts of the Sahara (northern Africa) and of the Nefud (Arabian Peninsular), are dominated by a *dry* climate. They are located between a latitude

2. Methodology

from around 10° to 30° north. The north coasts of Morocco, Algeria, Tunisia, and Libya, as well as the northern borders of Syria, Iraq, and parts of Iran vary more towards a *temperate* climate. All these locations are above a latitude of 30° north.

For building simulation contexts, a standardized weather, based on the buildings location, must be created and openly accessible to enable planners and operators to work on a unified base and make simulation outcomes predictable towards their real behavior in an environment. Therefore, the *World Meteorological Organization*, WMO, "defines climatological standard normals as "averages of climatological data computed for the following consecutive periods of 30 years: January 1, 1901 to December 31, 1930, January 1, 1931 to December 31, 1960, etc." (WMO, 1984). The latest global standard normals period is 1961-1990. The next standard normals period is January 1, 1991 – December 1, 2020." [29]. These so-called *normals* are not just averaged values over this periods as this would reduce the presence of local extrema that only occur for a short period during a year. "A more common approach has been to calculate parameters associated with the empirically derived frequency distribution. Common parameters used for this purpose include the number of days where an element is above or below a specified level (e.g. the number of days with temperatures greater than 30°C), the values of various quantiles of an element (e.g. the 10th or 90th percentile), and the extreme high and low values of an element over a specified period." [85, p. 5]. The cited report also includes a detailed description of the construction of these *normals*.

A different method is proposed by the *German Meteorological Service* (Deutscher Wetterdienst, DWD). There, "...a strategy is implemented, which is also used to synthesize time series for specific regions [...]. Therefore, time series are segmented and these segments are recombined to new time series." [86, p. 15]. The manual includes as well a detailed description for the construction of these so-called *Test Reference Years*, TRYs, for simulation applications. This method is partly included in the weather generation software *Meteonorm* by *Meteotest*. It is wide spread for many applications and various scenarios. The data is generated by interpolation of available data from the six closest weather stations and with different models for radiation and temperature. The user can select the different models to generate a weather data set for a specific location. The uncertainty deviates between 2 and 10%, dependent on the distances to the six closest weather stations and their available weather data [87]. Further, the software offers the option to export to various file formats for other applications. The outside climate defines the external heat gains resp. losses from or to the environment. The method for the calculations of those energy exchanges are presented in Section 2.3.3.

Radiation gains \dot{Q}_{Irr}

Normally, the weather data is a set of climatic parameters for a specific location in an hourly resolution. This data includes the local time, for example as hour of the year, HoY and values for the air state. This are the outdoor dry and wet bulb temperature, $\vartheta_{ODA,dry}$ and $\vartheta_{ODA,wet}$, the air pressure p_{ODA} , the humidity, as relative φ or absolute x values, the windspeed w and direction FF . Further, all values for a radiation calculation must be included. Usually, this encompasses the total, direct and diffuse radiation Irr_{tot} , Irr_{dir} and Irr_{dif} on a horizontal surface and the direct normal irradiation DNI , also known as beam radiation. The direct radiation on a tilted surface is calculated with Equation 2.5. There, the angle of incidence θ is needed besides the DNI . It is important to calculate the angle of incidence θ of the incoming direct radiation for each individual surface, based on its orientation and tilt angle. The full calculation is presented in Equation 2.6. For the calculation, the declination angle δ , the observers latitude ϕ , the tilt angle β , the hour angle ω and the solar azimuth angle A_{ZS} , are needed.

$$Irr_{dir,tilt} = DNI \cdot \cos\theta \quad (2.5)$$

$$\begin{aligned} \cos\theta = & \sin\delta \sin\phi \cos\beta + \sin\delta \cos\phi \sin\beta \cos A_{ZS} \\ & + \cos\delta \cos\phi \cos\beta \cos\omega - \cos\delta \sin\phi \sin\beta \cos A_{ZS} \cos\omega \\ & - \cos\delta \sin\beta \sin A_{ZS} \sin\omega \end{aligned} \quad (2.6)$$

The direct radiation on a tilted surface $I_{dir,tilt}$ can only be calculated with the help of the incidence angle. Also, the diffuse radiation onto a surface must be calculated. Here, physical models to determine the indirect radiation from the sky have to be used. It is hard to calculate the diffuse radiation, as the "... direction of diffused radiation is highly variable and difficult to determine. It is function of condition of cloudiness and atmospheric clearness which are extremely unpredictable. [...] In general the diffuse fraction of radiation on inclined surface is composed of isotropic, circumsolar and horizon brightening factors" [88, p. 99]. Two methods to do this calculation is to use an *isotropic sky model* or an *anisotropic sky model*. Both methods can be applied through several possibilities. Three of each are compared by Shukla et al. (2015). The three isotropic sky models are the so called *Badescu*, BA, model, the *Liu and Jordan*, LI, model and the *Koronakis*, KO model. All include the direct radiation $Irr_{dir,tilt}$ on an inclined surface (see Equation 2.5). They all differ in the calculation of the diffuse radiation $I_{diff,hor}$ from an isotropic sky. They come to the conclusion that the model with the lowest mean bias error and root mean square error is the *Badescu*, BA, model. It is directly followed by the performance of the *Liu and Jordan*, LI, model and the *Koronakis*, KO model, which perform equally good. A different result was found by Mbah et al. (2018) where they describe that "... the *Liu and Jordan* model manifested significant superiority over the other models tested." [89, p. 5]. The main difference between those sources is the climatic context in which the reference measurements were undertaken. Shukla et al. compared their calculations with measurements in Bhopal, India while Mbah et al. undertook their measurements in Nsukka, Nigeria. A third study in Dar El Beida, Algeria, by Mesri et. al (2015), came to the result that "... all the methods presented in this study are able to predict global radiation within little limits for the chosen station." [90, p. 481].

Equation 2.7 presents the overall calculation for the radiation gains onto a surface. It is based on the *Liu and Jordan* model. In his handbook for planning of solar thermal systems, Charčenko (1995) suggested, to use the *Liu and Jordan* model for solar applications [91]. Hence, this model will be used, due to its generalized approach and normative character of the book. This radiation is transmitted through transparent surfaces into a room. The resulting radiation into a room is dependent on the transmissivity of these surfaces. this g value is multiplied with the total incoming radiation on a surface to calculate \dot{Q}_{Irr} . The calculation is presented in Equation 2.8.

$$Irr_{tot,tilt} = Irr_{dir,tilt} + Irr_{tot,hor} \cdot \rho \cdot \frac{(1 - \cos\beta)}{2} + I_{diff,hor} \cdot \frac{(1 + \cos\beta)}{2} \quad (2.7)$$

$$\dot{Q}_{Irr} = Irr_{tot,tilt} \cdot g \quad (2.8)$$

Transmission gains \dot{Q}_{trans}

The heat transfer through surfaces under stationary conditions is described in Equation 2.9. For the calculation, the Area A , the temperature difference between in- and outdoor air $\vartheta_{ext} - \theta_{int}$, and the so-called u value is needed. Its calculation is presented in Equation 2.10. It is based on the heat conduction inside a construction element, which is made out of n material layers with a certain thickness thk_i and conductivity λ_i . This calculation method is standardized, for example in *DIN 4108* [92]. This heat transfer happens also through the transparent surfaces of a building.

2. Methodology

$$\dot{Q}_{trans} = u \cdot A \cdot (\vartheta_{ext} - \vartheta_{int}) \quad (2.9)$$

$$u = \frac{1}{R_{int}} + \sum_{i=1}^n \frac{\lambda_i}{thk_i} + \frac{1}{R_{ext}} \quad (2.10)$$

Further, the heat capacity c_i and density ρ_i of each layer have to be accounted to consider the heat storage and releasing effects in a transient simulation. This is presented within the Subsection 2.3.4. In total, the daily variation of the outside temperature condition is shifted and reduced through this effect of the building construction.

Ventilation gains \dot{Q}_{vent}

These are the gains through air exchange with and infiltration from the environment. The energy flow \dot{Q}_{vent} can be calculated with Equation 2.11. \dot{m} is the mass flow rate into the room. This can be caused by natural or forced ventilation, as well as through infiltration through air gaps. It is multiplied by the enthalpy difference of the inner and outer air $h_{ext} - h_{int}$ is needed.

$$\dot{H}_{vent} = \dot{m} \cdot (h_{ext} - h_{int}) \quad (2.11)$$

Modeling of internal gains \dot{Q}_{int}

The second main influencing factor for the building energy demand is the hosted user and their behavior inside a room. This includes the set temperatures, their own heat emissions through their metabolism \dot{Q}_{pers} and use of heat emitting sources like lighting \dot{Q}_{bulbs} , electric devices, stoves and ovens \dot{Q}_{mach} , heat transfer from/to neighboring rooms \dot{Q}_{room} , material throughput \dot{Q}_{mat} or other heat sources \dot{Q}_{misc} . The calculation was presented in Equation 2.4 on page 28. All these sources are not always present but follow a daily, weekly and annual schedule. Naturally, these user profiles are highly probabilistic. They can vary tremendously between socio-cultural different groups and regions and even drastically between single individuals of the same apartment. In many regions, detailed energy surveys and user behavior studies have been undertaken to evaluate the boundaries of thermal comfort [93] and the impact of individual boundaries, like gender or clothing [94].

Statistical models for the user behavior and their demands, the use of internal heat sources, and the energy load calculations have been created for the North American and European Region in various standards like the *ASHRAE Standard 55* or the *VDI 2078* [95][62]. Some studies can be found which analyze these boundaries for countries of the MENA region. For example, S. Attia et al. (2012) compiled these usage conditions for typical Egyptian residential applications. All these methods cumulate in specific user profiles for different types of applications and tables with specific heat emissions. The *DIN V 18599 - Part 10* includes 41 profiles for user presence and device usage in various residential, commercial or industrial applications. Further, heat emissions of internal sources can be assumed according to the floor space of a certain use case or in detail by heat emissions of each individual source, like lighting or IT infrastructure. Also, these sources have an impact on the energy load calculation according to a specific determined usage profile [84]. Yan et al. (2015) "... provided a comprehensive overview of the state-of-the-art and future research and industry needs with regards to occupant-related data collection and monitoring, modeling approaches, model evaluation, and finally model implementation into simulation tools" [96, p. 276]. They conclude that the current problem is the uncertainties in the user behavior. The results of a simulation can vary exceptionally from real observed/measured demands. Therefore, Junghans et al. suggest a method to identify "... the influence of the input variable of the occupant behavior on the robustness of the optimization process" [97, p. 486]. This enables

the conductor of a building energy model to find parameters which are critical on the energy demand calculation and rate their input with the needed care.

Newest studies investigate on predictive control strategies, where an algorithm learns about the specific user behavior in a certain context and optimizes the building supply systems according to a predictive user behavior [98].

2.3.4. HVAC component models

The following subsection describes the modeling methodology for the thermal system components. At first, this is the air cooling unit itself. Its main purpose is to cool an air flow and a connected air volume. Second is a water cooling system, which is the same kind of machine but cooling a secondary water loop instead of an air volume. Third, the thermal storage models are presented. This includes the cold water storage and building mass.

Air cooling unit

The main component inside an air cooling unit is the heat pump. The underlying thermodynamic principles are concluded in many standards, such as contained in the handbook *ASHRAE HVAC Systems and Equipment* [100]. The air cooling unit uses electricity to foster a thermodynamic cycle. Therefore, an electric compressor moves and pressurizes a coolant with mechanical work $\dot{W}_{compressor}$. The coolant rejects heat $\dot{Q}_{condenser}$ to the environment by condensing inside a condenser. This rejected heat $\dot{Q}_{condenser}$ is the sum of the previously absorbed heat $\dot{Q}_{evaporator}$ and the mechanical work $\dot{W}_{compressor}$ as shown in Equation 2.12. The absorbed thermal energy $\dot{Q}_{evaporator}$ is gained after an expansion and evaporation process inside an evaporator. This absorbed heat is, from an outer perspective, the effective cooling capacity $\dot{Q}_{cooling}$ (see Equation 2.13).

$$\dot{Q}_{condenser} = \dot{Q}_{evaporator} + \dot{W}_{compressor} \quad (2.12)$$

$$\dot{Q}_{evaporator} \equiv \dot{Q}_{cooling} \quad (2.13)$$

The amount of electricity for the compression process $P_{electric}$ is determined by the efficiency of the compressor and the motor $\eta_{electric}$ (see Equation 2.14). The ratio of the cooling capacity $\dot{Q}_{cooling}$ and the input power $P_{electric}$ is one of the key performance indicators of an air conditioner and is called Coefficient of Performance (COP_{AC}) as illustrated in Equation 2.15.

$$\dot{W}_{compressor} = P_{electric} \cdot \eta_{electric} \quad (2.14)$$

$$COP_{AC} = \frac{\dot{Q}_{cooling}}{P_{electric}} \equiv \frac{\dot{Q}_{evaporator}}{P_{electric}} \quad (2.15)$$

The COP_{AC} of an air conditioner is normally given by the manufacturer through its data sheet. Those given $COPs$ are determined under specific, so called nominal, boundary conditions $COP_{nominal}$. The following diagram in Figure 2.9 on page 35, shows this cooling cycle with the nominal conditions of an exemplary market available packaged air conditioning system with *R-22* as working fluid. Chlordifluoromethane (*R-22*) replaced the highly ozone depleting refrigerants *R-11* and *R-12* due to its much lower ozone depleting potential *ODP*. Today, even its lower global warming potential *GWP* is considered too high. Nowadays, more and more refrigeration systems use much less harmful refrigerants such as the so called natural refrigerants *Carbon dioxide (R-744)* itself or *Propane (R-290)*. These refrigerants have a much lower *GWP* and, most important, no *ODP*. However, many air conditioners remain to be operated with *R-22*. It is commonly used in many countries of the MENA region [99].

The temperature ϑ is indicated in $^{\circ}C$ on the y-axis while the x-axis shows the specific entropy s in $J/(kgK)$. Further, isobaric lines are highlighted in red on the top x-axis. The isenthalps are drawn

2. Methodology

in blue and indicated on the lower x-axis. Additionally, lines of constant specific volume are given in green. For better readability, the x-axis is cut out for the intervals from $\vartheta = -40^\circ\text{C}$ to $\vartheta = 0^\circ\text{C}$ and from $\vartheta = 100^\circ\text{C}$ to $\vartheta = 200^\circ\text{C}$.

Four temperatures are highlighted by horizontal lines. These are the nominal condenser and evaporator temperatures as well as their corresponding exterior and interior air temperatures. This example of a refrigeration cycle commences with the polytropic compression of the refrigerant from point 1 to point 2. The compressor adds mechanical work $\dot{W}_{compressor}$ to the process to increase the refrigerants pressure. Dependent on its efficiency $\eta_{electric}$, the needed electrical power input $P_{electric}$ can be determined (see Equation 2.14). For comparative reasons, the reversible isentropic compression is shown from point 1 to point 2' (dashed grey arrow).

The process continues inside the condenser from point 2 to point 3 at a constant pressure. There, the refrigerant is cooled down by a fan that ventilates environmental air at a temperature of $\vartheta_{exterior} = 30^\circ\text{C}$ until the temperature of the refrigerant drops to the condensation point where it condenses. Here, it is the nominal condensation temperature $\vartheta_{condenser,nominal} = 35^\circ\text{C}$ of *R-22* of the given exemplary split-unit. Further, it is slightly subcooled before it enters the expansion valve in point 3. In this process (from point 2 to 3), the heat stream $\dot{Q}_{condenser}$ is rejected to the environment. After the expansion valve, the refrigerant is relaxed isenthalpically from point 3 to 4. Following, its entropy S increases further and the refrigerant continues to evaporate until it is again fully gaseous in point 1'. The temperature is increased further before it enters the compressor in point 1. In this process (from point 4 to 1), the heat stream $\dot{Q}_{evaporator}$ is extracted from the room air.

The *COP* of any such thermodynamic process is dependent on the upper and lower temperature at which the condensation and the evaporation happen. In an ideal cooling cycle this efficiency is called Carnot efficiency COP_{Carnot} . In terms of cooling it is described in the following equation. The *COP* gets bigger, when the temperature difference between evaporator and condenser gets smaller and/or the heat source temperature increases. The shown example process from Figure 2.9 has a maximum Coefficient of Performance of $COP_{Carnot} = 9.3$.

$$COP_{cooling,Carnot} = \frac{T_{evaporator}}{(T_{condenser} - T_{evaporator})} \quad (2.16)$$

In any real thermodynamic cycle, different losses occur and this theoretical maximum is never achieved. These losses vary with the type of components, working fluids and boundary conditions which are used to drive the refrigeration cycle.

Manufactures of refrigeration machines state the efficiency of their systems with a nominal coefficient of performance $COP_{nominal}$ which is given at standardized boundary conditions. The previously described exemplary split-unit cooling system has a $COP_{nominal} = 2.5$. It has a nominal cooling capacity of $\dot{Q}_{cooling,nominal} = 3000\text{W}$ at a rated input power of $P_{electric,nominal} = 1200\text{W}$. This power demand includes auxiliary power $P_{auxiliary,nominal}$ for the interior and exterior fans and the control system.

$$COP_{nominal} = \frac{\dot{Q}_{cooling,nominal}}{P_{electric,nominal}} \quad (2.17)$$

Here, it is assumed that the ratio of the actual $COP_{current}$ to the Carnot efficiency at current heat source and sink temperatures $COP_{Carnot,current}$ is the same, as the ratio between the efficiency at nominal conditions $COP_{nominal}$ to the Carnot efficiency at the nominal conditions $COP_{Carnot,nominal}$ and its respective source and sink temperatures. This way to model the performance of a compression chiller is part of a well evaluated building system simulation library [26].

$$\frac{COP_{current}}{COP_{Carnot,current}} = \frac{COP_{nominal}}{COP_{Carnot,nominal}} = const. \quad (2.18)$$

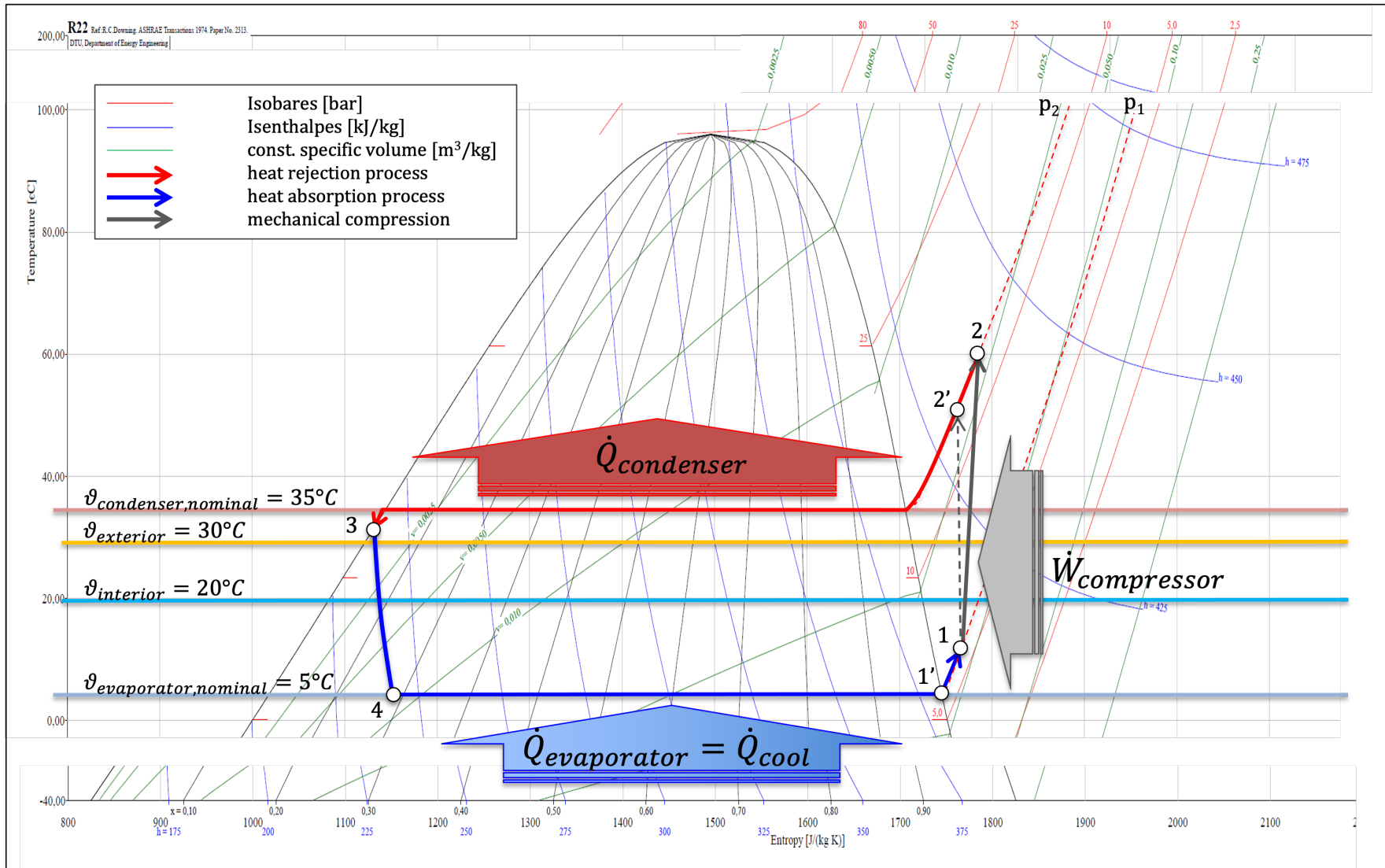


Figure 2.9.: Example process of an R22 compression chiller in the T-S-Diagram, modified from [15] with chiller data from [16]. Cut out x-axis intervals from $\vartheta = -40^{\circ}C$ to $\vartheta = 0^{\circ}C$ and from $\vartheta = 100^{\circ}C$ to $\vartheta = 200^{\circ}C$.

2. Methodology

The previous equation is rearranged to calculate the current $COP_{current}$. It is the Carnot efficiency at the current heat source and sink temperature $COP_{Carnot,current}$ scaled with the ratio of the manufacturers $COP_{nominal}$ to Carnot efficiency at those nominal boundary conditions $COP_{Carnot,nominal}$

$$COP_{current} = \frac{COP_{nominal}}{COP_{Carnot,nominal}} \cdot COP_{Carnot,current} \quad (2.19)$$

In conclusion, the system receives heat at the evaporator $\dot{Q}_{evaporator}$ and mechanical work from the compressor $\dot{W}_{compressor}$ and rejects it at the condenser $\dot{Q}_{condenser}$. The motor efficiency $\eta_{electric}$ adds to the electric power demand $P_{electric}$ of the entire air cooling unit. This demand varies depending on the part load behavior, resp. the efficiency of the motor at various load states. For the motor of a heat pump it can be simplified with a specific polynomial equation as it is often done for variable frequencies drives. Here, this modeling is not described further, as most of the analyzed packaged unitary air conditioning systems operate with a simple hysteresis control where the motor of the heat pump is operated always under full load. This control regime will be presented in more detail in Section 3.4 on page 51. Finally, the current electric power demand $P_{electric,current}$ can be calculated by combining Equation 2.15 and 2.19 to Equation 2.20.

$$P_{electric,current} = \frac{\dot{Q}_{cooling,current}}{COP_{current}} \quad (2.20)$$

The simulation library *BuildingSystems* allows to model various compression chillers with this approach. The model will calculate the system according to the performance under nominal conditions and extrapolate to other boundary conditions as described before. The library contains examples for small scale systems up to $\dot{Q}_{cool} = 3kW$. Further, the data for specific large scale compressors up to $\dot{Q}_{cool} = 635kW$ is included.

Water cooling system

A water chilling system operates with a secondary cooling loop which transports the heat from the room to the chiller by a water pipe network. In most systems, the "coldness" is supplied in exactly the same way as in the previously described working principle of a split-unit A/C system. A compressor densifies the refrigerant which is liquified inside the air cooled compressor. Thereby, the heat is rejected to the environment. From there, the refrigerant is relaxed and vaporizes inside the evaporator. Instead of the blower, which recirculates the room air over the evaporator in the split-unit A/C system, a water loop is connected by a heat exchanger to the evaporator. The working diagram is presented in the scheme in Figure 2.10. These systems are most common for air cooling applications beyond a cooling capacity of 10 kW as multiple consumers can be connected through a wide spread piping network. Even various subsystems, like cooling coils or cooling ceilings can be supplied.

The large air cooled condensers are seen around the world on rooftops or in detached areas besides a building with high cooling demands. The primary cooling loop in the chiller cools the connected secondary cold water network until the return flow falls below a certain level, e.g. 12°C. Afterwards, a water pump circulates the chilled water until the return flow exceeds a certain temperature, e.g. 14°C. The connected pipework can have enough capacity to work as sufficient storage for longer operation times of the primary cooling loop. Otherwise, a buffer tank is needed. The focus of this thesis are smaller cooling systems which supply only some rooms or a single apartment. The presence of a cold water storage can be beneficial, as a means of storage for peak load shifting.

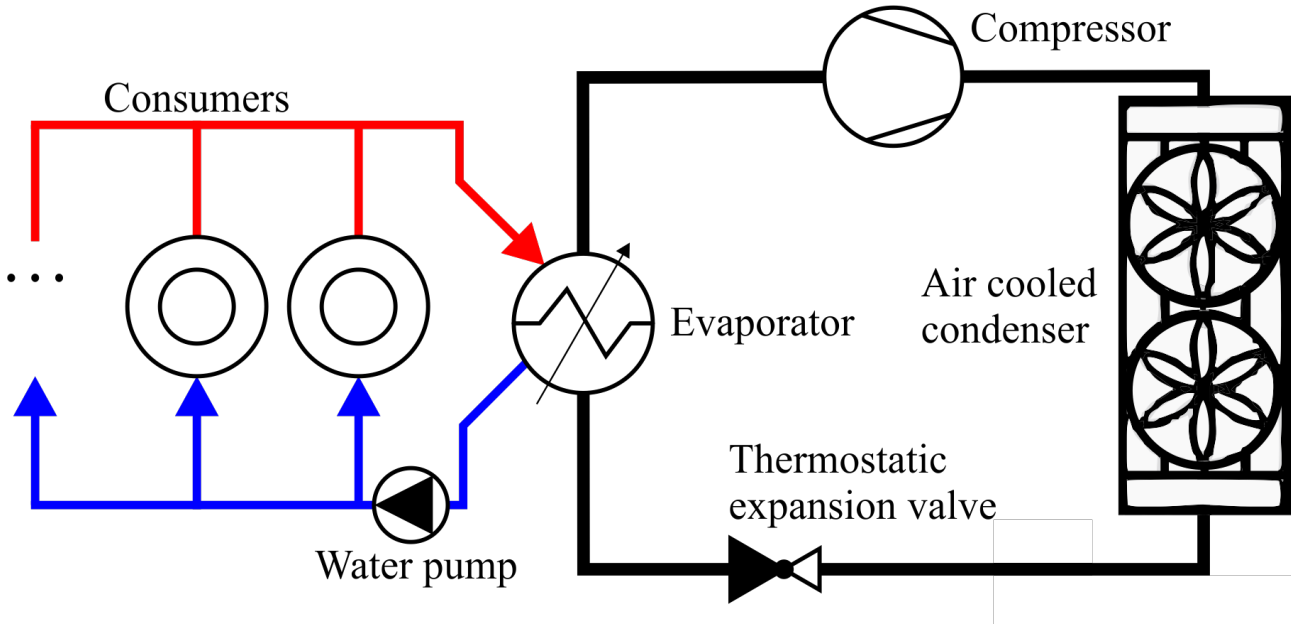


Figure 2.10.: Working scheme of an air cooled compression chiller which is supplying a connected cold water loop, based on [17, p. 6].

Thermal storage

The next two paragraphs describe two ways to store sensible heat. First the storage in solid building bodies, like walls or floors is described. Second, the storage in a liquid, like a water storage tank of any supply system, is described.

Sensible heat storage in building masses

A thermal mass, like a multi layer construction element of a building, can store thermal energy Q_{mass} . According to the research by C.A. Balaras (1996) a "... 5-10 cm wall thickness is usable for heat absorption, storage and release on a daily basis" [101, p. 3]. The amount of each layer i within this usable layer is dependent on the heat capacity $c_{p,i}$, the mass m_i and its temperature difference towards an environment $\vartheta_{ext} - \vartheta_{int}$. It can be calculated according to the following equation.

$$Q_{mass} = \sum_{i=1}^n m_i \cdot c_{p,i} \cdot (\vartheta_{ext} - \vartheta_{int}) \quad (2.21)$$

The temperature of each layer is dependent on the heat transport through the total construction element as it is described in Equation 2.9 on page 32. There are two heat transport effects. The first is the convection \dot{Q}_{conv} and its calculation is presented in Equation 2.22. The convective heat transport coefficient α can be increased through forced air movements along a surface with the area A . The second heat transport effect is the radiation between two room surfaces \dot{Q}_{rad} and is presented in Equation 2.23. The radiation exchange is dependent on multiple factors which are concluded in c_{12} and their areas A . The calculation of the view factor itself is dependent on the shape of the surfaces and the orientation between them. Further, the emissivity ε of both surfaces is needed for the calculation. These terms are multiplied with the *Stefan-Boltzmann* constant σ and the absolute temperature difference to the power of four.

2. Methodology

$$\dot{Q}_{conv} = \alpha \cdot A \cdot c_p \cdot i \cdot (\vartheta_{env} - \vartheta_i) \quad (2.22)$$

$$\dot{Q}_{rad} = c_{12} \cdot A \cdot \sigma \cdot (T_1^4 - T_2^4) \quad (2.23)$$

Cold water storage

The same equations as in the previous paragraph are valid for thermal energy storage in a water tank. The total sensible stored heat in a water tank Q_{sens} is dependent on the temperature difference of the environment to the average temperature of the total water mass $\vartheta_{env} - \vartheta_{store}$. A water storage of a certain height can be discretized into multiple layers with different temperatures to account for the thermal stratification inside such a tank. Coninck et al. (2013) developed a buoyancy model to discretize a water tank into n_{ele} different layers and calculate a resulting heat flow \dot{Q}_{flow} between each layer. This calculation is presented in Equation 2.24. The energy exchange is realized through the temperature difference between the layers ΔT , an exponent $exp_n Ele$, and the G value. It is empirically determined and has a different appearance for more than 10 layers. It is calculated with Equation 2.25.

$$\dot{Q}_{flow} = G \cdot \Delta T \cdot n_{ele}^{exp_n Ele} \quad (2.24)$$

$$G = \text{if } n_{ele} < 10 \text{ then } 0.8 \cdot n_{ele} + 16 \text{ else } 26 - 0.2571 \cdot n_{ele} \quad (2.25)$$

The "coldness", which is produced by any kind of chiller could be stored inside a thermal buffer tank instead of being directly supplied to a connected consumer. The system setup is shown in Figure 2.6 on page 26 and the working principle of a water cooling system is described in the previous Section 2.3.4. Therefore, another cooling loop needs to be connected. The principle is shown in the diagram in the following Figure 2.11. The primary water pump is operated until the entire cold water storage is cooled to a certain lower temperature limit. The connected primary cooling loop, which produces the "coldness", is operated during this period as well. The secondary water pump supplies the connected cold water network and its consumers. Thereby, the chilled water will be heated and the temperature of the cold water storage increased.

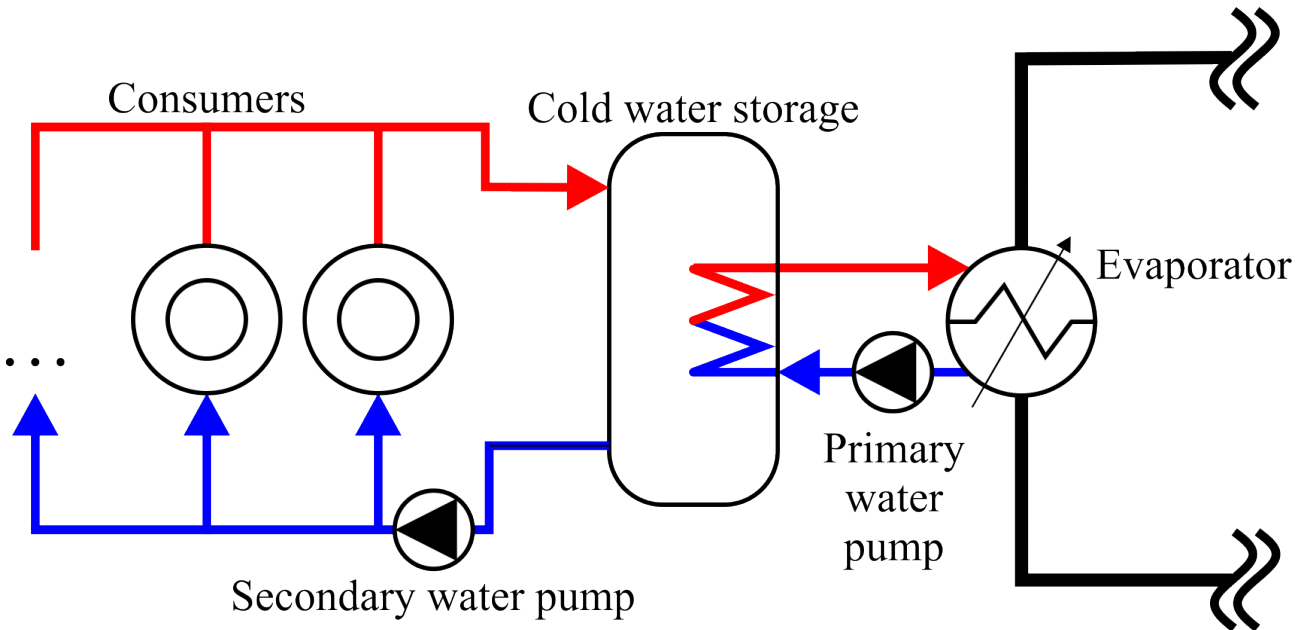


Figure 2.11.: Implementation of cold water network with a water storage tank as buffer.

The cooling capacity of the system can be extended by adding parallel connected chillers, consisting of the evaporator and air cooled condenser. Specific higher water inlet temperatures of different consumers could be realized with return flow mixing.

2.3.5. Electrical models

This section describes the electricity generation, transformation, storage and transportation models. This is the photovoltaic system, which generates direct current based on an incoming radiation, the battery storage system, which can chemically store direct current, the electricity transformation, which is needed to convert direct current, DC, to alternating current, AC, and last but not least the component to exchange AC electricity with a connected grid.

Photovoltaic system

The electric output of a photovoltaic system is dependent on the amount of incoming total solar radiation on its solar cells, how these cells are connected and which type of cell material is used. *Energy Informative* (2012) compares all used common solar cell technologies in terms of efficiency, pricing and durability. They conclude that more than 90% of the installed photovoltaic systems are crystalline silicon systems. Monocrystalline cells have the highest efficiency but are more expensive than polycrystalline cells. Thin film cells have an even lower efficiency at an increased price, but are flexible and light weighted. Further, they are much more resistant to high temperatures which makes them more attractive for hot and arid climate regions. Different applications demand different specifications and determine the best used photovoltaic technology [102]. The predicted output of PV systems can be assessed by computer simulations. The required parameters are gained through general properties of different technologies, manufacturers data sheets and standardized measurement trials. For example, a measured I-V curve of a solar panel can be used with a simplified I-V curve model [18]. More complex are the diode models of single solar cells. They can be modeled with one, two or three diodes with increasing complexity as the effort for parametrization and computation increases [103, p. 7]. All modeling approaches are shown in the following schemes in Figure 2.12.

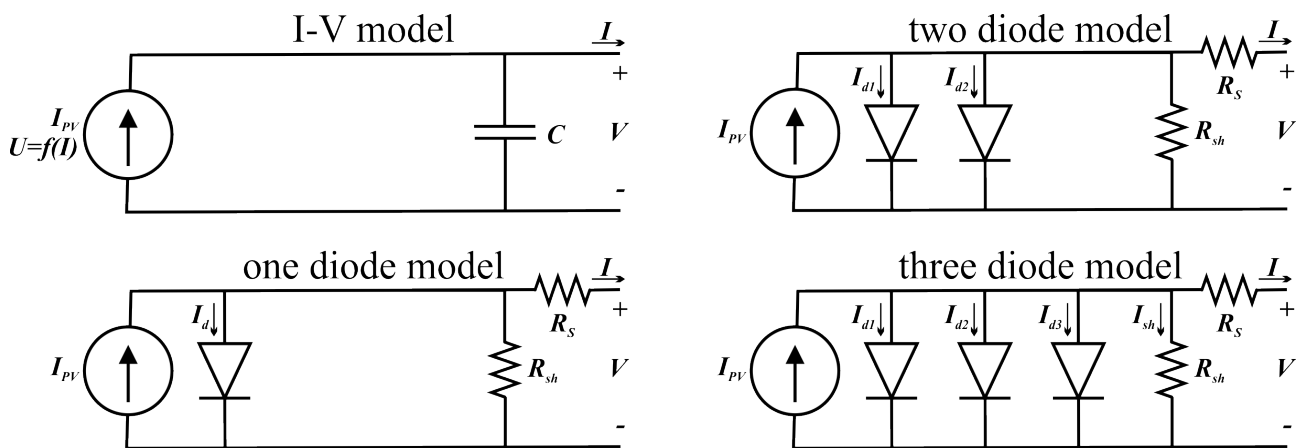


Figure 2.12.: I-V curve model for PV modules [18, p. 74], one and two diode cell model [19, p. 211] and three diode cell model [20, p. 107] for the modeling of photovoltaic systems.

All models calculate a current I_{pv} which is generated by a single photovoltaic cell under the incidence of light and with a resulting voltage V . The maximum flowing current is the short circuit current I_{sc} . It is scaled to the current power output of the module I_{pv} by scaling it from the short circuit current at standard test conditions STC. Therefore, I_{sc} is multiplied by the fraction of the incoming radiation

2. Methodology

G over the radiation at standard test condition $G_{STC} = 1000 \text{ W}$. It is reduced or increased by the temperature difference between the environmental temperature T and the temperature at standard test conditions $T_{STC} = 298.15 \text{ K}$ times a temperature coefficient k_0 . It can be calculated with the following Equation 2.26.

$$I_{pv} = I_{sc} \left(\frac{\dot{G}}{\dot{G}_{STC}} \right) - k_0(T - T_{STC}) \quad (2.26)$$

The cells are connected in series and in parallel to create a full PV module. The I-V model can be used to model an entire module at once by integrating a previously known I-V curve of any module. Thereby, all resistances and diode characteristics are directly added. The capacitor with the capacity C was included "... to improve model dynamics and substitute PN junction capacities" [18, p. 74]. This model is fast and easy to setup but not useful for simulations with changing illuminances as concluded by Bisenieks et al. (2008). The precision can be increased by including a diode to model each cell. Part of the generated current I_{PV} will flow through the diffusion and the recombination area of a silicon based solar cell and thereby produces a current I_d through the diode. Further, the resulting current I is reduced by two resistances: the series resistance R_S and the shunt resistance R_{Sh} . The latter will cause a current flow I_{Sh} inside the cell. This model is very accurate under varying illuminances and at the temperature which was used to parametrize the model. The error in the overall power calculation of a PV module can result into more than 2% when the surrounding temperature is varied. The diode current I_d can be split into its sub-components of the current through the diffusion area I_{d1} and through the recombination area I_{d2} . This will reduce the maximum error in the power calculation to around 1% [19, p. 213]. However, the accuracy decreases drastically in large scale PV modules as in industrial applications. Therefore, Khanna et al. (2015) suggested a three diode model. The currents through the diffusion and recombination area is combined again but the area itself is separated into three different areas. The first current I_{d1} is resulting as flow through the quasi neutral region (QNR), the second current I_{d2} is flowing through the space charge region (SCR) and the third current I_{d3} through defect regions and grain sites [20, p. 107]. This model can decrease the error of the calculated power by up to 10%, compared to the two diode model. However, the parametrization effort is enormous as the I-V curve for the modules have to be measured under varying conditions and a parameter fitting undertaken. The two diode model offers a sufficient accuracy and most parameters for setting up a simulation can be found in common data bases. Especially in building supply calculations the two diode model is commonly used. This was as well suggested in the thesis by P. Balekai [103]. The Equation 2.27 is used to calculate the resulting current I of a photovoltaic cell which is modeled with the two diode model.

$$I = I_{pv} - I_{d1} - I_{d2} - I_{Sh} \quad (2.27)$$

The resulting current I is the light induced photocurrent I_{pv} minus all internal current flows I_{d1} , I_{d2} and the shunt current I_{Sh} . The second and third term, I_{d1} and I_{d2} are the currents through the diodes and are calculated with equations 2.28 and 2.29. I_0 is the reverse saturation current at the first or second diode and is multiplied by the exponential fraction of the electron charge q , the open circuit voltage V , the series resistance R_s , the current I over the ideality factor of the diodes n_1 resp. n_2 times the Boltzmann constant k and the environmental temperature T .

Last but not least, the shunt current I_{Sh} is calculated with Equation 2.30 and the previously described

factors.

$$I_{d1} = I_{01} \left\{ \exp \left[\frac{q(V + IR_s)}{n_1 kT} \right] - 1 \right\} \quad (2.28)$$

$$I_{d2} = I_{02} \left\{ \exp \left[\frac{q(V + IR_s)}{n_2 kT} \right] - 1 \right\} \quad (2.29)$$

$$I_{Sh} = \frac{V + IR_s}{R_{Sh}} \quad (2.30)$$

The parameters which need to be defined or acquired for a successful simulation are k_0 , I_{01} , I_{02} , n_1 , n_2 , R_S and R_{Sh} . Those factors need to be calculated by square fitting a measured or given I-V curve.

Electrical battery storage system

The following paragraphs discuss first the selection process which led to the application of the *Kinetic Battery Model* in this thesis. The model and its extension during this research is described afterwards. This part of this research was already published under the title *Simplifying the Parametrization of the Extended Kinetic Battery Model to Calculate Voltage, Current, and a Variable Load Dependent Capacity* in the *Proceedings of IBPSA BuildingSimulation 2019*[104].

Battery modeling

In 2008, Jongerden et al. compared the performance and applicability of various battery models in their paper. There, they analyzed the performance of the chemical simulation software *Dualfoil* and compared it with the *Electrical Circuit* model, the model by *Peukert*, the model by *Rakhmatov*, the *Kinetic Battery* model, the model by *Chiasserini*, and the *Stochastic Kinetic Battery* model. Due to its accuracy, they classify the *Dualfoil* software as the reference model to check the performance of other models. The accuracy of the implemented model in the *Dualfoil* software comes with high computational efforts. Further, it is said about the *Kinetic Battery Model*, aka *KiBaM*, that it "... describes the battery in a more intuitive manner. The differential equations give a clear insight on how the battery behavior is modeled. This makes the *KiBaM* preferable over the model by *Rakhmatov*. [...] However, the *KiBaM* is designed to model a lead-acid battery, which is not used in wireless devices and has a more linear discharge behavior than the modern batteries" [105, p. 14f]. The use case of this paper is building energy supply simulations for air conditioning. Within these cases, lead acid batteries are widely used. They are used especially in large scale application because of their low production costs and wide availability. However, the *KiBaM* can be parameterized to work with Li-ion batteries as well [106]. The extension of the *KiBaM* can compute the terminal voltage [107, p. 285, equation 11]. In addition, this research offers the possibility to determine a variable overall battery energy capacity which is dependent on a varying applied load.

The Kinetic Battery Model

The battery model, which is developed in this thesis, is based on the Kinetic Battery Model (KiBaM). This was introduced by Manwell et al. in 1993. It describes an electro-chemical battery with two energy wells. One pretends to hold the so-called available energy, the other the so-called bound energy. It is capable to calculate a variable battery capacity which is caused by a varying load I_{load} . The state of charge (*SOC*) and the voltage can be calculated with the first extension of the model ([107]).

The scheme in Figure 2.13 shows the model, which is based on the original KiBaM. E_{ava} is the available energy and E_{bou} is the bound energy. Both are separated by a conjunction with a fixed constriction k . The factor c is the ratio between E_{ava} and E_{bou} . Simulation software, like *Polysun* offer tables with values of k and c . Unfortunately, these values are equal for a broad range of included batteries ([108])

2. Methodology

which indicates that they were not determined for each different battery. The current overall stored energy inside a battery E_{bat} is the sum of available and bound energy.

$$E_{bat} = E_{Ava} + E_{Bou} \quad (2.31)$$

The available and bound energy can be calculated with the height h and the width c of each well.

$$E_{ava} = h_1 \cdot c \quad (2.32)$$

$$E_{bou} = h_2 \cdot (1 - c) \quad (2.33)$$

E_{nom} is the nominal rated capacity at a $0.05C$ discharge rate. This is the battery's capacity C_{20} when it is discharged over a time of 20 hours. The batteries capacity can increase beyond its rated capacity if it is discharged at small currents of I_{load} . Many data sheets contain the C_{100} capacity at a discharge rate $0.0025C$, meaning a full discharge over 100 hours. This can be assumed to be the maximum battery capacity E_{max} . In contrast, the classic KiBaM by Manwell et al. suggests to use the nominal capacity E_{nom} as the maximum capacity E_{max} .

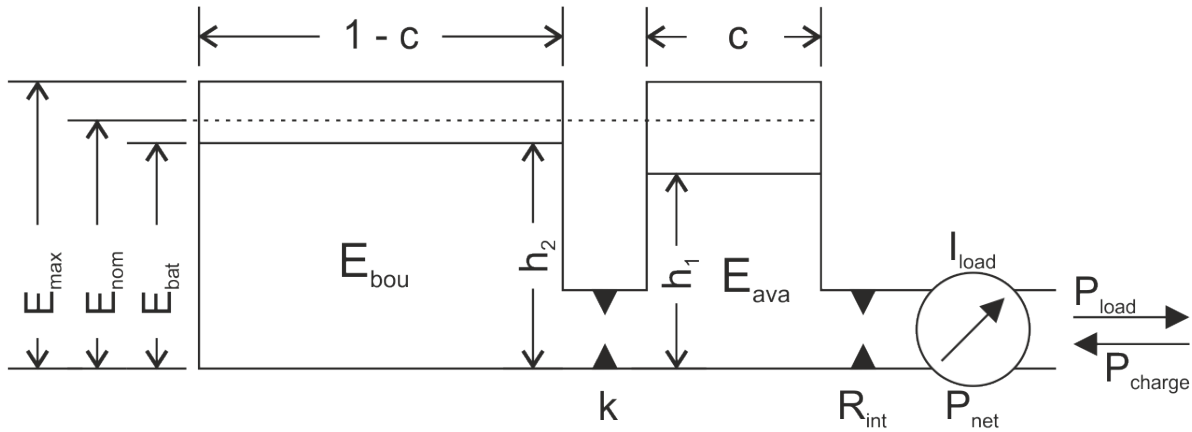


Figure 2.13.: *Applied kinetic battery model, based on Manwell (1993) [21, p. 400].*

The main difference of the original *KiBaM* by Manwell et al. (1993) to the implemented model is a power based approach of the model in this research. The original KiBaM takes the discharging current $I_{discharge}$ as a boundary condition. In contrast, this research is oriented towards the connected power. P_{net} is the resulting power, which is applied to the battery as a result of all charging and discharging loads. It is calculated by Equation 2.34. A positive P_{net} is charging the battery and a negative discharging it. The battery is discharged, if a load greater than a simultaneously applied charging power is applied to the battery.

$$P_{net} = P_{charge} - P_{load} \quad (2.34)$$

Furthermore, the charging process is modeled in accordance with [106, p. 36]. It limits the charging power at a state of charges close to $SOC = 1$. The actual state of charge SOC is defined by the following equation.

$$SOC = \frac{E_{bat}}{E_{nom}} \quad (2.35)$$

Charging and discharging loads are only applied to the available energy E_{ava} . The change of stored available energy is calculated with Equation 2.36. The equalization with the bound energy E_{bou} happens through the constriction k and can be calculated by Equation 2.37. Normally, the variable

capacity is modeled through the available energy E_{ava} : once it is empty, the battery is empty. However, this implies an accurate knowledge of k and c , which is not given in current available data sets. Previous simulation trials showed that the given parameters resulted in wrong battery capacities. Hence, these factors need to be determined by discharging trials and at least for each battery system. Alternatively, this paper suggest a variable capacity, which is applied through an additional capacity factor CF to the discharging load.

$$\begin{aligned} \frac{dE_{ava}}{dt} &= P_{charge,eff} - CF \cdot P_{load,ava} \\ &\quad + k \cdot (h_2 - h_1) \end{aligned} \quad (2.36)$$

$$\frac{dE_{bou}}{dt} = -k \cdot (h_2 - h_1) - CF \cdot P_{load,bou} \quad (2.37)$$

Battery charging

$P_{charge,eff}$ is the effectively resulting charging load. It is always positive and is calculated by the resulting load P_{net} and the charge efficiency η_{charge} of a battery. It is limited by a maximum charge rate factor a_{mcr} . This factor limits the charging rate at $SOCs$ near E_{nom} . Furthermore, it is limited by the maximum charging power of a battery $P_{charge,max}$

$$\lim_{P \rightarrow P_{charge,max}} f(P_{charge,eff}) = P_{net} \cdot \eta_{charge} \quad (2.38)$$

$$P_{charge,max} = a_{mcr} \cdot (E_{nom} - E_{bat}) \quad (2.39)$$

Battery discharging

CF is a discharging factor, which represents the battery's capacity at an applied discharge rate. It is based on the nominal capacity E_{nom} and the current total capacity E_{cur} . It is applied to the resulting loads $P_{load,ava}$ and $P_{load,bou}$. It is defined by the following equation.

$$CF = \frac{E_{nom}}{E_{cur}} \quad (2.40)$$

The current total capacity E_{cur} is calculated with Equation 2.41. There, the nominal discharge duration $t_{load,nom}$, 20 hours, the corresponding nominal load E_{nom} , the actual applied load $P_{load,eff}$ and the *Peukert* coefficient p are needed. This coefficient was developed by [109]. It describes the connection between two discharging curves of a battery and the varying overall battery capacity at various connected discharging loads and is valid between discharging rates $0.0025C < P_{load,eff} < 0.5C$. It can be calculated with Equation 2.42. Here, the nominal discharge time $t_{load,nom}$ and charge quantity $Charge_{nom}$ are required. Besides, a second discharging time t_2 and its corresponding charge quantity $Charge_2$ are needed. These data can be gained by measured discharging curves and are usually provided in data sheets as well.

$$E_{cur} = \left(\frac{Charge_{nom}}{t_{load,nom} \cdot P_{load,eff} / U_{cur}} \right)^p \cdot U_{cur} \cdot t_{load,nom} \cdot P_{load,eff} \quad (2.41)$$

$$p = \frac{\log\left(\frac{t_2}{t_{load,nom}}\right)}{\log\left(\frac{Charge_{nom}}{t_{load,nom}}\right) - \log\left(\frac{Charge_2}{t_2}\right)} \quad (2.42)$$

The sum of the loads $P_{load,ava}$ and $P_{load,bou}$ is the effective discharging load $P_{load,eff}$ (see Equation 2.43). The load on the available energy $P_{load,ava}$ is the resulting load P_{net} divided by the battery's

2. Methodology

discharging efficiency η_{load} . It is calculated by Equation 2.44 and becomes zero as soon, as the available Energy E_{ava} becomes zero. The resulting load on the bound energy $P_{load,bou}$ is the resulting difference between P_{net} and $P_{load,ava}$. Furthermore, standby losses due to self discharge are applied in this term. The discharging factor f_{dis} , gained by manufacturer data sheets, is multiplied with the current energy content of the battery E_{bat} .

The maximum discharging power $P_{load,max}$ is determined by each battery manufacturer and stated in data sheets as well. It limits each load. No load above this limit can be applied without damaging the battery immediately. Exceeding the maximum applied load must be prevented, as this damaging process is not part of the *Kinetic Battery Model*.

$$\lim_{P_{load} \rightarrow P_{max}} f(P_{load,eff}) = P_{load,ava} + P_{load,bou} \quad (2.43)$$

$$\lim_{E_{ava} \rightarrow 0} f(P_{load,ava}) = \frac{P_{net}}{\eta_{load}} \quad (2.44)$$

$$\lim_{SOC \rightarrow SOC_{min}} f(P_{bou,ava}) = \frac{P_{net}}{\eta_{load}} - P_{load,ava} + f_{dis} \cdot E_{bat} \quad (2.45)$$

Voltage model

Jongerson et al. (2008) summarize the extended kinetic battery model. This model was created by Manwell et al. (1994). It calculates the current voltage U_{cur} of a battery based on its voltage at $SOC = 1$, U_0 an applied load $I_{load,cur}$, the internal resistance of the battery R_{int} and multiple parameters and variables which are dependent on each individual battery A, C, D , and X . The calculation is described by Equation 2.46.

$$U_{cur} = U_0 - I_{load,cur} \cdot R_{int} + A \cdot X + \frac{C \cdot X}{D - X} \quad (2.46)$$

The initial terminal voltage of a fully charged battery U_0 is given by manufactures data sheets or can be measured. It is approximately 6% higher than the nominal voltage U_{nom} . The initial voltage drop while applying a load to the battery is described by the term $-I_{load,cur} \cdot R_{int}$. High discharging currents result in high initial voltage drops. Jongerson et al. (2008) describes the parameter A, C, D , and X as: "... E_0 [here: U_0] is the internal battery voltage of the fully charged battery, A is a parameter reflecting the initial linear variation of the internal battery voltage with the state of charge, C and D are parameters reflecting the decrease of the battery voltage when the battery is progressively discharged, and X is the normalized charge removed from the battery. These parameters can be obtained from discharge data. At least 3 sets of constant discharge data are needed for the non-linear least square curve fitting,..." [105, p. 9]. The measuring process of discharging batteries under various loads takes at least 20 hours to gain one measurement trial for the nominal battery capacity of an individual battery. Jongerson et al. (2008) suggest to run at least three measurement trials per battery. Gaining discharge curves for a general type of battery requires multiple measurement campaigns with many structurally identical batteries. Furthermore, it requires the needed equipment to discharge batteries under constant and high currents. Especially, in the early design stage of a building, the time to analyze single components like batteries is scarce. The time is crucial to calculate reliable results to determine fitting building supply technologies to continue with the building planning process. Hence, the battery characteristics and performance should be determined with easily available values, as gained from data sheets. Hence, the determination of the parameters A, C, D , and X is simplified.

Jongerden et al. (2008) A describes the initial linear voltage drop. It can be determined by the slope of the voltage drop between $SOC = 1.0$ to ≈ 0.5 . C . The parameter to model the slope near a $SOC = 0$ is C . It is the slope of the discharge curve between $SOC \approx 0.2$ and $SOC \approx 0.0$.

D is part of the denominator in Equation 2.46. It always has to be greater than the parameter X .

Thereby, its minimum value has to be the terminal voltage of a fully charged battery U_0 . X is described by Jongerden et al. (2008) as a removed charge, meaning it is dependent on the current state of charge. Equations 2.47 and 2.48 show the simplified determination of D and X .

$$D = U_{cur} \approx U_{nom} \cdot 1.06 \quad (2.47)$$

$$X = U_{nom} \cdot (1 - SOC_{cur}) \quad (2.48)$$

The resulting battery currents I_{net} , $I_{charge,eff}$, $I_{load,eff}$, and I_{bat} can be calculated with the corresponding powers and the battery voltage, which was calculated by Equation 2.46. I_{net} (Equation 2.49) is the overall electric current that is charging or discharging the battery. It is positive for charging and negative for discharging processes. $I_{charge,eff}$ (Equation 2.50) is the resulting current charged to the battery, based on the charge effectiveness and the applied charging power to the battery. $I_{load,eff}$ (Equation 2.51) is the equivalent to the discharging process. I_{cur} (Equation 2.52) is the real overall resulting current to or from the battery and it is based on the charging and discharging efficiency (or roundtrip efficiency) of a specific battery.

$$I_{net} = P_{net}/U_{cur} \quad (2.49)$$

$$I_{charge,eff} = P_{chare,eff}/U_{cur} \quad (2.50)$$

$$I_{load,eff} = P_{load,eff}/U_{cur} \quad (2.51)$$

$$I_{cur} = I_{charge,eff} - I_{load,eff} \quad (2.52)$$

Electricity transformation

The electricity supplied by the *Photovoltaic System* through the *Battery* is direct current (DC). It has to be transformed to an alternating current (AC) when it is used with a conventional compression chiller system. Furthermore, it has to be synchronized with the grid frequency, if it should be sold to the grid or to be used in a connected local grid. Within the lecture series by the educational equipment supplier *Festo Didactics* a typical performance curve of a DC/AC transformer is given [22, p. 48]. This curve is converted to a *.csv-file with *Plot Digitizer* [110] and shown in the following Figure 2.14. The graph shows the efficiency of the DC/AC transformer, η_{dcac} over its current load. The current load is defined by a *load factor* which is based on the current drawn power $P_{current}$ over the nominal capacity P_{nom} . This load factor is calculated below in Equation 2.53.

$$loadFactor = \frac{P_{current}}{P_{nom}} \quad (2.53)$$

Within the graph, the single values of the digitized plot are shown as blue dots. The rolling mean between 2 points is given as dotted blue line. This curve can be used to either create a look-up table or it can be used to find an equation which is capable to model the curve within an adequate accuracy. One possibility to describe this curve is given in Equation 2.54. This empirical equation calculates the resulting DC to AC conversion efficiency of the transformer η_{dcac} with an sufficient accuracy. The design efficiency on the name plate η_{max} is the upper limit for the efficiency of the transformer.

$$\eta_{dcac} = \eta_{max} + \frac{0.009 \cdot \ln(loadFactor/0.6)}{loadFactor} \quad (2.54)$$

The resulting curve is highlighted in Figure 2.14 in orange. It is well fitted to describe a general transformer cure above an applied load of more than 3%. Hence, a lower limit for the efficiency has to be established which limits the minimum power demand of the transformer. This should be the stand-by load of the transformer, i.e. the lost power of the nominal rated power output P_{nom} at its

2. Methodology

corresponding efficiency η_{max} . The lowest power demand could be $P_{min} = P_{nom} \cdot (1 - \eta_{max})$. However, when no load is applied, also the transformer should draw no current.

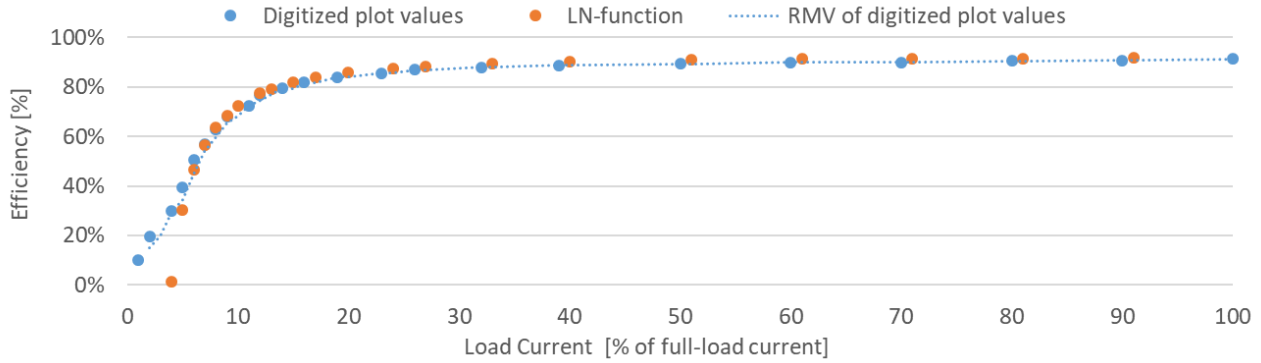


Figure 2.14.: General performance curve of an electric direct current to alternating current transformer, based on [22, p. 48].

Grid trading

Energy can be exchanged with a connected grid through the power P_{grid} . Electricity has to be drawn from the grid when a load is applied to the battery while its SOC is below its minimum charge level SOC_{min} . Furthermore, electricity can be supplied to a connected grid, as soon as the battery is fully charged and the power input of any connected source, like a photovoltaic system, is bigger than an applied load. Both processes are described in the following equations. The net power P_{net} is calculated by Equation 2.34 on page 42. The calculations and limitations of the effective charge and discharge power $P_{charge,eff}$ and $P_{load,eff}$ can be found the equations 2.38 resp. 2.43. P_{grid} is positive when power is supplied to the grid and negative when power is drawn from the grid.

$$P_{grid} = P_{net} - P_{Charge,eff}/\eta_{load} \quad (2.55)$$

$$P_{grid} = P_{net} + P_{load,eff} \cdot \eta_{load} \quad (2.56)$$

The integral of the P_{grid} is the overall energy balance for the system. In annual simulation a positive energy balance defines a plus-energy system, meaning that the system can supply more electric energy than needed for its own purposes over the period of one year. This value can be expressed as monetary value. When energy is supplied to the grid it could be either sold (e.g. at a fixed feed-in tariff), reverse a connected electric meter (so called *net-metering*), or satisfy other electric loads without drawing electricity at a current price from the grid.

3. System Design

This chapter is dedicated to define the design parameters for the previously described system setups (cf. 2.3.2, p. 23). First, the boundaries and properties are grouped into four fields and their dependencies are evaluated. Afterwards, a variation of optimization goals for the final system are presented. Based on this, the bandwidth of the outer boundaries is determined. Finally, the possible control strategies for the system components are analyzed.

A resulting solar powered air cooling for the MENA region needs to consider the following four interconnected fields:

1. Cooling demand, which is the heat that has to be rejected from a room to achieve thermal comfort and is based on the outside and inside boundaries,
2. Solar electricity, which is the amount of electric energy generated by a PV field and is dependent on the surrounding conditions and the module parameters,
3. Electrical systems, which are all electrical driven components, including the battery system and grid connection and which are dependent on the present appliances and the user behavior,
4. Thermal storages, which are sensible heat storages with a certain capacity to store "coldness" and are dependent on building properties.

Each field represents its own quality and quantity for the set up and operation. The interconnections and dependencies of each field are presented in the overview in Figure 3.1 on the following page.

The impact of each field on the system design is dependent on its properties and limits. Two of the main impacting parameters are the outside climate and the user behavior. The first has a massive impact on the cooling demand and solar offer, but influences as well the performance of the condenser of the electric driven cooling unit. The users on the other side, defines the internal loads and user presence but also when a room has to be cooled or to which extends the comfort conditions could be violated. They are demanding a best thermal comfort but can care as well about the costs to achieve it. This demand is satisfied by an unitary air conditioning system, like a split-unit. The needed electricity for its operation, is supplied by a connected electrical grid and/or a photovoltaic field. The solar field itself could be capable to supply electricity to a local or even national grid. Besides a direct satisfaction of the cooling load, "coldness" could be produced during off-peak hours and thermally stored in a cold water tank and/or the thermal building masses of an apartment. These masses could release "coldness" during times with high loads onto the electric grid and prevent thereby instabilities.

3. System Design

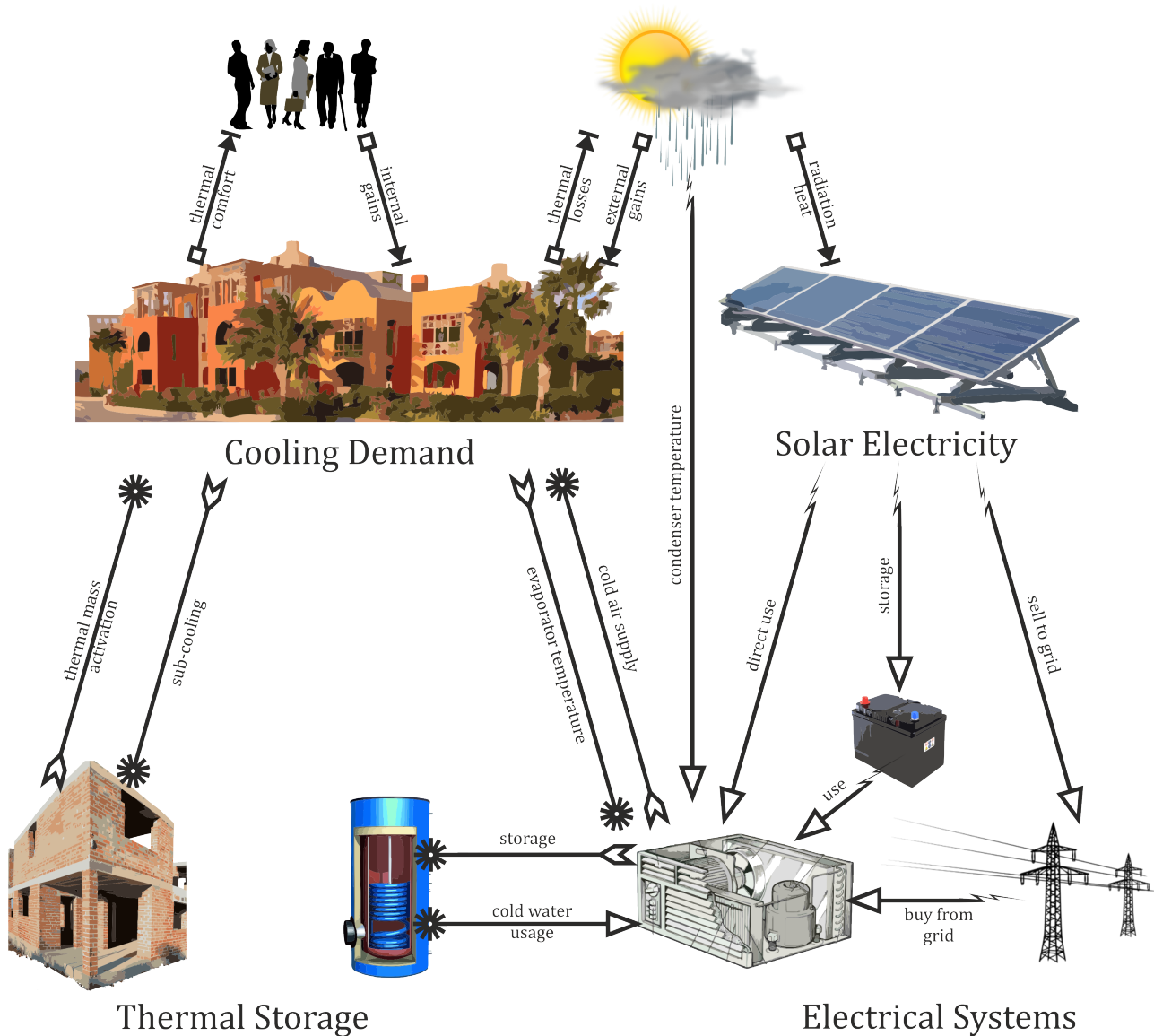


Figure 3.1.: System fields and interconnections, graphic based on vectorized images [23].

3.1. Climate condition bandwidth

The outer climate is defined by the location of a building or apartment and is the main impacting factor. It is only an external boundary condition with a one direction information flow. The only impacting factor of the systems are micro urban heat island effects, which can occur in dense city contexts or long term climate effects through fossil energy usage.

Within the MENA region, the climatic conditions are comparable but cannot be generalized (cf. Section 2.3.3, p. 29). Hence, the local weather conditions of a desired location have to be selected. Therefore, standardized weather data sets for certain cities [29] or specific locations [25] have to be used as input parameters. It is not recommended to use measured weather data. The annual deviation in climatic parameters can be tremendous. This deviation can be observed in the following graph in Figure 3.2. There, the daily average air temperature for an example location in the region is presented. The air temperature was measured for the years 2012 to 2018 at *KBC El Gouna* and provided for this

research [24]. Clearly visible is the annual trend in temperature and the drastic deviations between two successive days. The tremendous differences between the years can be found at a closer look. The smaller graph inside the red frame shows the last week of January for a better comparison. For example, the average air temperature on 26 January 2013 was $\vartheta_{ODA,26.01,2013} \sim 22^{\circ}\text{C}$. Three years later, in 2016, the temperature was $\vartheta_{ODA,26.01,2016} \sim 12^{\circ}\text{C}$, a deviation of 10 K . Hence, a standardized annual profile, like a so called test reference year TRY, is needed.

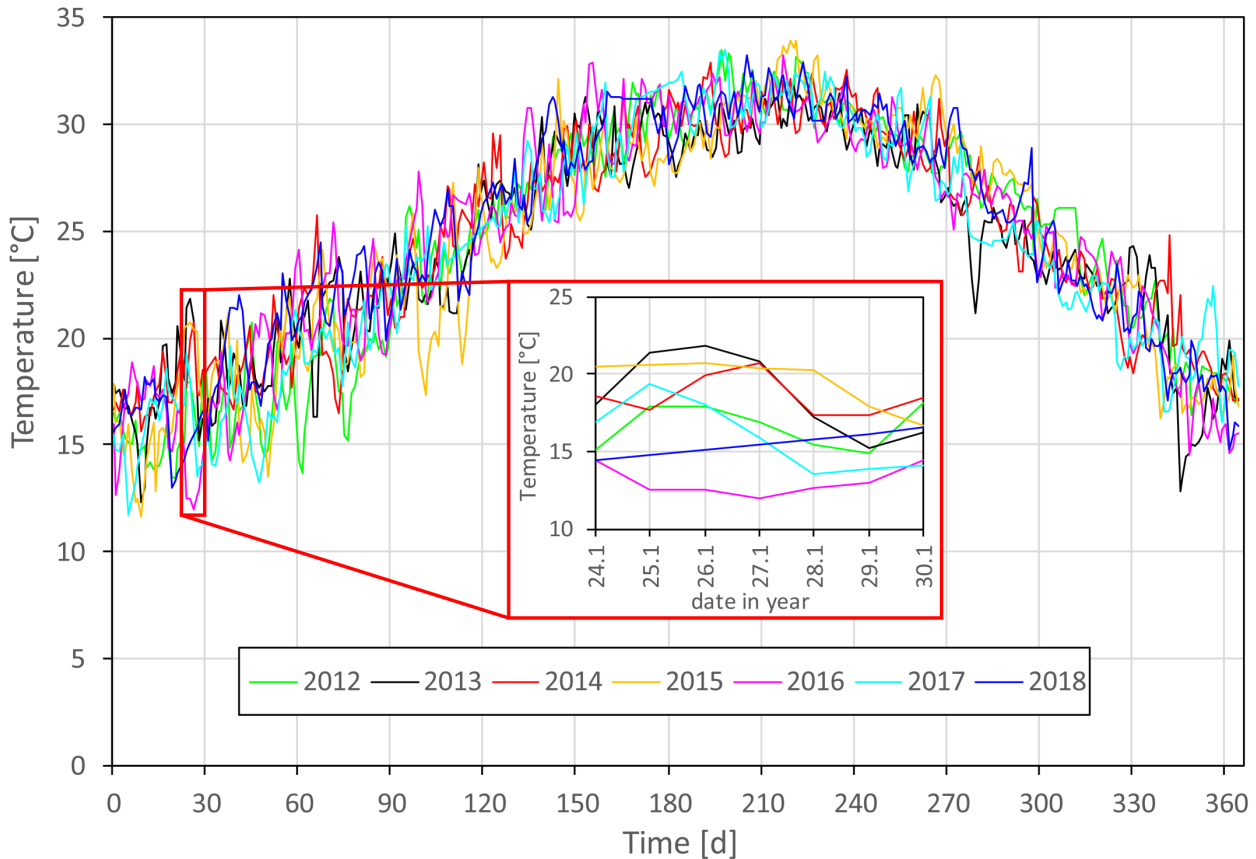


Figure 3.2.: Daily average weather temperature, measured from 2012 to 2018, data provided by KBC El Gouna [24].

Additionally, extreme weather data sets are available for specific locations. Those data sets include maximum and minimum temperatures as ten years extrema and can be used to evaluate the performance of a system under rare conditions. However, an analysis of the local weather should be undertaken and possible heat island effects manually encountered. The shadowing effect of the surrounding environment must be considered.

3.2. User behavior bandwidth

The user defines when and how much a room, apartment or building has to be cooled to a certain temperature. This temperature can vary with each user. Additionally, the user is also an internal heat load themselves. Further, other internal gains, like through light bulbs or machines, are caused by a user. The calculation process is described in Section 2.3.3 on page 32. A general profile has to be used for a standardized calculation method and to keep the results comparable. However, the results

3. System Design

can deviate between simulation demands and measured demands, as the assumed user behavior could be completely different to the real users behavior. Therefore the *IEA-EBC Annex 66* and *Annex 79* tasks were created. The goal of *Annex 66* is the "*Definition and Simulation of Occupant Behavior in Buildings*" [111]. There, the ideal user behavior is combined with stochastic models to evaluate relevant human feelings and resulting actions in terms of physiology, psychology and economics. The currently ongoing project *Annex 79* concluded for their task that "... *real operations of buildings show that man such models do not represent the manifold human interactions with a building appropriately enough, and that there is no guidance for designers and building managers on how to apply occupant behaviour models in everyday practice*" [112]. One new method to simulate such user dependent systems suggest a probabilistic agent based simulation [113]. The results of such simulation enable the researcher to determine a probability of a certain outcome of a simulation rather than a single digit result. This helps to increase the confidence into the simulations and evaluate weaknesses. However, this method requires a broad range of simulation trials to evaluate each possible outcome and determine the uncertainty of an averaged result. This in depth analysis is not part of this research due to the already present extensive simulation demand. Due to the similar socio-cultural background of the MENA region, a generalized user profile can be created which is used for a case study based analysis but has to be adopted for later use according to the planned demands of a certain user. This should include probabilistic agent based presence and usage.

3.3. Apartment design bandwidth

Also, the general construction, outer appearance and building material is similar through the MENA region. Nevertheless, its properties can deviate tremendously between two buildings. Unwanted changes in the quality of a building material or construction site assembly process can lead to big gaps between predicted and resulting energy demand of a building. However, these deviations are not part of this research either, as their occurrences are highly random and their impact is hard to model. Hence, generalized building material libraries and standardized apartment shapes are used in this thesis. The heat transfer processes from and to a room is presented in Section 2.3.3 on page 27.

Attia et al. (2012) described two different standard layouts for Egyptian flats. Both floor plans are shown in the following Figure 3.3. The typologies represent common buildings throughout the entire region. The floor plans highlight one flat per building, each with a kitchen, a bathroom and three sleeping rooms. According to a usage survey, the living room and two bedrooms are air conditioned [6, p. 273]. There, the energy demand of each typology is also determined within the three cities of Alexandria, Cairo and Asyut. It ranges from $Q_{annual} = 22.4 \text{ kWh/m}^2$ to 31.0 kWh/m^2 for typology 1 and from $Q_{annual} = 11.0 \text{ kWh/m}^2$ to 18.0 kWh/m^2 for typology 2. The energy demand increases, the further south a building is located.

The picture in Figure 1.7 on page 8 shows the presence of single room split-unit air conditioners in a broad range of buildings in the world. They can be installed in the parapet or above the window. This research focuses on single rooms and their separate air cooling units due to this distribution of A/C units. The supply systems are designed to match the needs of a single room and its user profile. For example, a hotel room could be considered as the shape of the bedroom and the bathroom and would be operated with the bedroom usage profiles. In a latter step, multiple rooms and their individual performance could be combined to the overall performance of an entire apartment. Those units could be combined to simulate the performance of an entire building. Finally, multiple buildings can be combined to simulate city quarters.

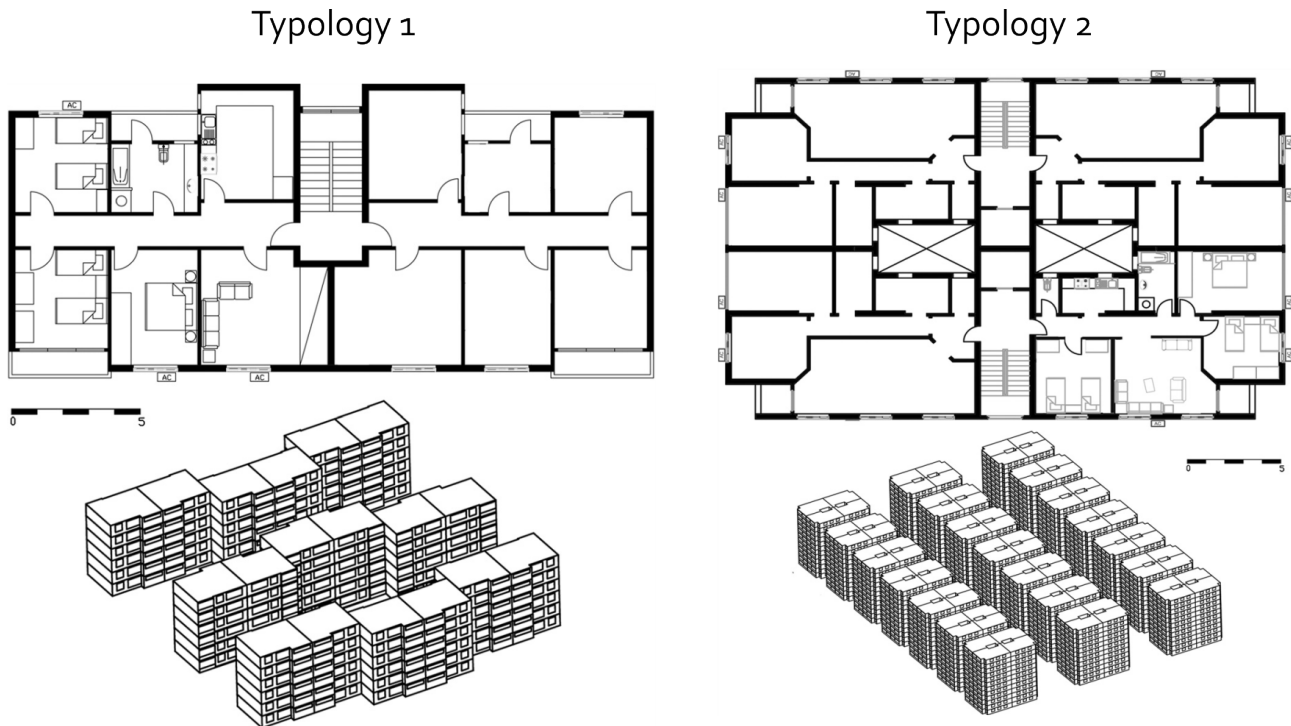


Figure 3.3.: Floor plans of building typology 1 and 2 and their urban context according to Attia et al. (2012), p. 274f.

3.4. System design spectrum

The different systems are introduced in Section 2.3.2 on page 23 in the previous chapter. The control strategies for each system are introduced. This main strategies lead to feasible system variants which are presented afterwards.

3.4.1. Reference system

The control logic of a standard supply system to cool down apartments within the MENA-region is shown in the schematic in figure 3.4. It is based on the reference cooling system in Figure 2.4, page 24. There the system components are shown in analogy to the overview in the table in Figure 2.3 on page 22 and their corresponding definitions. Electricity is taken from the *Grid Connection* which is used to supply the *House Connection* and the *Air Conditioner*. This is a standard split-unit compression chiller based room air cooling system which recirculates the room air and directly cools it through its through the evaporator in the *Air Outlet*. The control strategies for the grid controller $cntr_{grid}$ and air conditioner $cntr_{AC}$ are described in the following two subsections.

Electric grid

Power cuts in the region happen mainly on the 66kV to 22kV supply level. An electrical 66/22kV substation over sees the voltage U of the connected grid. When the voltage drops to 50kV, the transformers are switched of until the voltage is increased back to at least 55kV [114, p. 274]. This happens when the load on the grid is too high and it is not capable any more to satisfy the demand. It is outlined as a control scheme in the $cntr_{grid}$ controller in Figure 3.4. This control algorithm is out of reach of the user but necessary to understand the impact of many air conditioners to a grid.

3. System Design

Air conditioner

The user's impact on the system is the direct control of the air cooling unit. They select a certain indoor air temperature ϑ_{set} . The hysteresis controller measures the indoor room air temperature ϑ_{IDA} at the air inlet of a cooling system, or, in some cases, with a detached thermometer within the presence zone. It switches the air cooling unit on, when this temperature exceeds the set temperature by half of a programmed hysteresis $hyst$. The A/C is switched off, as soon as ϑ_{IDA} drops by this hysteresis to ϑ_{off} . This control algorithm is visualized in the $cntr_{AC}$ controller in the scheme in Figure 3.4.

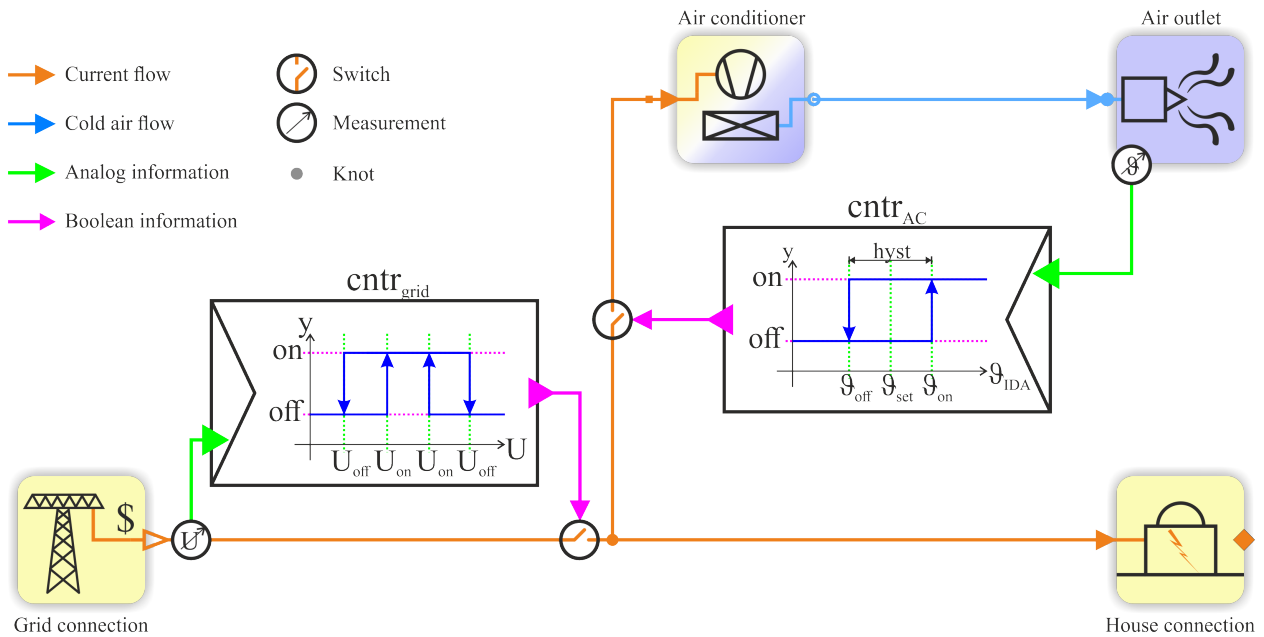


Figure 3.4.: Reference cooling supply system of a typical apartment in the MENA-region.

3.4.2. Electric energy exchange systems

The previously described control logic is extended to be used in a cooling system with an added photovoltaic field, a battery and a DC/AC transformer. Furthermore, the system is capable to transfer electricity to the hosting connected grid. The fundamentals are introduced in Section 2.3.2 on page 25. The additional control logic is presented in Figure 3.5. It is added besides the now simplified presented controllers of the reference system. The controller for the battery storage $cntr_{strg}$ is schematically presented as a graph in Figure 3.5. In this analysis, the battery is designed to supply the air conditioner as primary consumer. This is done to exclude the effects of various load duration profiles and different user dependent priorities of electricity needs. Practical applications of battery systems could include a user setting for prioritizing connected electrical sinks.

Battery storage systems

The PV field is connected to a battery system. The state of charge SOC is monitored and the data handled in the battery control logic $cntr_{strg}$. It connects the battery to the transformer and thereby to the air conditioner when the state of charge SOC of the battery is above a minimum level SOC_{min} . In this case, the grid supply is disconnected and the rest of the system can be supplied by the PV system. In case, a cooling load occurs, the air cooling unit is switched "on" through the $cntr_{AC}$ logic.

Selling and buying to/from public grid

As before, the air conditioner control logic $cntr_{AC}$ switches the air cooling unit "on", when a cooling load is present. Additional electricity from the PV field will be supplied to other consumers of the same household. Further excess energy can be supplied or sold to the connected grid. All solar generated electricity is supplied to the household or grid when the battery is fully charged and no cooling demand is present.

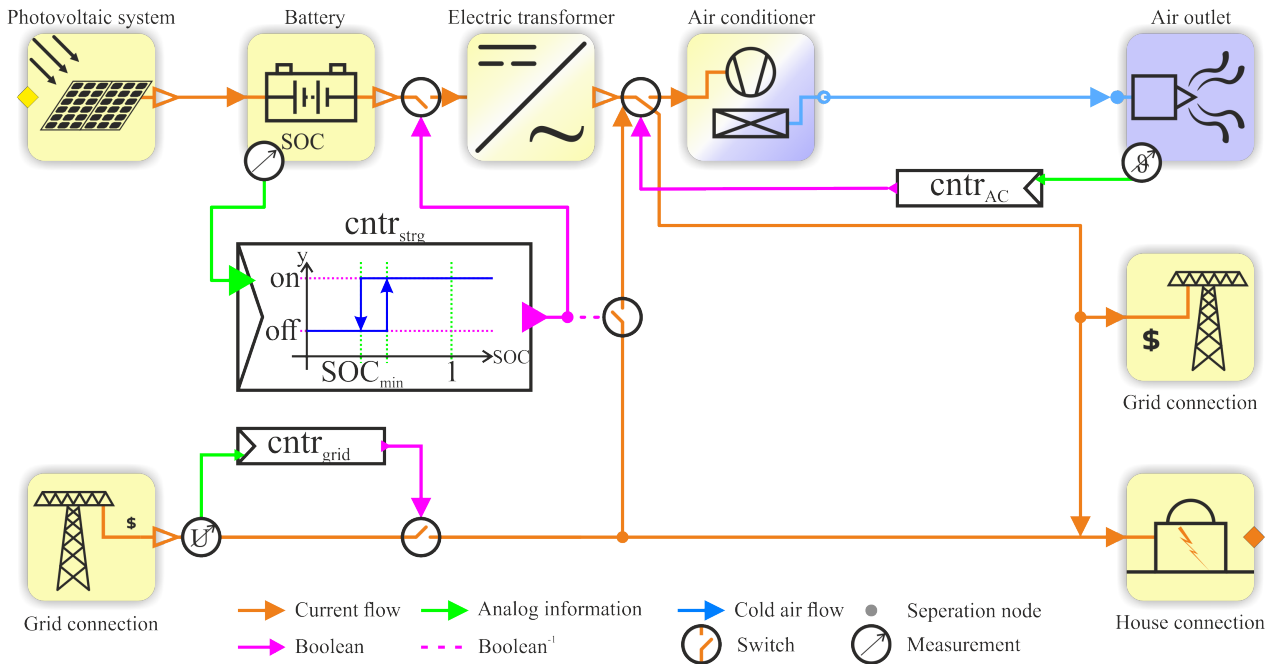


Figure 3.5.: Cooling system with a PV and battery system and a grid connection.

3.4.3. Thermal energy storage systems

According to the system description, there are two possible thermal storages available to extend the reference system. One is working with the building mass (cf. Section 2.3.2, p. 25) and the other with a cold water storage (cf. Section 2.3.2, p. 26). Control strategies for both systems are presented below in Figure 3.8 and 3.9.

Building mass activation

The first storage possibility is to thermally activate the existing building mass. Therefore, the room has to be sub-cooled so that the temperature of the room surfaces becomes lower than the set temperature. This could mean to exceed the lower limit of thermal comfort. This should only be done, while no occupant is present in the room. This storage comes for free with every building as the room enclosing surfaces. However, its efficiency is relatively low as it can only be cooled with the room air itself and approximately only the first 7.5 to 10cm of a construction are available. This was shown by D. Chiras in *The Solar House*[115]. Furthermore, it is connected to the outside or neighboring rooms which causes increased losses to the environment or other apartments. Hence, only the available building mass should be considered and the installation of any additional storage capacities by adding additional wall layers should be avoided. The following pictures in Figure 3.6 and Figure 3.7 show the general operation modes to charge and discharge the thermal mass of a building. Figure 3.6 shows the charging mode to thermally activate the building mass.

3. System Design

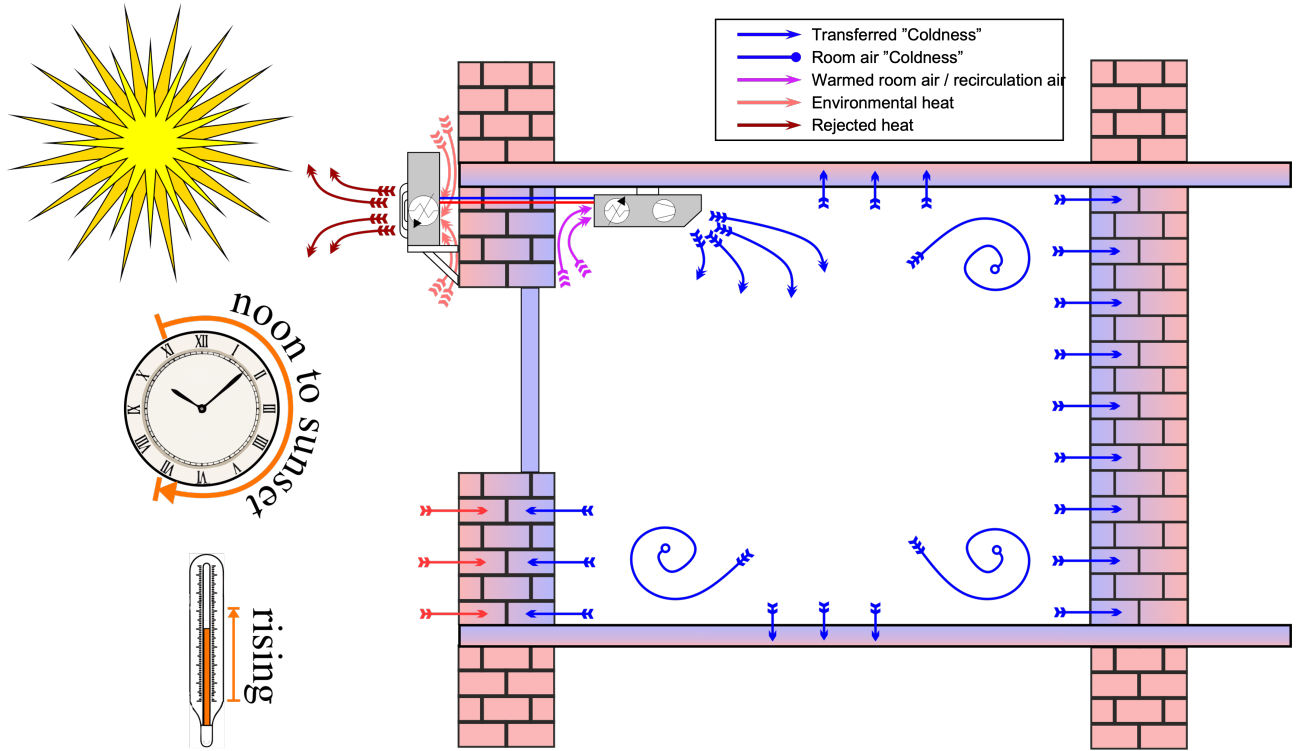


Figure 3.6.: Charging of building mass during day time and no occupancy.

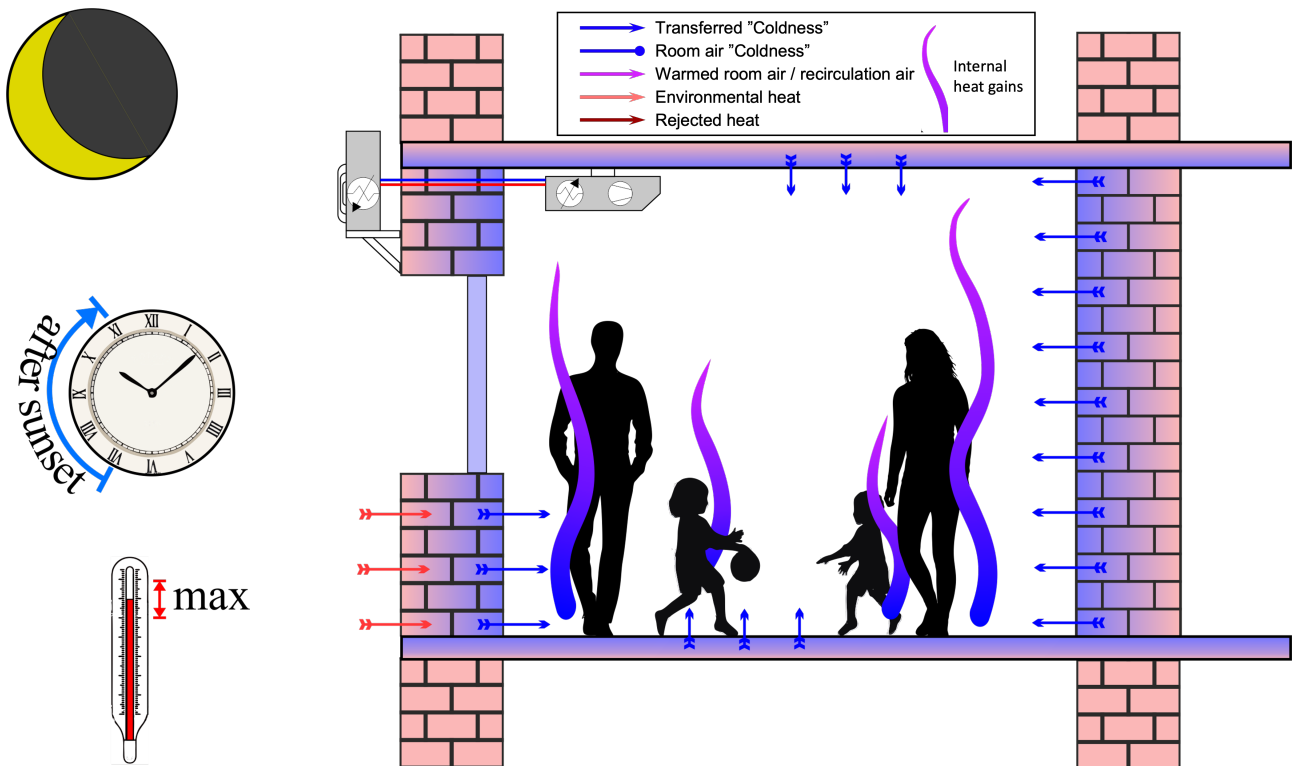


Figure 3.7.: Use of building mass as thermal sink during occupancy and after peak demand time.

During day times, when no user is present, the air conditioner could still be operated and cool or even sub-cool the room to a temperature of as low as $T_{room} 16^{\circ}C$. The air will cool the room surfaces and building mass through convection. Thereby, the mass will be charged with "coldness". The discharge process is shown in Figure 3.7. After sunset, when users come home and the peak load demand is reached, the air cooling unit can be switched off and the building mass used as heat sink for the room air.

A corresponding control scheme is presented in Figure 3.8. The controller $cntr_{occ}$ reduces the set temperature of the A/C controller $cntr_{AC}$ by a defined value x when the room is empty. The value is reset as soon as one user is present or is expected in the near future. Further, the A/C is switched off when the state of charge of the building mass is at $SOC_{mass} = 100\%$. The state of charge of the building mass is defined by its potential. This is the temperature difference to the set temperature while a user is present. It can be determined with a temperature measurement in the first 10cm of the walls. This is the thermally active building material, as described in Section 2.3.4 on page 37. The control is done with an equivalent control as for the battery storage $cntr_{strg}$.

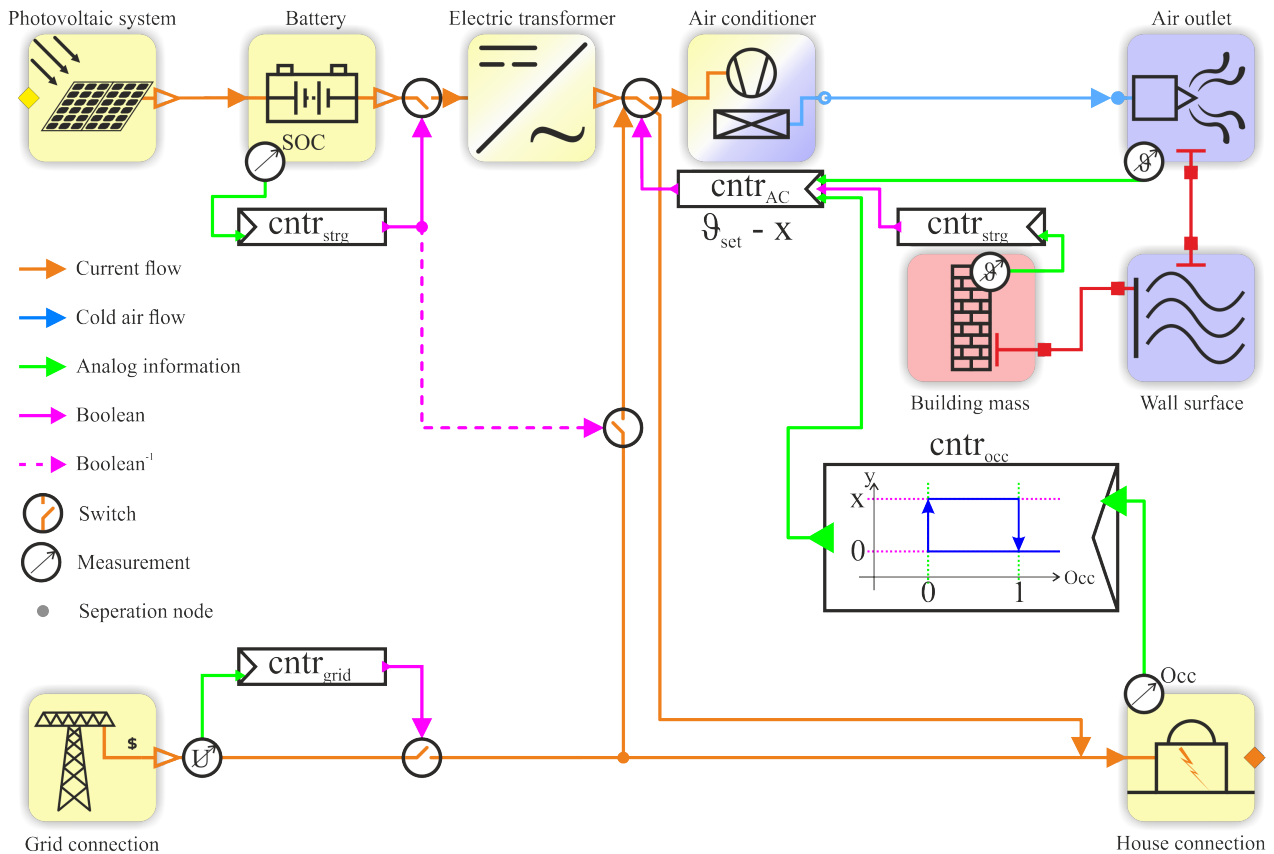


Figure 3.8.: Extended system with a sub-cooling control algorithm to thermally activate the building mass.

Cold water storage systems

A system with a cold water storage is the most complex system of this research. As previously described, it needs a cold water production and a connected distribution system to supply a cooling coil and/or a cooling surface. Within this system, a cold water storage can be utilized as alternative or support for an electric battery and/or thermally activated building masses. Also, the cold water could

3. System Design

be used in surface activation systems such as cooling ceilings. The scheme in Figure 3.9 shows the control strategy for such a system. The air conditioner, the occupancy controller and the building mass controller are represented as one controller $cntr_{AC+occ}$. In this case, it activates a cold water pump, which supplies a fan coil unit and/or a cooling surface. The newly introduced cold water storage has at least two temperature sensors: one at the top ϑ_{up} and one at the bottom ϑ_{dwn} . The storage can be charged as soon as the temperature in the top layer rises above the set temperature ϑ_{set} . It is fully charged when the temperature at the bottom has reached this set temperature.

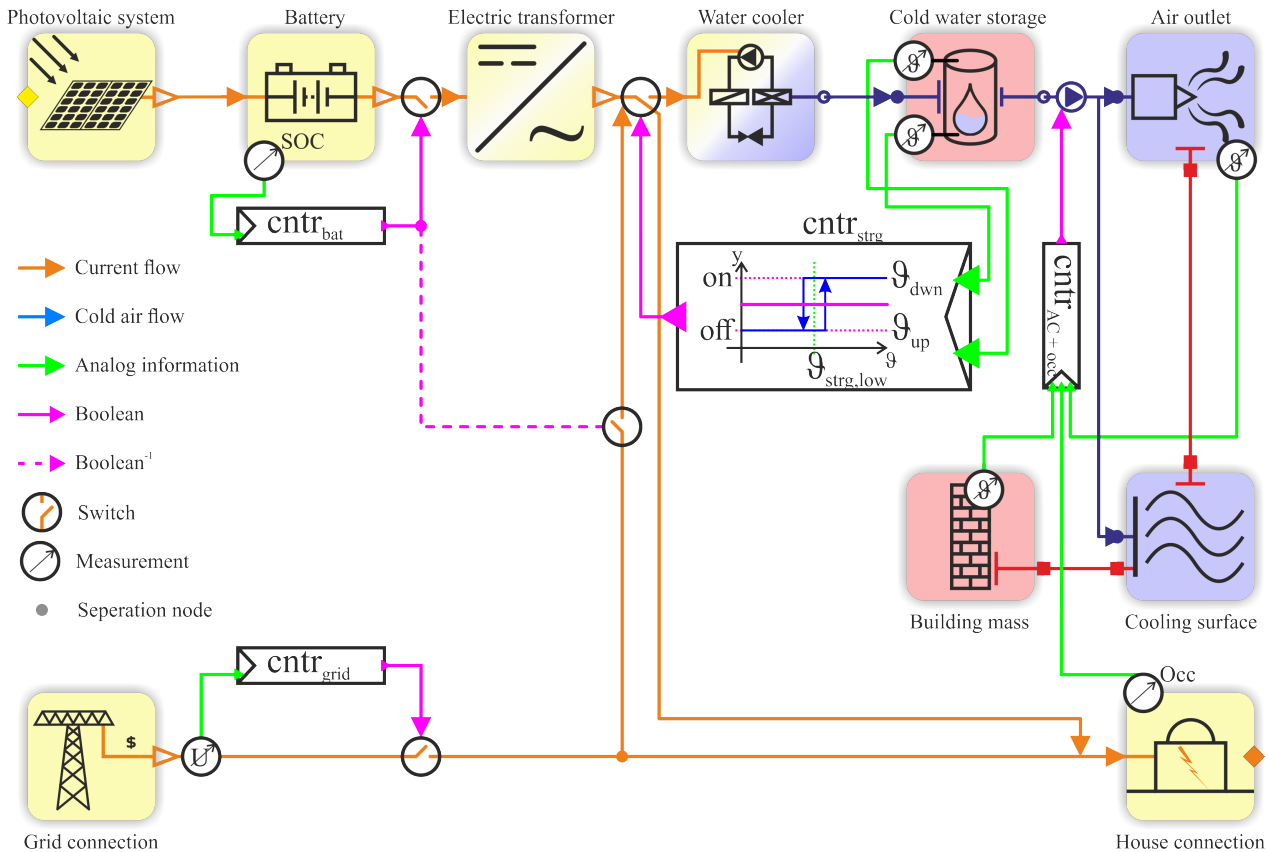


Figure 3.9.: *Extended system with a water chiller, cold water storage, cooling coil and thermally activated building mass.*

3.5. Feasible system variants

Researchers, engineers, planners and developers need to evaluate if their plans and suggestions are feasible. There are various definitions and scopes to estimate the feasibility of a solution. All of them conclude multiple dimensions that should be vetted. Heathcote et al. defined in their book for project management for information technologies the basic categories to evaluate the feasibility of a project. These are the technical, economic, legal, operational and scheduling feasibility [116]. Newer manuals, especially within the engineering and planning field highlight further the importance of ecologic and socio-cultural feasibility, as it was done by Urkiaga et al. in 2006 [117].

First of all, the scope of this research is the technical feasibility. Can the system work as proposed and are all used components and systems available on the market with the defined properties? Afterwards, the economic and ecologic feasibility has to be evaluated. Is the investment into additional components worth it for an investor, the user itself or a higher entity? What are the global and local impacts on

the environment of such a proposed system? Finally, as well some socio-cultural aspects of a proposed systems will be evaluated. How could such a system be implemented? How could users or investors be convinced besides financial benefits?

Optimization goals are defined to evaluate the performance of a possible system. Thereby, only technical feasible systems will be analyzed. This means that only market available products and components will define the properties of any suggested system. Based on this, the economic feasibility is evaluated by calculating the levelized costs of electricity, $LCOE$. This is the price for electric generation per kilowatt-hour over the life time of an energy supply system, including fuel costs and interest rates and it is as well a major part of the socio-cultural feasibility. The economic feasibility can be calculated as well by comparing the levelized costs of cooling, $LCOC$. This calculation includes the investment and financial costs for additional equipment, operation and maintenance costs, the costs for electricity and the possible revenues of a solar system by selling electricity to a connected grid. A similar calculation is also done for the ecologic impact. The energy savings are compared against the needed energy for the production and installation of the additional components. Also, this could be a major decision criteria for an ecological aware user. Other optimization goals, like improving the grid stability, increase the degree of autonomy or achieve the best thermal comfort must be evaluated under the light of the economic and ecologic impact of alternative solutions that achieve the same goal. This thesis will start by comparing the results of these categories of a reference system against various system variants. These performance indicators are used to determine all previously described dimensions of the feasibility.

3.5.1. Grid stability

The first variant is specially designed to keep the burden of A/C systems onto the electrical grid as small as possible. The annual report of the Fraunhofer Solar institute writes about grid supporting buildings. Those buildings can contribute to match the volatile offer of fluctuating renewable energy sources with demand side management and other load shifting techniques [118, p. 54]. Hollinger et al. suggested already in 2013 a charging scheme for a battery which is connected to a PV system to reduce the impact of the noon peak [119]. The scheme suggests to use a battery storage to cut of the high solar offer by charging this battery during this time of day. Systems, which are not grid friendly operated, would charge the battery immediately when the solar offer is bigger than the electricity demand. In most cases, the battery would be sufficiently charged during noon and pushing all solar generated electricity to the grid.

However, the solar generated electricity is not yet a problem in the MENA region (cf. Section 2.1.2, p. 17). The main problem for the grid is the high peak demand due to the growing use of A/C systems. Therefore, the impact of them must be reduced. This impact was discussed in Section 1.3.3 on page 9. In particular, the tremendous evening peak in electric energy demand (cf. 1.12, p. 11) causes massive blackouts or forces rolled power cuts. Nevertheless, both strategies should be directly applied in future developments.

The main idea is presented in the following Figure 3.10. The load profile of 2012 of the city of El Gouna, Egypt is averaged for the main cooling period from June to September and the resulting average load duration curve is presented in blue. In contrast, the daily average total horizontal radiation $Irr_{tot,hor}$ is outlined in red and on the secondary y-axis. This solar offer should be cut off from 8am to 3pm by charging a battery. The potential is indicated by the red striped area. Finally, this stored energy should be used to cut off the demand peak from 4 to 10pm, which is marked with a blue striped area. The main design criteria for the needed storage capacities are based on this peak shift capability. The energy storage capacity E_{strg} should be sufficient to supply enough cooling energy $Q_{cool,peak}$ during the peak demand hours. Further, the installed photovoltaic system has to supply the needed PV generated electricity around noon $E_{PV,noon}$ to charge the battery adequately.

3. System Design

$$E_{strg} \sim Q_{cool,peak} \sim E_{PV,noon} \quad (3.1)$$

This system design focus on the bigger picture and the overall benefit of all grid connected users of a local or national electricity grid. The stabilizing effect of demand response on the daily load duration curve was also described by the IEA in 2018: "During the hours when supply is scarce or electricity networks are congested, connected devices such as smart ACs can be switched off or run at lower load automatically. These connected devices can reduce or shift consumption to other periods when supply is abundant, for example, when the sun shines, the wind blows or when there are no technical problems with the electricity grid"[10, p. 51]. The impact of single or scattered applicants would barely have a stabilizing effect.

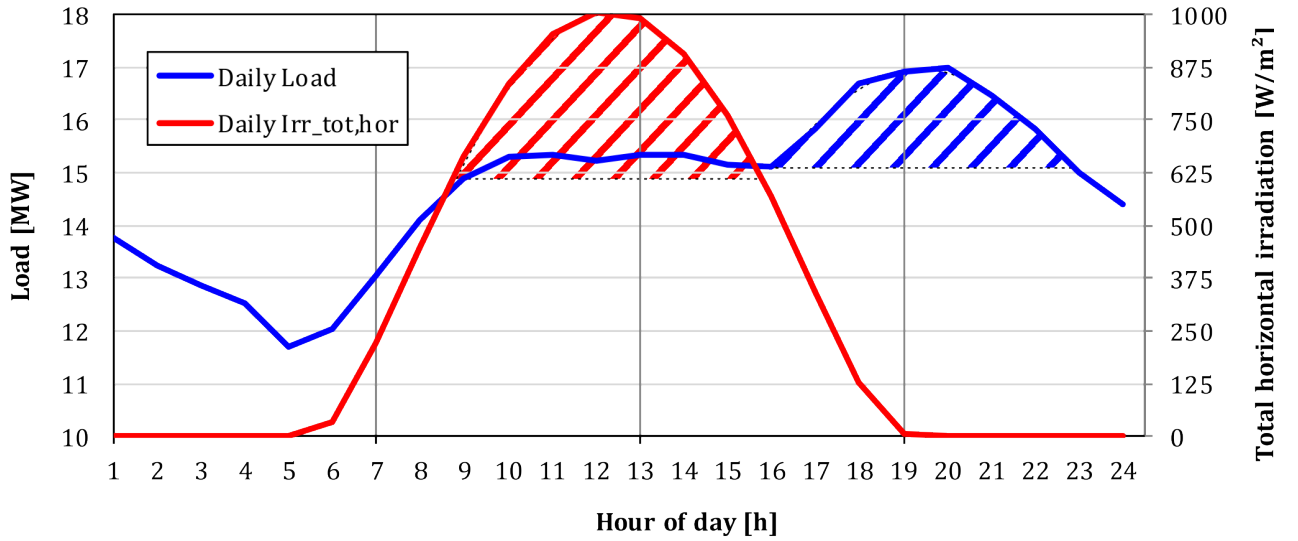


Figure 3.10.: Average load duration [11] and total horizontal irradiation profile from June to September in El Gouna [25].

3.5.2. Maximum solar coverage rate and solar autonomy

The extreme of this scenario could be for an island systems or a method to become electric autonomously. The estimation can be done for the air cooling unit solely or the entire connected household. In both cases, the energy storage capacity E_{strg} has to be sufficient to satisfy the demands E_{dmd} on the worst possible day. Also, the PV system must generate enough electricity E_{PV} before this particular day to supply this amount of energy (cf. Equation 3.2). The easiest but most expensive way to satisfy the storage demands would be a sufficiently big battery system $E_{strg,bat}$. However, the cooling energy could be stored alternatively in a sensible heat storage like a cold water tank $E_{strg,water}$ or the building mass $E_{strg,mass}$ (cf. Equation 3.3).

$$(E_{dmd})_{max} \leq E_{strg} \leq E_{PV} : (E_{dmd,max}) \quad (3.2)$$

$$(E_{strg}) = E_{strg,bat} + E_{strg,water} + E_{strg,mass} \quad (3.3)$$

The size of each possible storage capacity is defined by its costs and availability. The building mass should be used as much as possible, as it comes for free with a building. The cold water storage is the cheapest additional energy storage possibility. It should be used to satisfy the cooling energy demand during peak and night hours. Only the rest of the cooling demand should be supplied with an expensive

battery storage system.

An important factor to evaluate the annual energy balance of solar supplied systems is the solar coverage rate, SCR . It is shown in Equation 3.4 and calculated by dividing all used solar electricity $Q_{elect,solar} * \eta_{DCAC}$ with the annual electricity demand $Q_{elect,annual}$.

$$SCR = \frac{Q_{elect,solar} * \eta_{DCAC}}{Q_{elect,annual}} \quad (3.4)$$

The calculation can be related to the total annual electricity demand or the electricity demand for solely cooling. The solar cooling autonomy, SCA , can be used to evaluate the grid independence of the cooling system. It is calculated with Equation 3.5. It is the fraction of the difference between the annual electric energy demand of a split-unit $E_{elect,split}$ and the annual bought grid electricity for the operation of the split-unit $E_{import,split}$ over again the annual electric energy demand of the split-unit itself.

$$SCA = \frac{E_{elect,split} - E_{import,split}}{E_{elect,split}} \quad (3.5)$$

The SCA is 1 when no electricity is bought from the grid to power the A/C. This means that all cooling energy is supplied by local solar power directly or through one of the storage systems. A small solar cooling autonomy indicates a high grid electricity demand used of cooling purposes. However, it does not indicate the time distribution of the power demand and can only be a first indicator if an air conditioning system is a burden for a connected electrical grid.

3.5.3. Minimum investment costs

This optimization strategy is as well a fixed, additional boundary condition. In many private households, the decision for any additional system component is not driven by net present value or return on investment calculations. Often, the limiting factor is the available or obtainable money for such investments. However, the user expects the highest possible energy or cost savings. Hence, this boundary condition can be added to all previous scenarios and limits the maximum costs of a proposed system. The lower boundary of this system is a minimum system with a small scale photovoltaic system and battery storage system. This system is used to extend an reference model without changing boundary parameters such as thermal building mass or user profiles. The additional components are given in the following table. The detailed modelling of each component is evaluated in the following chapter. The components are selected according to their availability in the case study location *Hurghada, Egypt*. The prices are online search results on a Chinese retailer website. The overall minimum additional system components sum up to $C_{sys,min} = 845 \text{ USD}$. Additionally, the customer needs to pay for a charge controller, wiring and installation.

The second half of the table includes the additional components which are needed for a water cooling system. There, the price for the air-water heat pump is given as it must be additionally purchased to replace the existing air to air heat pump of a split-unit system. Further a cold water buffer storage tank is needed. Both components increase the minimum price to $C_{water-sys,min} = 2070 \text{ USD}$. This tremendous increase can be found in the exchange of the cold water production system. However, the found air to water chiller is oversized by its capacity and at least capable to exhaust the cooling load of an entire apartment or multiple interior fan coil units. Additionally, the costs for installation effort and further components (such the water piping system) will occur.

3. System Design

Table 3.1.: Overview of additional system components with minimum investment costs.

Component	Parameter	Symbol	Value
Photovoltaic system	Type		SpectraVolt 100M36S
	Nominal power	$P_{el,nom}$	100 W
	Number of models	n_{mod}	15
	Tilt angle	$degTilt$	30°
	Azimuth angle	$degAzi$	0°
	Price per module	$USD/module$	35 \$*
Battery system	Type		Chloride CLH12-200
	Nominal capacity	E_{nom}	200 Ah
	Number of batteries	n_{bat}	1
	Price per battery	Cst	120 USD/unit*
	Specific prices	cst	62.5 USD/kWh _{elect}
Transformer	Type		General DC-AC converter
	Nominal capacity	P_{nom}	3000 W
	Maximum efficiency	η_{max}	0.92
	Price per inverter	$USD/inverter$	200 \$*
Air-water heat pump	Type		Ruidong RLSFW
	Nominal power	$P_{cool,nom}$	7.1kW
	Price per unit	$USD/unit$	1000 \$**
Water Storage	Type		FJI-100A-NH
	Water capacity		300l
	Insulation thickness	thk_i	0.01m
	Heat conductivity	λ_i	0.05W/mK
	Price per unit	Cst	50 USD/unit**
	Specific prices	cst	166.67 USD/m ³
Room transfer unit	Type		AIKE FP-68
	Nominal power	$P_{cool,nom}$	3.6kW
	Price per unit	$USD/unit$	150 USD/unit**

* prices evaluated on www.alibaba.com on 9 November 2019

** price evaluated on www.alibaba.com on 27 December 2019

3.5.4. Minimum life cycle costs

Instead of making the whole system grid independent, the goal for minimum life cycle costs is to reduce the levelized cost of electricity $LCOE$. The calculation, as done by the Egyptian office of the Fraunhofer ISE, is presented in Equation 3.6[13, p.25]. The numerator contains all costs of the system, including the initial investment cost I_0 and all continuous annual costs A_t of each year for the lifetime of the supply system. The divisor is the total sum of the electrical power output over the lifetime $M_{t,el}$. It includes possible degeneration through an interest rate i .

$$LCOE_{ISE} = \frac{I_0 + \sum_{t=1}^n \frac{A_t}{(1+i)^t}}{\sum_{t=1}^n \frac{M_{t,el}}{(1+i)^t}} \quad (3.6)$$

For this work, the calculation is specified and the resulting formula is presented in Equation 3.7. The life time costs include the investment costs I_0 for all system components as shown in the previous Table 3.1. Further, operation and maintenance Cst_{OM} cost are includes. The sum of all specified costs is divided by the life time energy output E_{total} . A degradation factor d is included to account for the annual decreasing power output of a solar system.

$$LCOE = \frac{I_0 + \sum_{t=1}^n (\frac{I_0}{(1+i)^t} + Cst_{OM})}{\sum_{t=1}^n \frac{E_{y0}}{(1+d)^t}} \quad (3.7)$$

The needed additional parameter are presented in the following Table 3.2. The input data is based on the previous shown system with minimum investment cost and a study on LCOE for renewable energy technologies in Egypt by the *Fraunhofer ISE* (2016)[13].

Table 3.2.: Parameters and variables for LCOE cost calculation as presented by Hussein et al. (2016)[13] for small scale residential applications of photovoltaic systems on Egypt's Red Sea cost

Parameter	names	Unit	Value
I_0	Initial investment costs	USD	845*
n	System lifetime	a	25
i	Interest rate	%	8.5
Cst_{OM}	Annual operation and maintenance costs	USD/(kW _{Peak} * a)	34
E_{y0}	Initial annual energy output of PV fields	kWh/kW _{Peak}	1800*
d	Annual degradation of PV modules	%	0.09

*variables calculated based on system with minimized investment costs

An alternative way to evaluate the performance directly in terms of cooling is the levelized cost of cooling, $LCOC$. These cost are the amount of money which is spent per kilowatt-hour of cooling energy Q_{cool} . The overall money is the difference of the supplied electricity from the grid E_{grid} at its purchasing costs Cst_{elect} to the income from sold electric energy E_{sell} at the revenue price Rvn_{elect} . The calculation is shown in the following equation.

$$LCOC = \frac{Cst_{elect} * E_{grid} - Rvn_{elect} * E_{sell}}{Q_{cool}} \quad (3.8)$$

3.5.5. Minimum environmental impact

This system should minimize the annual fossil fuel consumption and thereby reduce the environmental impact of a room air cooling system. Reducing the prime energy demand to zero would indicate no use of fossil fuels during operation. However, the tremendous amount of energy for the production of the energy supply systems are considered. This includes the photovoltaic modules, transformers and the battery storage system. The solar coverage rate should be maximized while keeping the environmental impact as low as possible. This could be done by comparing the lifetime savings of carbon equivalent emissions for the system operation Em_{op} with the additional amount of carbon equivalent emissions for manufacturing and installing n new system components Em_{sys}

3. System Design

$$\sum_{i=1}^n Em_{sys} \leq Em_{op} \quad (3.9)$$

The so called carbon accounting for the energy savings can be done by comparing the reduced energy demand $\Delta E_{dmd,grid}$ and multiplying it with a corresponding prime energy factor PEF and the carbon equivalent emissions $CO_{2,equiv}$. These emissions unify the harmfulness of various emissions sources of greenhouse gases to the harmfulness of carbon dioxide. Thereby, the overall environmental impact of a system can be evaluated with a single comparable value. The equivalent carbon emissions for new system components can be gathered through databases.

3.5.6. Thermal comfort bandwidth

The thermal comfort inside a room should be achieved by all previous systems. However, exceeding or deceeding the limits of comfort could be tolerated if the system would become otherwise economically or ecologically unfeasible. Some renewable air cooling is still better than no renewable power supply. Alternatively, an increased room air temperature to $28^{\circ}C$ or even $30^{\circ}C$ could be tolerated in residential applications. This upper set temperature limit has to be defined according to the boundaries of the cooled room. Sensible use scenarios where heat stress has to be prevented, like hospitals or high class holiday apartments, should be designed to keep the temperature within the thermal comfort area, below $26^{\circ}C$.

The set temperature is an additional boundary condition which can be combined with all previous optimization goals, as the willingness to exceed an upper temperature is highly connected with the will to save money or reduce the electric energy consumption for other reasons (such as environmental concerns).

A further possibility, to evaluate the thermal user comfort, is the radiation asymmetry. People feel uncomfortable, when the surface temperature of a wall exceeds the room air temperature by 2K. This was already shown by Fanger et al. in in 1972 [93]. A sum of all hours is made over a whole year, multiplied by the temperature difference to the upper thermal comfortable limit of $\vartheta_{air,room,max} = 26^{\circ}C$ plus 2K of tolerizeable temperature limit. This amount is calculated in $(^{\circ}*h)/a$.

$$\sum_{i=1}^{n=8760} \Delta\vartheta = \vartheta_{wall}(n) - \vartheta_{air}(n) \text{ if } \vartheta_{wall}(n) \geq \vartheta_{air}(n) + 2K \quad (3.10)$$

3.5.7. Optimization boundaries

The influencing parameters, which are defined by the user specifications, are the number of PV modules, n_{PV} , the number of batteries, n_{bat} and the volume of a possible cold water storage V_{cw} . Additionally, the price for selling $cost_{rvn}$ and buying $cost_{buy}$ electricity to/from a connected grid has a major impact on the economics of any supply system. The upper and lower boundary of each parameter is given in Table 3.3.

The number of PV modules n_{PV} is limited by the amount of available investment money, the price of the modules and the available roofspace. At least one module has to be purchased for the purpose of this thesis. The normally available roof space on a *Typology 2* building would only allow for 2 modules per room. However, the entire roof area of a single top floor apartment is assumed to be available for the maximum solar system size. This limits the number of modules to 30. The number of batteries should be varied between 1 and 11. Again, at least 1 battery should be present. 11 batteries is a reasonable amount to be stored in a shelf and controlled with a single residential available charge controller.

To evaluate the economic feasibility of a system, the boundaries of the electricity price have to be evaluated. Therefore, the price to buy electricity from the grid is varied, as well as the revenue when electricity is sold to the grid. The levelized costs of electricity $LCOE$ can be seen as lower boundary for both prices. As long as the electricity price is below this value, any alternative energetic supply system is not comparable with the reference system being connected solely to a grid. The upper boundary for the electricity price is set to 200% of the highest current electricity price which was reported to be $cst_{elect} = 26USD/kWh$ in *Oman* (see Table D.3 on page XXXI).

Table 3.3.: Design parameters for optimization.

Name	Parameter	Minimum	Maximum	Type
Number of PV modules	n_{PV}	1	30	Integer
Number of Batteries	n_{Bat}	1	11	Integer
Electricity costs	cst_{elect}	$LCOE$	$0.52 USD/kWh$	Continuous
Electricity revenue	cst_{rvn}	0	cst_{elect}	Continuous
Volume water storage	V_{strg}	$0.06m^3$	$0.3m^3$	Discrete

4. System Modeling

This chapter describes the modeling process of the previously described system components and implements the interconnection between them. Therefore, the in- and outputs from data sheets, previous studies and local boundary conditions to software programs or programming environments are defined. The overview of the information flow is shown in Figure 4.1 in the following section.

Afterwards, the realizations of the introduced system components in various tools are presented. The inputs and outputs of each sub component are highlighted. The variety of input parameters are indicated and the possible data sets for the MENA region and the selected 26 locations highlighted. The performance of newly developed components under the given boundary conditions is directly discussed to prove the usability of each part for the undertaken research. This was done for the new developed standardized load profile (cf. Section 4.5.3, p. 90), an extended battery model (cf. Section 4.5.2, p. 82), the split-unit A/C model (cf. Section 4.6.2, p. 98), the thermal activated building mass (cf. Section 4.6.5, p. 102), the electric transformer (cf. Section 4.5.2, p. 88) and the grid trading process (cf. Section 4.5.2, p. 90).

4.1. In- and outputs

The following overview in Figure 4.1 shows the input, processing tools and output data. The first software tool *Meteonorm* by *Meteotest* is used to generate generalized weather data sets for the selected locations. The generated data set can be directly exported to the simulation software *IDA ICE* by *Equa*. *IDA ICE* simulates the building energy demand and is used as well to evaluate thermal comfort and thermal stratification. Therefore, additional knowledge about the properties of the building materials and constructions, as well as about the user behavior, their demands, and the further presence of internal gains is necessary. The software will simulate the thermal energy demands according to Chapter 2, Section 2.3.3 on page 27.

The resulting load profile is used as demand side model within a created *Modelica* model. The needed weather data set from *Meteonorm* can be imported with the *NetCDF* library for *Modelica* by *J. Rädler*. Additional boundary data for performance curves and properties of system components are entered as parameter to the simulation model. Thereby, a template for all possible system set ups is created. It is a *Modelica* representation of the system in Figure 2.6 on page 26 but with a water cooler or a split-unit to supply coldness.

The boundary conditions of the systems define the final shape and properties of the resulting system set up (cf. Section 3.4, p. 51). This set up is generated with the code templating tool *CoTeTo* for *Modelica* code generation by *C. Nytsch-Geusen*. The resulting code is a *Modelica* simulation model.

This model can be used to run an optimization with *GenOpt*. The target function for the optimization process has to be defined. It is based on the optimization goals which were presented in Chapter 2, Section 3.5 on page 56. The result is the best feasible system set up for a solar powered air cooling system *SPA/CS* for the given boundaries and goal. It has to be evaluated according to all dimensions of feasibility (cf. Section 3.5, p. 56). This evaluation could be used to adopt the boundary parameters for the system simulation or optimization goals, in case other aspects, like socio-cultural prejudices, prevent a successful implementation of the suggested *SPA/CS*. Furthermore, the input parameters should be varied to determine the vulnerability of the system and determine the uncertainties of the simulated performance.

4. System Modeling

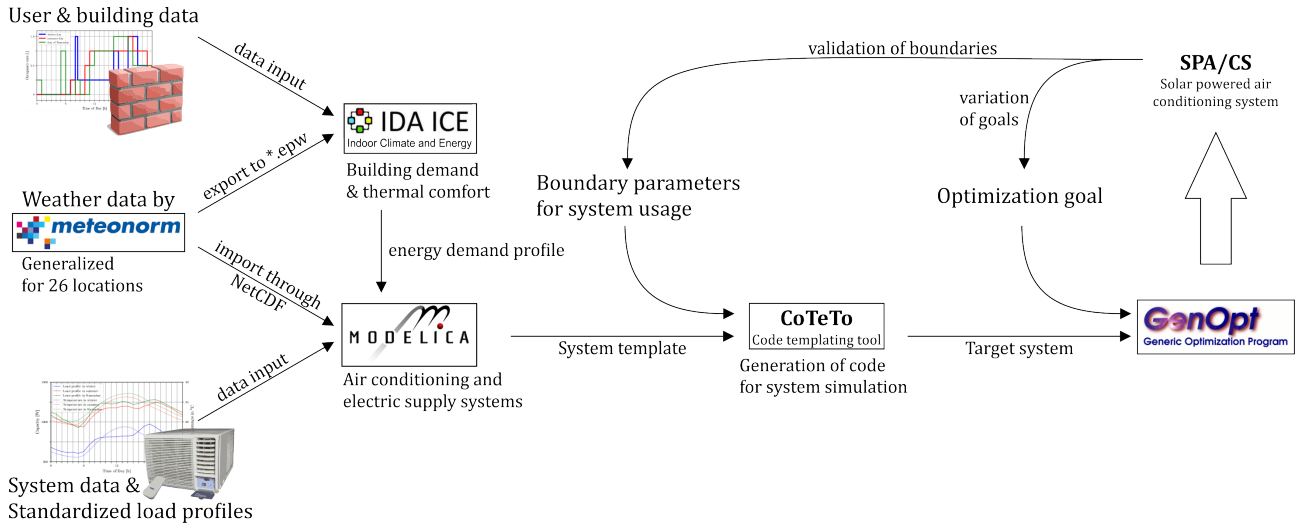


Figure 4.1.: In- and outputs to and from used modeling and simulation software.

4.2. System template

The key component is the Modelica model of the *System template*. This model includes all possible system set-ups and can be modified to work under all possible boundary conditions. The single components inside will be activated and connected according to the given boundary conditions. Its performance will be evaluated according to the desired optimization goals. The following scheme in Figure 4.2 shows the appearance of this template. The various system parts are highlighted with a red dashed box.

The *Weather data* part is the model which reads any data set containing the outside conditions, including the longitude and latitude of a location. The temperature data is needed for the photovoltaic system, the split-unit or the water cooler, and the building demand model. The radiation data is transferred to the building surfaces of the *Demand models* and the *Radiation transformation*. The later calculates the direct and diffused radiation onto an inclined surface. In particular, it calculates the radiation onto a defined photovoltaic system. This system is part of the *Electricity supply models*. Here, the radiation is transformed to direct current, according to the boundaries of a photovoltaic module. The resulting power is transferred to a battery, any chiller or a connected grid.

The chillers (a split-unit or a water cooler) are part of the thermal supply model. This could additionally contain a cold water storage or a surface cooling system which is in radiation exchange with the building *Demand models*. The cooling surface can be parameterized to work as indoor fan coil unit which is in convective heat exchange with the room air and is supplied by a cold water production system.

Each part and its components are introduced in the following sections. The input, outputs and processes in between are described for every part. The *battery* system was extended and improved throughout this thesis. The electrical *transformer* is a newly developed component which was needed to fulfill the goals of this research. The *splitUnit*, the *waterCooler* and the *coolingSurface* are new components which are created with existing models from the *Modelica* standard and the *BuildingSystems* library.

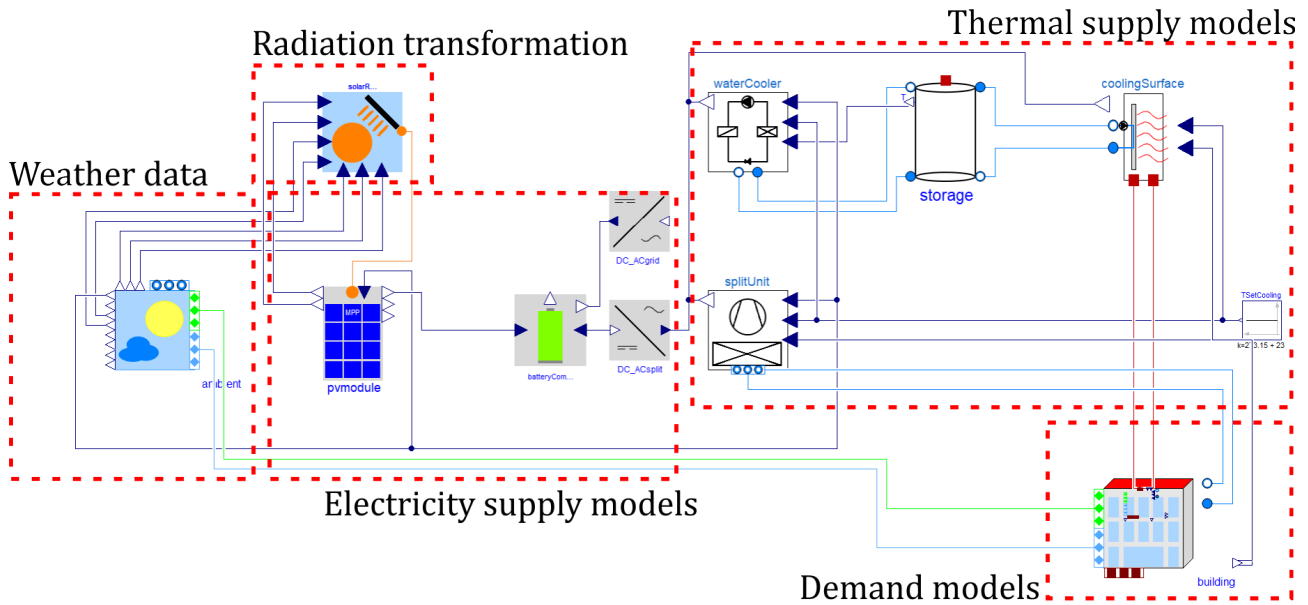


Figure 4.2.: Modelica simulation template for parametric code generation and optimization, shown in Dymola with new and existing components from the BuildingSystems library [26].

4.3. Weather data and radiation transformation

Following, the components for the reading of the ambient weather data and the transformation to a radiation onto an inclined surface are described. First, their in- and outputs are shown and their interconnections between each other and to other components are visualized. Afterwards, the location in the MENA region is concluded and described in particular for 26 cities of the region. These are Abu Dhabi (UEA), Al Hudaydah (Yemen), Alexandria (Egypt), Algiers (Algeria), Aqaba (Jordan), Asyut (Egypt), Baghdad (Iraq), Bandar Abass (Iran), Beirut (Lebanon), Casablanca (Morocco), Damascus (Syria), Doha (Qatar), Eilat (Israel), Hurghada resp. El Gouna (Egypt), Jerusalem (Israel), Kuwait City (Kuwait), Manama (Bahrain), Masirah (Oman), Riyadh (Saudi Arabia), Safawi (Jordan), Sharurah (Yemen), Tabriz (Iran), Tamarasset (Algeria), Tehran (Iran), Tripoli (Lybia), Tunis (Tunisia). The weather for Hurghada is exemplarily presented in more detail.

4.3.1. In- and outputs of the weather data models

Below in Figure 4.3, the in- and outputs, and data exchanges between the different components to handle the weather information are shown. The only user input is the selection of the location. The longitude `longitudeDeg`, the latitude `latitudeDeg` and the latitude of the locations time zone `latitudeDeg0` are provided by the weather data set and are shared between the *Ambient* and the *SolarRadiationTransformer*. Further, the *Ambient* model reads and provides the outdoor air temperature `t_amb`, and the direct and diffuse radiation `Irr_dir` and `Irr_diff`. Last but not least, the component supplies a vector for all air paths `toAirPorts` and surfaces `toSurfacePorts` between a building and the environment.

The *SolarRadiationTransformer* needs the azimuth `angleDegAzi` and the tilt angle `angleDegTil`. This data is provided by the electrical component of the *pvmodule* (cf. Section 4.5.1, p. 80). Alternatively, the model is capable of providing a calculated tilt angle if the modules are one-axis tracked. Result of the weather data and radiation transformation part is a radiation vector `radiationPort` which contains

4. System Modeling

the direct and diffuse radiation onto the given inclined surface. The *SolarRadiationTransformer* has to be used multiple times if different oriented modules are present.

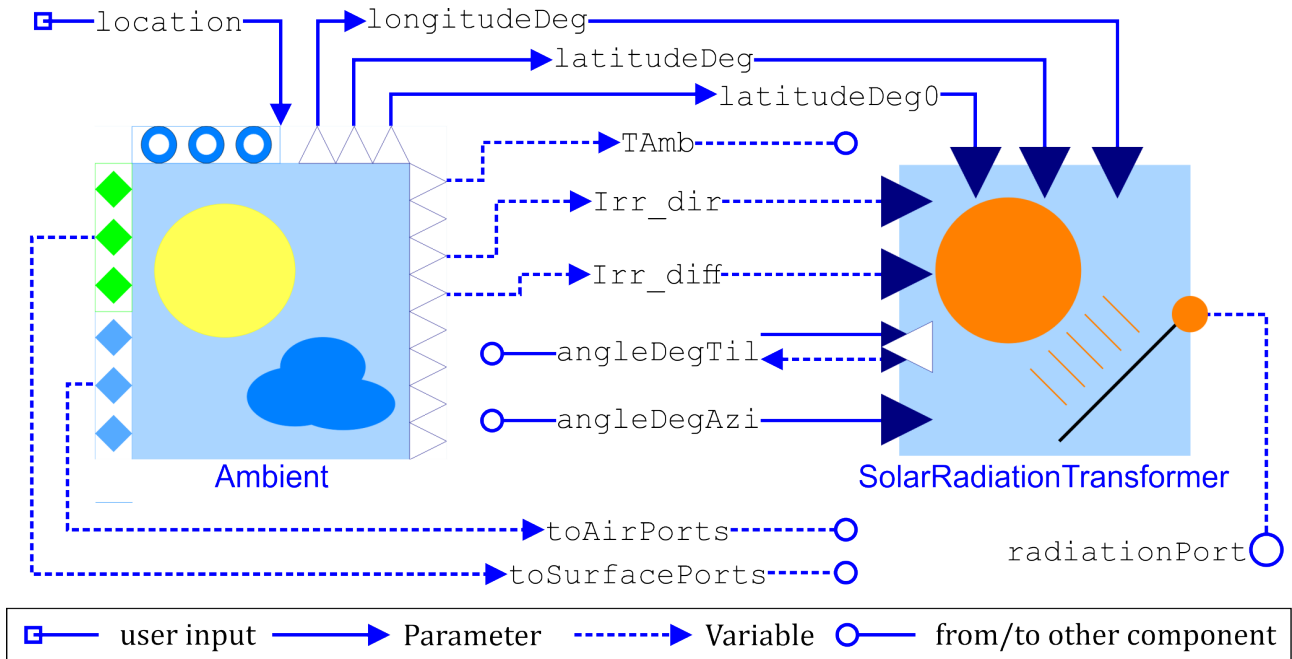


Figure 4.3.: In- and outputs to and from the ambient and the *SolarRadiationTransformation* model within Modelica.

Location: climate in the MENA region

As compared before, the dominant climate zone of the region is the *dry-hot, desert zone*. 26 cities are selected as a representation for the various climatic boundary conditions of the region and are shown in the map of the MENA region in Figure 4.4. They are selected according to the availability of data by weather stations by the World Meteorological Organization, WMO. A weather data file is generated for each location based on the provided data with the software *Meteonorm* [25]. Below, the characteristics of each outdoor climate boundary conditions of all 26 cities are compared. The official WMO station code is stated in brackets at each name.

The *Encyclopaedia Britannica* defines the tropical and subtropical climate as follows: "... cloud cover is uncommon (fewer than 30 days per year have clouds in some areas). Precipitation amounts are mostly in the range 0–25 cm, although the unreliability of precipitation is more significant than the small totals." [120]. This results into very high annual solar radiation. The overall amount of incoming radiation is shown as well in Figure 4.4. The color ranges from blue to red, indicating an annual total radiation from 1,500 kWh to 2,000 kWh (blue colored) and from 2,000 kWh to 2,500 kWh (red colored). The size of each circle indicates the overall number of cooling degree days (CDD). They are defined by the European Environment Agency as all days of the year in which the air temperatures outside are above a threshold of 22°C multiplied by the average daily temperature difference to this threshold [121, p. 18]. The calculations of the CDD are done with *BizEE* as average over the years 2015 to 2019 for each weather station.

4.3. Weather data and radiation transformation

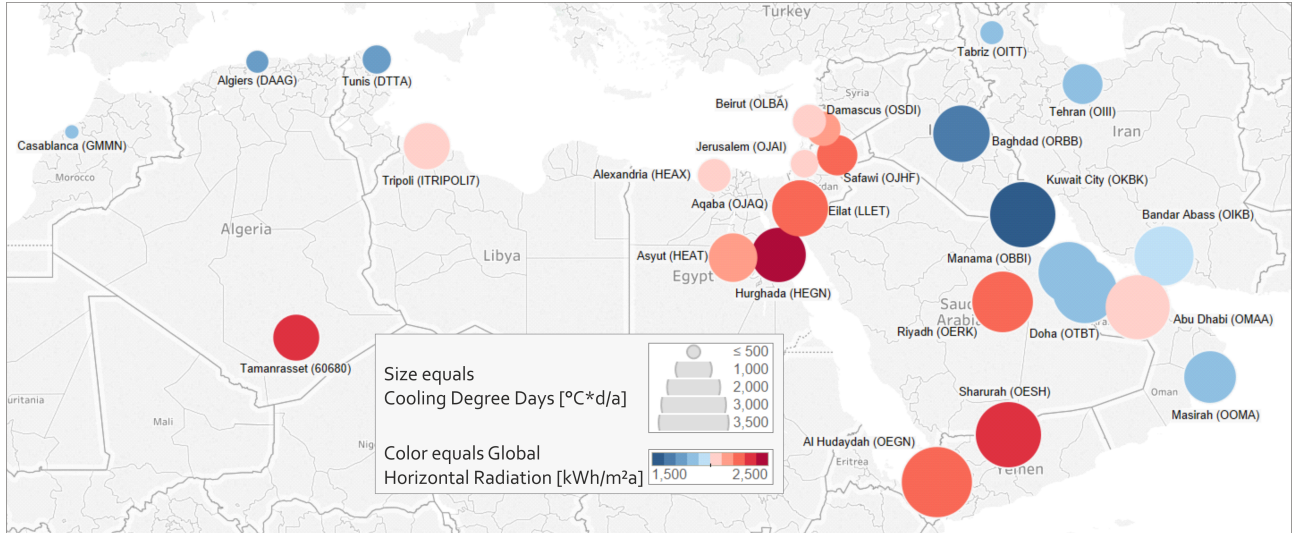


Figure 4.4.: Climatic boundary condition of each city and WMO weather station code. Radiation data generated with *Meteonorm* [25], CDD with *BizEE* [27].

In Baghdad (Iraq) and Kuwait City (Kuwait) the annual total solar radiation is only around $\dot{Q}_{solar} \sim 1,500 \text{ kWh/a}$. This is mainly caused by the near Zargos mountains in northern Iraq and along the border to Iran. However, about 2,400 (Baghdad) resp. 2,800 (Kuwait City) cooling degree days accumulate in both cities. On the one side of the MENA region, cities close to the Atlantic and Mediterranean, like Casablanca, Algiers and Tunis, have a low total global radiation and a low number of cooling degree hours. On the other side, cities close to the deserts of the Sahara or the Nefud are dominated by a high total incoming radiation. The city of Tamanrasset (Algeria), Hurghada resp. El Gouna (Egypt) and Shahrura (Saudi Arabia) have each an incoming radiation of about $\dot{Q}_{solar} \sim 2,500 \text{ kWh}$. Simultaneously, Hurghada and Shahrura have high cooling degree days: each above $2,000^\circ\text{C} \cdot \text{d/a}$.

The following Figure 4.5 shows the resulting heating and cooling degree days of the analyzed 26 cities. As previously described, each cooling degree day (CDD) counts for a day with an outdoor air temperature above $T_{ODA} > 22^\circ\text{C}$ and the temperature difference to this threshold [121, p. 19]. They are highlighted in blue. Red are the heating degree days (HDD). These are the days per year on which the temperature is below $T_{ODA} < 15.5^\circ\text{C}$ multiplied by the temperature difference of each day to this temperature [121, p. 19]. Both indicators are calculated with the software *BizEE*.

According to the *Encyclopaedia Britannica*, "temperatures are high, with monthly means in the range of 21 to 32°C. Daily temperature variations are extreme. Ranges of 35°C are not unknown when daytime maxima in excess of 40°C are followed by a rapid nocturnal temperature drop brought about by the limited capacity of the dry, cloudless desert air to emit infrared radiation to the ground to offset radiation loss from the surface at night." [120]. The cities are arranged by a rising number of CDD per year as the previous definition indicates a clear dominance of cooling demand in the MENA region.

A clear trend is visible: the more cooling degree hours occur, the less heating degree hours are present. Five of the selected cities have more HDD than CDH. Outstanding is the city of Tabriz (Iran). It has more than $HDD > 2,100 \text{ K} \cdot \text{d/a}$ due to its elevated location in the mountains. Still, there are 584 CDD present. The lowest number of CDD are found in Casablanca (Morocco) and Algiers (Algeria). However, they have a relatively low number of HDD. On the other side, there are 21 cities with a higher amount of CDD than HDD. The cities Masirah (Oman) and Al Hadaydah (Jemen) don't even have any HDD while Al Hadaydah even has the highest number of $CDD > 3,400 \text{ K} \cdot \text{d/a}$.

Worth mentioning is Tehran (Iran). There, the CDD and HDD are almost equal around $1,000 \text{ K} \cdot \text{d/a}$,

4. System Modeling

accounting for the second highest number of heating degree days. In most cities with $HDD < 100 K \cdot d/a$ no air heaters are installed. The energy demand for heating can often be satisfied by internal gains. Nevertheless, small decentralized electric heaters are often present to supply heat during seldom low temperatures.

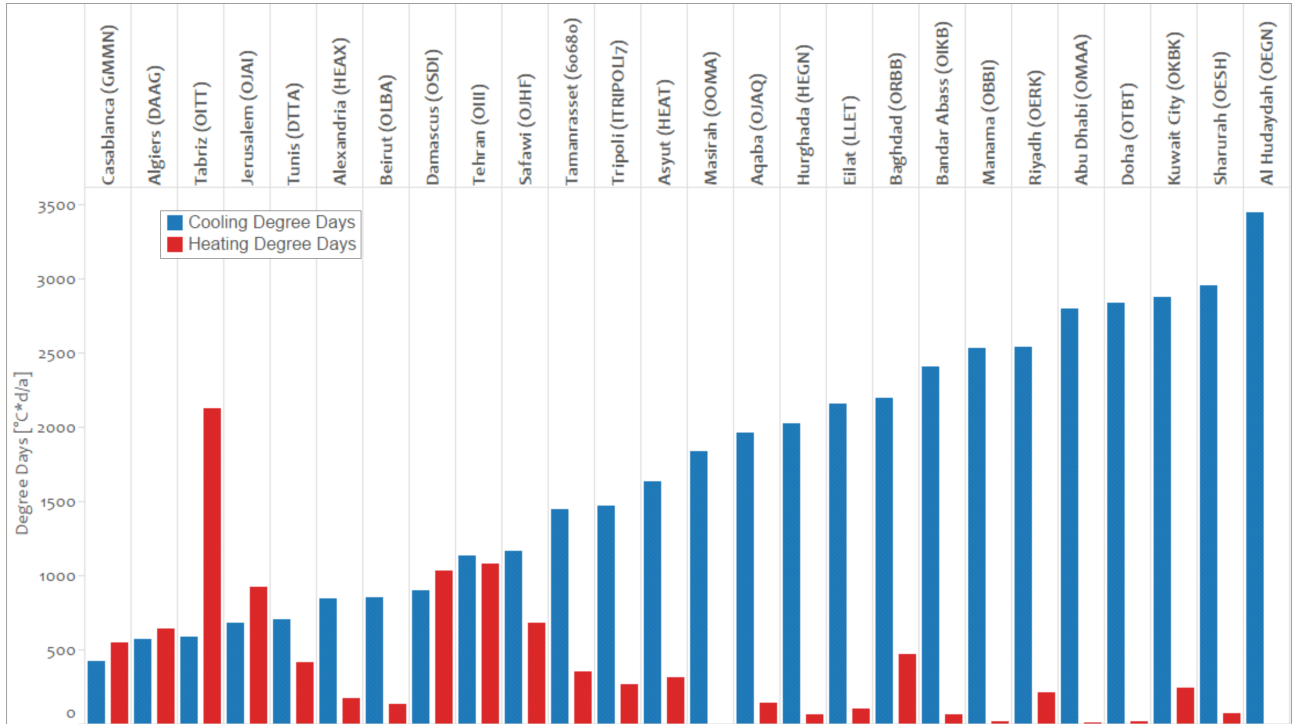


Figure 4.5.: Cooling and heating degree days per year and city, based on weather data of each weather station, calculated with BizEE [27]

Example location: data for Hurghada, Egypt

The previous described situation was observed in the Red Sea town resort El Gouna, which is a detached part of the city Hurghada (Egypt). The outside weather condition for this location are concluded in the graph in Figure 4.6. The monthly average temperature is show as red circles. The graph includes the standard deviation of the outdoor air temperature of each month and the corresponding minimum and maximum temperature in blue. Additionally, the monthly global horizontal radiation is indicated on the right y-axis and in orange.

The outdoor temperature can fall below $10^{\circ}C$ during the night time of the winter months December, January and February, but regularly reaches temperatures around $20^{\circ}C$ during the daytime. During July and August the temperature never falls below $24^{\circ}C$ and can reach up to $41^{\circ}C$ in the early afternoon. The incoming solar radiation is always above $100 kWh/(m^2 * month)$, reaching more than $200 kWh/(m^2 * month)$ in May, June, July and August. The precipitation is neglectable. The highest rainfall expectation is during May where 12mm of rain are usual. Around 7mm can be anticipated during September and October [25].

Monthly air temperatures and incoming radiation in Hurghada

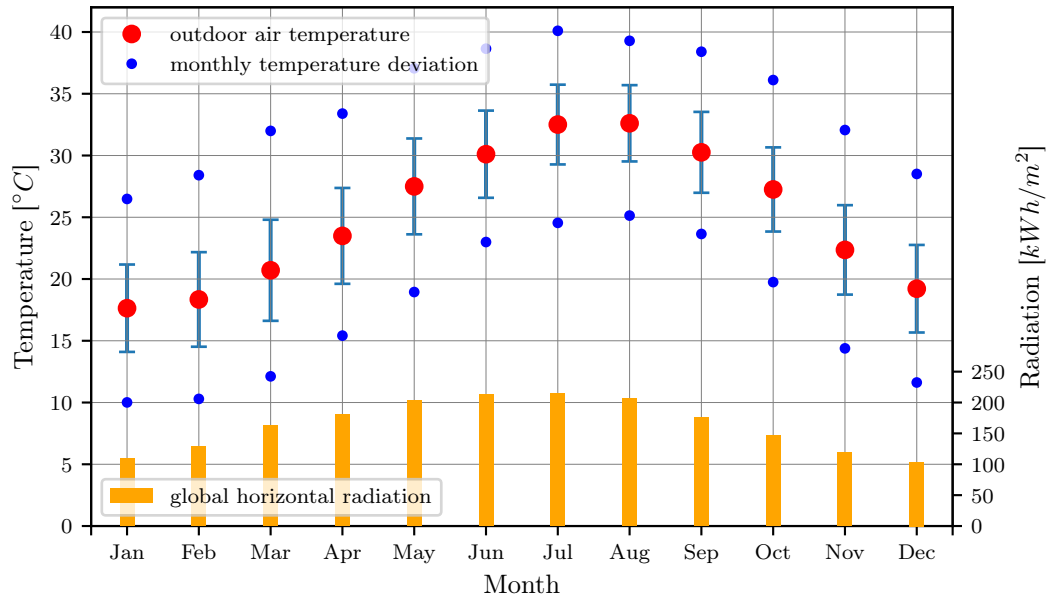


Figure 4.6.: Monthly average outdoor air temperature (red dots), its standard deviation (blue bars) and monthly maxima values (blue dots) over monthly incoming total horizontal radiation (orange bars), data generated with Meteonorm [25].

4.4. Demand models

Next, the building energy demand model and its in- and outputs are introduced. This is done for the simulation tool of *IDA ICE* and *Modelica*. The first is used for a detailed simulation to validate the results of the simplified *Modelica* model. The latter is presented as a scheme in the beginning of this subsection. Afterwards, the set points for the thermal comfort as main user behavior are defined. Further, a profile for the user presence, as main cooling energy demand trigger and additional heat source, is concluded. Last, the common physical properties of buildings in the MENA region are presented.

4.4.1. In- and outputs of the building demand model

The *Building* needs a lot of input data from other components and further values which are defined by the user. These in- and outputs are shown in Figure 4.7. Variable inputs from other components are the radiative and convective heat gains resp. losses through the `heatPortRad` and `heatPortCon`. Here, internal gains through humans or other inner sources are defined as `IntRad` and `IntCon`. The exchange to the *Ambient* environment happens through the `toAirPorts` and `toSurfacePorts` (cf. Section 4.3.1, p. 67). Additionally, the building could be connected to a controlled ventilation system. The energy exchange would happen to the supply and exhaust air ports `port_SUP_app` and `port_EHA_app`.

The building construction like the properties of the walls, windows, and the shape and orientation of the building are user defined boundaries but can be varied throughout the optimization process. For example, the thermal resistance or mass could be varied by changing the input parameter of `construction.thermal`. This value could be varied with each simulation trial to find an optimum wall thickness, the best glazing or building orientation `angleDegAziBuilding`.

Part of the demand models is as well the desired set temperature for room air cooling `TSetCooling`

4. System Modeling

which needs to be set according to the given boundary conditions by the user. The main control output of the *Building* model is the average room temperature of the zones inside the building T_{Air} .

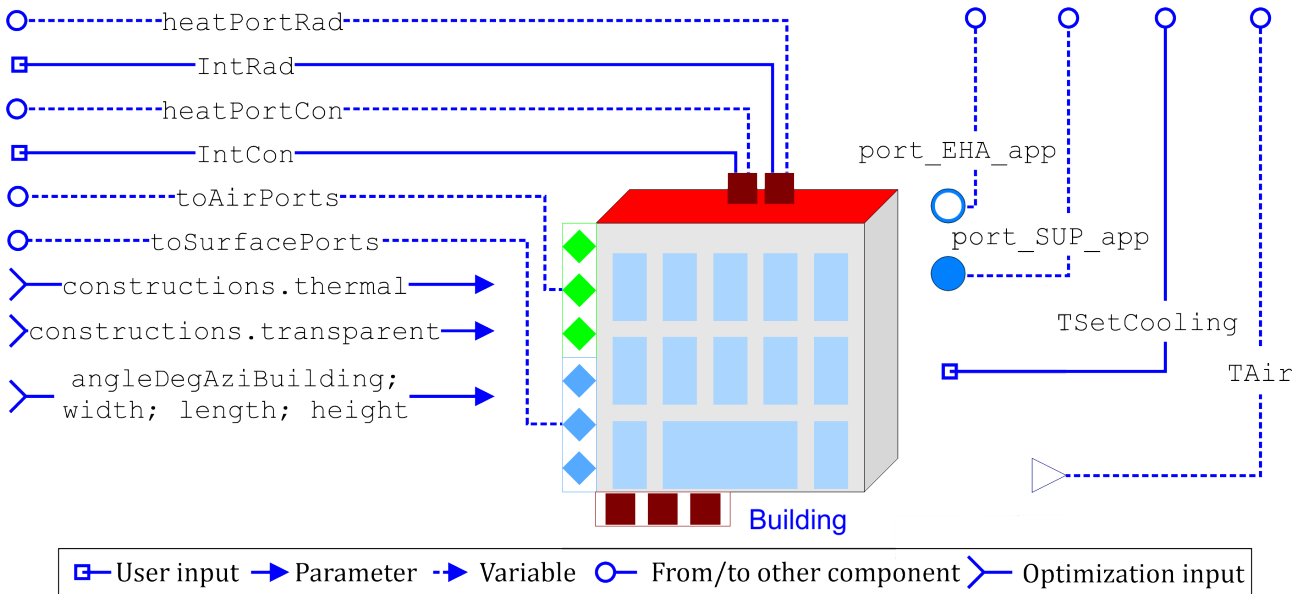


Figure 4.7.: In- and outputs to and from the building demand model within Modelica.

4.4.2. Set points - boundaries of indoor comfort

The next two subsections describe the limits of individual user comfort inside a room in the MENA region. Thereby, the limits of the operative room air temperature are needed to define the limits of thermal comfort. Further, the ventilation behavior and energy exchange with the outdoor air environment need to be generalized to perform accurate simulations.

Thermal comfort

Evaluations of user behavior of air conditioner operation shows that owners operate their air conditioning systems extensively as soon as they possess one [122]. Especially in the MENA region, ACs are operated all day long, due to low electricity prices and lack of energy saving awareness. The authors observations indicate that the cooling set temperature $T_{set,cool}$ is often set to the lowest possible temperature, which can be down to $16^{\circ}C$ (observations made in Egypt, 2012-2019). This user behavior should not be mimicked in building energy demand simulations, as the energy saving potential of adapted user behavior and increased cooling set points is well known and educated more and more around the region. Therefore, the users of an apartment should be modeled to operate their apartment according to standardized thermal comfortable indoor climate conditions. Attia et al. (2012) suggest to use a set-point for cooling of $T_{set,cooling} = 24^{\circ}C$. The ASHRAE Standard 55 (2010) defines the optimum temperature for summer times as $24.5^{\circ}C$ and $21.5^{\circ}C$ for winter times with an acceptable range of $\pm 1.5 K$ [123, p. 5] [124, p. 7]. However, further studies showed that especially in dry-hot climates the area of thermal comfort can be extended to even $28^{\circ}C$ [125, p. 6]. Therefore, the set points are placed on the outer limit of the standardized thermal comfort range at $T_{set,cool} = 26^{\circ}C$ and $T_{set,heat} = 20^{\circ}C$. A cooling or heating system is activated, as soon as the air temperature leaves these boundaries. Still, the operative room temperature (also know as "felt" room temperature) can exceed the limits of thermal comfort as result of high temperatures of the surrounding surfaces. This temperature can go up to $28^{\circ}C$ without a negative impact on the thermal comfort as shown by Akande

et al. (2010). However, these effects must be considered within the simulations to take the user comfort into account as well.

The given limits can be violated during times in which a room is not occupied. In residential applications, it is also acceptable to start the air conditioner as soon as the room is being used. However, the air temperature should be always within the thermal comfort limits in comfort oriented use cases. This includes hotel apartments or medical applications like retirement homes or hospitals [126].

Most of the used split-unit air cooling units only cool down the room air. No humidity control is applied. Condensing water, which is accumulated if the air is cooled below the dew point, is displaced directly on site.

In some cases, the heat pump of the air conditioner is reversible, meaning it can supply heating and cooling energy. In the heating case, the recirculated air is heated by the indoor unit. However, in most cases, no or additional electric heating systems are used in apartments throughout the MENA region (authors own observations).

Indoor air quality

A further important driving factor of the energy demand is the ventilation behavior or the user. Standards, like the *ANSI 62*, define lower and upper limits for fresh air supply for an acceptable indoor air, IDA, quality. These values are represented in building supply system planning handbooks like the *ASHRAE Handbook for HVAC systems*. Normally, a person needs 10 to 45 m^3/h of fresh outdoor air, ODA. This value depends on the quality of the ODA itself and the activity level of a person. For residential applications, this value can be formalized to an hourly air change rate, ACH, which describes how often the entire air of a room needs to be exchanged per hour. For residential application, this value is calculated to be $ACH = 0.5 h^{-1}$ [95] [100]. In simulation programs, this value would be translated to a constant air supply stream from the outside. This outdoor air needs to be conditioned by local A/C systems to the desired thermal comfort conditions. This volumetric flow rate is needed to remove air pollutants, odors, carbon dioxide and achieve a comfortable environment.

However, the authors own observations in the MENA region show that no window or mechanical ventilation systems are applied. The windows are always kept closed due to the bad outdoor air quality in the streets of big cities like Cairo, Egypt. Also high noise levels in the streets limit the manual ventilation efforts. A minimum air exchange is given through the leakages of the building surfaces. Windows have visible gaps and the enclosing of packaged A/C systems is poor. The windows are normally only opened during or after cooking or when the indoor air quality is reduced to a level where negative effects, like weariness, can be directly linked to the poor indoor air. It is impossible to model these leakages and find a realistic air exchange model. In this case, the fresh but unconditioned air supply can be modeled by an upper carbon dioxide level $CO_{2,max}$ inside the room. The *ANSI 55* standard recommend an upper limit of $CO_{2,max} = 1000 ppm$, as weariness and a lack of concentration become measurable at this level. "*Thus indoor CO2 concentrations of 1000 to 1200 ppm in spaces housing sedentary people is an indicator that a substantial majority of visitors entering the space will be satisfied with respect to human bioeffluents (body odor)*" [95, appendix D].

4. System Modeling

4.4.3. User presence

Another important influencing factor is the usage of the building and the corresponding presence of the users and their lighting usage. An apartment can be sub-cooled during times of no presence. Lighting is mainly done with incandescent light bulbs. Those emit additional heat inside the apartment. Shady Attia et al. (2012) defined a typical residential usage profile for Egyptian households. There, the year is divided into 3 seasons:

1. Season 1 (summer), from 1 June to 30 September
2. Season 2 (winter), from 1 October to 31 May
3. Ramadan, around 30 days from 31 August to 29 September in 2014.

Each season has 4 profiles. Two for the presence of the number of people of a typical Egyptian 4 person household and two for their lighting usage. A profile is given each for a living room and a bedroom. The resulting twelve profiles are shown in the following four graphs in Figure 4.8 and 4.9 on page 75 for the occupancy of a living resp. a bedroom and in Figure 4.10 and 4.11 on page 76 for the lighting usage in those rooms. In all diagrams, a typical winter day is represented in blue, a summer day in red and a day during Ramadan in green. Ramadan days are used as well for holidays and the weekend. The weekend is on Fridays and Saturdays due to the importance of the Friday Prayer in the entire MENA region [6].

The average Egyptian family wakes up around 7 am and assembles together for breakfast at 8 am in the living room. During Ramadan, the family meets shortly before sunrise, around 5 am, in the living room to have breakfast and continues sleeping afterwards until 8 am. In summer or during holidays, all family members will be awake and either in the living-, bedroom or outside until 12 pm. In winter times the bedroom is also used as additional living space inside the flat. All inhabitants will go to sleep at 11 pm during winter, 12 am during summer, and 1 am during Holidays or Ramadan. The lighting usage evolves according to the presence schedule. Lighting is used, as soon as a room is occupied after sunset. The latter can be established by a predictive analysis of the given user profiles.

During times of no occupancy, a room air conditioner unit could be switched off to save electricity. Alternatively, the air conditioner could be set to a maximum cooling of the room to store cooling energy in the walls and decrease the demand during times of occupancy. This could be done, while access electricity is available, no person is in the room and a cooling demand will be expected at the return of a person in the future.

Holiday apartments, e.g. hotel rooms, can be simulated with the bedroom profiles. The facilities, like the restaurant, lobby and bar of the hotel, can be assumed to substitute for the lack of a living room in most hotels. These occupancy and lighting schedule are assumed as profiles in all 25 analyzed cities of the MENA region, due to their socio-cultural similarity and lack of other available sources. Nevertheless, using the same schedules and load profile makes the comparison of the performance of all later defined system variants possible as the impact of a varying user behavior can be excluded.

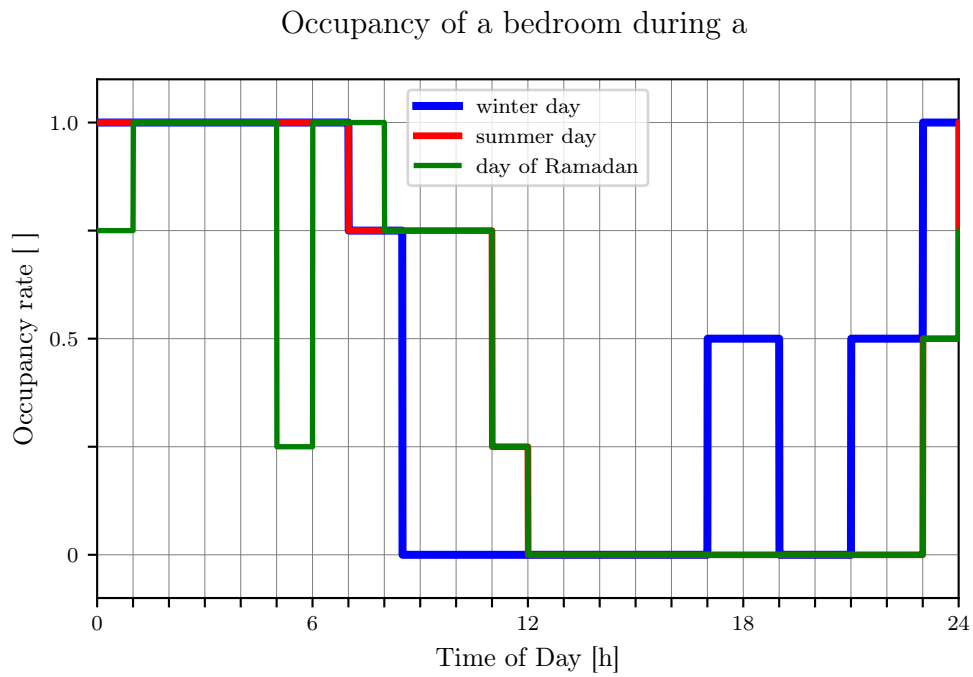


Figure 4.8.: Occupancy of a bedroom in a typical Egyptian flat [6, p. 278].

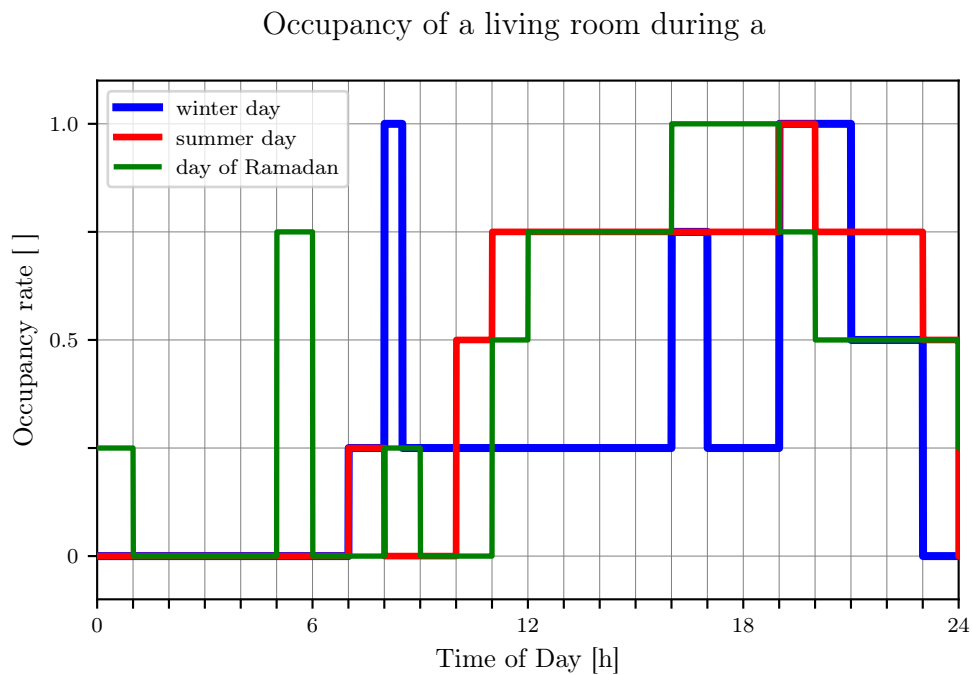


Figure 4.9.: Occupancy of a living room in a typical Egyptian flat [6, p. 278].

4. System Modeling

Lighting of a bedroom during a

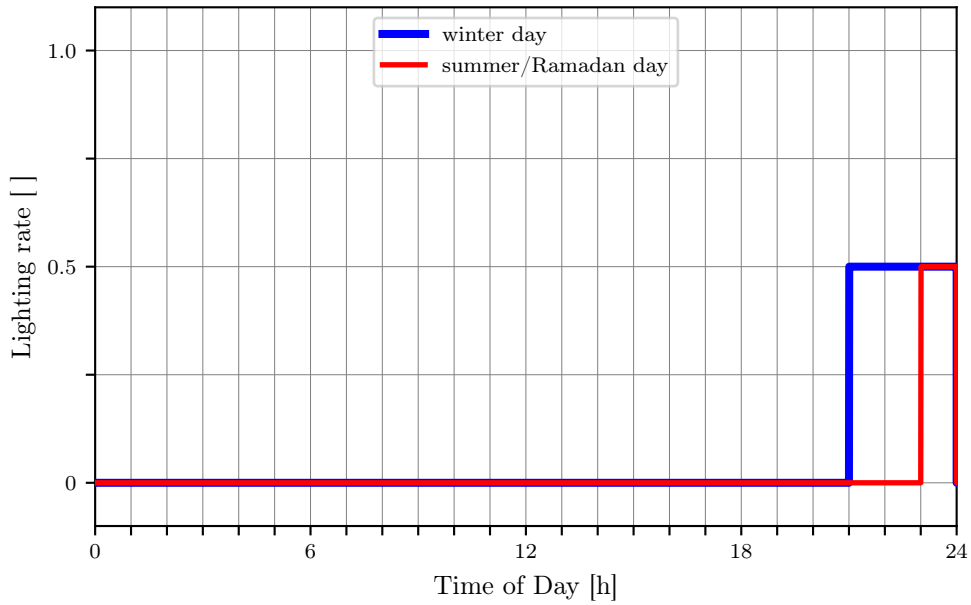


Figure 4.10.: *Lighting of a bedroom in a typical Egyptian flat [6, p. 278].*

Lighting of a living room during a

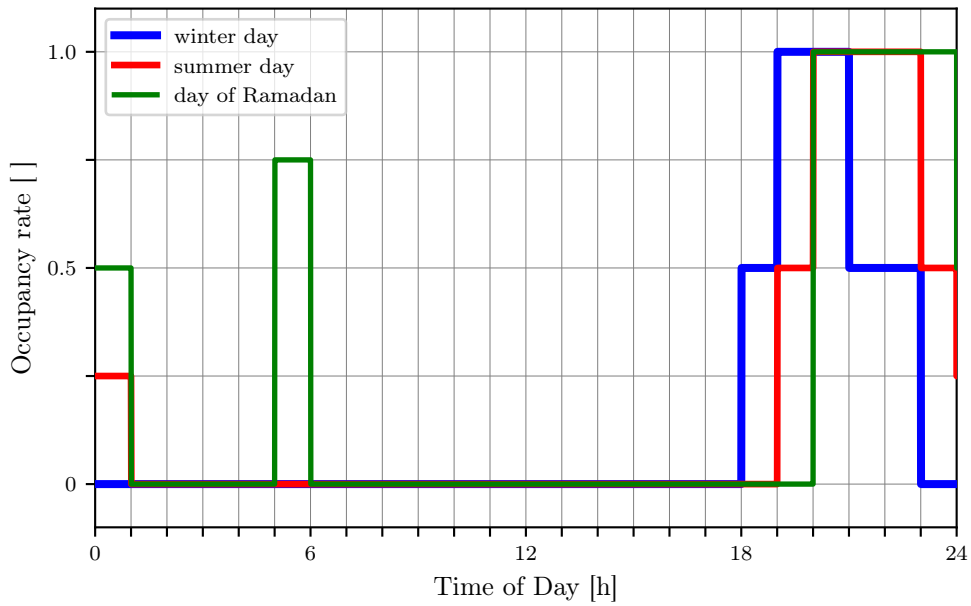


Figure 4.11.: *Lighting of a living room in a typical Egyptian flat [6, p. 278].*

4.4.4. Building properties in the MENA region

The construction type of most buildings is the same throughout the region. A skeleton construction is erected by reinforced concrete. Walls often are reduced to one or even a half brick layer [127]. The value of a building is only defined by its outer appearance and not its physical quality. However, there are two different types of used bricks. Massive clay mud bricks and vertical coring bricks. Both can be coated by a layer of lime plaster. The bricks are used for domed ceilings as well but most of the roofs are constructed equally to the construction of ceilings by reinforced concrete which often isn't coated from the downside but covered with lime sand stone tiles on the top. The thermal properties of all common used material is shown in the following Table 4.1. These values are assumed to be valid for the entire MENA region due to similarities in house constructions.

Table 4.1.: *Physical properties of common used building material.*

	Thermal Conductivity λ in W/m^2K	Density ρ in kg/m^3	Specific Heat Capacity c in J/kgK
Mud clay bricks [128]	0.90	1788	545
Vertical coring bricks [34]	0.18	765	850
Lime plaster [128]	0.70	1600	850
Lime sand stone [128]	1.00	1900	1000
Reinforced concrete [128]	0.46	2300	880

The given materials are combined to construction components like walls and ceilings. Observations of construction sites have shown that the difference between a costly building and an average multi-story apartment building is an additional layer of outer plaster and coloring or decorative panels (authors own observations in Egypt, 2012-2019). A typical housing situation in the Greater Cairo Area is shown as example in the photograph in Figure 4.12. There, the typical situation of uncoated walls is shown. Further, it can be observed that no additional efforts for roofs are made. Ceilings are kept as concrete slabs for further vertical expansion.

The U-value of a typical residential building in this region is defined to be as low as U-value = $2.5 W/m^2K$ when using typical clay mud bricks [6, p. 275]. The increased use of vertical coring bricks and a light render is reducing the U-value to at least U-value = $0.72 W/m^2K$ [34, p. 170]. The calculation of the U-value of typical construction components of Egyptian buildings are given in the following Table 4.2.

Walls and ceilings with coating can be used for apartments with a higher standard. The thickness of the brick or concrete layer has to be adopted according to the real boundary conditions of the observed apartment. Their thickness can be part of the variable boundary conditions to increase the thermal capacity and storage capabilities of the room enclosing surfaces.

4. System Modeling

Table 4.2.: *Layers and U-values of construction components.*

	thickness <i>m</i>	U-value <i>W/m²K</i>	<i>C_{area}</i> <i>kJ/m²K</i>
Base plate	0.765	1.44	1455.4
Lime sand stone	0.750		
Reinforced concrete	0.015		
Ceiling	0.200	3.33	401.1
Lime sand stone	0.030		
Reinforced concrete	0.170		
Ceiling with coating	0.201	3.32	402.4
Lime sand stone	0.030		
Reinforced concrete	0.170		
Lime plaster	0.001		
Walls	0.22	2.41	214.4
Mud clay brick	0.22		
Walls with coating	0.222	0.72	145.8
Lime plaster	0.001		
Vertical coring bricks	0.22		
Lime plaster	0.001		



Figure 4.12.: *Residential buildings in Giza (Abd El Latif Street on 25 April 2015).*

Last but not least, the window properties are given in the following Table 4.3. They are based on a typical residential apartment in Egypt.

The construction is valid for both, rural and urban applications. The only difference between both installation situations is the frame fraction. In rural areas the windows include a smaller section which can be opened separately but is protected by a mosquito net. This additional feature increases the needed wooden construction around the glazed area.

Table 4.3.: *Window properties for a typical building [34, p. 170]*

	Symbol	Value	Unit
Thermal transmittance	U-value	5.8	W/m^2K
Solar Heat Gain Coefficient	g	0.85	
Solar transmittance	ST	0.83	
Visible Transmittance	T _{vis}	0.9	
Internal emissivity	e_{int}	0.837	
External emissivity	e_{ext}	0.837	
Frame fraction urban/rural		0.4/0.6	
Frame thermal transmittance	U-value	2.0	W/m^2K

4.5. Electricity supply system

The following overview in Figure 4.13 shows the in- and outputs of the electrical supply models. The *PVmodule* contains and processes all information of the photovoltaic system. Therefore, a database with all the relevant module data `pVModuleData` must be supplied. The optimization algorithm can select different modules and should decide how many modules have to be installed.

The main input to the PV system is the `radiationPort` which gets the direct and diffuse radiation from the *SolarRadiationTransformer* (cf. Figure 4.3, p. 68). For this calculation, the azimuth `angleDegAzi` and tilt angle `angleDegTil` are given as user input. These values can be optimized by the optimization algorithm as well. Another option would be the one axis tracking. In this case, the tilt angle is supplied by the *SolarRadiationTransformer*. The *PVmodule* will calculate the resulting power, based on a 2-diode model and with a maximum power point tracking MPP. This means that the modules will be operated in the point where the product of the voltage U and current I is the highest.

The *Battery* is connected to this power supply. Here, also the user has to specify a certain battery or the algorithm could select the type and amount. This will define all needed boundary parameters through the `batteryData`. The integrated charging logic will take care of the power supply to the battery, based on its state of charge `SOC`. Any electrical load `PLoad` is connected through a DC/AC transformer *DCACtoSplit*. In case of this research, this load is the electricity demand `P_Split` of the *splitUnit*. The charge controller inside the *Battery* component will automatically supply electricity from the grid in case the battery is not sufficiently charged and no solar power is supplied. The efficiency of the transformer is specified by its nominal capacity `P_nom` and its highest efficiency η_{max} . The calculated efficiency curve is presented in Section 2.3.5 on page 45.

Also, the excess electricity, which could be supplied to a connected grid or the corresponding household, is calculated inside the *Battery* component. Electricity can be used for other purposes, if the output of the photovoltaic system is bigger than the sum of the connected load of the split-unit and the charging power to the battery.

The *DCACtoGrid* component is calculating the transformer losses equally to the *DCACtoSplit* component. However, here a standard load profile `SLP` is needed to evaluate how much electricity can be used on side and how much has to be sold to the grid.

4. System Modeling

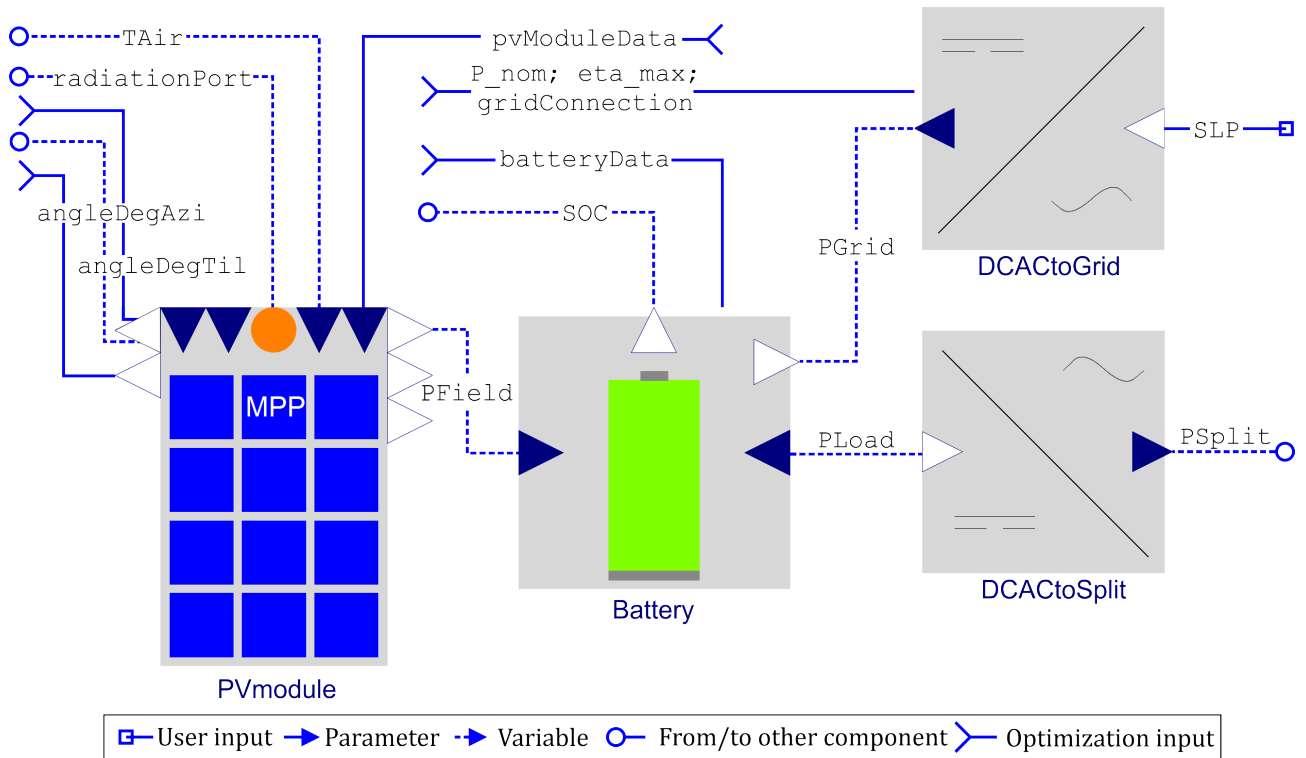


Figure 4.13.: In- and outputs to and from the entire electrical system models and graphical representation in Modelica.

4.5.1. Photovoltaic system model

This section shows the modeling and implementation of the photovoltaic model. Therefore, the general introduction to the used PV modules is given, which is followed by the concrete implementation with *Modelica*.

Overview

The following overview in Figure 4.14 shows the data in- and outputs of the *PVmodules* component. Many of the needed parameters are available through manufacturers data sheets. These are the dimensions width and height, the short circuit current I_{k0} , the open circuit voltage U_{10} , the number of cells in series and parallel n_{CelSer} and n_{CelPar} and the nominal power output $P_{EL_nominal}$ and the temperature coefficients for the current and voltage τ_{Ik0} and τ_{U10} . The band gap E_g is dependent on the used cell material.

Further, current over voltage U_I curves are needed to determine further parameters for the calculation with the 2-diode model (cf. Section 2.3.5, p. 39). The curves are provided from the manufacturer. However, they can deviate between specific modules of the same type. Hence, measured curves for single modules should be used to create exact models of existing panels.

The further in- and outputs are shown in the following figure and where briefly described in the previous section. The total number of used modules for the PV system is the product of the number of parallel n_{ModPar} and serial n_{ModSer} connected cells. The arrangement in parallel and serial strings has no effect on the calculated power output P_{Field} but the resulting voltage U_{Field} and I_{Field} .

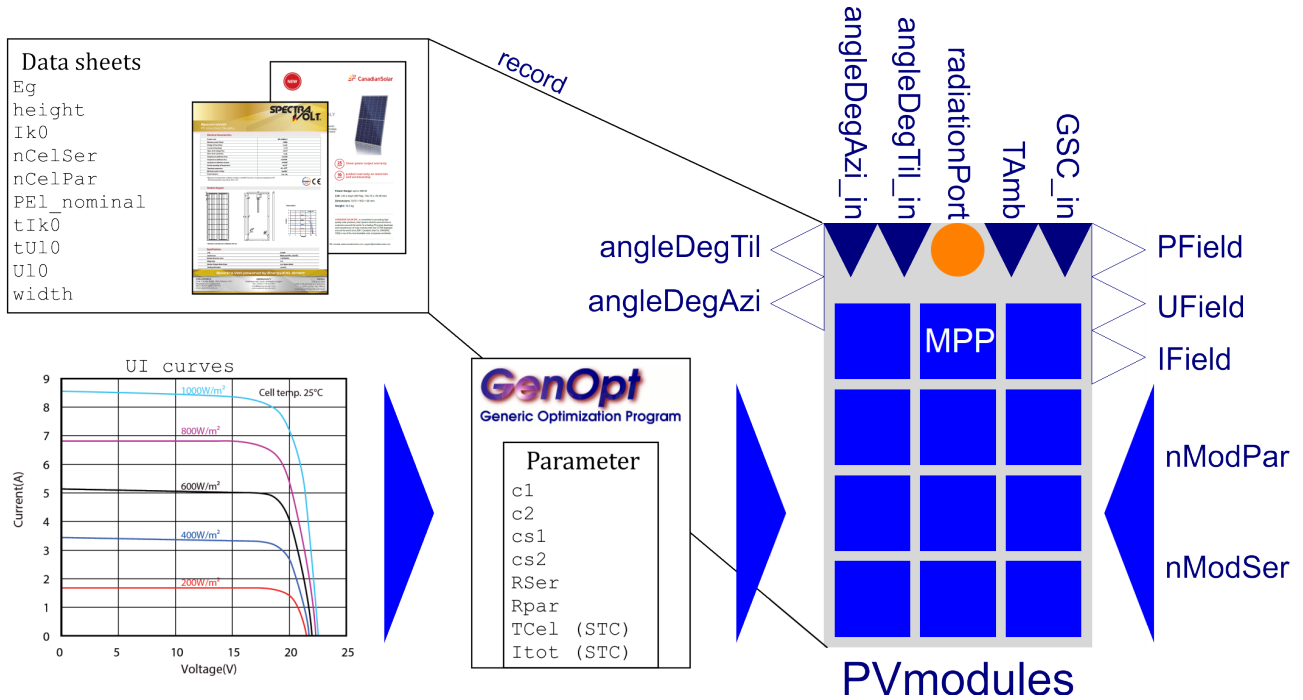


Figure 4.14.: In- and outputs to and from the PV_{module} system component and graphical representation in *Modelica*.

PV module parameter acquisition

The main data source are manufacturers data sheets. They offer a more or less full set of needed information. Missing parameters can be assumed in adequate accuracy, based on the module type and cell connections. The acquired parameters are concluded in the following table.

Table 4.4.: Given and determined parameters for two different PV module types.

Parameter Name	Parameter	Symbol	Unit	TSM-220PC05	SPV-100M36S
Peak power output	PEL_nominal	$P_{nom,max}$	W	230	100
Open circuit voltage	U10	U_{OC}	V	8.26	22.74
Short circuit voltage	Ik0	I_{SC}	A	37.0	5.9
Width	width	l	m	0.992	0.545
Height	height	h	m	1.650	1.195
Current temp. coefficient	tIk0	t_{Ik0}	$\%/K$	4.13	1.659
Voltage temp. coefficient	tU10	t_{U10}	$\%/K$	-0.1295	-0.060
1st coefficient IPho	c1	c_1	m^2/V	0.000613641954555	0.005493984
2nd coefficient IPho	c2	c_2	$m^2/(kV \cdot K)$	0.000139642340029	0.00033398822
1st coefficient ISat1	cs1	cs_1	A/K^3	0.113159968903	1.4269971
2nd coefficient ISat2	cs2	cs_2	A/K^5	0.000640010305878	0.000504
Serial resistance	Rser	R_{ser}	Ω	0.0309282623867	0.006629844
Parallel resistance	Rpar	R_{par}	Ω	9.21908843302	935.8011

Further, some databases, like the one which is integrated in *Polysun*, offer additional information like the parameters which are needed for the 2-diode model. P. Balekai (2018) developed in his Master thesis a method to undertake a square root parameter fitting with *Modelica* and *GenOpt* [103] to

4. System Modeling

determine the missing values. There, he analyzed and determined the data set for the *TSM230PC05* from *Trina Solar* [129]. His method was used in this research to determine the missing parameter for the *100M36S* modules from *SpectraVolt* [130].

4.5.2. Battery systems

The electric battery storage system, the electric transformer and the electricity trading with the grid are described in the following section. The additional energy demand from a connected grid is directly modeled within the battery storage system. In this way, the connected loads are always supplied with electricity, even when a connected battery is empty and no additional charging power is applied. However, the battery can only supply direct current electric energy. Connected alternating current systems, like the grid connection, have to be connected through an DC/AC transformer.

The presented data is already published within the aforementioned *Proceedings of IBPSA BuildingSimulation 2019* as case study to the described method to extend the *Kinetic Battery Model*[104]

Overview

The electric storage model consist of a model of an electro-chemical battery storage and the possibility to exchange electricity with a connected grid. All processes are programmed into an existing battery model. This model is based on a simplified battery model of the *BuildingSystems* library, written in *Modelica* [26]. The model calculates the state of a battery based on charging and discharging powers. The electro-chemical charging and discharging process is extended by modifying the *Kinetic Battery Model* as described in subsection 2.3.5, page 41. The electricity exchange process is highlighted in subsection 2.3.5, page 46. The inputs and sources are shown as an overview in the following Figure 4.15. There, inputs, processes, and outputs of the electric storage model are given as an overview.

The battery is defined by manufacturer *data sheets*. They are entered as records and can be selected within the model. The record defines all needed and battery type dependent parameters, which are needed for the simulation. The acquisition is described in table 4.5, on page 85. Furthermore, the battery needs a connected charging and discharging source, *PCharge* and *PLoad*. Both values can be zero but need to be connected to a valid electricity source/sink. The state of charge (*SOC*), the batteries voltage (*UBattery*), and the current which is drawn or supplied to the battery (*IBattery*) is calculated according to the methodology described in subsection 2.3.5, on page 41. The grid connection is modeled into the battery model. Electricity from a grid is automatically supplied to an occurring electricity demand if the *SOC* falls below the given minimum charge level *SOC_min* and while $P_{Net} < 0$. The accumulated charged, discharged and grid electricity is calculated through the model.

The electricity, supplied by a battery, is direct current (DC). It has to be transformed to alternating current (AC), for the use in conventional air cooling systems as they are usually operated with alternating current. This is done with the component of an electric DC/AC transformer. It is connected through the *PLoad* connector and the *DCACTrafo_load*. This transformer supplies the needed power to the connected devices. The efficiency is dependent on the currently applied load as a dependency of the nominal load.

The electricity supplied and taken from the grid is also alternating current. Its frequency has to be synchronized when the electricity is supplied through an DC/AC transformer to the grid. The alternating current of the grid has to be transformed to direct current, if the grid should be also used to charge the battery. This is optionally done through the *PGrid* connector of the battery model which is connected to the *P_1* connection of a *DCACTrafo_grid*. The discharge to and the supply from the grid can be done within one component.

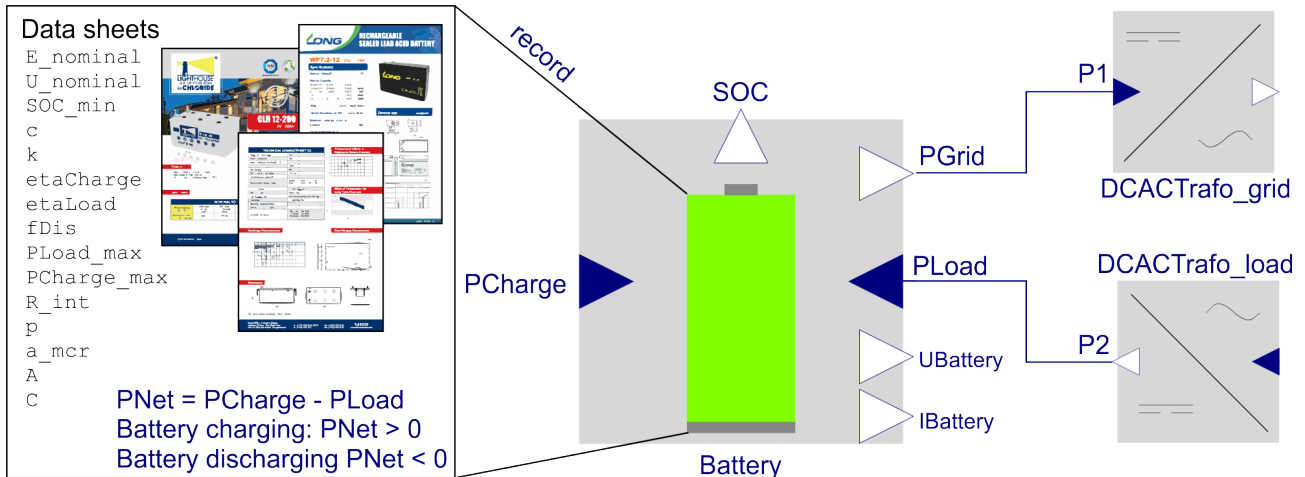


Figure 4.15.: Graphical representation of the electric battery component in Modelica.

Battery parameter acquisition

Various parameters, determined by data sheets, are needed for the simulation. The *BuildingSystems* library already contains some battery data sets. For the purpose of this thesis, the data records are extended with a small and a medium scale lead acid battery. The small scale battery is a *Long WP7.2-12* battery with a nominal capacity of $E_{nom} = 7.2 \text{ Ah} (\equiv 86.4 \text{ Wh at } 12 \text{ V})$ [131]. The medium scale battery is a *Chloride CLH 12-200* battery with a nominal capacity of $E_{nom} = 200 \text{ Ah} (\equiv 2400 \text{ Wh at } 12 \text{ V})$ [132]. The parameters of each record set are shown in figure 4.15. The corresponding values of each battery are given in table 4.5 on page 85.

The nominal voltage U_{nom} is directly stated on the battery's name plates. The nominal capacity E_{nom} in J can be obtained by combining the stated nominal capacity with the nominal voltage.

The minimum state of charges SOC_{min} limits the lower discharge limit of the battery. Any further occurring load has to be satisfied by other sources, e.g. a connected PV field or electricity grid. The minimum SOC can be gathered by cycle service life diagrams. The depth of discharge of each charging/discharging cycle should be limited as this is the main influencing factor. The battery should at least last 700 cycles in terms of building energy supply systems with a connected PV field. In this case, the battery goes through a daily charging and discharging cycle. Most probably, 700 cycles will be completed in less than 2 years. The SOC_{min} is strongly dependent on the battery type and should be limited to $SOC_{min} = 0.6$ for lead acid batteries.

The rate $c = 0.315$, to determine the size of the available and bound energy well, E_{ava} and E_{bou} , and the constriction $k = 1.24/s$ to define the rate of energy exchange between both wells, are gained from the *Polysun*-software database. They are similar for each battery type like lead acid batteries. This accounts as well for the charge and discharge efficiency, $\eta_{charge} = 0.92736$ and $\eta_{load} = 0.92736$, of the battery. The *Polysun* database contains the so called round trip efficiency. Its square root can be assumed to be the charge and discharge efficiency.

The self discharge rate $f_{dis} = 1.27e^{-8}/s$ resp. $f_{dis} = 1.65e^{-8}/s$ is usually stated on battery data sheets. Often it is given as "Battery retention" [131], indicating a SOC after a certain time period. This value needs to be transformed to a unit of s^{-1} .

The maximum charge and discharge capacities, $P_{charge,max}$ and $P_{load,max}$ are normally given in W . They need to be transformed to A by using the nominal voltage U_{nom} . Also, the internal resistance R_{int} is given in data sheets. Their dimension is mainly dependent on the battery type and its size.

The *Peukert* p coefficient can be calculated with Equation 2.42 on page 43. Therefore, two capacities and their corresponding discharging times are needed. These values are given by most data sheets. The values for the newly implemented lead acid batteries are $p = 1.08$ resp. $p = 1.17$

4. System Modeling

The maximum charge rate a_{mcr} defines how the battery is charged at high SOC . Normally, most types of batteries can be charged to approximately 80% with the maximum charging power $P_{charge,max}$. Afterwards, the charging power should be reduced to prevent damages to the battery. Real charge controllers do this by limiting the maximum voltage. When this voltage is reached, the charged current is gradually reduced to keep the voltage constant until a $SOC = 1$ is reached. The limit of Equation 2.38 on page 43 mimics this behavior at $a_{mcr} = 2.6e^{-4} W/J$.

Many data sheets contain discharge curves for various discharge rates. These curves are needed to determine the parameters A and C . The determination for both batteries is shown in figure 4.16. For calculating the parameters, the discharge curves for the nominal capacity, the $C20$ -rate, is chosen. This curve is highlighted in both diagrams in figure 4.16 in red.

A and C indicate the slope at the beginning and end of discharging a battery. A represents the slope at the beginning of a discharging process. The best results were obtained by determination of the slope in voltage drop between a SOC from 1.0 to 0.5. This area is highlighted in both diagrams in bright blue. The area, marked in bright red, is used to determine the parameter C . It corresponds to the slope between a SOC of 0.2 to 0.05. The resulting slopes of both batteries for both parameters are highlighted in blue.

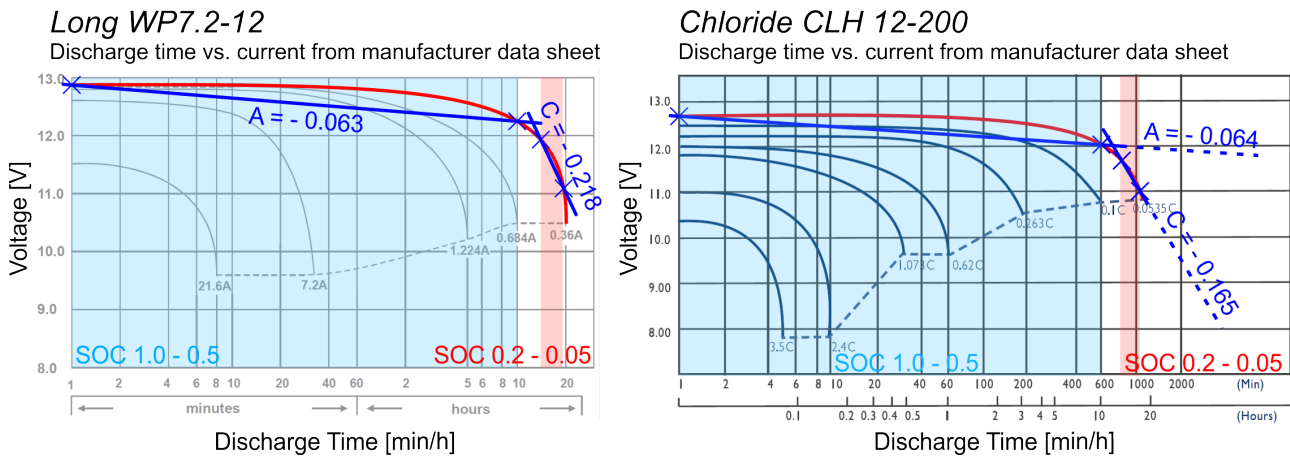


Figure 4.16.: Terminal voltage of two different batteries over time at various discharging currents, $C20$ -rate in red, resulting slope parameter in blue

Battery modeling in Modelica

The whole battery is modeled with the programming language *Modelica*. The model is created according to the methodology described in chapter 2.3.5, page 41. The names of each variable or parameter and their corresponding physical value are stated in the previous table 4.5. The exact code is presented in listing E.1, Appendix page XXXV and contains the calculation method for the basic parameters of the battery simulation. The variables h_1 and h_2 are helping variables, as shown in Figure 2.13 on page 42, and are not described in table 4.5. They are needed in further modeling to simulate the energy flow between the available energy E_{Ava} and bound energy E_{Bou} . The current energy E within the battery is calculated as sum of both energies. The state of charge SOC describes the current energy bound in battery in relation to its nominal capacity $E_{nominal}$. P_{Net} is needed to determine, if the battery is being charged or discharged.

Further, $P_{ChargeEff}$ is limited by the *BuildinSystem*-function *smoothLimit*. This function is used to smoothly fade towards an upper and lower limit and also prevents sudden and discrete changes of a state and thereby preventing an increase simulation time. Its lower limit is 0.0 as a negative charging would be a discharging process. This is modeled with a different equation. The upper limit of charg-

Table 4.5.: Parameters in data record for two newly introduced lead acid batteries

Parameter	Symbol	Name	Unit	Value of WP7.2-12	Values of CLH 12-200
Nominal Voltage	U_{nom}	U_nominal	V	12	12
Rated capacity	E_{nom}	E_nominal	J	311,040	8,640,000
minimum State of Charge	SOC_{min}	SOC_min		0.6	0.6
Available to bound energy rate	c	c		0.315	0.315
Constriction	k	k	1/s	1.24	1.24
Charge efficiency	η_{charge}	etaCharge		0.92736	0.92736
Discharge efficiency	η_{load}	etaLoad		0.92736	0.92736
Self discharge rate	f_{dis}	fDis	1/s	1.27e-8	1.65e-8
Maximum discharge capacity	$P_{load,max}$	PLoad_max	W	1296	8400
Maximum charge capacity	$P_{charge,max}$	PCharge_max	W	25.9	336.0
Internal Resistance	R_{int}	R_int	Ω	0.022	0.0027
Peukert coefficient	p	p		1.08	1.17
Maximum charge rate	a_{mcr}	a_mcr	W/J	2.6e-4	2.6e-4
Slope at high SOCs	A	A		-0.063	-0.064
Slope at low SOCs	C	C		-0.218	-0.165

ing power is defined by a further `smoothLimit`-function. It limits the overall charging power to the maximum allowed power `P_ChargeMax` which is determined by manufacturer data sheets. Further, it is decreased close to the nominal capacity of the battery. `PCharge_max` which was presented in Equation 2.39 on page 43.

The battery model includes an equation to model the exchange with electricity taken and transferred to a connected grid, `PGrid`. It is positive while electricity is taken from the grid and negative while electricity is supplied to the grid. `PGrid` is the sum of the difference of the delta between net power `PNet` and the incoming charging power `PLoad` and the delta between net power and applied discharging power `PLoad`. Both terms are smoothed with the help of a `tanh` function close to the transition time between supplying of or taking electricity from the grid.

For time period based comparisons, like annual energy analysis, the overall charged and discharged electricity is summed to `E_charged` resp. `E_discharged`.

This partial battery model is extended to a simple, on the one side, and a more complex battery model, on the other side. All equations and variables of the previous described partial model are valid. The simple model basically sums up the charged and discharged power and concludes the balance based on the nominal capacity. A dependency on the current battery capacity, based on the current discharge rate is not considered. The extension towards a more complex model is shown in listing E.2. `EAv` and `EBou` have to be determined to calculate the current energy `E` which is present in the battery. The effective energy which is charged to the battery `PChargeEff` is calculated by Equation 2.38, page 43. This function is combined with a tangens hyperbolicus `tanh()` to allow a smooth transition when the battery is fully discharged. Due to the self discharge the simulation time would drastically increase when the battery is fully charged. This modeling method was developed by Jörg Rädler in 2010 [133] to prevent sudden and discrete events.

`E_current` is needed to adopt the drawn power from the battery according to its current capacity

4. System Modeling

based on an actual applied discharging current. This capacity factor CF was presented in Equation 2.40 on page 43. E_{current} is calculated according to Equation 2.41. This capacity is limited with the `smoothLimit`-function to 0, at infinite high discharge rates, or to a maximum capacity of E_{max} , as the capacity would increase to infinity at low discharge currents. The maximum capacity E_{max} is based on the $C100$ -rate (also known as discharging current to discharge within 100 hours) and is usually given through data sheets as well. The resulting ratio between the nominal and current capacity is applied to P_{LoadAva} and P_{LoadBou} . Both discharging powers are limited similar to $P_{\text{ChargeEff}}$ with a `smoothLimit`. Both loads will be reduced smoothly to 0.0 around the minimum state of charge SOC_{min} with the help of the `tanh()`-function. Furthermore, they are limited to the maximum discharge power $P_{\text{Load}_{\text{max}}}$ which is acquired from data sheets. Both values, P_{LoadAva} and P_{LoadBou} are combined as a sum to P_{LoadEff} . This ensures that the available energy of the battery is discharged before the bound energy is used to satisfy the power being discharged.

Battery simulation performance

The graphs below compare the performance of the modeled battery with the before stated parameters (see Table 4.5) in comparison to the given discharge curves of the manufacturers data sheets. The first graph in Figure 4.17, page 86, shows the terminal voltage during discharging processes of the small scale lead acid battery *Long WP7.2-12*. The second graph in Figure 4.18, page 87, shows discharging processes of the *Chloride CLH12-200* battery. Both graphs compare the simulated voltage of the modeled battery *UBattery* (highlighted in blue) versus the terminal voltage given by manufacturers' discharging curves. The continuous red and blue line represent in both graphs the discharging process at a $1C$ -rate. This rate is equivalent to a constant drawn current I in $[A]$ which is equal to the nominal charge quantity $\text{Charge}_{\text{nom}}$ in $[Ah]$. The dashed lines represent the discharge curves at a $0.1C$ -rate. These curves represent a voltage drop over time at a constant discharge current I which will discharge the battery in 10 hours. Equivalent, the voltage drop curves for the $0.05C$ -rate represent a discharging with a constant voltage to fully discharge the battery in 20 hours. The result is the nominal charge quantity. The corresponding curves are highlighted with filled circles.

The average difference between the given and simulated voltage is $\text{RMSD}_{\text{WP7},1C,100\%} = 0.957 \text{ V}$. At a discharging at the $0.1C$ -rate, the corresponding deviation is only $\text{RMSD}_{\text{WP7},0.1C,100\%} = 0.123 \text{ V}$. This value increases to $\text{RMSD}_{\text{WP7},0.05C,100\%} = 0.305 \text{ V}$ while discharging at a $0.05C$ -rate.

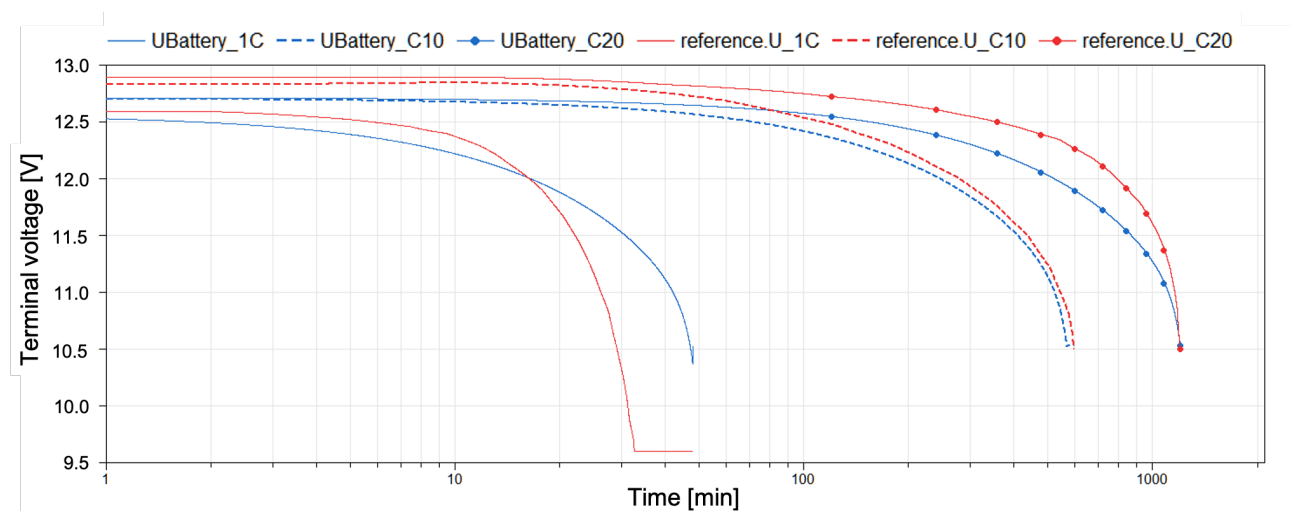


Figure 4.17.: Terminal voltage of simulation vs. data sheet during $1C$, $C10$, and $C20$ discharging of *Long WP7.2-12* battery

The average deviation when fully discharging both batteries with a $1C$, $0.1C$, or $0.05C$ -rate is 0.47 V (3.92% of U_{nom}). The deviation at the $0.05C$ -rate alone is 0.35 V (2.92%). The difference can be drastically reduced, when only calculating the deviation for a $DoD = 80\%$. This would reduce the average the RMSD to 0.03 V (0.25%).

Within all sets of comparative simulations, the root mean square deviation, $RMSD$ has been calculated for the resulting difference in given and simulated voltage drop. The average deviations of the simulated and given Voltages are compared in Figure 4.19 for the 3 selected discharging rates.

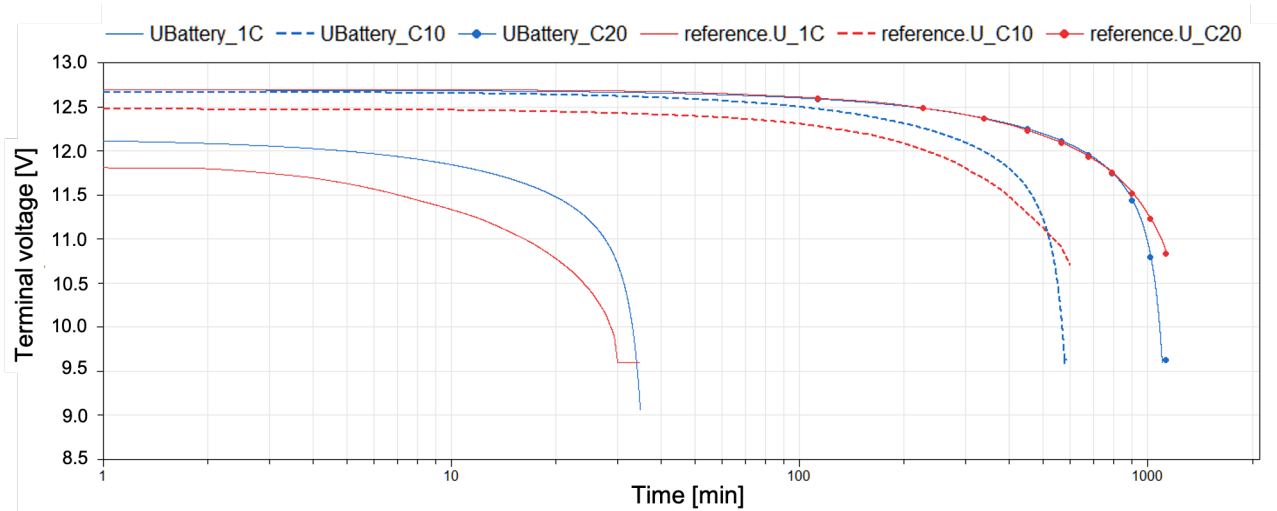


Figure 4.18.: Terminal voltage of simulation vs. data sheet during $1C$, $C10$, and $C20$ discharging of Chloride $CLH12-200$ battery

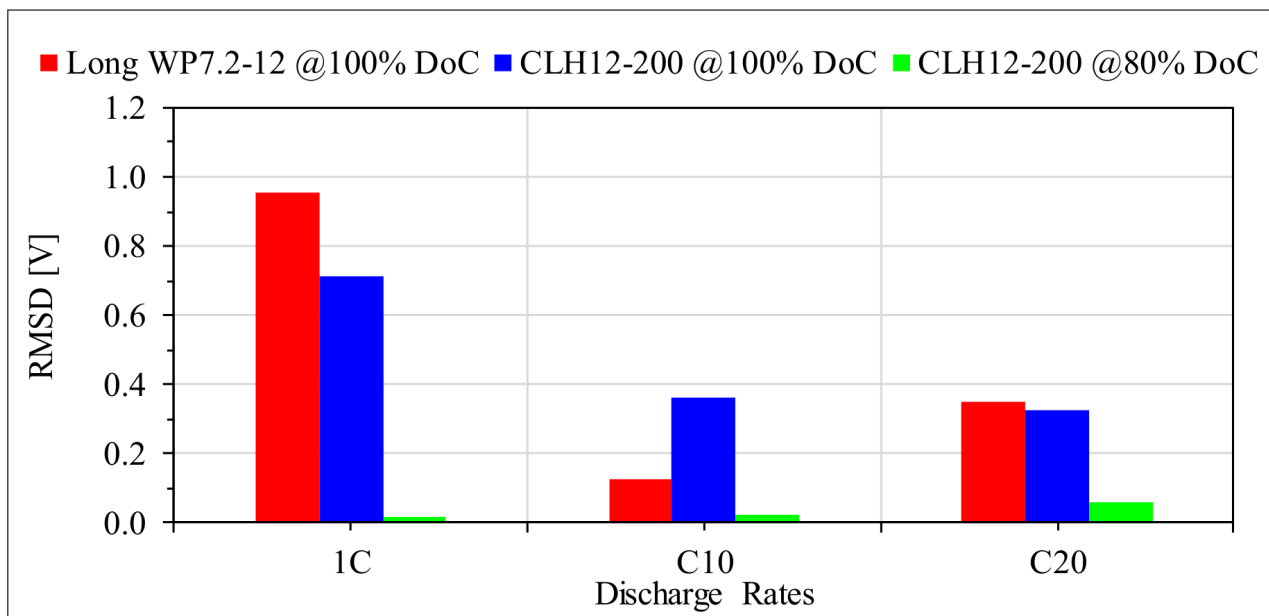


Figure 4.19.: Comparison of $RMSDs$ for both batteries and for a depth of discharge of 100% and 80%.

Battery simulation conclusion

Both simulated batteries show a good performance when compared at the nominal discharge rate

4. System Modeling

$0.05C$, as the parameters A and C have been calculated based on the corresponding given discharge curves. However, the improvements of the simulation results in comparison to the $0.1C$ and $1C$ -rate are minor, if the parameters are based on their given discharge curves. The resulting deviation within the other curves is, in these cases, tremendous.

Further, manufacturers suggest to limit the discharging of the batteries technically. Deep discharging cycles decrease the overall number of battery cycles drastically. Hence, it is suggested, to limit the depth of discharge to a minimum state of charge of $SOC_{min} > 0.2$. The resulting error of the *CLH12-200* battery is reduced to 0.13% of the nominal voltage U_{nom} (RMSD = 0.015V). The other errors are reduced as well to 0.21% (RMSD = 0.0254V), resp. 4.7% (RMSD = 0.566V). This effect occurs as well when this limit is applied to the *WP7.2-12* battery. The resulting deviations correspond to an error in current calculations of $\delta_I = 0.2$ to 5%. This relative error is acceptable for the terms of building simulation calculations.

Electric transformer

Transformer parameter acquisition

A general transformer performance curve is taken and modeled through an equation as described in Equation 2.54 in section 2.3.5 on page 45. Two further parameters need to be defined: the nominal rated power of the transformer, P_{nom} , and the maximum efficiency at this output, η_{max} . The transformer has to be selected to match the capacity of the connected cooling system, for example an electric capacity of 2000W. The efficiency at this load is limited to $\eta_{max} = 0.91$, as described in the previous mentioned modeling chapter, section 2.3.5.

Transformer modeling in *Modelica*

The transformer is also modeled with the programming language *Modelica* within the environment of *Dymola*. The *Modelica* code, shown in listing E.3 in the Appendix on page XXXVI shows the equation section of the modeled system. The calculation of the load factor `loadFactor` was described in Equation 2.53 on page 45. For the calculation, the absolute value of `P1` over `P_nom` is needed to avoid negative logarithms within the efficiency calculation. By this, the transformer can be used to simulate electricity supply to the grid. `P_grid` Additionally, the additional term of 0.001 is needed so that the load factor is never zero. This is needed to avoid a division by zero when no load is applied and to enable the calculation of the efficiency of the transformer `eta_dcac`. A `smoothMax` function is used to limit the lower efficiency to 20% to avoid a negative efficiency and describe a minimum stand by load as described in the transformer modeling section. Setting a lower minimum efficiency would result in unrealistic power demand peaks at a load factor of around 4%. The transition to this lower limit is done within an interval of 0.1 % of the load factor. Another limit is set to the minimum drawn power `P2` to model the minimum electricity demand of the transformers control electronics. However, new transformers have close to zero energy demand while no load is applied. Therefore, a `tanh` function is introduced to switch the electric to zero when the output power `P1` falls below 0.01 W.

`P2` calculates the input power which is needed to satisfy the connected load. It is defined by `load P1` over the current transformer efficiency `eta_dcac`. The whole power demand is limited with the function `smoothMax`. This is modeled so that the minimum power which is drawn from a connected source is the lost power at nominal performance. This is calculated by the nominal power `P_nom` multiplied with the transformer losses $(1-\eta_{max})$. It can be assumed that this power is the stand-by electricity demand of the transformer and thereby its lowest power demand. Besides this, normal transformer switch themselves off completely when no load is applied. This is modeled through a `tanh` function. It will switch the power demand `P2` to zero below a load factor of 0.01.

Further, two service variables are introduced, to integrate the drawn and supplied power, `P2` and `P1`, of the transformer. The energies `E_in` and `E_out` can be used to evaluate the average efficiency of

the transformer over a certain time period or calculate costs or sale margins when the transformer is connected to an electric grid.

Transformer simulation performance

The resulting efficiency curve is shown in the following picture 4.20. The graph highlights the range from 0 to 120% of connected nominal load. Clearly visible is the lower limit of $\eta_{min} = 0.3$ below a $loadFactor < 0.5$. The transition period of 1% is indicated as the small slope between a constant and the rising efficiency. The overall curves approximates the upper efficiency limit η_{max} .

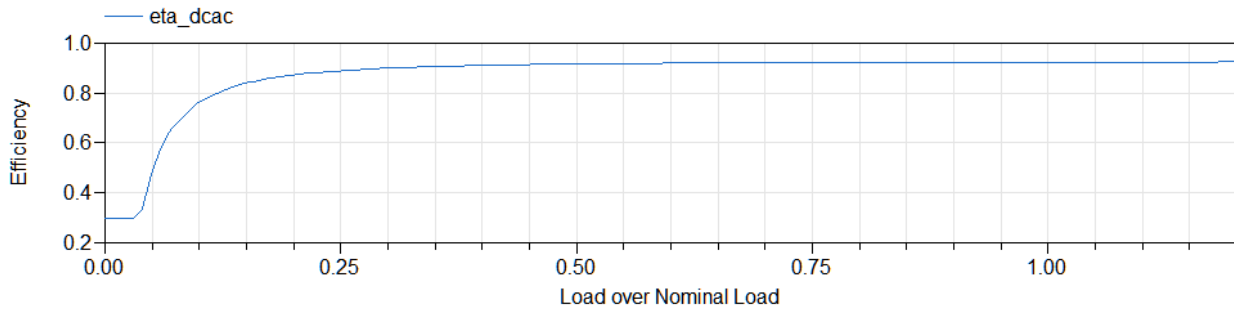


Figure 4.20.: Transformer efficiency at the corresponding fraction of the applied load

The following graph 4.21 shows the power output of the transformer P_{out} (red) and the power input to the transformer P_{in} (blue) at their corresponding nominal load. The power output is defined by a connected load which has to be satisfied. The input power is the load which has to be drawn from a connected DC electricity source to satisfy this load. The power curves are given for a nominal converter load ranging from a load of 0 to 120%. The efficiency drastically drops below a load factor of 4% due to Equation 2.54 which is used to model the transformer performance but is limited as described in listing E.3. This results into the slight rise in power demand P_{in} below a load factor of 0.05. Additionally, the minimum power demand can be observed below a load factor of 0.03. There, the input power P_{in} deviates clearly from the output power P_{out} in red. The sharp drop to zero reflects the total switching off when no load is applied to the transformer.

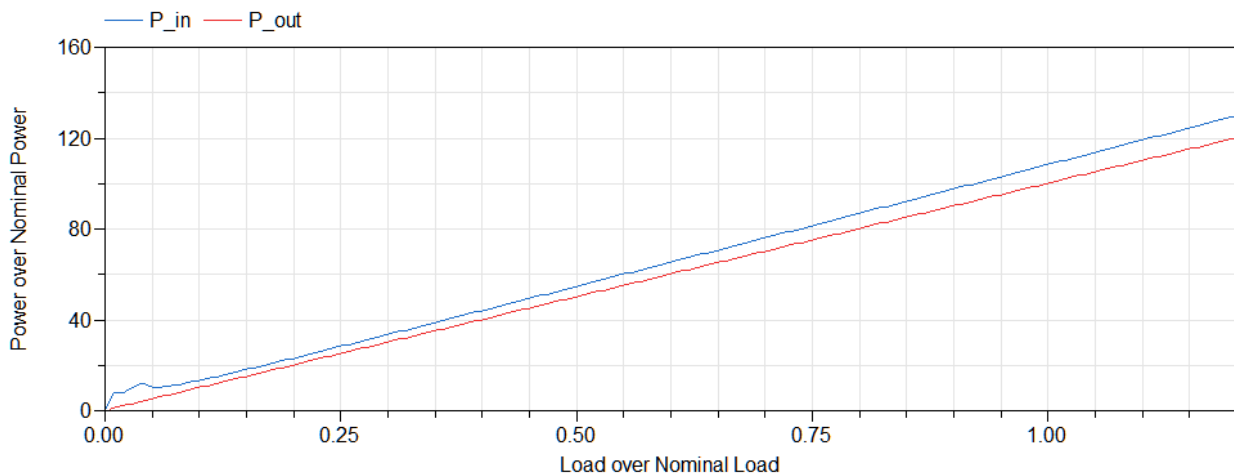


Figure 4.21.: Power output of and power input to the transformer at the corresponding fraction of the applied load

Transformer simulation conclusion

The transformer model was introduced to the overall system to account for the additional losses within the proposed system. The overall system is designed to refurbish existing systems or help to solarize common planned new systems. Most of the existing split-unit systems are operated with an AC driven compressor. Hence, a DC/AC transformer is needed to supply the electricity. On the other side, the transformer is used to transfer electricity to a connected grid. This could consist of other household devices, a local or the national grid. This would further introduce the need of a frequency synchronization. This level of detail is not included in this thesis.

A data base of common used transformers, including their nominal load and a look up table for their performance curve, can be developed in the future to extend the *BuildingSystems* library. The use of a transformer can be avoided when the split-unit is operated with DC electricity.

Energy trading with the electricity grid

Using grid electricity P_{grid} is necessary, to satisfy the electric demand when the battery is discharged to its minimum state of charge level SOC_{min} and no electricity is supplied from a connected source like photovoltaic modules. On the other side, electricity can be supplied to a connected grid in times, when the battery is fully charged and the incoming power P_{charge} is bigger then the power demand P_{load} of a connected system. The modeling is done according to the system overview in Figure 4.15 on page 83. The model is extended for this purpose. The *Modelica* code can be found in the Appendix, in Listing E.3 on page XXXVI. A new boolean parameter `gridConnection` is added to the code. The transformer efficiency `eta_dcac` is switched between two modes: electricity taken from the grid and electricity supplied to the grid. The switch is done with a `tanh()` function which will alter the efficiency when the connected load in `p1` becomes positive. This is the case, when electricity is taken from the grid. Alternating current from the grid can be directly used to supply the connected load. Hence, no transformer is needed. This is expressed by setting the transformer efficiency `eta_dcac` to 1. The transformer losses are modeled according to the previous section with the given efficiency curve. Less energy is forwarded to the grid than supplied by the excess energy from the connected energy source. Further development of the grid exchange model through the transformer should include additional losses through the frequency adoption which is needed to feed power into a connected grid. This could be done with an individual component or within the transformer itself. Finally, individual data sets should be created which represent the real performance curves of various transformer and frequency rectifiers.

4.5.3. Grid connection and SLP

A standardized electric load profile is needed for the analyzed apartment and building structures. They help to evaluate the potential energy savings, determine the additional energy which is needed from the grid, or calculate the amount of excess electricity which could be supplied to the grid. PV generated electricity can be used directly on side if a demand is present or has to be fed/sold to a connected grid. Otherwise, this electricity would be wasted. So called standard load profiles, SLP, have been created for multiple use case scenarios in Europe. This includes a residential usage profile *H0* besides other commercial or industrial profiles. It contains 3 profiles, each for a working day, Saturdays and Sundays. The Sunday profiles are used as well for holidays [134, p. 26]. The curves add up to an annual electricity demand of exactly $Q_{electr} = 1000 \text{ kWh}$. These demand curves must be adopted for the varying demand throughout an average year due to the varying demand in different seasons [135, p. 9]. The accuracy of the energy demand prediction through the profiles increases with an increased number of consumers which are modeled with a SLP. Misfits or local extremes vanish in the statistical uniform behavior of an increasing number of users. These profiles are used in many countries with a

moderate climate and underlie a constant review and adaptation process, for example, to introduce additional demand through electric vehicles [136].

However, these profiles cannot be used in countries in *tropical* or *subtropical* climate regions. There, the electric load is significantly higher during the summer season than in *moderate* climate regions. Hence, an alternative load profile needs to be created for the use in *dry, hot* climate regions. Therefore, the annual electric demand curve of the Red Sea town resort *El Gouna* is available with an hourly resolution for the year 2014 [11]. This curve is presented in Figure 4.22 in blue and indicated on the left y-axis in the graph. The shown graph is the resulting rolling mean over a period of 24 hours. The maximum grid load in 2014 was $Q_{electric,peak} = 21.5 \text{ MW}$. The sharp drops in summer are the results of blackouts which lasted for at least 5 hours. Within 2014, a total number of 17 black outs with a minimum duration of at least 1 hour occurred. Further, an uncounted number of smaller black outs, lasting less than 60 seconds, happened.

The amount of electricity, which is needed by the city, depends on the number of present tourists and the current outdoor air temperature. The city's population is highly dominated by the capacity of 25 hotels and hundreds of private holiday apartments. The occupancy rate of an average sized hotel is available for the year 2014 [137]. This is used to determine the occupancy rate of the entire town, based on the available capacity of 20,000 beds [138]. The resulting daily amount of city inhabitants is presented in green and also on the left y-axis in the graph in Figure 4.22. The total number of present people deviates in 2014 between 16'700 and 10'800.

Additionally, the 24 hours rolling mean of the outdoor air temperature in 2014 is presented in the Figure. It is indicated in red on the right y-axis. The data is provided by a weather station close to the shore at the northern edge of *El Gouna* [24]. The minimum outdoor temperature is $T_{ODA,min} = 8.9^\circ\text{C}$ and the highest is $T_{ODA,max} = 40.5^\circ\text{C}$.

Electric load, occupancy and outdoor temperature in El Gouna in 2014

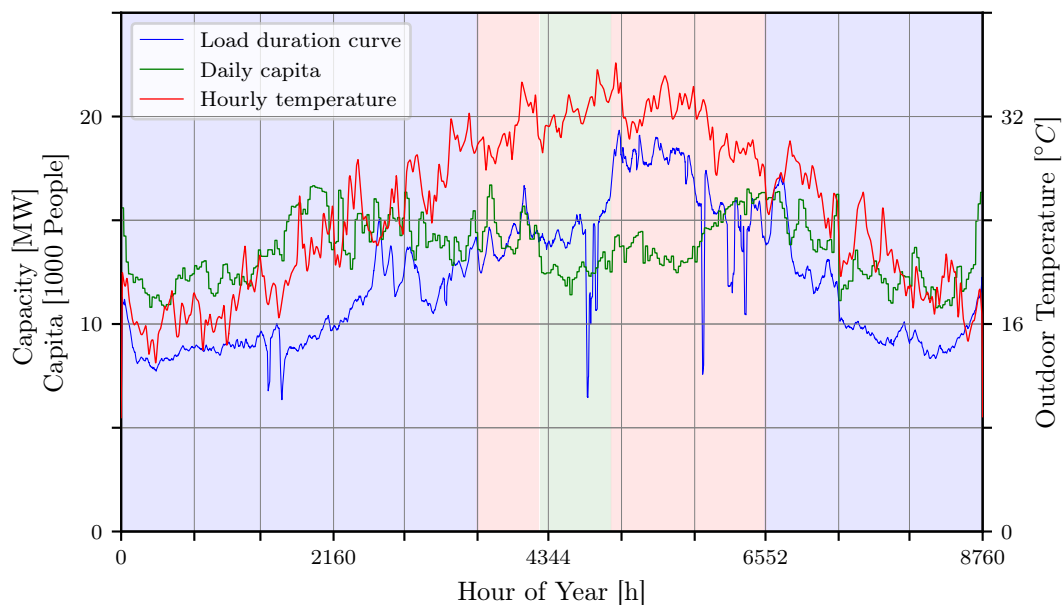


Figure 4.22.: Annual electric, occupancy and temperature profile for the highlighted seasons winter (blue background), summer (red background) and Ramadan (green background), according to Attia et al. (2012).

The three different seasons, according to the listing in paragraph 3 on page 74, are represented by the light background colors. The winter period is outlined by a blue area, summer by a red area and

4. System Modeling

Ramadan by a green area.

The energy demand and occupancy is quite high at the beginning and the end of the year, due to Christmas and new years eve celebrations, where a lot of domestic tourists stay within the town. Especially during the winter season, the electric demand is mainly dependent on the occupancy rate of the city. During the beginning of the summer season, indicated by the red area, the demand is rapidly rising due to increasing outdoor air temperatures. The sharp rise is interrupted by the holy season of Ramadan, which is outlined by a light green background color. During this time, the city is not much visited by tourists. Domestic tourists return to El Gouna towards the end of Ramadan, the feast of *Eid al-Fitr*. The demand peaks during the following summer month of August. The cooling demand reaches its peak, as air temperatures and incoming radiation reach their maximum. Within the following winter season the demand follows the decreasing number of tourists and outdoor temperatures.

This load duration profile is standardized for the three different seasons to work as general electric load profile for a single user. Therefore, the load duration curves of each season are averaged over all days. No significant difference was found in profiles for different days of a week, due to the holiday destination character of the town which provided the data. Additionally, the same is done for the outdoor air temperature in each season. Thereby, three load profiles and three temperature profiles are created. They are shown in the following Figure 4.23. Blue is used to highlight the average winter day, red for a summer day and green for a day during Ramadan. Solid lines represent the daily load duration profiles, ranging from 606 W in winter to 1282 W during Ramadan. They are marked on the left y-axis. The right y-axis indicates the temperatures by dotted lines.

Clearly visible is the constant demand during the daytime of about 700W in winter and around 1200W during summer and Ramadan. A sharp peak to almost 1000W resp. 1300W occurs during the early evening hours of each day. In winter, the demand peaks at 6pm, while in it is shifted by an hour to 7pm. Afterwards, the demand slopes down during the night time towards its minimum around sunrise, when daytime activities start and hotel kitchens commence operation to prepare breakfast.

Load profile for one user and average hourly temperature on a

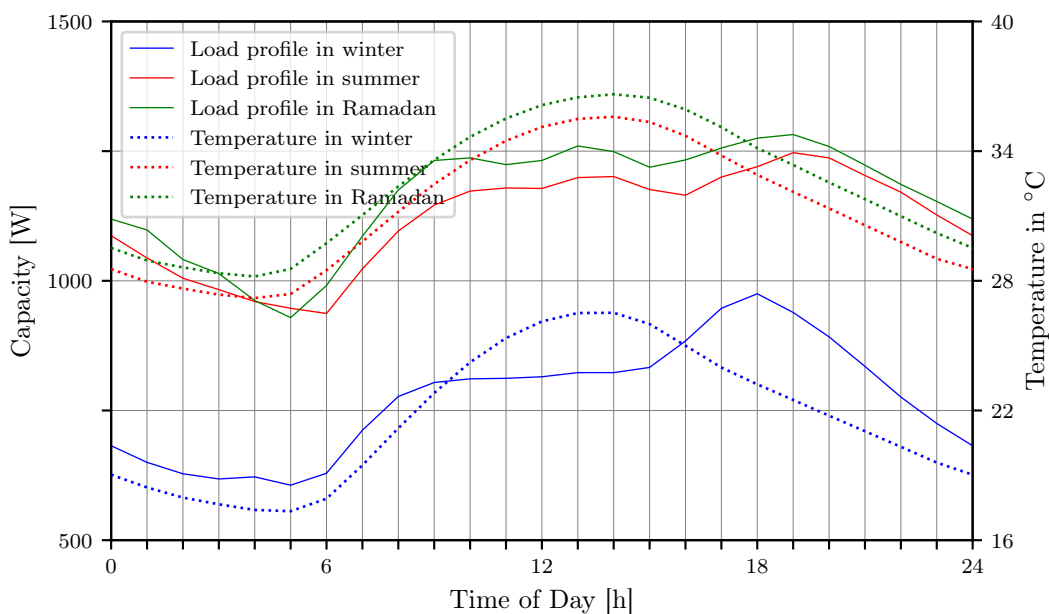


Figure 4.23.: Electric load and temperature profiles for all three seasons, based on the electricity demand curve and outdoor air temperature of El Gouna in 2014.

The electric load curve of each season is divided by the temperature curve of the corresponding season to generate load duration curves, which are dependent on the number of inhabitants and the outdoor air temperature. The resulting curves are shown in the graph in Figure 4.24. Each load duration curve represents the power demand (W) of one inhabitant (cpt) in each season per outdoor temperature degree ($^{\circ}C$). They are applied as more detailed standardized load profile for annual simulations and to make them applicable for all climatic boundaries within the MENA region.

Load profile for one user per Kelvin

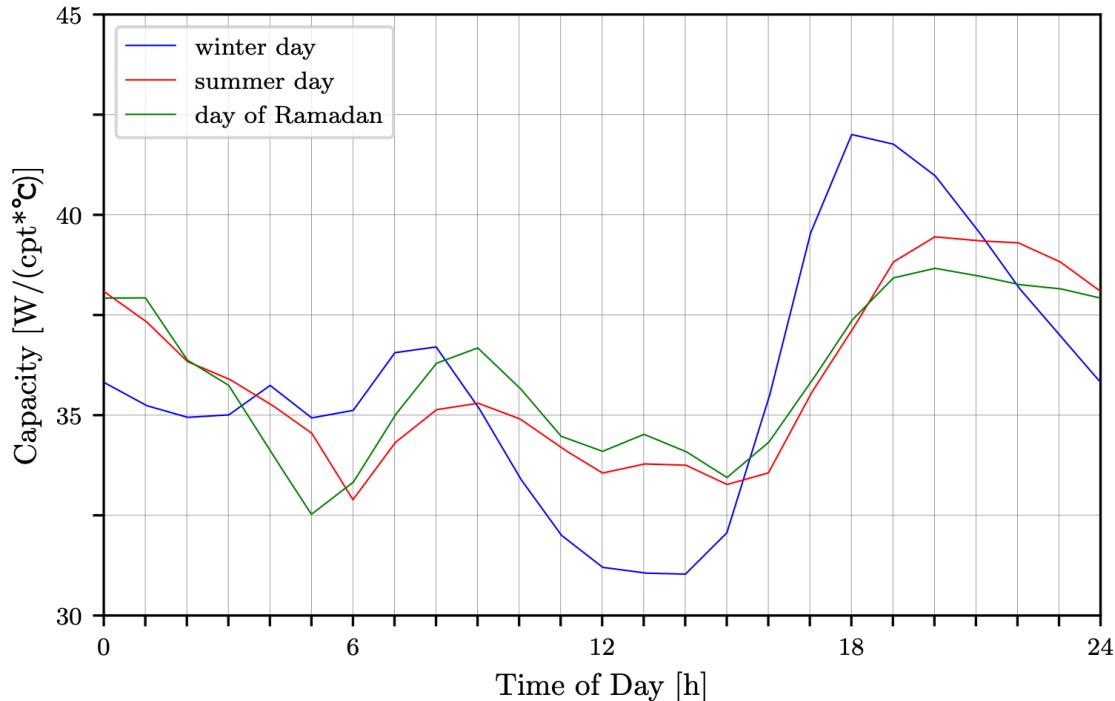


Figure 4.24.: Standardized load profile per capita and Kelvin for all three seasons, based on data for El Gouna in 2014.

On a winter day (blue line) the electric demand would peak at 6pm (18h) with about $42W/(cpt^{\circ}C)$. This would account for $P_{winter,hot} = 840W$ on a warm winter day with an outside temperature of $\vartheta_{ext} = 20^{\circ}C$ at 6pm. At this time, the sun just set. However, a still warm outside temperature at this time of day would indicate a sunny and relatively hot air temperature. Around 6pm, the maximum cooling load would reach the interior. This power demand would drop to only $P_{winter,cold} = 420W$ on a cold winter day with only $\vartheta_{ext} = 10^{\circ}C$ at 6pm.

The seasonal profiles of Figure 4.23 and 4.24 are each combined to a full standardized load profile of one year, according to the seasonal schedule on page 74. Thereby, two standardized annual load profiles are created. Their performance is evaluated against the measured load duration profile from which they originated. The monthly electric energy demands of each profile are shown in the following graph in Figure 4.25 in MWh on the left y-axis. The green bars represent the monthly measured demand of El Gouna in 2014. The blue bars sum up the monthly demand, which is dependent on the season and the given occupancy. Highlighted in red are the demands, which are additionally subject to the dry bulb outdoor temperature. On the far right, the annual sum of each profile is presented in GWh on the right y-axis.

4. System Modeling

Over the whole year, both two standardized load profiles sum up to an equally close demand compared to the measured demand of $Q_{ElGouna,measured} = 105.6 \text{ GWh}$. The profile which is solely based on the occupancy is slightly closer to the measured profile with a simulated demand of $Q_{ElGouna,user-SLP} = 106.7 \text{ GWh}$ compared to $Q_{ElGouna,user\&temp-SLP} = 108.2 \text{ GWh}$. Especially, as the electricity demand due to electricity cuts and black-outs is missing in the measured data. This sums up to $\Delta Q_{missing} 1.1 \text{ GWh}$, nearly nullifying the annual difference between the measured and solely occupancy based load profile. However, the following month of August is the worst for both profiles. The reason is the sharp increase in demand due to the end of Ramadan. The monthly demands of the user and temperature based SLP is always above the measured consumption, except during the winter months January, February and December, and the demand anomaly in August. A detailed analysis for the performance is undertaken for a week during Ramadan (Figure 4.26), summer (Figure 4.27) and winter (Figure 4.28).

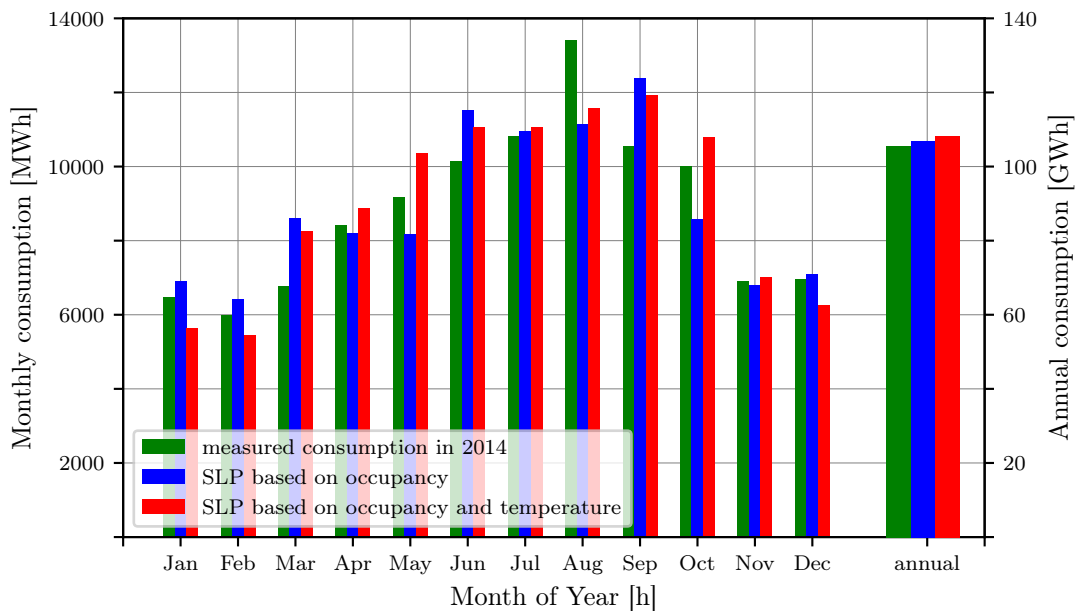


Figure 4.25.: Comparison of the monthly electricity demand between the measured values (green) and the demand, which is scaled to the occupancy (blue) and additionally to the outdoor air temperature (red).

The performance of both created standardized load profiles match during Ramadan. The temperature dependent load profile always slightly exceeds the measured profile, except on Sunday, Friday and Saturday. The overall shape follows the given measured curve: steep rise in the morning hours to a plateau which increases to a peak in the early evening hours with a steep drop afterwards. Even the small peaks during noon match the measured profile. Both created profiles underestimate the performance on Friday and Saturday. The given days, 25 and 26 July 2014 where the last days of Ramadan, ramping up the overall demand of the city due to the preparations for *Eid al-Fitr*. This mismatch can be observed in the following graph in Figure 4.27.

During the summer week from 27 July to 3 August 2014, the measured demand is always above the created load profiles, except on Tuesday, where the temperature dependent curve matches the measured. This exceeding demand causes the anomaly in the electricity demand for August. Towards the end of the week, no clear daily peaks are visible and the demand drop during night time is reduced. The performance of the simulation of the other days of August match the load duration curve as close

as during Ramadan.

Within the shown week in Season 2, from 5 to 12 October, the temperature dependent standardized load profile matches the measured profile closely. Especially the evening peak is well visible and time coherent. The performance of the solely occupancy based profile always underestimates the demand but follows its shape. Both profiles are not capable to predict the noon peak on Tuesday, Wednesday and Thursday. However, both match the real performance during the heating season in the winter months of December, January and February.

The occupancy and temperature dependent standardized load profile is scaled to the overall energy demand of Egypt. Therefore, the peak load profile of the years 2013 and 2014 are compared against a scaled SLP. The measured load duration curves are given for the 6 August 2013 and 12 August 2014 [28, p. 10]. Further, the population and the climatic boundaries are needed. The population was 89.8 million in 2013 resp. 91.8 in 2014 [44]. The temperature profile is acquired for the city of Cairo, where more than a quarter of the Egyptian population is concentrated [29].

With this data, the standardized load profile is constructed. The resulting curves are presented in the graph in Figure 4.29. The year 2013 is presented by dashed lines, while 2014 is highlighted with solid lines. Green are the measured peak load profiles, blue the standardized load duration curves and the outdoor air temperatures in red and on the right y-axis. The population of Egypt has been limited to 25% of the given numbers. This is done to match the peak demand during the day. This factor indicates that the individual electricity demand of the observed resort town El Gouna is four times higher than the demand of the rest of the country, despite additional industrial demands on a national scale.

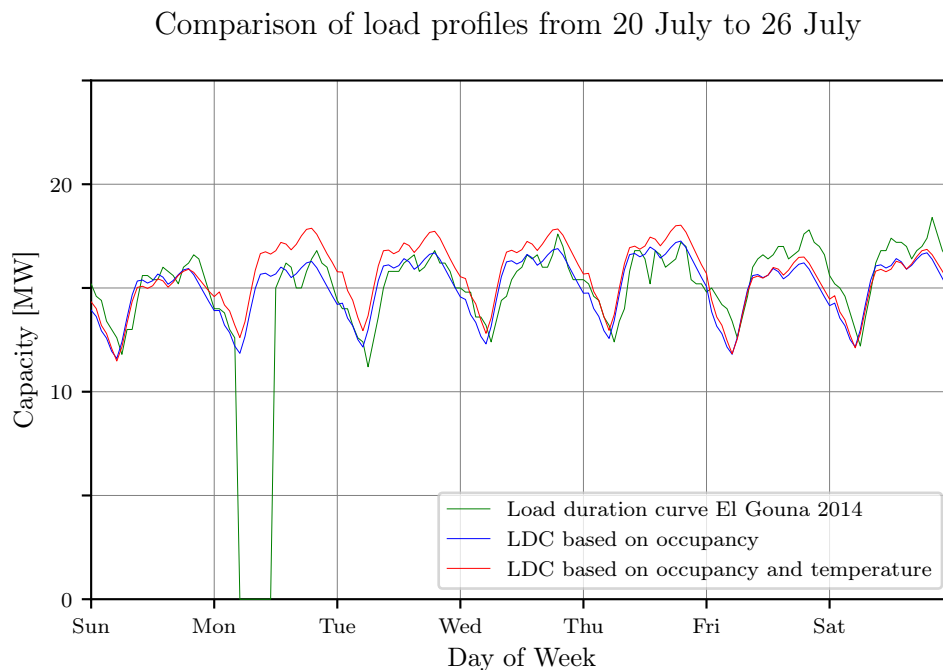


Figure 4.26.: Comparison of different load profiles of a week during Ramadan.

4. System Modeling

Comparison of load profiles from 27 July to 3 August

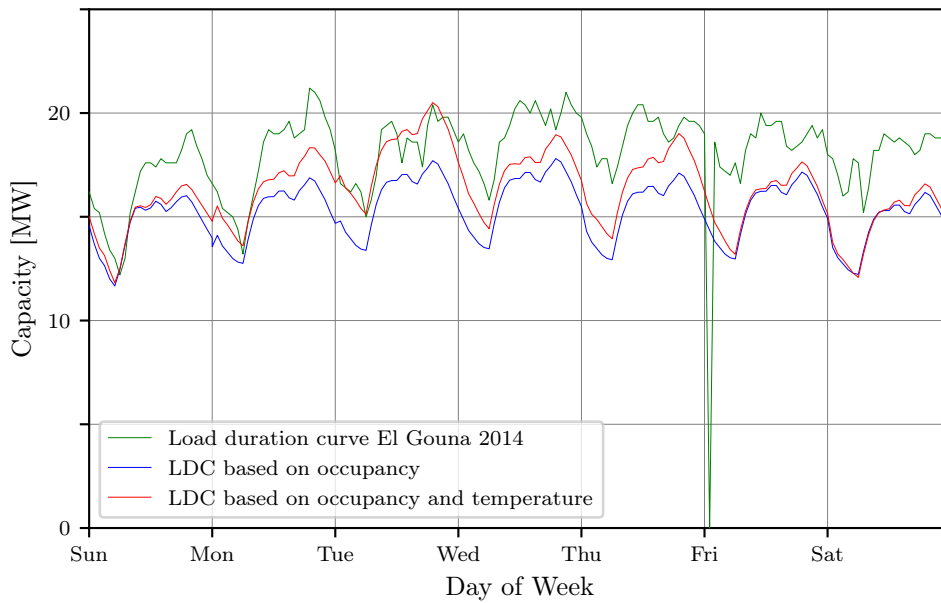


Figure 4.27.: Comparison of different load profiles of a week during Season 1.

Comparison of load profiles from 5 to 12 October

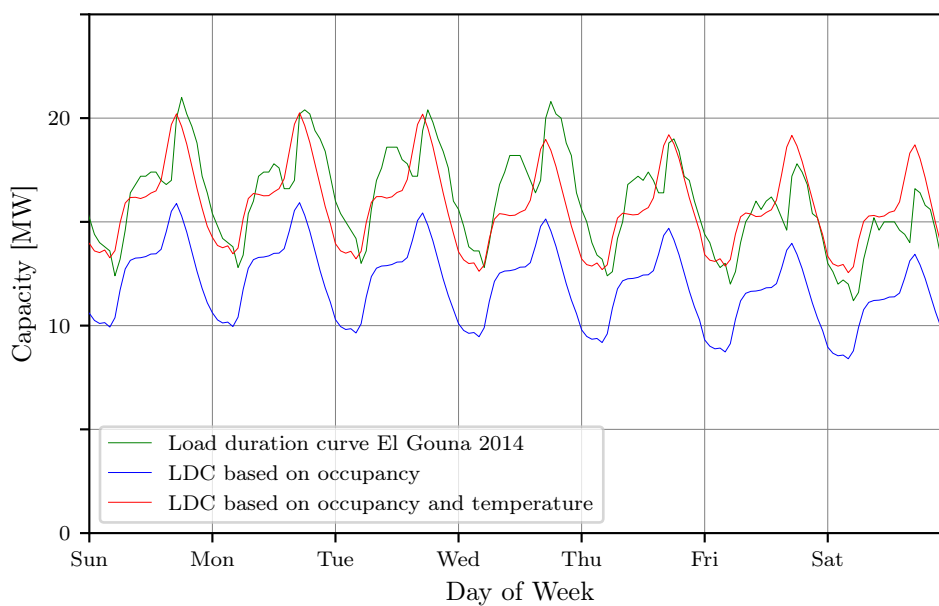


Figure 4.28.: Comparison of different load profiles of a week during Season 2.

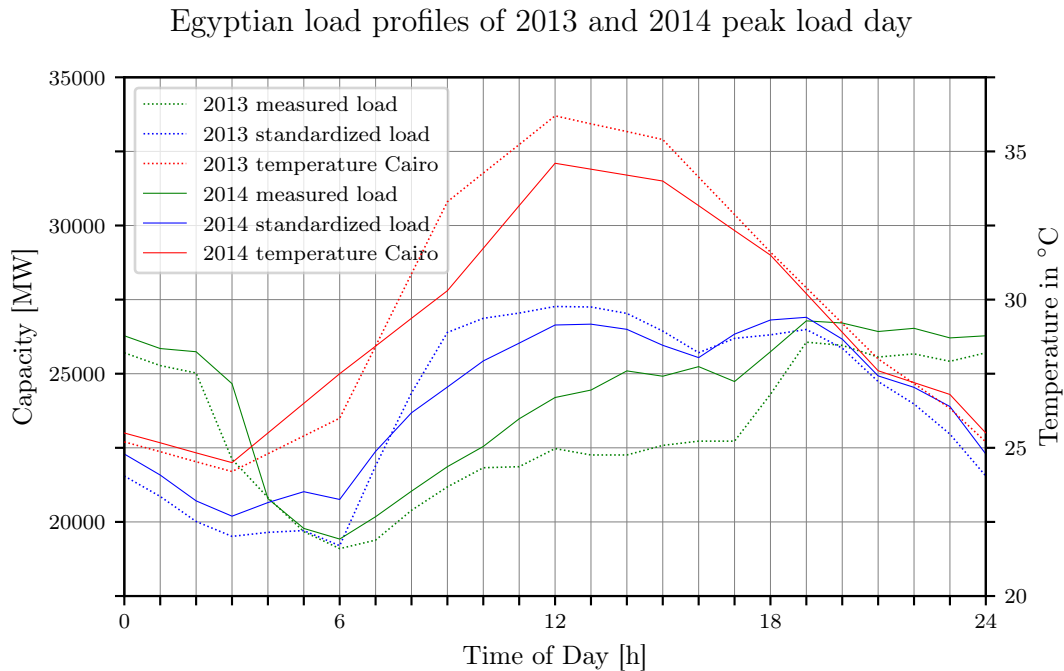


Figure 4.29.: Comparison of peak load profiles [28] and outdoor air temperatures [29] for 6 August 2013 (dashed lines) and 12 August 2014 (solid lines).

The main difference between the performance of the overall Egyptian demand curve and the applied standardized load profiles is during the evening hours. Within Egypt, no clear peak is visible. The demand spikes around 7pm in all profiles. However, it stays on a high level in the measured curve and first drop around 3am. The result of the SLPs drop already around 7pm. Also, the rising demand after sunrise is visible in the measured and constructed profiles, but their rise is slighter in the measured data of Egypt. Here, a tremendous difference is visible for the year 2013.

The constructed temperature dependent SLP will be applied within this thesis as household demand curve. Temperature data will be always available as it is simultaneously needed for the simulation of the PV generated electricity. Its use should be limited to residential applications and smaller local boundaries as shown by the scaling to an entire country.

The resulting individual electric demand curve can be used to determine how much electricity can be used on side and how much has to be distributed to a connected grid or would be wasted otherwise. Furthermore, it allows to calculate internal heat sources, as most electric devices emit the used electricity to the enclosing room air.

4.6. Thermal supply system

This section describes the modeling process of the thermal system components. The split-unit air conditioner is introduced and followed by the water cooling system. Finally, the storage capabilities of a cold water storage and the building mass are modeled.

4.6.1. Overview

The following scheme in 4.30 shows the in- and outputs to and from the thermal energy exchange system components. This includes the electric driven "coldness" generation, which are the *splitUnit* and the *waterCooler* and the thermal storage systems, which are the *fluidStorage* and the *coolingSurface*. The reference system is based on the *splitUnit* (cf. Section 2.3.2, p. 24). The split-unit air conditioners main user input is the system size which is defined by the cooling capacity Q_{cool} . The second user

4. System Modeling

input is the set temperature $T_{SetCooling}$ according to the thermal comfort bandwidth. This value is evaluated against the room air temperature T_{Air} . The heat is extracted from the room through the two flow ports for the exhaust air $port_EHA_app$ and returned by the supply air $port_SUP_app$. Additionally the outdoor air temperature T_{Amb} is needed to calculate the external heat exchanger performance. The connection to the rest of the electric system is realized through the power demand P_{Split} . In case of a water based cooling system the upper section of the scheme becomes activated and the *splitUnit* is deactivated. The *waterCooler* is connected to a *fluidStorage* through the flow ports $port_Return$ and $port_Flow$. The chiller is activated when the lower storage temperature T_{Strg} exceeds a set temperature and it is deactivated when upper storage temperature deceeds that set temperature. The user only needs to define the height $storage.h$ and volume $storage.V$. This cold water storage is connected to a *coolingSurface* through the flow ports $port_Flow_cs$ and $port_Return_cs$. The heat from a room is extracted through the radiation and convective heat ports $heatPortRad$ and $heatPortCon$. The share of each part is dependent on the properties of the cooling surface and if it is either an active or passive construction element. Each component is described in the following subsections.

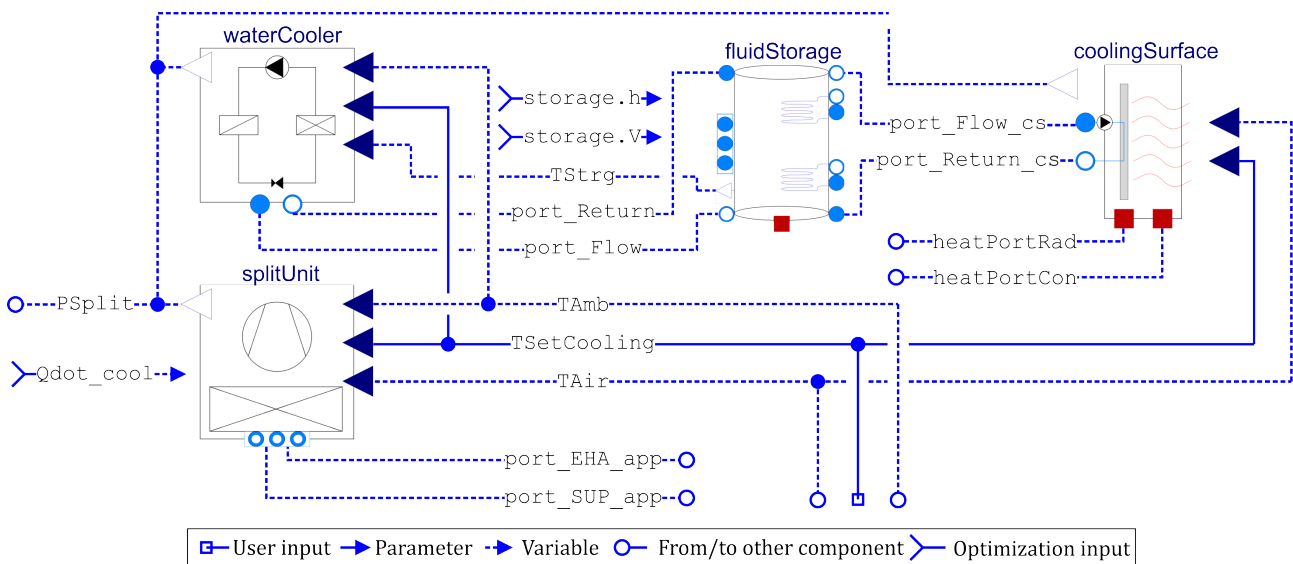


Figure 4.30.: *In- and outputs of the thermal supply model components*

4.6.2. Split-unit A/C system

split-unit air conditioning systems are a subcategory of unitary air conditioners and are the most common way to cool down the room air [7][43]. Their integration in residential applications is shown in Subsection 2.3.2 on page 23 and is illustrated in Figure 2.4. The in- and outputs to this system component are shown in the graphical representation of *Modelica* in Figure 4.31.

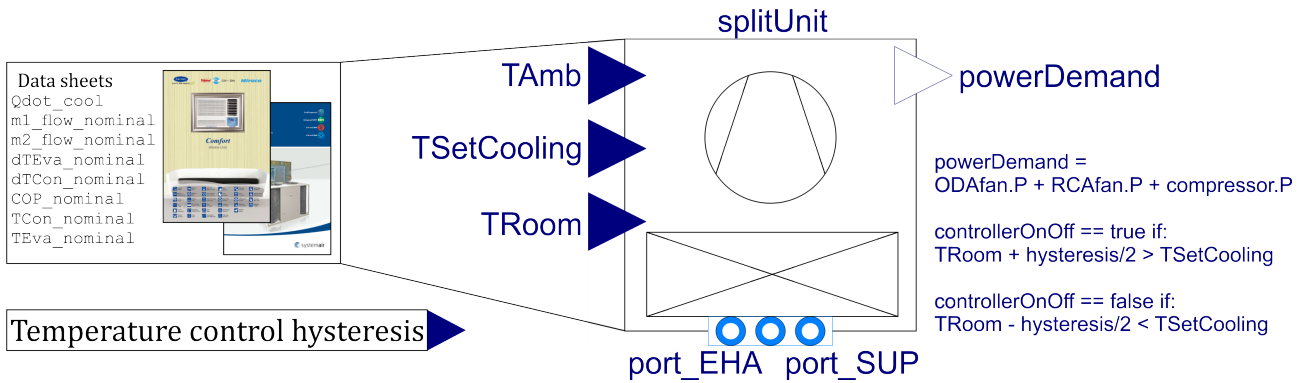


Figure 4.31.: In- and outputs of the `splitUnit` component in Modelica.

The following pictures in Figure 4.32 show the appearance of two different types of split-units. The scheme on the left illustrates the working principle: a circulating refrigerant is eased by the expansion valve inside the evaporator in the indoor unit/section. The blower recirculates the indoor air over the evaporator coil and thereby cools it. Afterwards, the now gaseous refrigerant is pumped by the compressor to the outdoor unit/section. There it is densified and condenses inside the condenser coils. A fan blows outdoor air over the heated coils to transfer the thermal energy to the environment. Afterwards, a gas-liquid separator makes sure that no gaseous refrigerant enters the evaporator. A classic split-unit is shown in the top right. The outdoor unit is normally placed on the outside wall or the roof while the indoor unit is mounted on an inside wall surface. The connecting pipes directly transport the liquid or gaseous refrigerant. Both parts can be directly put together to a packaged system which is shown on the lower right. In this case no pipework needs to be done and the system can be directly installed inside a hole of an outer wall of a room.

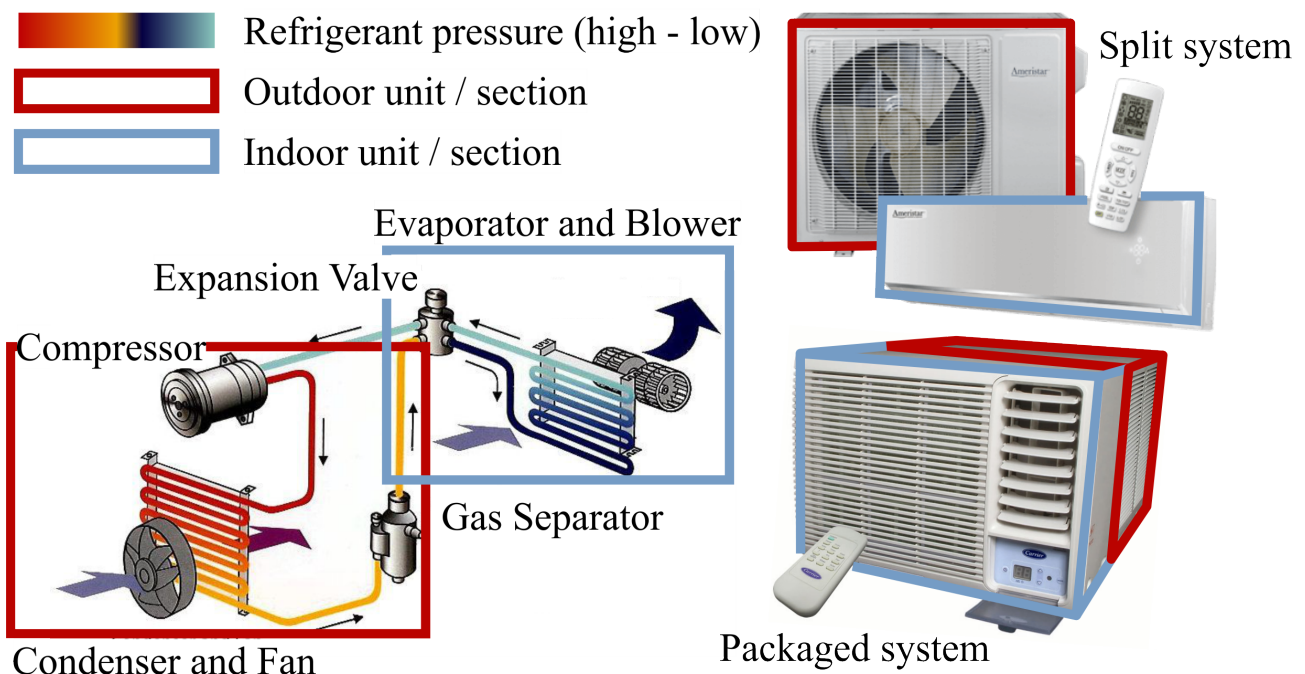


Figure 4.32.: Outdoor and indoor unit of a unitary air conditioner (left) [30] and examples of a split system [31] and a packaged system [16].

Both examples are common methods to cool down the room air. They are operated in the same

4. System Modeling

way. The main difference is the length of the pipework which is separating the indoor and outdoor part of the air conditioner. The classic split system can supply multiple indoor units but requires more installation effort as pipework needs to be built to connect the evaporator and the condenser. A packaged system is a more simple solution to supply a single room with air cooling as the pipework is completely encapsulated in the system itself. The downside is a lower coefficient of performance due to heat bridges between the sections and possible losses due to air overflows.

Various types of compression chillers are operated with different refrigerants and different compressor types. In general, they are operated as shown in the scheme above. Different refrigerants, like R22 or R134a, have different shapes of the blue separation area between the liquid and gaseous state. Still, R22 is one of the most used refrigerants but is succeeded by R134a because of its much lower global warming potential. For example, R22 will be phased out completely until 2020 in the USA [139]. Optimized compressors try to limit the increasing entropy and come as close as possible to an isentropic compression.

The table below concludes the different input parameters for a typical split-unit air conditioner as it is available throughout the region. The data was derived as much as possible from a *Carrier* data sheet for the *Comfort Window Unit* packaged system [16]. However, this data sheet does not offer detailed data like the secondary mass flows of cooling air at the condenser \dot{m}_{cond} or of the amount of recirculated air at the evaporator \dot{m}_{eva} , nor the temperature differences, and the pressure differences over the condenser and evaporator. This data has been derived from a comparable but three times bigger compression chiller from *Systemair Airwell SAS* which had the same COP and operation limits as the used A/C. These values are marked with an "*" in the table [35]. The standby power demand $P_{standBy}$ is calculated as a percentage of the cooling capacity and was concluded from the same data sheet.

Table 4.6.: Parameters from data sheet from comparable A/C split-unit [16]/[35].

Parameter	Symbol	Name	Unit	Value
Rated cooling capacity	\dot{Q}_{cool}	Qdot_cool	W	3,000
Temp. hysteresis	$hyst$	hysteresis	K	4
Coefficient of performance	COP_{nom}	COP_nominal		2.55
Standby power demand for IDA recirculation*	P_{sBy}	P_standBy	W	$0.01\dot{Q}_{cool}$
Condenser nom. mass flow*	\dot{m}_{cond}	m1_flow_nominal	kg/s	0.303
Evaporator nom. mass flow*	\dot{m}_{eva}	m2_flow_nominal	kg/s	0.157
Temp. difference evaporator between outlet-inlet*	ΔT	dTEva_nominal	K	-9.8
Temp. difference condenser between outlet-inlet*	ΔT	dTCon_nominal	K	26.3
Pressure diff. over condenser*	Δp	dp1_nominal	Pa	25
Pressure diff. over evaporator*	Δp	dp2_nominal	Pa	25

*scaled values

4.6.3. Water cooling system

The following scheme in Figure 4.33 shows the system component of the water cooling system. It is only used, when a water based cooling system, including a cold water distribution system, is used. The working principle is described in Section 2.3.4 on page 36 and the main means of controlling is presented in Section 3.4.3 on page 55. The performance parameters are taken from the packed split-unit in Table 4.6 to keep the simulation results comparable. Here, also the ambient air temperature T_{Amb} is used

to calculate the performance of the outdoor heat exchanger. The internal control compares the set temperature $T_{SetCooling}$ with the set hysteresis against the temperature of a cold water storage or the return flow temperature T_{Strg} of a connected cooling system. It is switched on, when the return flow temperature exceeds the set limit and is turned off when this temperature limit minus half the hysteresis is exceeded.

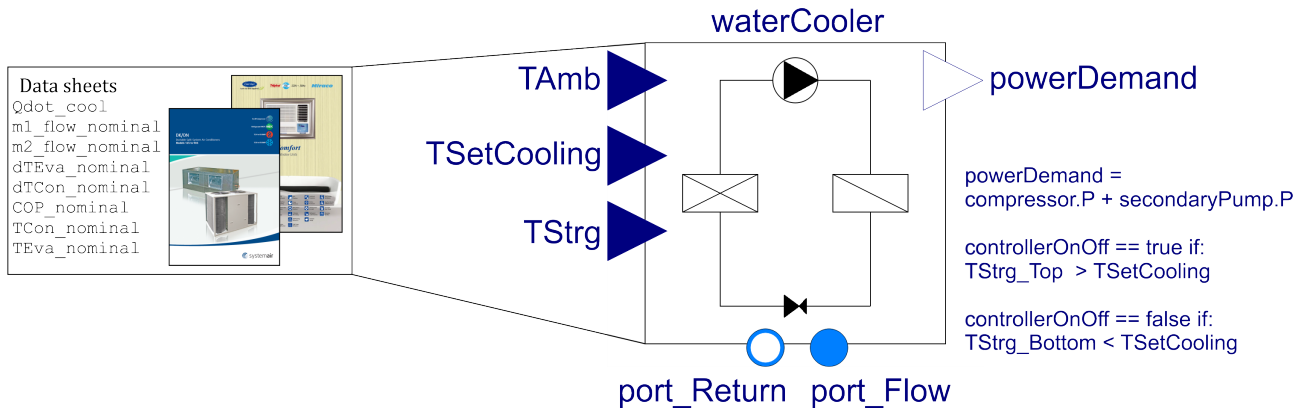


Figure 4.33.: In- and outputs of the `waterCooler` component, graphical representation in Modelica.

The component is connected through the flow ports `port_Flow` and `port_Return` to the cold water distribution system. The main calculated variable is the power demand `powerDemand` which is based on the compressor and the circulation pump energy demand `compressor.P` and `secondaryPump.P`. No standby power demand is calculated as the activation temperature is measured within the water storage system.

4.6.4. Cold water storage

Below, in Figure 4.34, the cold water storage is presented. It is connected through the flow ports `port_Flow` and `port_Return` to the water cooler and through the flow ports `port_Flow_cs` and `port_Return_cs` to the cooling surface. The size of the storage `storage.Volume` is limited by the available space or bearing capacity of the hosting floor. It can be reduced to zero if no cold water storage is present. The number of layers `layers.nEle` is defined by the user and should be chosen on the storage height. Thereby, the thermal stratification inside the volume is considered. The control strategy is based on this and the number of simulated layers should be at least 2. The cold water from the chiller is brought into the storage in the layer at the bottom. The return flow is located at the warmest layer at the top of the storage. Also, the connected cooling device draws cold water from the bottom and returns the heated fluid on top. The primary cooling loop through the water cooler is activated, when the storage is empty. This is the case when the lowest layer exceeds the set temperature. The storage is fully charged, when the top layer exceeds the set temperature. The storage transfers all temperature layers through a vector `TStrg[]`. The heat gains from the environment are as well considered through the `heatPort`. The losses are dependent on the surface area of the storage and the heat transfer through this shell. This can be reduced by insulation. Hence, the thickness of this insulation `insulation.thickness` has to be defined by the user.

The fluid storage is part of the *BuildingSystems* library and its parameters are kept according to the predefined values. They are valid for water storage systems in normal water tanks for residential applications. The semilinear buoyancy model with fixed coefficients from literature was first implemented by C. Tugores (2013) [81].

The component is capable to be extended for additional simulation cases. There, the storage can be extended with a heat exchanger in the top and/or bottom layer of the water tank. These options are

4. System Modeling

indicated by the additional flow ports in the given scheme. However, these possibilities are not used within this research to limit the amount of possible system setups and optimization parameters.

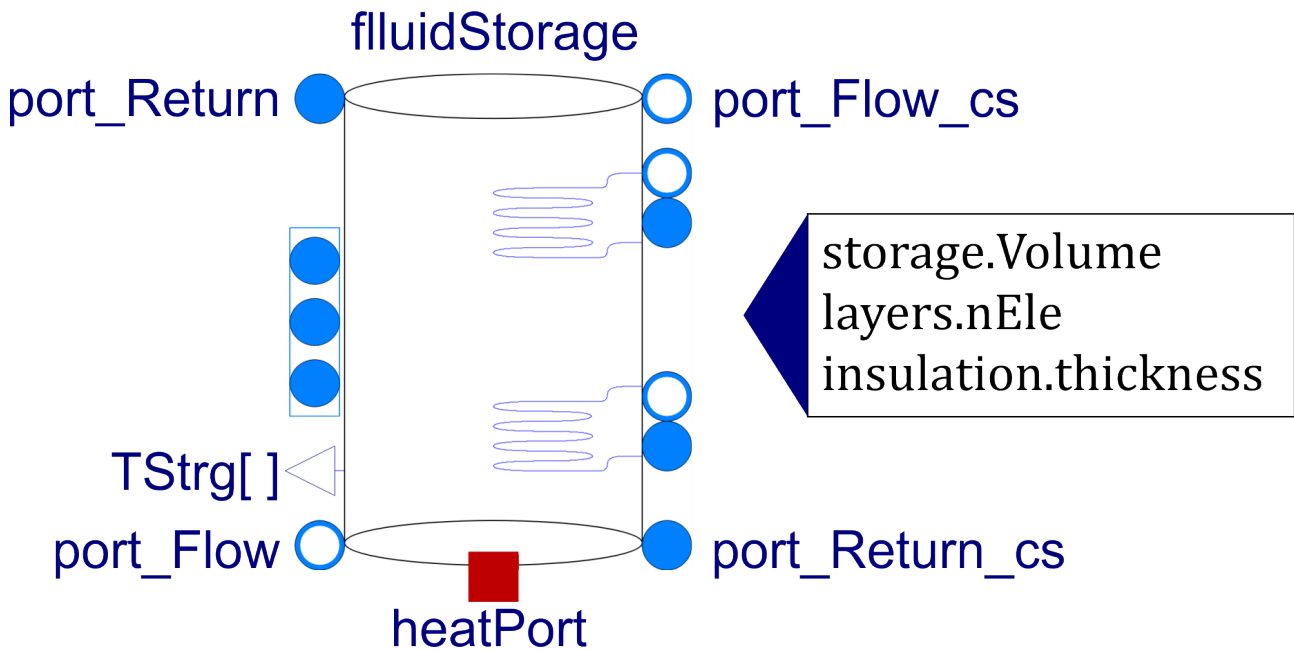


Figure 4.34.: In- and outputs of the *fluidStorage* component, graphical representation in Modelica.

4.6.5. Thermal storage in building masses

The last needed component for a water based cooling system is a room heat exchanger. This can be a cooling surface, like a cooling ceiling which is connected to the secondary cold water loop through the storage tank. Its functionality is described in general in Section 2.3.4 on page 37. The general mode of operation is outlined in Section 3.4.3 on page 53. The component itself is represented in the following scheme in Figure 4.35. This cooled water is supplied through the flow port `port_Flow_ss` and rejects the heat through the return flow port `port_Return:sc`. Here, also the current room temperature `TRoom` is compared against a set temperature `TSetCooling`. The secondary cooling loop is activated when the room temperature exceeds the set temperature by half the hysteresis. The energy demand for the cold water pump `powerDemand` is an output of the component and needed for the electric demand calculations. The cooling surface is connected through the heat ports for radiation and convection `heatPortRad` and `heatPortCon` to the room itself. Additionally, the size of the cooling surface `coolingSurface.A` and its heat capacity of the first thermally active 10 cm `coolingSurface.cp` have to be given by the user.

This system component can be parameterized to work as fan coil unit. This is a room air cooling system which recirculates the room air over a cooling coil which is supplied by cold water. This is done through reducing the radiative heat transfer to zero and only extracting heat through the convective heat port. In this case, the additional power demand of the recirculation fan has to be considered as well.

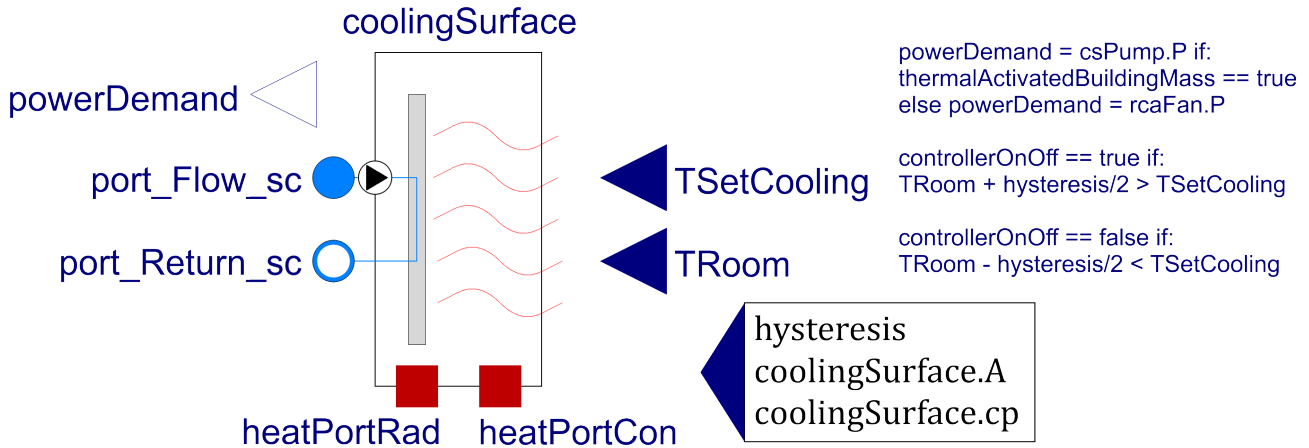


Figure 4.35.: In- and outputs of the `coolingSurface` component, graphical representation in Modelica.

4.6.6. Optimization modelling

The optimization is done with a particle swarm optimization, *PSO*. This method is applied through the simulation environment of *GenOpt*, a parametric optimization program for various simulation environments. It was developed by M. Wetter at the Lawrence Berkeley National Laboratory. The detailed program internal modelling of the *PSO* can be found in the current version of the software documentation [140, p. 32ff.]. This method allows to search a wide area for a global best solution and is inspired by the movement of migrating birds. The initial conditions are selected randomly across the entire searching boundaries. These n_{part} initial points are called *particles*. The value of each variable is deviated for each *particle* according to the distance to a local and the current global minimum. A newly discovered local minimum has an impact on the movement of a single *particle* while a newly discovered global maximum has an impact on all *particles*. Each movement step of all particles is called a *generation*. Overall, the number of generations is limited by a previously defined boundary n_{gen} . The movement of a particle towards its own local minimum is called *cognitive acceleration*, c_{1} , while its movement towards the global minimum is called *social acceleration*, c_{2} . A random factor $0 < r < 2$ is applied to each step distance to statistically cover a large area of points and vary the covered distance between each generation. The step size is limited by the maximum velocity v_{max} . The inertia weight defines, how fast particles convey towards a minimum. The following table shows all design parameter for the *PSO* algorithm with inertia weight w_{inert} .

The resulting number of simulations of each optimization process is the number of particles times the number of generations. 2000 simulations are done when 4 parameters are varied and 2500 are varied when 5 parameters are varied. The system has to be simplified to handle this amount of simulations in a reasonable time with a reasonable computational effort. Therefore, the case study location *Hurghada, Egypt* is selected as the reference location. The simulation time is reduced to the simulation of one single day. The 1 August is selected as this day. The energy demands of this day have to be scaled by 362.39 days to account for a whole year. The initial conditions of the air, water and wall temperatures, as well as the initial state of charge are calculated with an annual simulation. Further, the difference in stored energy between the initial and final state of charge of any storage system is added as additional cost or revenue to the system costs.

4. System Modeling

Table 4.7.: *Design parameters for particle swarm optimization.*

Name	Meaning	Symbol	Value
Neighborhood Topology	Type of search	lbest	local best
	Neighborhood size	izen_s	4
Number of particles	Sets of variables	n_part	$10 * n_{variables}$
Number of generations	Optimization steps	n_gen	50
Cognitive acceleration	Speed towards a local minimum	c1	2
Social acceleration	Speed towards the global minimum	c2	1
Maximum velocity	Distance between	v_max	3
Initial inertia weight	Pull towards a local minimum in generation 1	w_inert_start	0.7
Final inertia weight	Pull towards a local minimum in last generation	w_inert_end P_{nom}	0.2 3000 W

5. Simulations and results

This chapter shows and describes the results of the simulation runs which were designed and modelled in accordance to the presented methodology of the previous chapters. At first, an entire typical building model is presented according to the described *Typology II* as it was first introduced in Section 1.3.2 on page 5. This reference building is modeled in *IDA-ICE* and simulated for all 26 locations which were presented in Section 4.3.1 on page 68. The simulation results of a single bed and living room are analyzed in depth for the reference location of *Hurghada, Egypt*. These results are compared with the simulations written in *Modelica* to confirm the usability and accuracy of the presented models. The *Modelica* models are used to calculate the annual cooling energy and electric power demand for room air cooling purposes in all 26 locations for a living and a bed room. The results are analyzed in terms of their impact on the grid stability and electric supply security, in terms of operation costs and greenhouse gas emissions, in terms of thermal user comfort, and in terms of sensible energy storage throughput.

The grid influence is determined by calculating the share of the peak electricity demand on the total cooling energy demand of both room types. The evaluation process was first described in Section 3.5.1 on page 57. Another influencing factor is the number of on and off switching cycles of compression chillers. Their three times higher power demand during startup only last for a split second but can sum up to an enormous burden for an electric grid if thousands of split-units are involved.

The economic and ecologic impact is based on the typical electricity prices and carbon emission factors of each grid. The calculations are shown in Section 3.5.4 and 3.5.5, starting on page 60.

The thermal comfort is determined by the amount of hours in which the wall temperature is by at least 2K above an upper room temperature of 26°C, as it was presented in Section 3.5.6 on page 62.

Lastly, the thermal energy storage throughput through the wall masses is calculated as sum of all stored and released heat energy, as it was presented in Section 4.6.5 on page 102.

A monthly analysis is done for all previous indicators for the example location of *Hurghada, Egypt*. This typical location in the MENA region is used to evaluate the annual performance in depth and to analyze the performances of the presented systems in detail. Hereby, the plausibility and usability of the simulation results can be confirmed.

Afterwards, a simple standard photovoltaic system with a battery storage is evaluated in the same manner. Therefore, two further performance parameters are used: the solar coverage rate *SCR* and the solar cooling autonomy *SCA*. The calculation of these parameters was introduced in Section 3.4 on page 59. They are calculated for the previously described reference system for all locations and the room type of a bed room and a living room.

This case is analyzed in detail for the location of *Hurghada, Egypt*. The monthly and annual performances of all indicators are compared to evaluate the validity of the simulation and gain a deep understanding of solar powered cooling systems in the *MENA* region.

Finally, variable parameters of system are defined and varied with a particle swarm optimization process to search through a wide field of variable parameters with multiple local minima. This method is applied to find the best possible system in terms of solar coverage rate *SCR* and the solar cooling autonomy *SCA*.

5. Simulations and results

Table 5.1.: Resulting building parameter

	Symbol	Value	Unit
Ground area	A_{grnd}	494.0	m^2
Total floor area	A_{tot}	5,566.7	m^2
Total building volume	V_{tot}	14,010.9	m^3
Building envelope area	A_{surf}	3,971.8	m^2
Building surface to volume ratio	S/V	0.2835	m^2/m^3
Window to envelope area		16.9	%
Average U-value	u_{tot}	2.214	$W/(m^2K)$

5.1. Reference system

The reference system was presented first in Section 2.3.2 on page 24 and represents the worldwide dominant room air cooling system: a unitary air conditioning system with a parapet installation of a split-unit. At first, the performance of the entire building structure is shown before the performances of a single bed room and living room are evaluated. Afterwards, the performance of these rooms is shown when they are equipped with an *UAC* system.

5.1.1. Performance of reference model

The reference building was first modeled in *IDA-ICE* to evaluate the performance of the *Modelica* model which is present secondly. The following two subsections show the results of the *IDA-ICE* simulation. First, the outcome of the entire building simulation for all 26 locations. Second, the performance of the single rooms are shown. Afterwards, the results are compared between both simulation tools. Therefore, the room models are virtually placed in the climate conditions of *Cairo, Egypt* as their benchmarking model was created for this urban area.

Apartment building

The typical physical properties of a building within the MENA region are described in detail in Section 4.4.4 on page 77. The resulting boundaries are concluded in the following table. The building is quite compact as it is indicated with a surface to volume ratio of $S/V = 0.2835$. The window area is given as 16.9% of the entire envelope area. The overall U-value is calculated to be $u_{tot} = 2.214 W/(m^2K)$. The single zoning is presented in the following figure in the left picture. There, the naming of each apartment and the building orientation are given. The results of the average floor and its four average flats are multiplied by 10 to account for a 12 story building. Further, the figure includes the simulated ideal heating and cooling loads in the top right graph. Heating loads are drawn in red while cooling loads are presented in blue. The bright area indicated the hourly deviation and the thick lines the rolling mean over 24 hours.

In the lower right corner, the monthly energy balance of the entire building is presented. This balance is also calculated for the example location of Hurghada. The bars above the zero line represent thermal gains while the bars below the zero line represent losses. The absolute values of each month are equal. The sources and sinks of the heat transfer processes are stated in the legend below the graph.

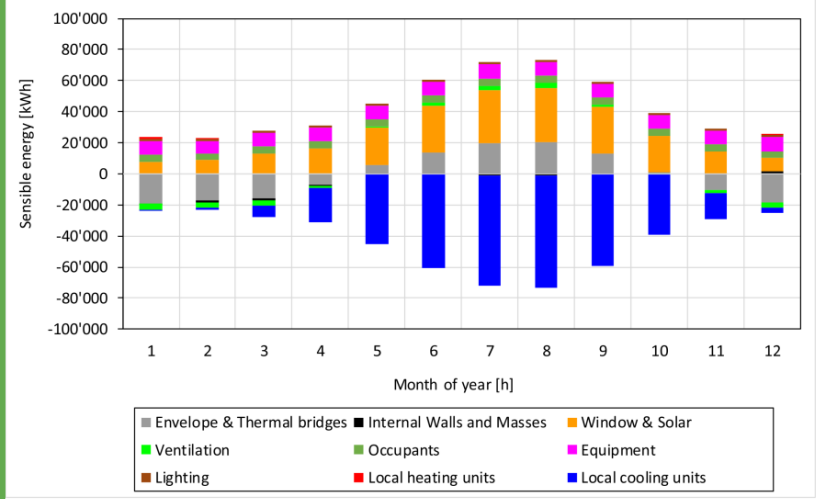
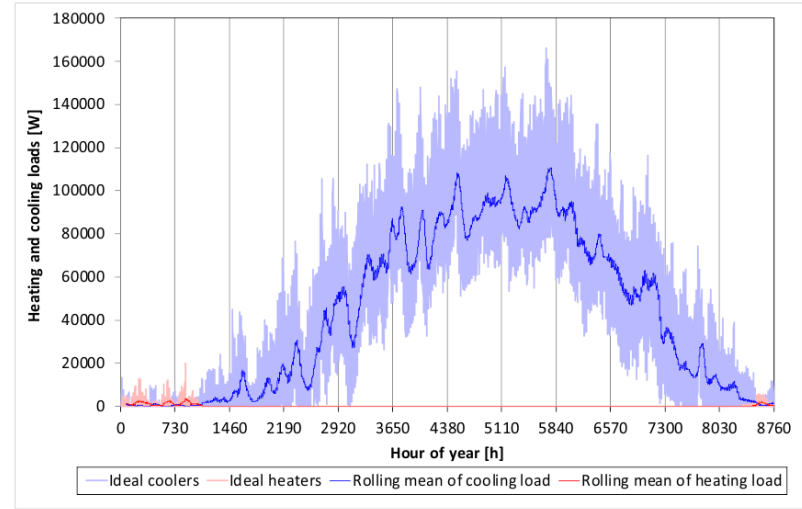
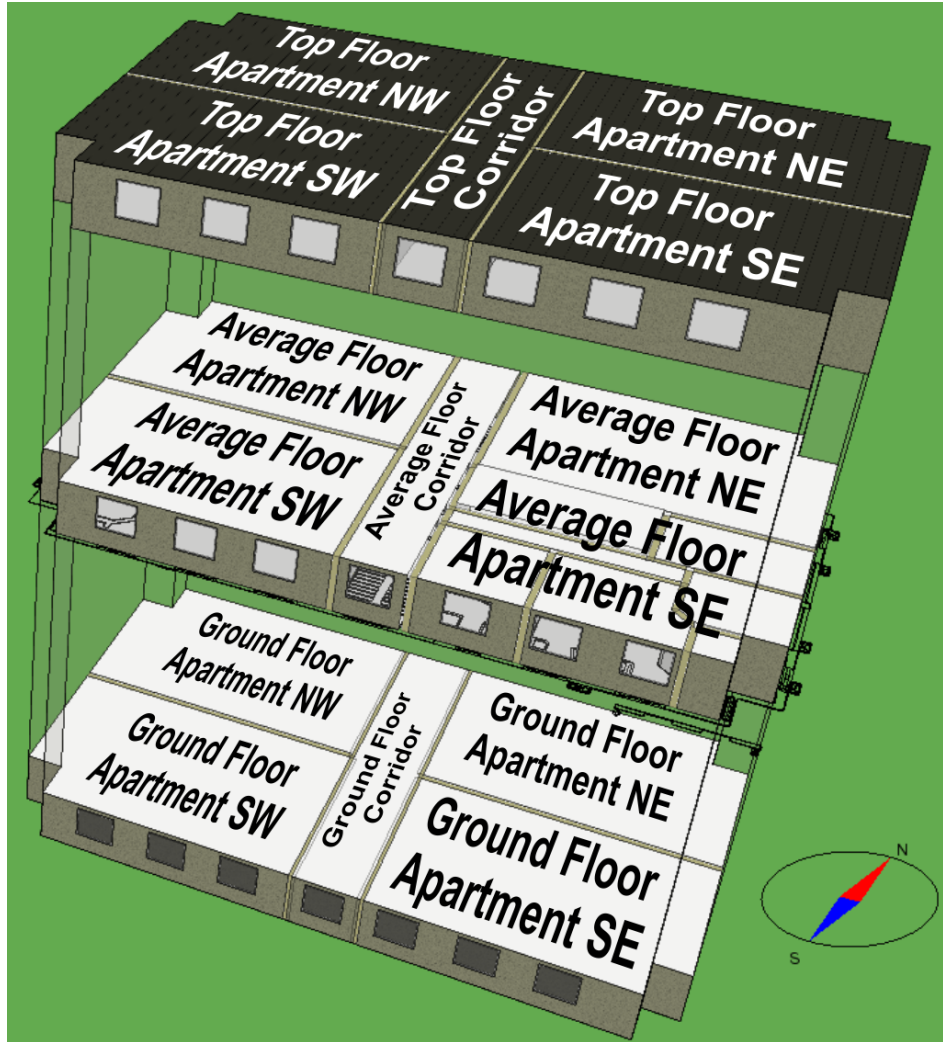


Figure 5.1.: IDA ICE simulation model of a typical apartment building with zone names (left), and example results for Hurghada, Egypt of the ideal heating and cooling loads (top right) and monthly room air energy balance (bottom left).

5. Simulations and results

Clearly visible is the dominance of the cooling demand, at least for the example location. The heating capacity can almost be neglected and is not part of the analysis of this dissertation. The overall cooling capacity is highest during the months of May, June, July, August and September with almost identical peaks in June, July and August. During this time of year, the daily and hourly deviation in needed cooling capacity can be tremendous.

The needed big cooling capacity is mainly the result of heat gains through the windows. Even with the applied shadowing strategy, the heat gains through the windows are dominating. This is indicated by the orange bars in the lower right graph of Figure 5.1. This is due to their poor heat resistance $R_{window} = 0.172 \text{ m}^2\text{K}/\text{W}$ as indicated by the given U-value in Table 4.3 on page 79. The second biggest heat source are the external walls (grey). The comparatively high gains through equipment (purple) can be explained by the still dominant presence of incandescent light bulbs in the region. The external walls become a heat sink in the months from November to April and reduce the needed cooling energy demand. This increases drastically in the main cooling period from May to October. This simulation is undertaken for all 26 locations. The resulting ideal annual heating and cooling demands are presented besides the needed installed capacities in Figure 5.2. All values are given in the appendix in Table D.2 on page XXX. The red bars above the zero line show the specific ideal heating demands of each location while the blue bars indicate the specific cooling energy demand. The green triangles on top show the specific demand of the heating capacity of the building in each location. The specific cooling capacities are indicated as purple diamonds.

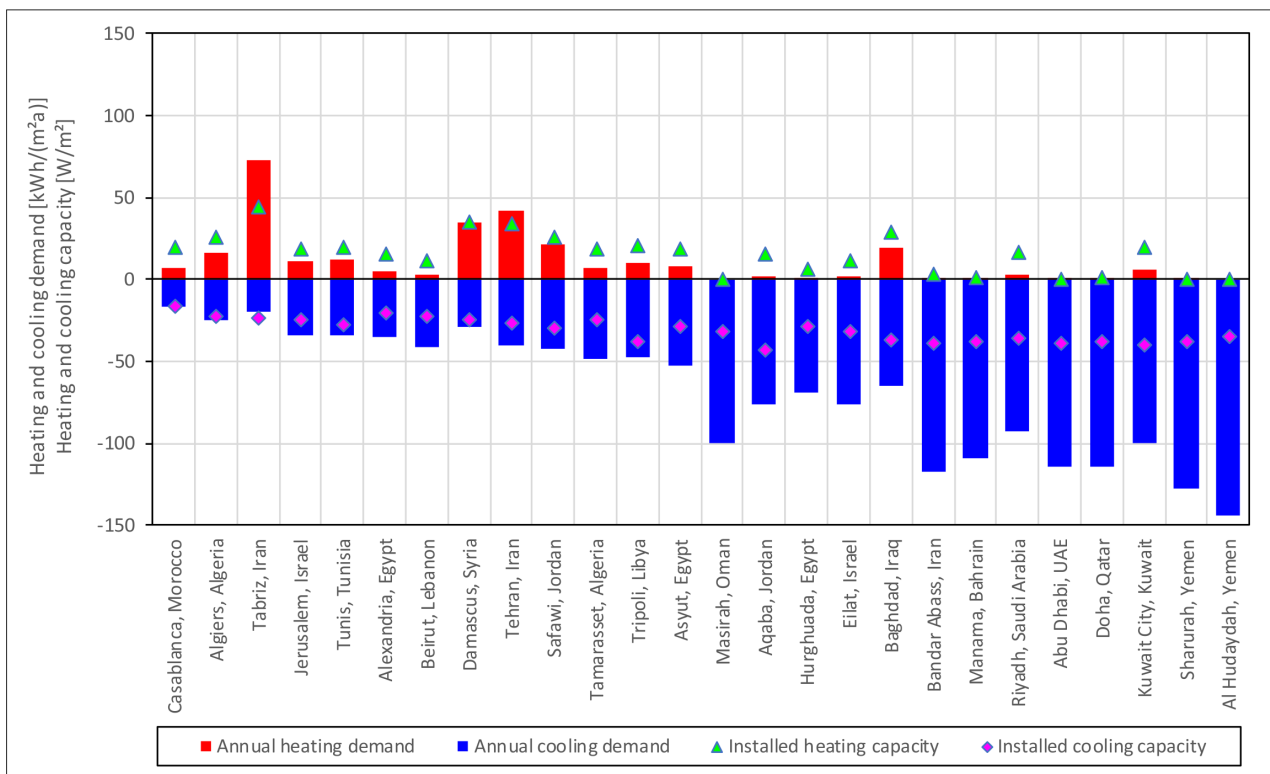


Figure 5.2.: IDA ICE simulation results of annual heating (red bars) and cooling energy demand (blue bars) of all 26 locations and their corresponding needed ideal heating (green triangles) and cooling (purple squares) loads.

The average heating capacity is only $\dot{q}_{heat} = 10.8 \text{ W}/\text{m}^2$ compared to the average cooling capacity

of $\dot{q}_{cool} = 68.1 \text{ W/m}^2$. However, the standard deviation of the heating capacity is with $\delta\dot{q}_{heat} = 16.2 \text{ W/m}^2$ much bigger than the average capacity. Multiple locations have a relatively high need for heating and accumulate much more heating energy demand throughout the year. These cities are mainly located in the inland and further away from water masses like *Tabriz (Iran)*, *Damascus (Syria)*, *Tehran (Iran)*, *Safawi (Jordan)* or *Baghdad (Iran)*. Most of the cities have no or close to none heating demand.

The standard deviation of cooling capacity is with $\delta\dot{q}_{cool} = 37 \text{ W/m}^2$ much smaller in relation to the total average installed capacity. In most locations with a high number of cooling degree days, the needed capacity is almost constant. However, the annual energy demand for cooling increases. This is a clear indication that the installed systems can be similar but only their operation times are extended with increasing cooling degree days.

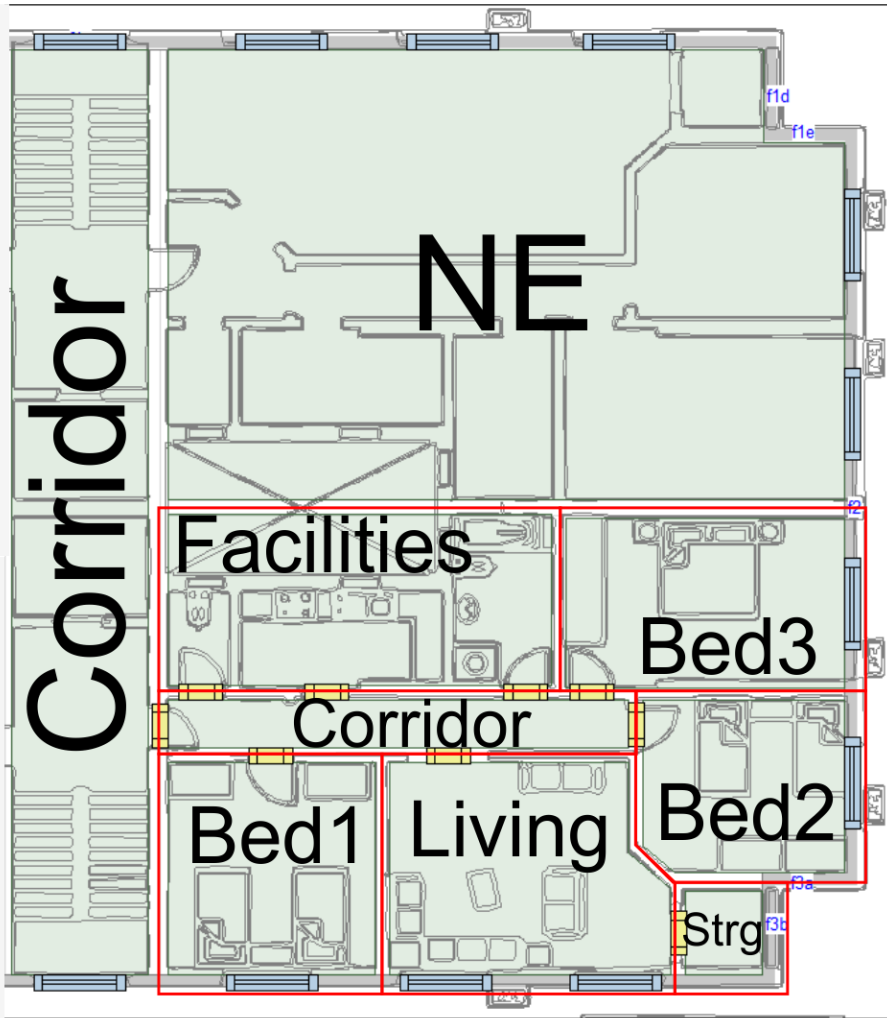
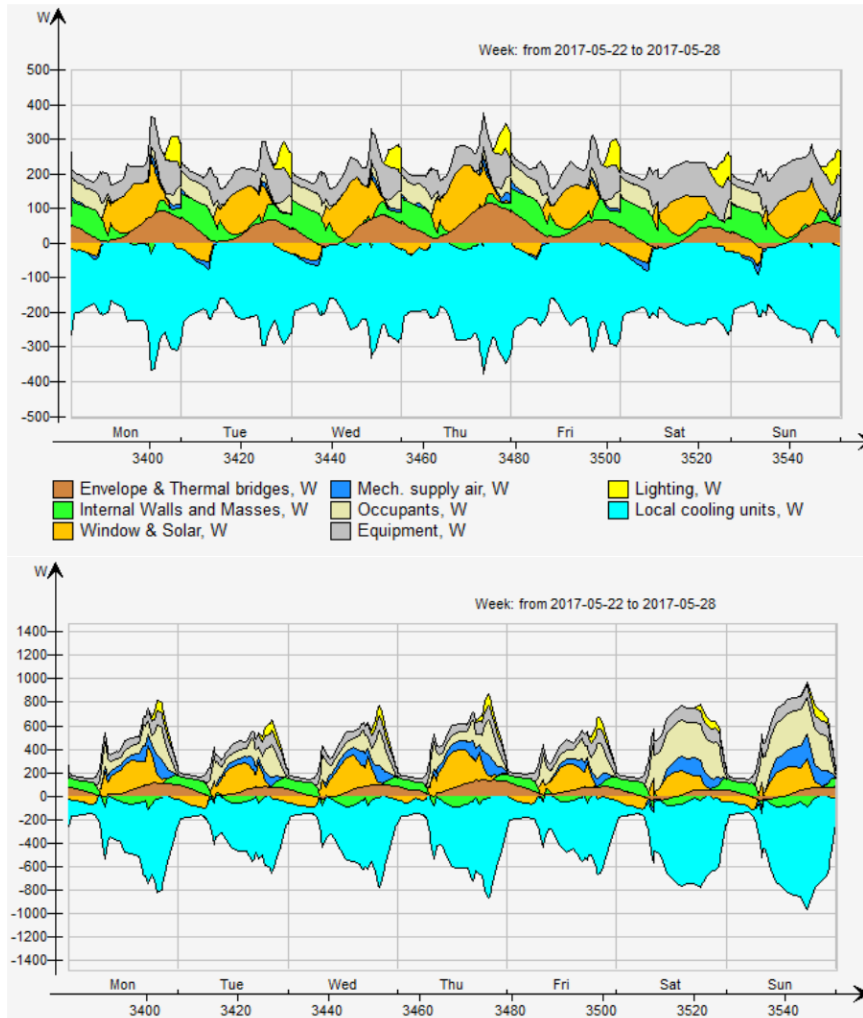
Room performance

The thermal performance of the *IDA-ICE* simulation model is evaluated in detail through the graphs in Figure 5.3. On the right side, the eastern section of the floor plan for the average apartments is presented. The boundaries of single rooms are highlighted in red. The name of each zone is presented right on the plan. The overall apartment has a total floor area of $A_{apt} = 107.2 \text{ m}^2$. For comparative reasons the bedroom *bed1* and the living room *Living* are analyzed for a week within the transition period in spring (22 to 28 May). Both rooms are facing south but have totally different user presence and equipment usage profiles. The bed room has a floor area of $A_{bed} = 15.57 \text{ m}^2$ and the living room a floor area of $A_{liv} = 19.5 \text{ m}^2$.

The different colors for the present heat sources and sinks is equivalent to Figure 5.1 and indicated in the legend in between both graphs.

The energy balance of the stated week is presented on the left side of the figure. Clearly visible is the continuous cooling energy demand (bright blue) which is particularly high in the evening hours. The thermal transport through the windows is presented in orange and is positive during the day and negative during the night. Internal walls work as buffer storage for the heat. The thermal energy which is stored and released from the walls is drawn in green. It increases the cooling energy demand especially in the bed room. However, the walls reject the heat in the living room during times of the smallest cooling demand. Here, they absorb the heat during the mid of the day and reduce the power demand during this time.

Performance of room *Bed1*



Performance of room *Living*

Figure 5.3.: Western side of standard floor in reference building from typology 2 and rooms in the south eastern apartment (right) and comparison of room energy balance for the bed room (top left) and the living room (bottom left) for an example week in the transition period (22 to 28 May).

Comparison of IDA ICE and Modelica

A *Modelica* model is created which includes the bed and living room. Both submodels are presented as their graphical representation in *Dymola* in Figure 5.4. The upper model is the bed room and the lower the living room model. *Cairo, Egypt* is selected as ambient climatic boundary condition for both room models and in both simulation environments.

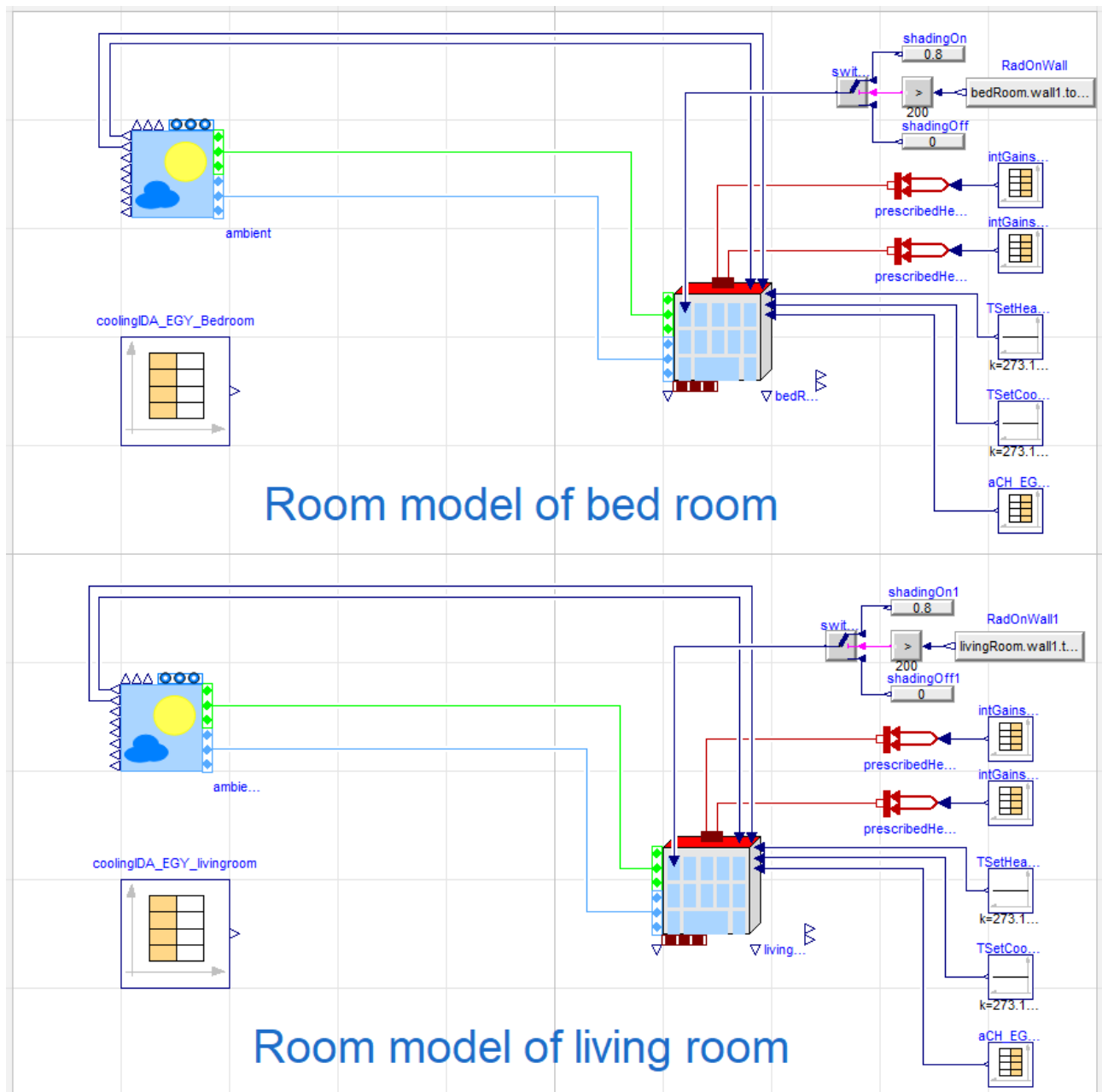


Figure 5.4.: *Modelica* set up for the comparative simulation between *IDA ICE* and *Modelica* for the bed room (top) and the living room (bottom).

The results of the cooling demand calculation in *IDA-ICE* are included to the simulation for data processing reasons. The base for each ambient model for both simulation programs are generated with *Meteonorm*. The rooms themselves are modelled equally to the *IDA-ICE* system by using the same

5. Simulations and results

physical properties and same set temperatures. The convective and radiative heat gains are exported from the results of the *IDA-ICE* simulations for each location. The simulation results from *IDA-ICE* of the air change per hour and the convective and radiative internal gains are used as model inputs for the room operation. Further, the same shading control strategy is applied. A shading factor of 0.8 is applied when the radiation onto the external wall exceeds $\dot{q}_{solar} \geq 200W/m^2$.

The following two figures compares the simulation results of both software environments for the example location of *Hurghada, Egypt*. Figure 5.5 shows both cooling energy demands for the living room. Figure 5.6 compares the results for a living room. The results which are achieved with *Modelica*, simulated with the commercial tool *Dymola*, are presented in blue. The *IDA-ICE* results are outlined in green. The differences between both tools are the result of the deviations in the building energy demand calculations of each month and for the annual calculation on the right y-axis.

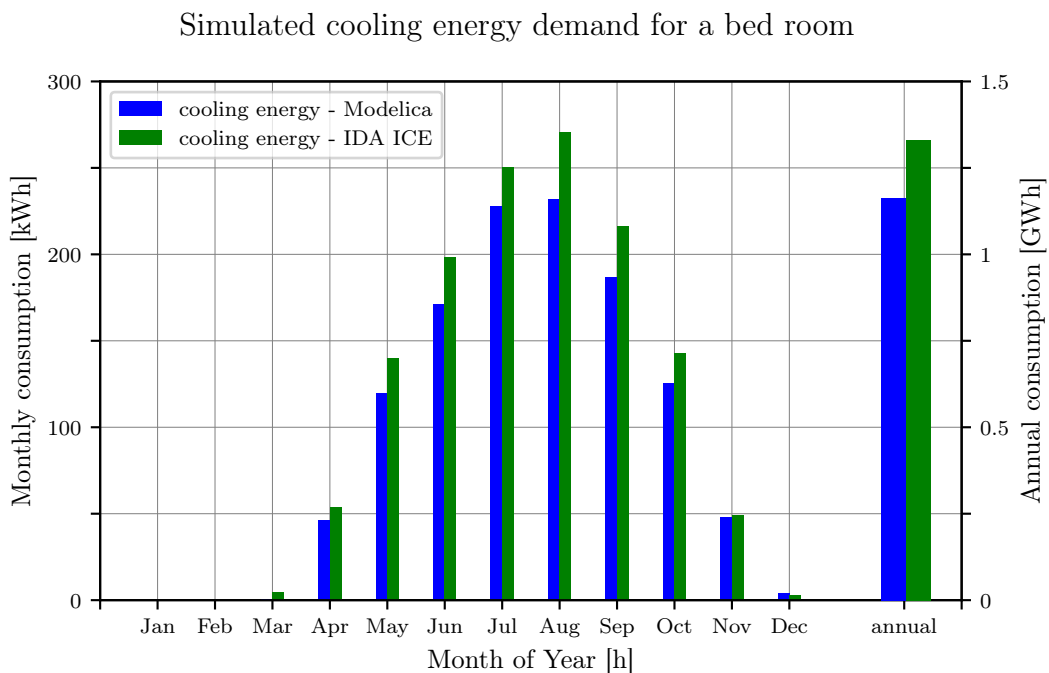


Figure 5.5.: Comparison of simulated cooling energy demand for the bed room between the reference model of *IDA ICE* (green) and the system which will be used for optimizations with *Modelica* (blue).

The calculated cooling energy demand for the bed room is overall less when simulated within *Modelica*. This is also true for each single month, except December. The annual difference is less than 250 kWh. A different picture is drawn when comparing the living room results. Here, the results of the *Modelica* models are always higher than the *IDA-ICE* results. However, the overall difference of the annual demands is equally smaller with 250 kWh.

The explanation for the switch in the difference of the annual cooling energy demand can only be explained with the heat emission through users and lighting. The window surface and internal wall areas are almost similar in both rooms which result in similar solar gains. The exact calculation of the heat gains from occupants in *IDA-ICE* is unknown to the author. The heat gains from lighting is directly given as convective heat source. However, the heat gains in *Modelica* are modeled by a load profile which is transferred each by 50% by convection and radiation to the room in terms of users and light.

Both simulation tools determine an equal amount of cooling energy demand. The outputs of the

specialized building energy demand tool *IDA-ICE* helped to improve the accuracy of the *Modelica* model. The latter model is being used to model the reference system for the bed and living room as the simulation time for an annual simulation is much faster than compared with *IDA-ICE*. The sole room simulation model only needs less than a minute for an annual simulation while it takes more than five minutes in *IDA-ICE*. Further, the use of *Modelica* allows the author to gain full access and control over the supply system modeling.

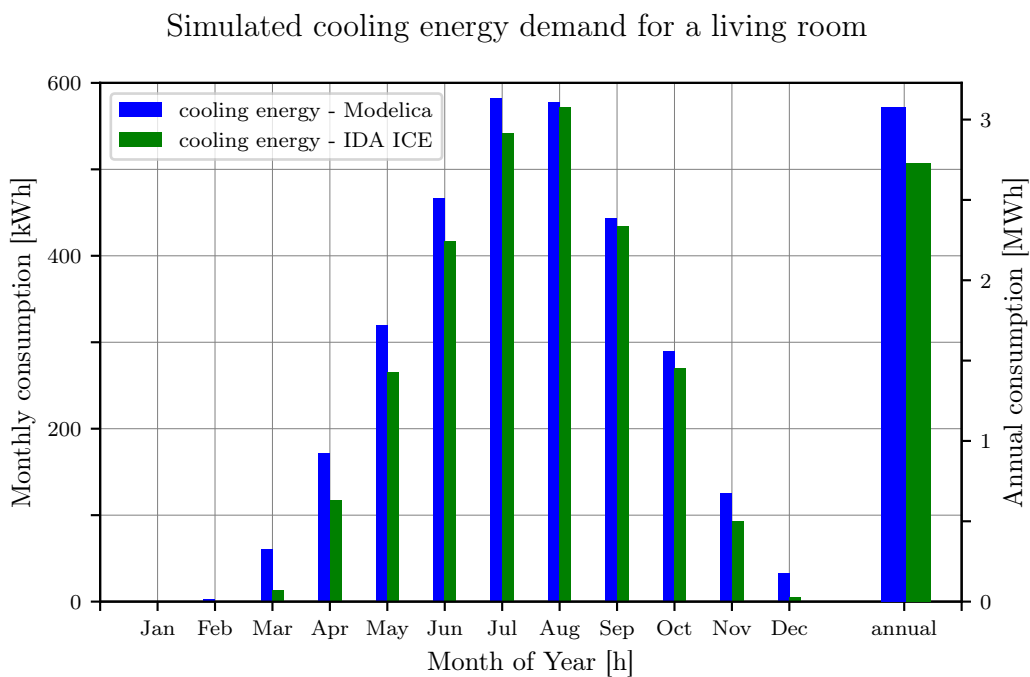


Figure 5.6.: Comparison of simulated cooling energy demand for the living room between the reference model of IDA ICE (green) and the system which will be used for optimizations with Modelica (blue).

5.2. System performance

The following section presents the results of all simulated room air cooling system for the various locations. These systems were described in Section 2.3.2, beginning on page 23. First, the overall performance of the reference system is shown. For this evaluation, the annual energy demand of both rooms in all 26 locations are displayed. Afterwards, the impacts of each room cooling system are compared. This comprises the cost for cooling and the caused greenhouse gas emissions, the impact on the grid stability, the thermal comfort and the sensible energy storage throughput.

The subsequent section analysis these performance parameters for a system to optimize the grid stability.

5. Simulations and results

5.2.1. Reference system - performance in the MENA region

The reference system is simulated for all 26 selected locations which represent the MENA region in this work. It is a simplification of the *Modelica* simulation template which was presented in Figure 4.2 on page 67. The split-unit is directly connected to the electric grid. No PV system nor battery storage or transformers are simulated. No water coolers or cold water storages are present. This system is parameterized for the bed and the living room. The results are presented in the following subsections. The subsections are separated to show and compare the annual performance of all 26 locations in the *Mena region*. After each of this comparisons, the performance is analyzed on a monthly basis for the case study location of *Hurghada, Egypt*.

Annual energy demands of the bed room in all 26 locations

The following graph in Figure 5.7 shows the simulated energy demands. The results for both rooms are given by values in Table D.2 in the appendix on page XXX. Blue is used to highlight the annual thermal cooling energy demand. Red outlines the needed electric energy demand for the simulated split-unit to exhaust these loads.

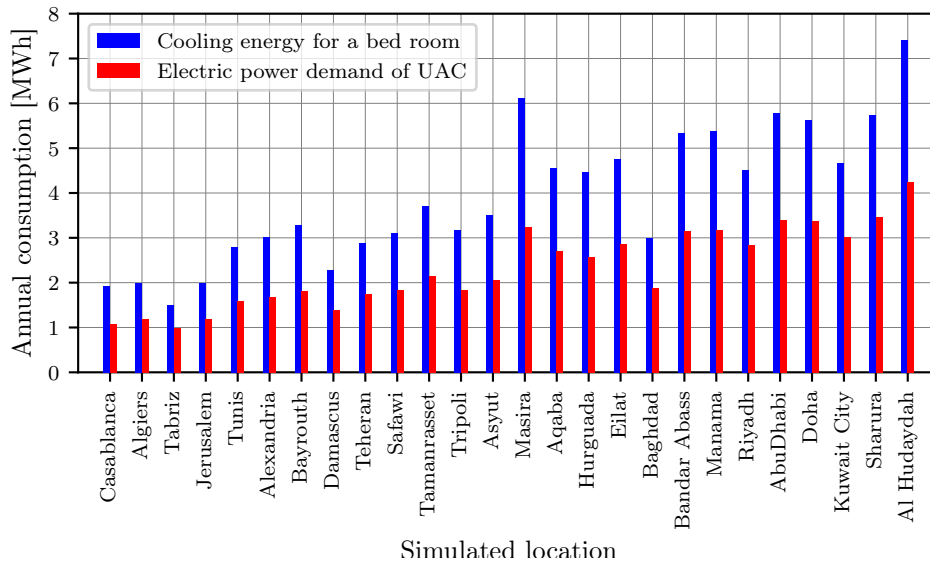


Figure 5.7.: Comparison of the annual cooling energy demands for a bed room (blue) and the corresponding annual electrical power demand for the split-unit air conditioner (red).

The difference between both values is the average coefficient of performance. In all cases, the average resulting COP is below $COP_{location} \leq 2.0$ ($COP_{avg,bed,sim} = 1.7$) which is lower than the average stated COP on the data sheet of $COP_{nom} = 2.55$. The main reason for this difference is the standby energy demand of the modeled split-unit. This power consumption is $P_{sb} \sim 30 W$ for the minimum fan setting to move the air through the indoor section of the unit and evaluate the room air temperature. This leads to the lowest COP of 1.55 for the location of *Tabriz, Iran* as here the split-unit runs idle throughout most of the times of the year.

Cooling energy demand for a bed room in the case study location Hurghada

The cooling energy demand is exemplarily analyzed on a monthly basis for the case study location in the urban region of *Hurghada, Egypt*. This is done, to gain a deeper insight to the annual cooling demand distribution.

The following graphs in Figure 5.8 and 5.10 show the monthly energy demands for a bed resp. a living room in the location. The monthly cooling energy demand are given in blue. The resulting monthly electric energy demand to satisfy those loads are given in red. A table with the detailed results of both graphs can be found in Appendix D.6 on page XXXIII.

The average daily cooling energy demand for a bed room in *Hurghada, Egypt* is $Q_{cool,bed,HRG} = 12.25 \text{ kWh/d}$ and the average daily electricity energy demand is $Q_{electr,bed,HRG} = 7.06 \text{ kWh/d}$. This divides to an annual average coefficient of performance of $COP_{bed,HRG} = 1.74$. A cooling demand is only present during the months from April to November with the highest demand of $Q_{cool,bed,max} = 815.35 \text{ kWh}$ in August. During this time, the outdoor air temperature reaches its maximum. This second highest consumption is in July. Then, also the outdoor temperatures are high and additionally, the holy season of Ramadan was celebrated, meaning that people are long and often present at home during peak load hours. The minor electric demand of $Q_{electr,bed,winter} = 22 \text{ kWh/month}$ is the result of the constant operation of the recirculating fan in standby.

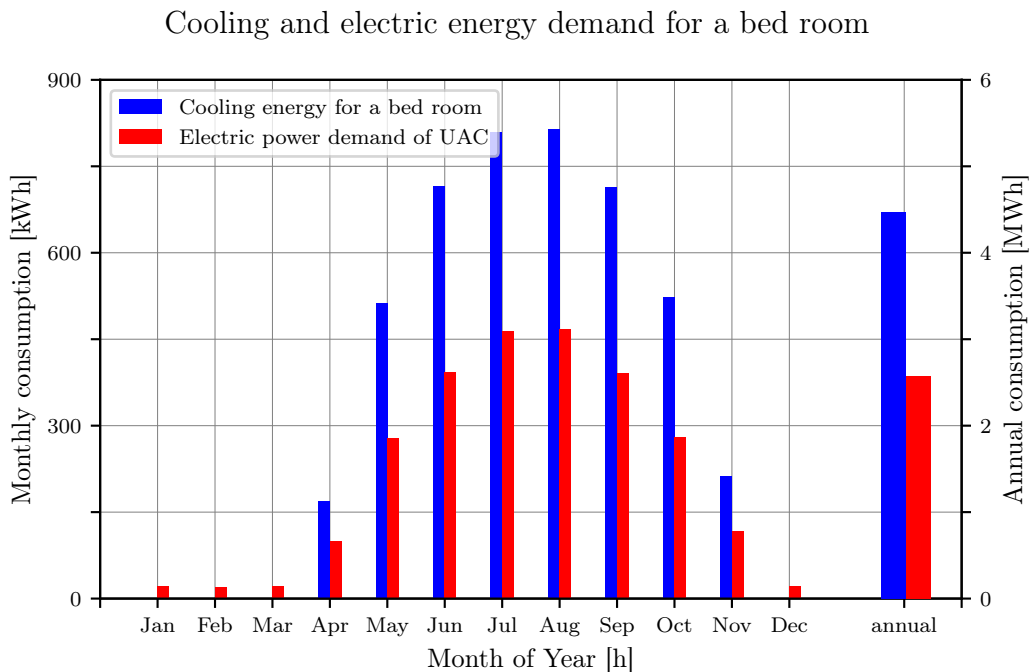


Figure 5.8.: Comparison of monthly cooling energy demands for a bed room (blue) and the corresponding monthly electrical power demand for the split-unit air conditioner (red).

5. Simulations and results

Annual energy demands of the living room in all 26 locations

Similar to the previous two sections, the results for the living room are presented for all 26 locations and in particular for the case study location of *Hurghada, Egypt*. The results in Figure 5.9 display the annual thermal (blue) and electric (red) energy demand for air cooling of an air conditioner in a living room. These results are given as well in Table D.2 in the appendix on page XXX.

As before, the difference between both values is the annual average COP. The average COP over all locations is, with $COP_{avg,liv,sim} = 1.8$, slightly higher than in the bed room. This is mainly due to the overall higher and more frequent cooling energy demand inside a living room. This reduces the stand by losses of the systems. The average COP in *Casablanca* is even above 2 ($COP_{avg,liv,MA} = 2.07$). This is due to the better performance of an electric driven compression chiller in colder environments. The worst average COP for both room types occurs in *Kuwait City* ($COP_{avg,bed,KW} = 1.54$ and $COP_{avg,liv,KW} = 1.61$). High outdoor temperatures throughout the entire cooling season reduce the efficiency of the split-unit.

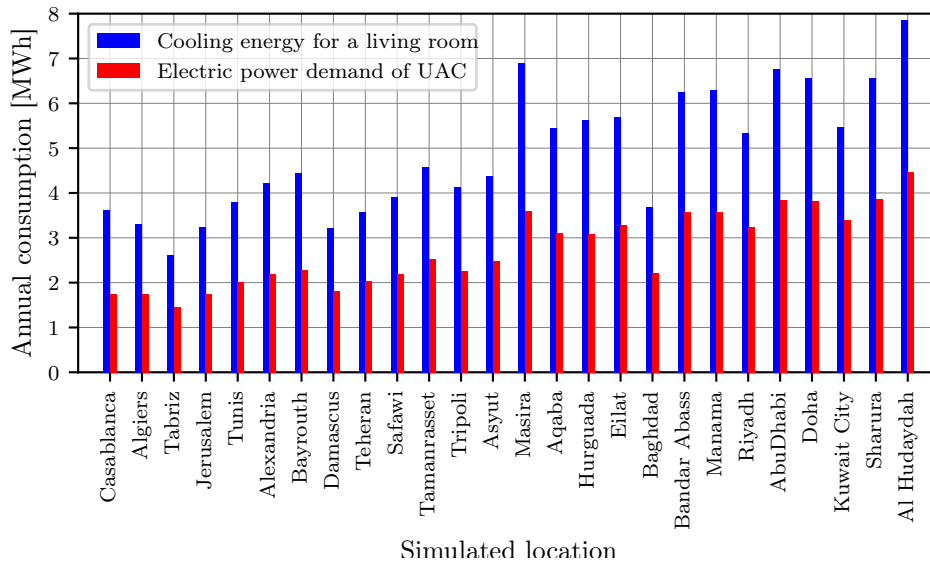


Figure 5.9.: Comparison of the annual cooling energy demands for a living room (blue) and the corresponding annual electrical power demand for the split-unit air conditioner (red) for all 26 locations.

Cooling energy demand for a living room in the case study location Hurghada

As before, the needed cooling energy and the resulting electric energy is compared on a monthly basis for the case study location of the Egyptian Red Sea region *Hurghada*. The same trend, as in the results for a bed room, can be observed in the following graph, showing the results for the living room.

Here, the average daily cooling energy demand for a living room is $Q_{cool,liv,HRG} = 15.40 \text{ kWh/d}$ and the average daily electricity energy demand is $Q_{electr,bed,HRG} = 8.46 \text{ kWh/d}$. This divides to a higher annual average coefficient of performance of $COP_{bed,HRG} = 1.82$. This is mainly due to the decreased standby losses as cooling demand is present during all months except January. Also, July and August have the highest overall cooling and electric energy demands.

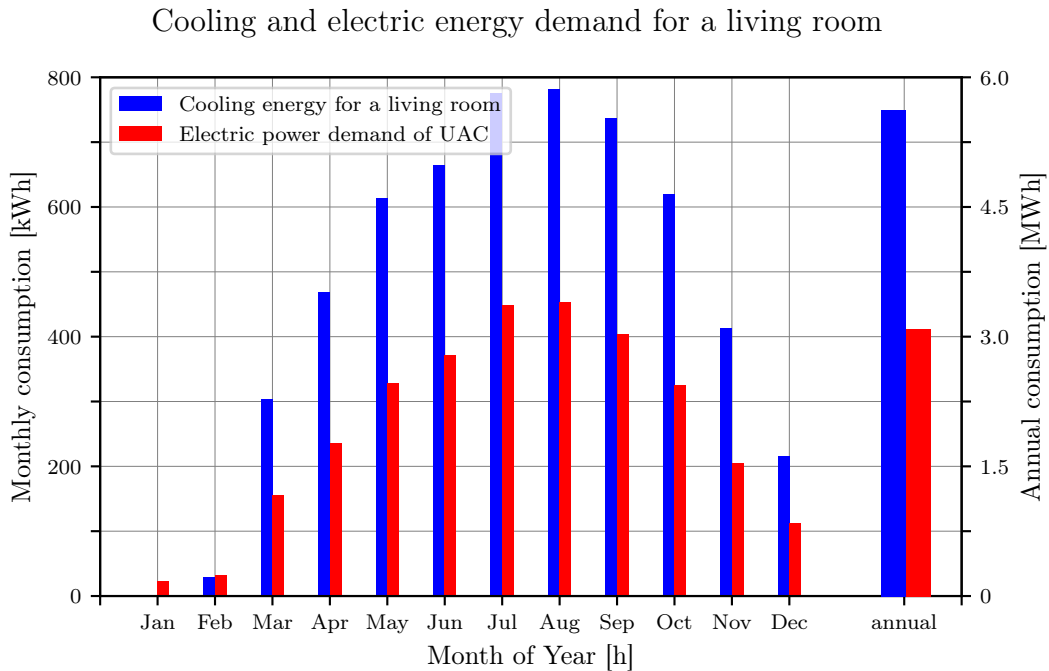


Figure 5.10.: Comparison of monthly cooling energy demands for a living room (blue) and the corresponding monthly electrical power demand for the split-unit air conditioner (red) in Hurghada, Egypt.

Costs and greenhouse gas emissions for room air cooling

The following graph concludes the annual costs and GHG emissions for both rooms in all 26 locations. The specific costs and emissions are concluded as values in Table D.3 in the appendix on page XXXI. The costs are given in USD/kWh and are calculated with the average consumer electricity prices of 2018 [12], except for Lebanon [141], Oman [142], Libya [143], Kuwait [144], Yemen [145] and Syria [146]. The electricity prices for the first 5 countries are given for 2012, the electricity price for Syria is given for 2015. The average price of electricity over all 26 nations is $C_{elect,avg} = 0.08 \text{ \$/kWh}$. The resulting costs to cool a bedroom are indicated in the graph in Figure 5.11 as blue bars. The annual costs to cool a living room in each location are stated as red bars.

The annual GHG emissions are based on the equivalent CO_2 emissions of the electric grids of each country in the year 2009 [32], except for Iran and Israel. There, the regions average emissions per used kilowatt hour are taken. The average GHG emissions in the region are $EM_{GHG,avg} = 0.658 \text{ kgCO}_{2,equiv}/kWh$. The emissions which are caused for cooling the bed room are indicated as green diamonds and on the right y-axis. There, also the GHG emission of the living room A/C are highlighted as green triangles. For comparative reasons, the annual carbon budget per person to reduce global warming to 2 K is drawn as dashed orange line.

Location with a low electric energy demand for cooling and a low electricity price have a low budget need for room air cooling purposes consequently. This includes locations like *Algiers*, *Morocco* or *Tabriz*, *Iran*. A particular outlier is *Masirah*, *Oman*. The high cooling energy demand and highest electricity price of the region ($0.26 \text{ \$/kWh}$) causes a tremendous budget need for room air cooling. The same accounts for *Tripoli*, *Lybia* as it has the second highest electricity prices ($0.21 \text{ \$/kWh}$). The other end of the spectrum is *Doha*, *Qatar*. Here, the electricity price is one of the lowest ($0.03 \text{ \$/kWh}$) and keeps the budget need for room air cooling very limited despite the fact that it has the third highest electric energy demand of all simulations. Locations in *Kuwait* and *Yemen* have a particular high operation cost demand even besides their low electricity costs ($0.03 \text{ \$/kWh}$ resp. $0.07 \text{ \$/kWh}$).

5. Simulations and results

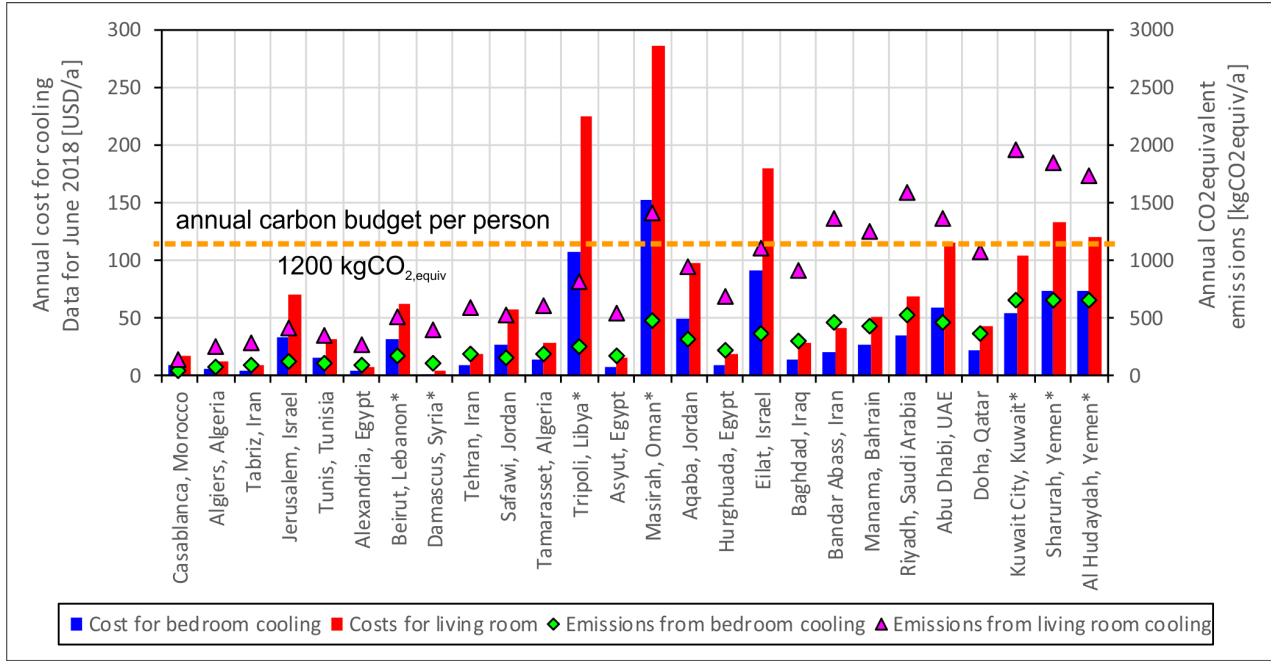


Figure 5.11.: Annual costs for cooling (left y-axis) for all 26 selected locations for a bedroom (blue bars) and a living room (red bars), based on electricity prices from 2018 [12] (except locations marked with an asterisk) and annual carbon emissions (right y-axis) for a bedroom (green squares) and a living room (purple triangles), based on El Khoury (2009)[32] (except Iran and Israel, their emissions are the regions average). The orange line marks the annual carbon equivalent emissions budget per person to reduce global warming to 2K [33].

Impact on grid stability in all 26 locations

Next, the impact on a local connect grid is evaluated for both room types and all 26 locations. Therefore, the annual ratio of the electricity demand, which is needed for room air cooling during peak load hours, over the overall annual energy demand for room air cooling is calculated. The results for these shares are presented in Figure 5.12. The corresponding Table D.4 with all results is presented in the appendix on page XXXII. Results for the bedroom are indicated in blue, for the living room in red. The average share of the peak demand over all 26 locations is 0.240 for the bed room and 0.252 for the living room.

The highest shares for both rooms are reached in *Casablanca, Morocco* with 0.295 for both rooms. The shares are smaller in locations with a higher overall cooling energy demand and are lowest in *Doha, Qatar* with 0.215 and 0.219. The shares of a living room are always higher than those of the bed room. This is due to the user profile, as living rooms are mainly and extensively used during peak load hours. Another burden for the grid is the number of on and off switching cycles of the air cooling system. This is due to the peak electricity demand of a compression chiller in the startup phase. A compression chiller needs 3 times more power in the first split of a second when activated. This small but dramatic spike in electricity demand has a high impact on the grid stability. The graph in Figure 5.13 shows the annual sum of on/off switching cycles in all 26 locations. As before, the numbers for a bed room are indicated in blue and for a living room in red. The detailed table with all calculated values can be found in Appendix D.4 on page XXXII. The average number of cycles is around 12000/a for a bed room and about 17250/a for a living room.

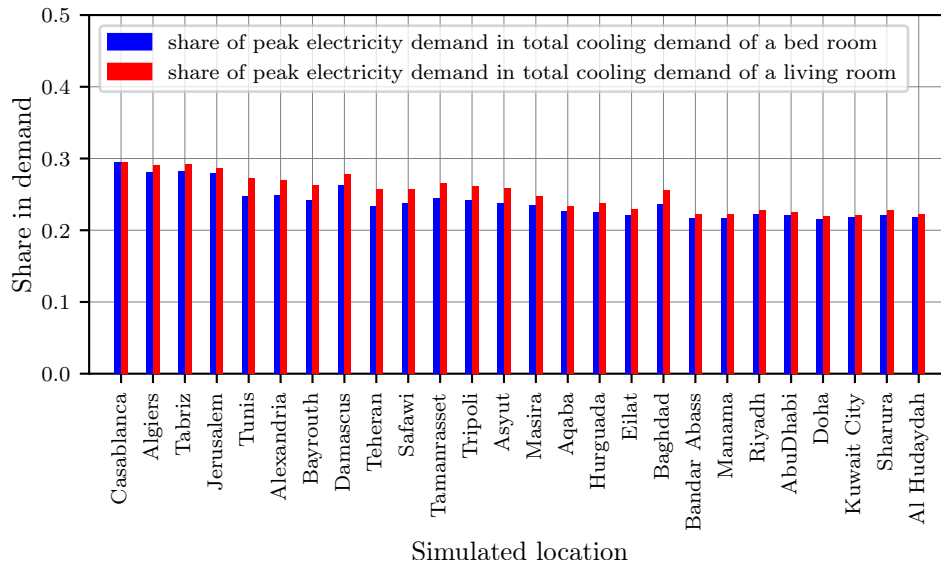


Figure 5.12.: Average share of the electricity demand for air cooling during peak load hours (5 to 9pm) in the total daily electricity demand for air cooling of a bed room (blue) and a living room (red) in all 26 locations.

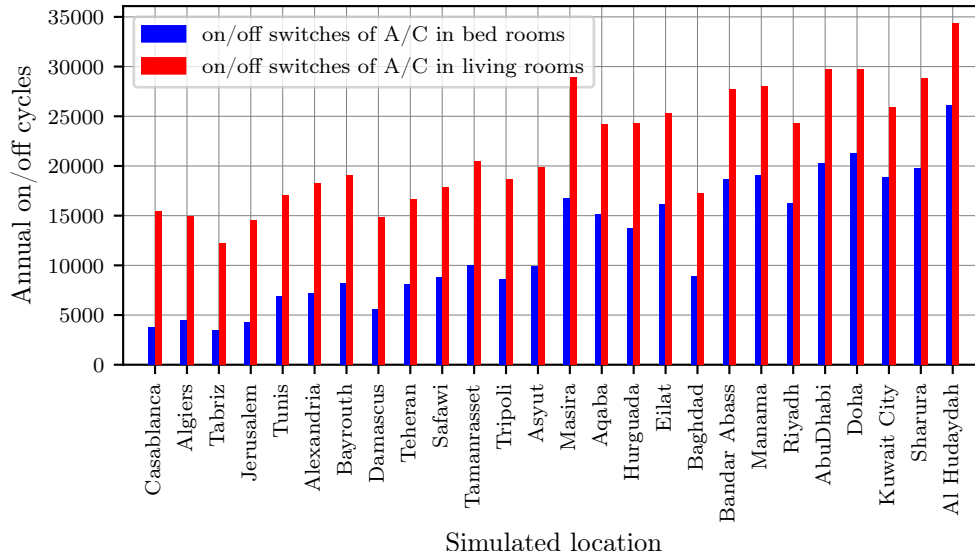


Figure 5.13.: Annual number of on/off switching cycles of the reference A/C in a bed room (blue) and a living room (red) in all 26 locations.

Here, also the clear trend is visible: the more cooling degree hours a location has, the more often an A/C is switched on and off. Due to the higher overall cooling energy demand, an A/C is always cycled more often in a living room. The lowest number of cycles was simulated for both room types in *Tabriz, Iran* with 3469 cycles in the bed room and 12250 cycles in the living room. The cities of *Masira, Oman* and *Baghdad, Iraq* are the biggest outliers on the overall trend line. *Masira's* hot summers increase

5. Simulations and results

the air conditioner use in the cooling season tremendously and thereby increasing the number of cycles to up to 50 on a single hot summer day. *Baghdad* is much below the trend line. Due to its continental climate, which is comparable to *Tehran, Iran*, the number of switching cycles is comparable low, even during the main cooling season.

Impact on local electric grid in the case study location Hurghada

The average daily load profile is created for all typical three seasons (winter, summer and ramadan) in the *MENA* region. First, the average load duration curves for the electric energy demand of a bed room are shown in Figure 5.14. Afterwards, the resulting curves for a living room are shown in 5.15. In both diagrams, the red line draws the electricity demand during summer, the blue line for the winter period and the green line during Ramadan. These three curves are each an average over all days of each certain time period of a year. They are the results of the *Modelica* simulations.

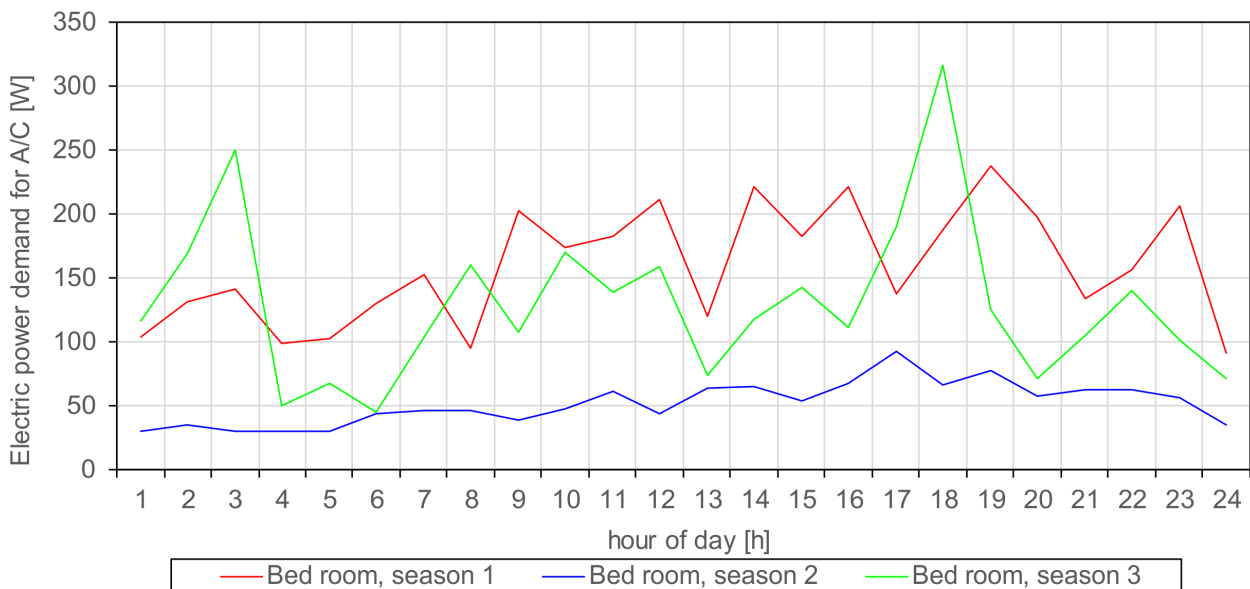


Figure 5.14.: Average daily electric demand profile for an air cooling in a typical bed room in Hurghada, Egypt during summer (season 1, highlighted in red), during winter (season 2, outlined in blue), and during Ramadan (season 3, indicated in green).

During winter the demand is almost constant and around $P_{electr,bed,winter,avg} \sim 50 W$. This is more or less the power demand in stand by. The cooling demand is only present in April and November and in the early night hours around 5 to 7pm. This is visible by the slightly increases average daily load duration curve to $P_{electr,bed,winter,max} \sim 90 W$. A similar picture is drawn during summer. The demand curve increases softly from around 100 W around midnight to 250 W at 7pm. The profile is mainly dominated by the present users in the room. During the morning and noon hours, the bed room is not occupied. Hence, the cooling load is reduced during this times. The occupation and thermal delayed cooling load create the peak at 7pm. A complete different picture is drawn during Ramadan. People go to bed late and create a dramatic peak around 3am. The bed room is unoccupied shortly before sunrise and than again used until noon. It is again much used in the hours before sunset. Then, also the thermal cooling load, due to the thermal delayed transfer of the outdoor heat, peaks.

A different picture is drawn for the average load profiles in the living room. No cooling load is present

from midnight to sunrise. The first loads appear with the first occupants around 6am. In the afternoon (from 2pm to 8pm), the load is constantly slightly below 200W, as most family members spent their time here during the days. This profile is escalated in summer. Also, only minor cooling loads need to be satisfied in the night hours until sunrise. The electric energy demand follows the outdoor temperature profile and peaks around 4pm. A second peak is visible around 8pm, when the cooling load due to thermal transmittance and the amount of present users are high. This is also the reason for the drastic peaks around this time during Ramadan. People gather together after sunset to break the feasting together.

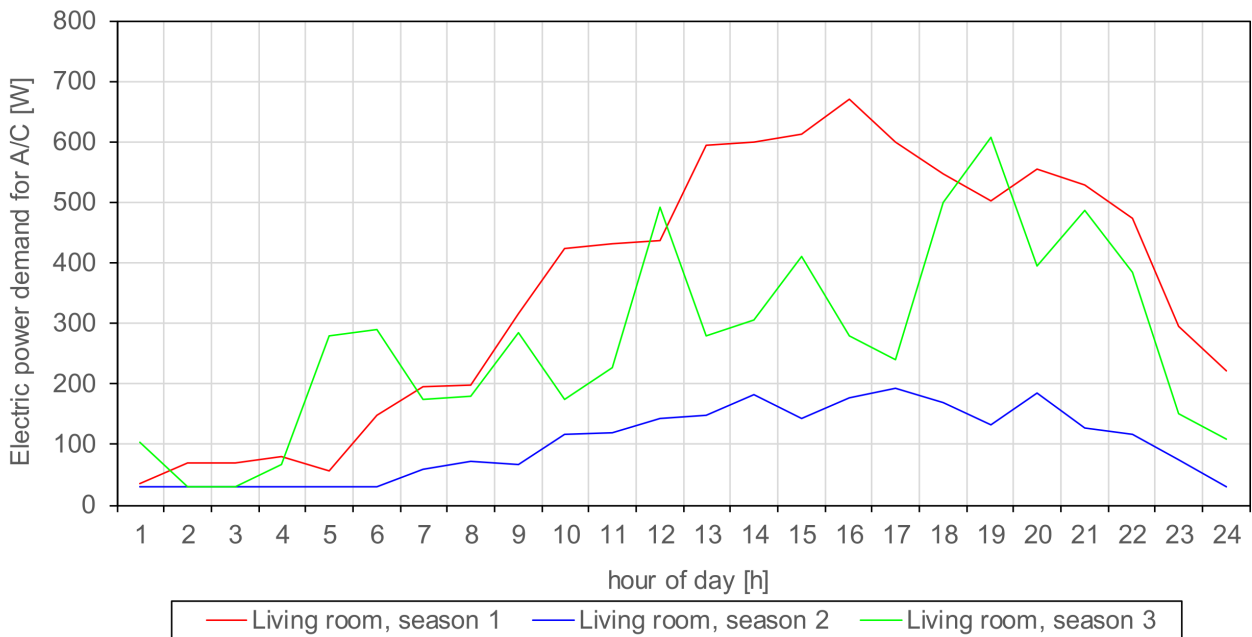


Figure 5.15.: Average daily electric demand profile for an air conditioner in a typical living room in Hurghada, Egypt during summer (season 1, highlighted in red), during winter (season 2, outlined in blue), and during Ramadan (season 3, indicated in green).

The number of on/off switching cycles is further summed up. The results are shown in the following Figure 5.16. The results for a bed room are given in blue, the ones for a living room are drawn in red. In average, an A/C is switched on and off 100 times per day ($\equiv 4 /h$ in a bed room and 170 times per day ($\equiv 7 /h$) in a living room. The full table with the results can be found in Appendix D.7 on page XXXIV.

The number of switching cycles follows the general annual trend of the cooling load. An air conditioner is cycled most often during July and August with close to no difference in total cycles. The numbers break down to $n_{on/off,bed} = 10 /h$ and $n_{on/off,liv} = 15 /h$. The toggle rate is especially high when the internal gains are high. The convective shares of cooling loads from lighting, occupants and devices have an immediate impact on the air temperature. These loads can only be exhausted by the recirculating air through the split-unit system, as the walls are too hot to store thermal energy or transfer heat to the outside.

5. Simulations and results

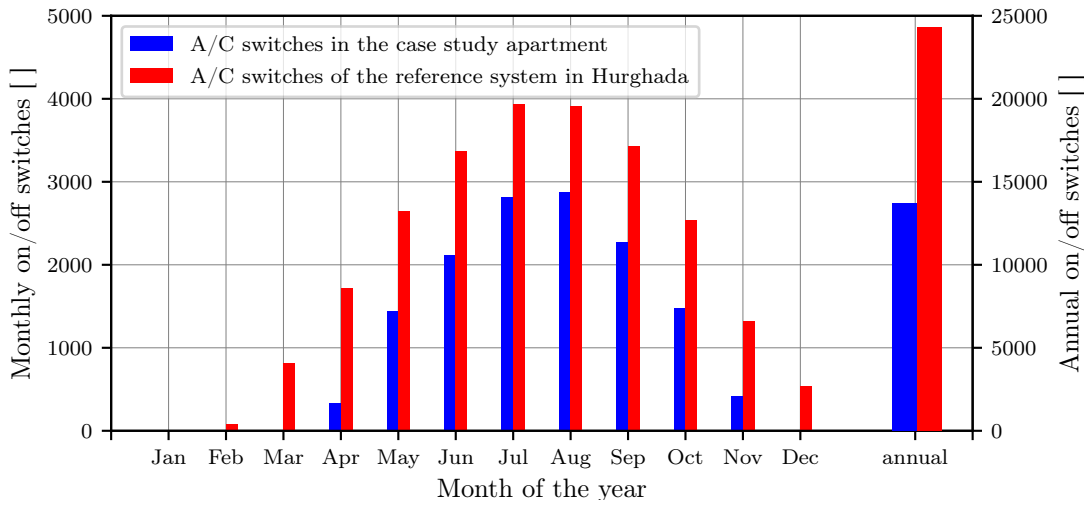


Figure 5.16.: Monthly (left y-axis) and annual (right y-axis) number of on/off switching cycles of the reference A/C in a bed room (blue) and a living room (red) in Hurghada, Egypt.

Thermal comfort in all 26 locations

The temperature difference $\Delta T_{wall-air}$ is the difference of the outer wall temperature to the room air temperature and is summed up while the inner surface temperature of the wall is more than 28°C to evaluate the annual thermal discomfort. This was described in Subsection 4.4.2 on page 72. The results are presented in the following graph. Blue are the degree hours of the bed room, red of the living room. The average sum over all 26 locations is $8208^{\circ} * h$ in the bed room and $10008^{\circ} * h$ in the living room. The detailed table of all results is presented in Annex D.5 on page XXXIII.

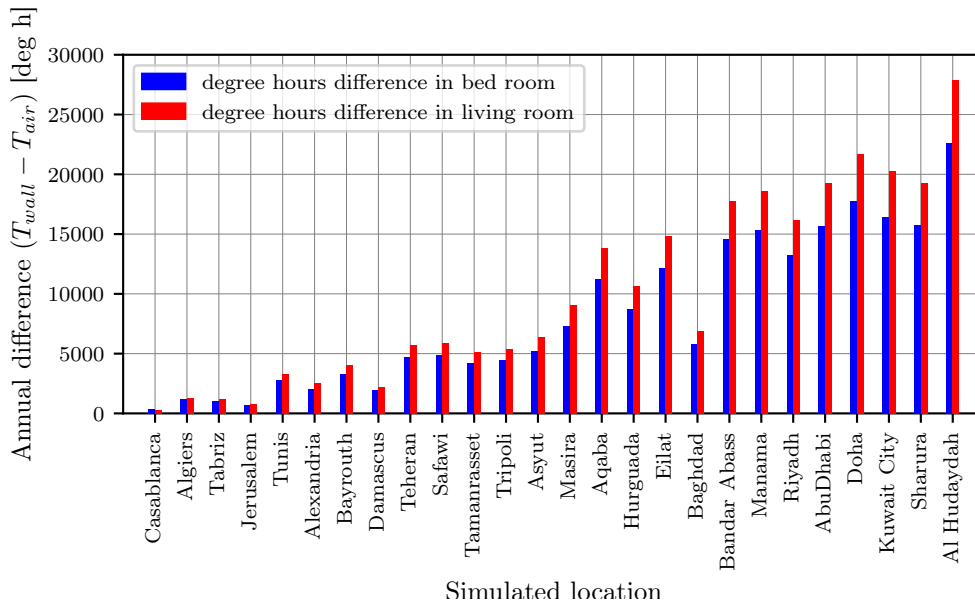


Figure 5.17.: Absolute annual (right y-axis) hourly accumulated degrees difference between room air temperature and the outer wall surface temperature of a bed room (blue) and a living room (red) of all locations. Only the hours where the wall surface temperature is above 28°C are accounted.

The shown trend correlate with the previous given results: the higher the overall number of cooling degree hours of a location the higher the degree hours difference between the wall surface temperature and the room air. The lowest amount is summed up to 341 *deg h* resp. 291 *deg h* in *Casablanca, Morocco*. This is also the only location where the sum is higher in the bed room. The biggest amounts are calculated with 22589 *deg h* resp. 27843 *deg h* for *Al Hudaydah, Jemen*. The general trend line is again broken most significant by *Baghdad, Iraq*. There the amounts are similar to *Tehran, Iran*, with a similar continental climate profile.

Thermal comfort in the case study location Hurghada

Next, the thermal comfort is evaluated with the help of the inner surface temperature of the outer walls of both rooms. The concept of the temperature degree hours to evaluate this performance was introduced in the previous sections. The monthly and annual sums are presented in the graph in Figure 5.18. Blue is used for the accumulated degree hours in a bed room and red in a living room. The annual sum for a bed room is $degH_{bed,HRG} = 7879.5^\circ * h$ and is for a living room $degH_{bed,HRG} = 10237.9^\circ * h$. A detailed table with the results can be found as well in Appendix D.7 on page XXXIV.

The wall surface temperature exceed first $28^\circ C$ in April and last in November. Clearly the highest values are reached in both rooms during August. There, the temperature difference between surface and air accumulates to $degH_{bed,August} = 2144.9^\circ * h$ resp. $degH_{liv,August} = 2692.8^\circ * h$. This means that during an average day in August, the wall surface temperature is $\Delta\vartheta_{bed} = 2.88K$ resp. $\Delta\vartheta_{liv} = 3.62K$ above $28^\circ C$ while the room air temperature still is $26^\circ C$ on average.

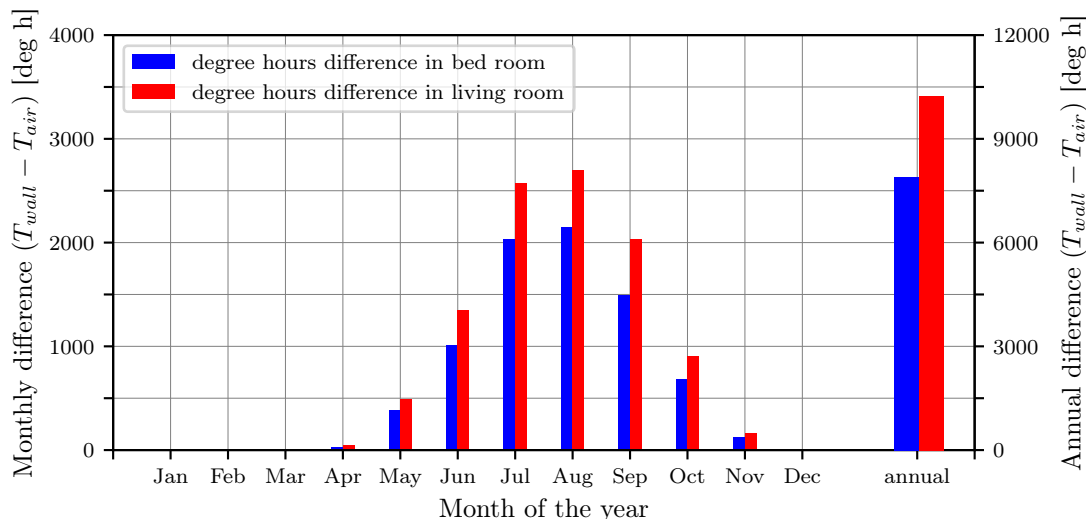


Figure 5.18.: Absolute monthly (left *y-axis*) and annual (right *y-axis*) hourly accumulated degrees difference between room air temperature and the outer wall surface temperature of a bed room (blue) and a living room (red) in Hurghada, Egypt. Only the hours where the wall surface temperature is above $28^\circ C$ are accounted.

Sensible energy storage throughput in all 26 locations

The sensible energy which is stored and released from internal wall surfaces is a good indicator to evaluate the storage capacity of the building masses. The performance of the building integrated thermal storage system, the room surfaces, is evaluated according to Subsection 4.6.5 on page 102. The absolute values of the stored and released thermal energy is summed up for every location for an entire year. These final evaluation parameters are outlined in the graph below. Blue is used for the energy

5. Simulations and results

throughput through interior walls of bed rooms, red is used for the results of living rooms. The results can be found in the same table as the previous results in Appendix D.5 on page XXXIII. In average, 272.8 kWh/a of sensible energy are stored and released from the interior wall surfaces of a bed room. The average energy throughput through the interior surfaces of living rooms sums up to 386.4 kWh/a. Also, this final performance evaluation parameter follows the previous calculated trends: increasing cooling degree hours of a certain location means an increasing amount of energy throughput. However, the trendline is not as steep as seen in other parameters. Always, the energy which is stored and released in living rooms is higher than in bed rooms. The main reason is the increased surface due to a bigger floor area. Again, *Baghdad, Iraq* is the most significant break of the trendline.

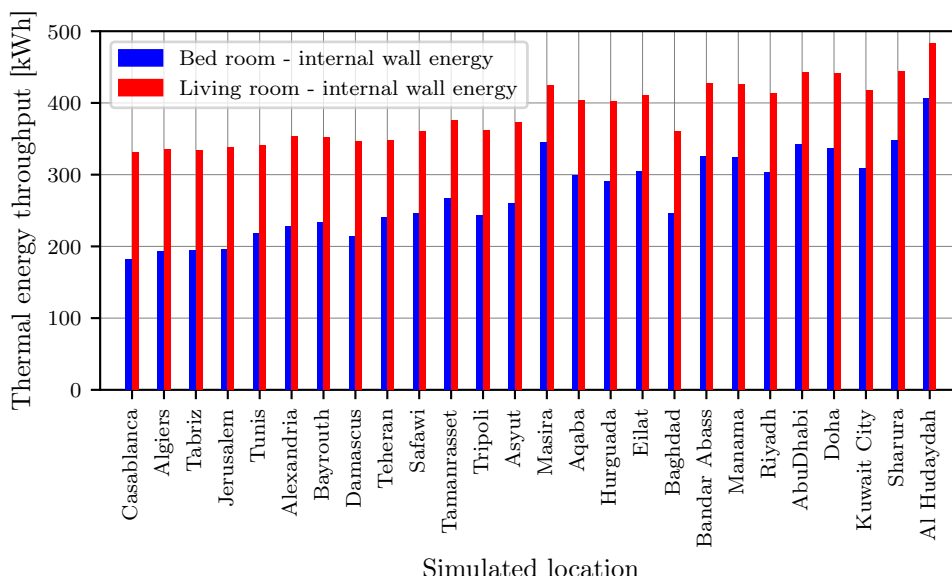


Figure 5.19.: Annual amount of roundtrip energy stored in the internal thermal masses of a bed room (blue) and a living room (red) in all 26 locations.

Sensible energy storage processes in the case study location Hurghada

The monthly sums in *Hurghada, Egypt* are presented in the following figure. Annually, 234.6 kWh are stored in and released from the room surfaces of a bed room (indicated in blue) and 358.2 kWh are cycled through the living room surfaces. Also these monthly values can be found in Appendix D.7 on page XXXIV.

The stored and released energy amount is biggest in July and August. In both months 32 kWh are cycled through the surfaces of a bed room and 36 kWh are cycled through living room surfaces. It is already more than 1.03 kWh/d resp. 1.16 kWh/d. These thermal capacities are almost 10% of the daily cooling energy demand.

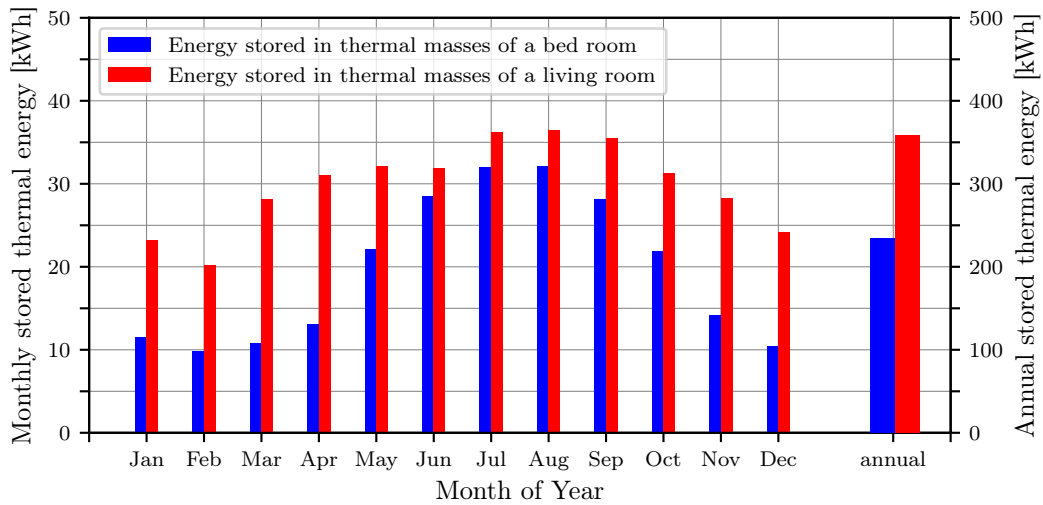


Figure 5.20.: Monthly (left y-axis) and annual (right y-axis) amount of roundtrip energy stored in the thermal masses of a bed room (blue) and a living room (red) in Hurghada, Egypt.

5.2.2. Performance with minimized investment costs

A minimum solar cooling system is introduced to evaluate the performance of a small scale photovoltaic system with a small battery system. This system and the used system components are shown in Section 3.5.3 on page 59. The resulting simulated model is shown as graphical representation in *Modelica* in the scheme in Figure 5.21 for the bed room. It is a reduced version of the system template in Figure 4.2 on page 67.

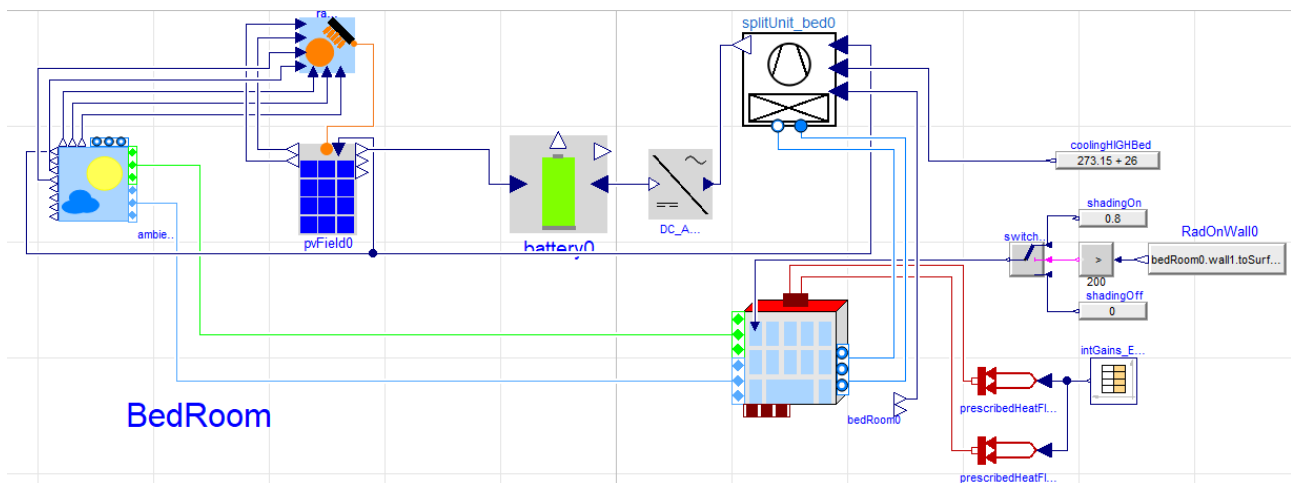


Figure 5.21.: Modelica set up for any location for the bed or living room (naming example for the bed room) with a small scale photovoltaic and battery system.

This small scale system expansion has no influence on the previous described parameters. The thermal comfort parameters are not changing and the overall cooling energy demand is not changed. Only the amount of grid supplied electricity deviates. The calculation of the solar coverage rate and solar cooling autonomy are introduced in Section 3.5.2 on page 58 to evaluate the impact on the energy balance and grid autonomy of a given system. Both values are presented for a bed room in the following graph in

5. Simulations and results

Figure 5.22 and for a living room in Figure 5.23. Also this results can be found as detailed table in Appendix D.8 on page XXVII. In a bed room, the average solar coverage rate over all 26 locations is $SCR_{avg,bed} = 0.929$ and the average solar autonomy rate is $SCA_{avg,bed} = 0.281$.

The hotter an environment is, the more cooling demand can be directly satisfied with on site generated electricity and thereby increasing the SCA . The overall high cooling energy demand reduces the SCR on the other side. The first twelve locations have a SCR bigger than one. This means that the overall annual electric output of this small scale PV system is higher than the annual electric energy demand for the split-unit system. Outstanding is the location of *Tabriz, Iran*. Here, two times more energy then needed for room air cooling is generated with the PV system. The lowest ratio is generated in *Al Hudaydah, Jemen*. There, the pv electricity can satisfy only 41% of the electric energy demand. However, the SCA is the highest with $SCA_{ALH} = 0.44$. This means that 44% of the electric cooling demand are directly satisfied by the photovoltaic generated electricity. This value is the lowest in *Casablanca, Morocco* with only $SCA_{Casa} = 0.17$. *Masira, Oman* has a very low SCR and high SCA despite its average annual cooling degree hours.

In a living room, the average solar coverage rate over all 26 locations is with $SCR_{avg,liv} = 0.731$ lower than in the bed rooms. However, the average solar autonomy rate is with $SCA_{avg,liv} = 0.368$ higher than in bed rooms. Also, the performance of the living rooms follow the general trends compared to the bed room. However, the highest SCR is only 1.36, again in *Tabriz, Iran*. This time, the lowest value is calculated for *Doha, Oman* with even only 0.37. *Al Hudaydah* has again the highest SCA rate with 0.48 which is 4 percentage points higher then in the bed room.

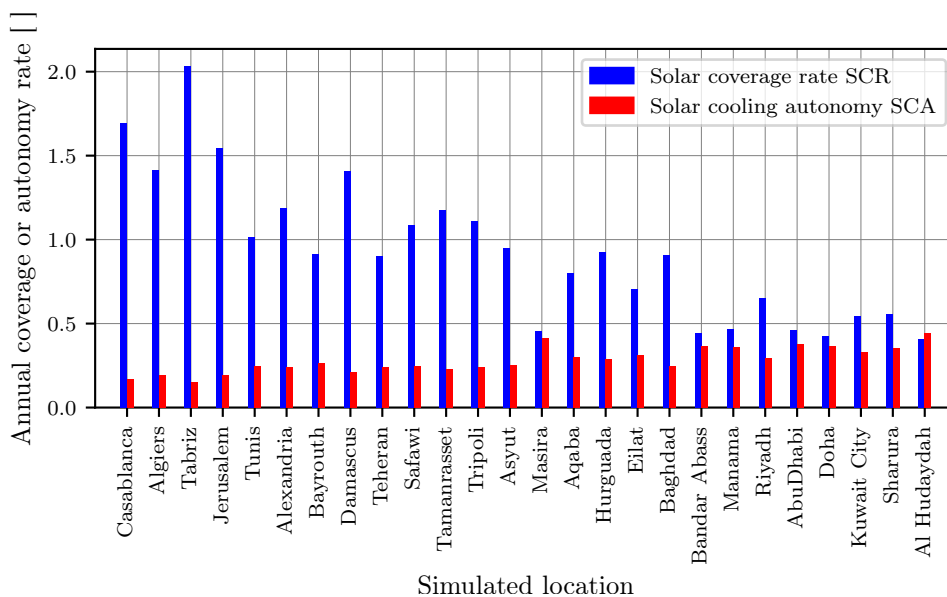


Figure 5.22.: *Bed room - annual solar coverage rate (red) and solar autonomy rate (blue) for a bed room with a minimum sized solar electric power system in all 26 locations.*

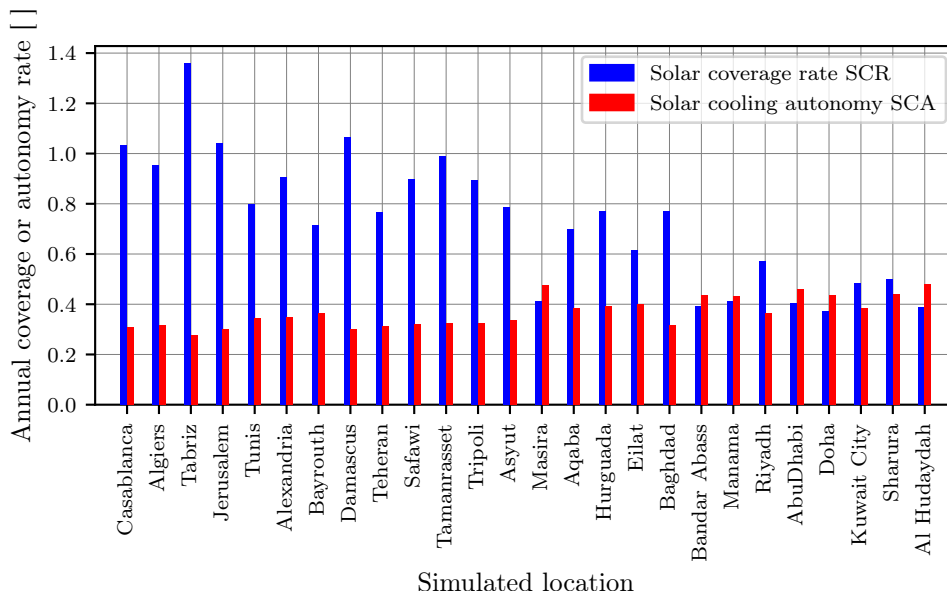


Figure 5.23.: Living room - annual solar coverage rate (red) and solar autonomy rate (blue) for a living room with a minimum sized solar electric power system in all 26 locations.

5.2.3. Performance of a water cooling system

The system is extended with a cold water loop to exhaust cooling loads with a water based room transfer unit, such as a cooling surface. Therefore, a cold water production system, a chiller, produces cold water which is stored in a buffer tank. The complete simulation set up in its graphical representation in *Dymola* is shown in the following picture in Figure 5.24. The general concept of this system was outlined in Section 2.3.2 on page 26. The various design parameter are given in Section 3.4.3 on page 55 and its modelling in Section 4.34 on page 102.

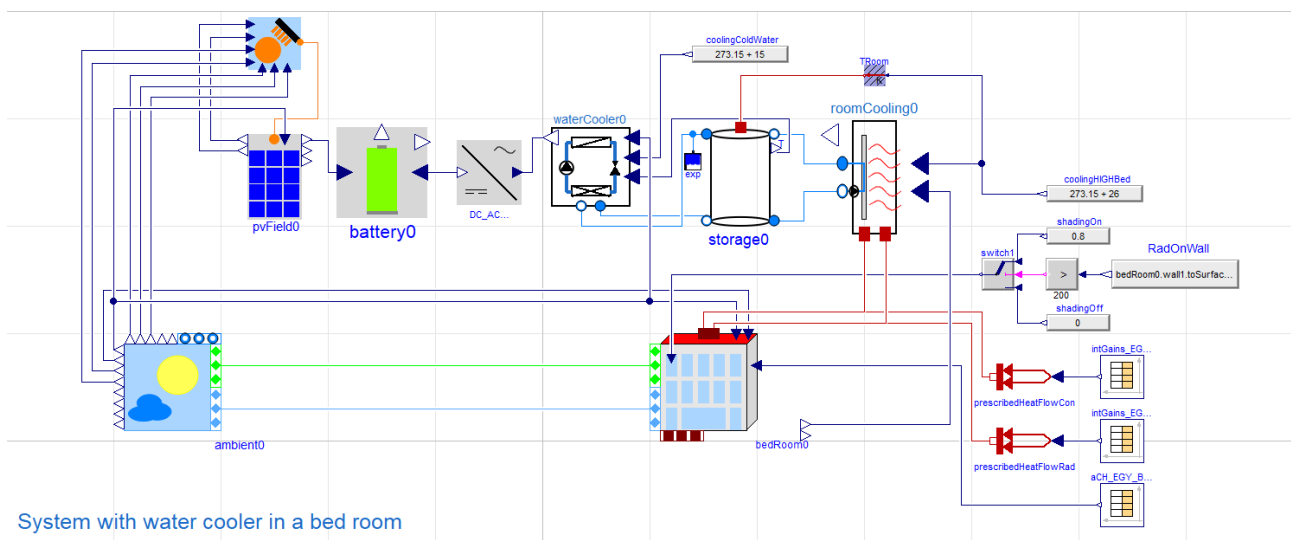


Figure 5.24.: Modelica set up for any location for the bed or living room (naming example for the bed room) with a small scale photovoltaic, battery and water cooling system which consists of a water cooler, a cold water storage and a room transfer unit.

5. Simulations and results

The performance is compared with the reference system. Therefore, the energy flows are compared in the following two graphs. They show the difference of the annual electric demands for air cooling. First, the annual power demands are compared to the reference case in blue. Second, the difference to the exported grid electricity are outlined in red. Third, the difference in electrical energy which needed to be bought, is presented in green.

The overall electricity demand is decreased in all simulations of a bed room. The most, it is reduced in Masirah, Oman. There, the energy demand drops by almost 25 %. In average, the demand is reduced by 19.4 %, which is a reduction of 425 kWh per year. The main reason for this reduction is the increased coefficient of performance of $COP_{chiller} = 3.0$ of the selected water chiller (according to the data sheet), the increased hysteresis in the cold water loop to $\Delta\vartheta_{storage} = 6 K$, and the smaller auxiliary power demand for the water transportation. The electricity, which is sold to the grid is also reduced in all cases and by 19.1 % in average. The main reason is the storage capacity by the cold water tank. This additionally storage is also the reason why the amount of bought energy decreases by 8.3 %.

The energy demand decreases only by 7.5 % on average in the living room. The savings are less, because the chiller is used more during the day. Hence, the effect of a better COP is reduced. This effect causes the electric energy demand to even increase in Kuwait City where the purchased power is 3.8 % higher. There, the outdoor temperature is especially hot and stays high even during the night. Thereby, the additional auxiliary demands are increased and overcome the savings by a better system. This can be observed by the change in electric energy which is bought from the grid. It is almost the same as with the UAC reference system which is smaller in only 11 of the 26 locations. In hot locations, like *Kuwait City*, up to 14 % of additional electricity have to be bought.

For comparative reasons, also the difference in the number of on- and off-switching cycles of the cooling units are analyzed. Thereby, the positive impact of even a small thermal storage system can be determined. The results for both room types are plotted in the following graph in Figure 5.27. Again, blue is used for the results of a bed room, and red for a living room.

As expected, the number of switching cycles is reduced in all cases. In *Masira, Oman* the number is reduced by almost 800 cycles in a bed room. The cycle amount is reduced less in a living room in all locations, except *Casablanca, Morocco*. There, the temperature of the night is sufficient to provide a cooling capacity, even during most summer days. Besides the switching cycles the share in peak load demand due to the water storage system are calculated. The changes are relatively small, with only 0.9 % less share of the peak load demand in the overall electric energy demand in a bed room, and at least 3.2 % less in a living room. The highest reduction of the peak load demand was achieved in a living room i *Baghdad, Iraq* with almost 5 %.

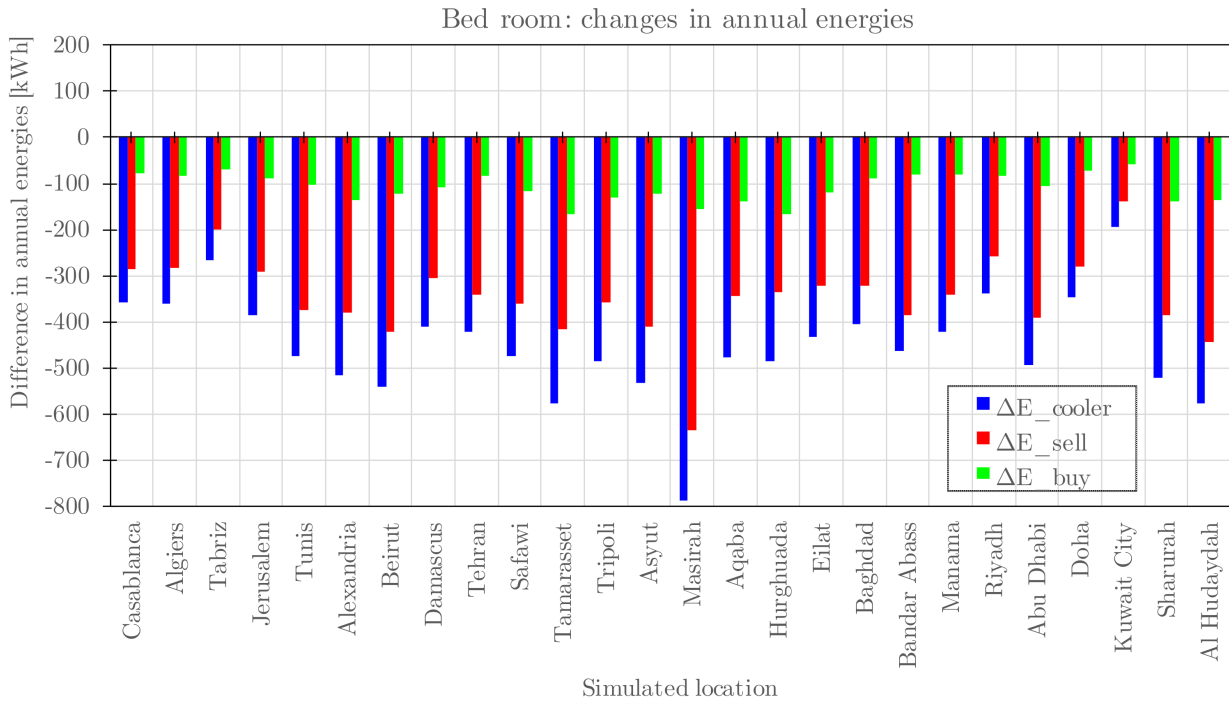


Figure 5.25.: Results for a bed room: change in annual energy demands for the chiller (blue), the annual amount of energy being sold to the grid (red), and the annual amount being purchased from the grid (green) for all 26 locations.

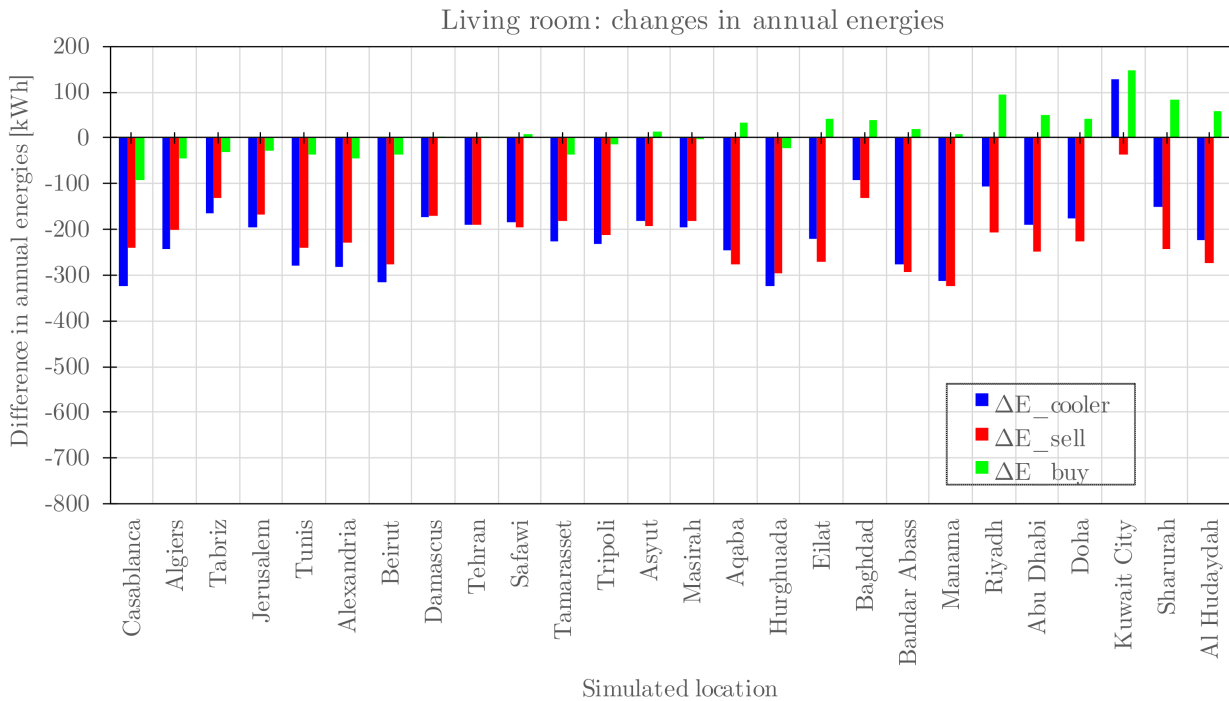


Figure 5.26.: Results for a living room: change in annual energy demands for the chiller (blue), the annual amount of energy being sold to the grid (red), and the annual amount being purchased from the grid (green) for all 26 locations.

5. Simulations and results

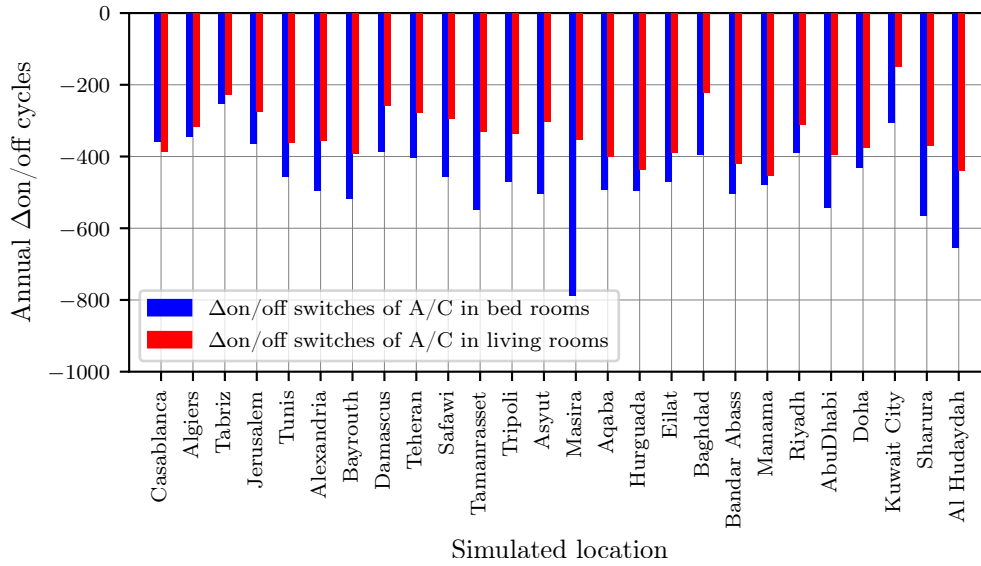


Figure 5.27.: Difference in number of on/off cycles between the water and the air cooling system for a bed room (blue) and a living room (red).

5.2.4. Evaluation of the LCOE and LCOC

Based on the previous analyses, the levelized costs of electricity $LCOE$ and the levelized costs of cooling $LCOC$ are calculated. The calculation methods for both indicators are presented in Section 3.5.4 on page 60. The calculations are not made for all 26 locations but can be easily repeated with the following steps and to determine the boundary conditions for other locations. The $LCOE$ is calculated for the case study location of *Hurghada, Egypt*. This is done to determine, when a small scale solar system is valuable to be used. Therefore, the performance of only a PV system is evaluated. The investment cost of all additional components are presented in Table 3.1 on page 60. The resulting $LCOE$ are compared in the graph in Figure 5.29. Three analyses are made. One for an investment period of 5 years (green), one for 15 years (red) and one for 25 years (blue). The period of 25 years is selected according to reference $LCOE$ calculations by the Fraunhofer ISE. This quite long period was chosen by the Fraunhofer ISE in 2016 for a $LCOE$ calculation for renewable energies in Egypt[13]. The curves are plotted against a growing installed solar peak power which is equivalent in an increase from 1 to 20 PV panels.

The levelized costs of electricity drop to 0.04 $\$/kWh_{elect}$ with more than 10 solar panels and at an investment period of 25 years. These costs are not much higher in terms of a 15 years investment period. The cost drop below 0.20 $\$/kWh_{elect}$ already with 6 PV panels when the investment period is viewed to be only 5 years. The electricity generation costs go down to 0.12 $\$/kWh_{elect}$ with 20 PV panels.

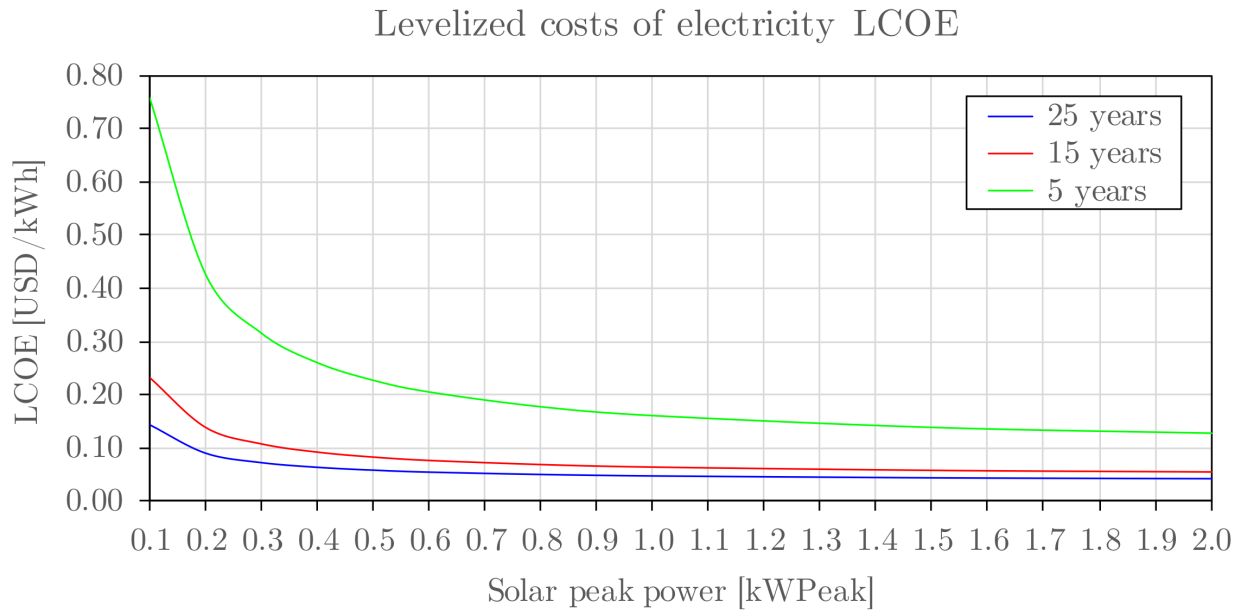


Figure 5.28.: Levelized cost of electricity for an increasing peak capacity of the pv field in Hurghada, Egypt for an investment period of 5 (green), 15 (red), and 25 (blue) years.

With these results in mind, the levelized costs of cooling are calculated in the next step. A current electricity price of $cst_{elect,HRG} = 0.02$ $\$/kWh_{elect}$ will bring the reference system to levelized cooling cost of about $LCOC_{ref,HRG} = 0.011$ $\$/kWh_{cool}$ to cool a bed or a living room. The specific cooling costs will increase to $LCOC_{minInv,bed,HRG} = 0.026$ $\$/kWh_{cool}$ for a bed room and to $LCOC_{minInv,liv,HRG} = 0.020$ $\$/kWh_{cool}$ for a living room in the case of a minimum investment approach (compare with the system in Section 5.2.2 on p. 125).

The parameters of this system are varied to find to lowest possible specific levelized costs of cooling. Therefore, the parameter field (see Table 3.3 on p. 63) is analyzed for two investment periods of 25 and 5 years. Afterwards, the costs are analyzed for the time period of 5 years as this is a much more realistic time horizon for small scale PV systems. The latter analysis is done for the solely PV and battery system as well as for the water cooling system.

The overall resulting savings are shown in the following graph. Highlighted on the y-axis are the differences in specific cooling cost compared to the reference cooling system at the equal electricity price. A negative price difference means that the levelized costs of cooling of a small scale PV and battery system are smaller than compared to the $LCOC$ for a bed room (blue) or the living room (red). The five year investment period is shown for the bed room in green and for the living room in purple. Yellow (bed room) and azure (living room) are the colors for a water cooling system. The box plot are the results of a particle swarm optimization which is set to a local best search and a neighborhood size of 4 increments. This optimization process was described in Section 4.6.6 on page 103. Each PV and battery system is simulated 2000 times while each PV, battery and cold water storage system is simulated 2500 times as an additional variable parameter is given. The model is simplified to handle this amount of simulations with a reasonable computational effort. The simplification process to simulate only the 24h of 1 August is described in the same section. The results of all simulation runs are compared with each other in the following box plots.

5. Simulations and results

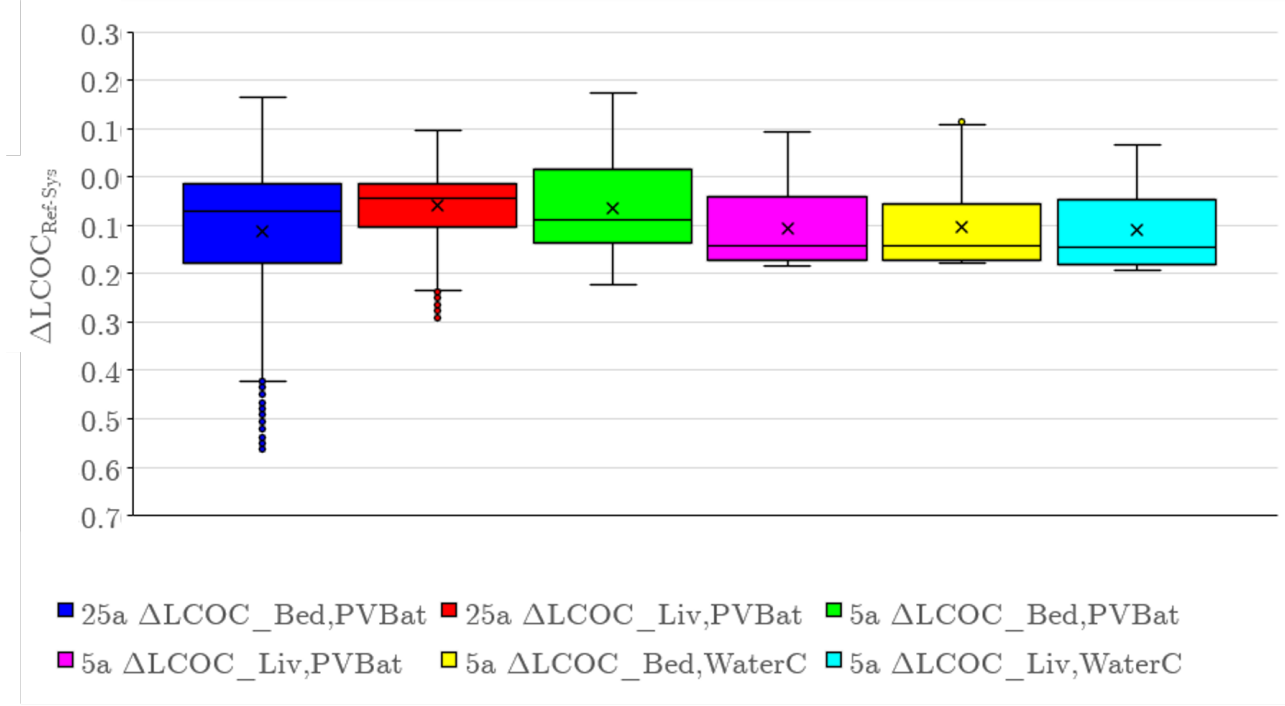


Figure 5.29.: Variability of the differences in the levelized costs of cooling for an investment period of 25 (blue and red) and 5 years. The first four box plots indicate a small scale PV system with a battery storage, while the last two indicate a chilled water system. Blue, green and yellow are used for an analyzing a bed room in Hurghada, Egypt. Red, purple and azure are used for a living room.

In both room types, a solar system becomes worthy to be installed, when the electricity price and revenue is around $C_{elect} \sim 0.05 \text{ \$/kWh}_{elect}$. This range was predicted by the LCOE calculation. Then, always the maximum number of solar modules should be installed. Within a bedroom, the highest savings in the $LCOC$ are up to $\Delta LCOC_{PVBat,bed,min} = -0.56 \text{ \$/kWh}_{cool}$ and $\Delta LCOC_{PVBat,liv,min} = -0.29 \text{ \$/kWh}_{cool}$ for the living room when only a PV and Battery system is installed and the investment period is 25 years. Most system combinations are more cost efficient than the reference system. Only low electricity prices and a high number of batteries increase the $LCOC$ beyond the reference. Within the simulations for a bed room, 50% of the results have levelized costs of cooling of a PV and batterie supported cooling system of $-0.09 < \Delta LCOC_{PVBat,bed} < 0.02 \text{ \$/kWh}_{cool}$ smaller than the reference cooling system. This is only 14.8% of the entire spectrum of a price difference of $\Delta LCOC$ from $-0.57 \text{ \$/kWh}_{cool}$ to $+0.16 \text{ \$/kWh}_{cool}$. Batteries pay off with an electricity price of $C_{elect} \sim 0.14 \text{ \$/kWh}_{elect}$. They get more worthy, the higher the electricity costs are. With an amount of 7 batteries and 20 solar panels, the system almost gets grid independent as the price difference for grid electricity to grid revenue plays a decreasing role. Within the simulations for a living room, 50% of the results have levelized costs of cooling of a PV and batterie supported cooling system of $-0.05 < \Delta LCOC_{PVBat,liv} < 0.01 \text{ \$/kWh}_{cool}$ smaller than the reference cooling system. This is only 16.0% of the entire spectrum of a price difference of $\Delta LCOC$ from $-0.29 \text{ \$/kWh}_{cool}$ to $+0.10 \text{ \$/kWh}_{cool}$. Batteries pay off already at an electricity price of $C_{elect} \sim 0.08 \text{ \$/kWh}_{elect}$, when the maximum number of PV panels is installed. The smallest grid dependency is achieved with 9 batteries and 27 PV modules.

The savings shrink when the PV and Battery system is evaluated at a five years investment period (green and purple). A PV system becomes cheaper for cooling purposes at around $cst_{elect} \sim 0.18 \text{ \$/kWh}_{elect}$ and for a battery assisted system at around $cst_{elect} \sim 0.30 \text{ \$/kWh}_{elect}$ for both room

types. At the maximum electricity price ($cst_{elect} = 0.52 \text{ \$/kWh}$), the cheapest cooling system has 27 to 30 PV modules and 1 to 3 batteries. The feed in tariff can be up to 30% smaller than the cost. Up to 10 batteries become worthy with an electricity price of $cst_{elect} = 0.46 \text{ \$/kWh}$, even without any possibility to sell electricity to a grid. With the currently highest electricity price of $cst_{elect,Bahrain} = 0.26 \text{ \$/kWh}$ it is worth to install 5 batteries and 14 PV panels, even when the feed in tariff is 70% smaller.

Similar results are achieved for the living room. Except that here even 7 batteries are being worth to be installed at $cst_{elect} > 0.18 \text{ \$/kWh}$ and no revenue on selling electricity to the grid.

It is not worthy to install a water cooling system with a big as possible cold water tank, as long as the feed-in tariff is higher than the electricity price. Then, it is always better to sell the electricity to the grid.

5.2.5. Evaluation of the SCR and SCA

Finally, the solar coverage rate, SCR , and the solar cooling autonomy, SCA , are analyzed for the case study location with an extended *Modelica* model and the parametric optimization tool *GenOpt*. The calculations are described in Section 3.5.2 on page 58. For a better readability, these values are rounded to the first decimal digit.

The reference bed room has 30 PV panels, 1 battery, and a cold water storage of $V_{strg} = 0.060 \text{ m}^3$. The price for electricity is the same as for the revenue with $cst_{elect} = rvn_{elect} = 0.30 \text{ \$/kWh}$. The investment period is set to 5 years.

The resulting calculated SCR and SCA are used to weight the overall total system costs, including capital costs and revenue. The bed room in *Hurghada, Egypt* has $(1 - SCR * cst)_{ref,bed} = 941 \text{ \$}$ and a solar coverage rate of $SCR_{ref,bed} = 0.889$. This bed room reference system has a weighted total cost in terms of solar cooling autonomy of $(1.1 - SCA * cst)_{ref,bed} = 2917 \text{ \$}$ with a solar cooling autonomy of $SCA_{ref,bed} = 0.505$.

The reference living room with the same boundary conditions has $(1 - SCR * cst)_{ref,bed} = 5305 \text{ \$}$ and a solar coverage rate of $SCR_{ref,liv} = 0.482$. This living room reference system has a weighted total cost in terms of solar cooling autonomy of $(1.1 - SCA * cst)_{ref,liv} = 7357 \text{ \$}$ with a solar cooling autonomy of $SCA_{ref,liv} = 0.419$.

The parameter field is varied again to search for local minimum and a global minimum point. The results of all simulations are presented in the following box plot in Figure 5.30. The boxes show the average difference of the simulated weighted cooling costs for 5 years in terms of the solar coverage rate (blue and red) and in terms of the solar cooling autonomy (green and purple). The bed rooms are outlined in blue and green and the living rooms in red and purple. Clearly visible is that the medians are much closer to the lowest possible results. Also, the lower quartile is very small in its range. Outliers can only be found in the direction to higher costs.

The median weighted cost of a bed room cooling system with a focus to the solar coverage rate are 926 \$ and thereby even 1.7 % smaller than those of the reference system. The costs can be reduced to 651 \$, which is 31.82 % smaller than the reference system. This system has 30 PV panels, 8 batteries, and a water storage with a capacity of $V_{strg} = 0.120 \text{ m}^3$. In this case, the electricity can be sold at the same price to the grid as it can be purchased $cst_{elect} = rvn_{elect}$. It will be the best system until a 40 % reduced revenue for feed in electricity. Here, the solar coverage rate increases to $SCR_{best,bed} = 0.903$. Up to 10 Batteries should be installed with a price difference of $rvn_{elect} = 0.50 * cst_{elect}$. This will result in weighted costs of 677 \$.

5. Simulations and results

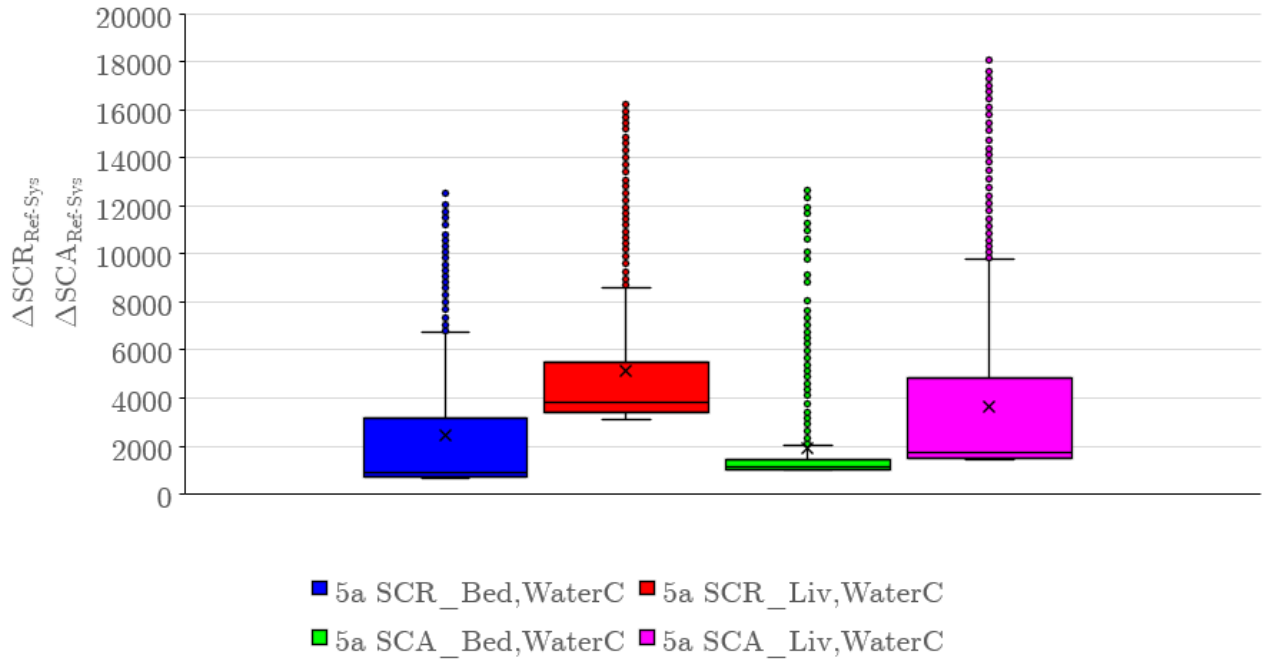


Figure 5.30.: Variability of the weighted solar coverage rate and solar cooling autonomy. The box plots indicate the variability of a small scale PV system with a battery and a cold water storage. The electricity price is fixed at $cst_{elect} = 0.30$ $\$/kWh$ and the investment period is set to 5 years. Blue and red indicate the SCR of the system when installed to a bed resp. a living room. The SCA is indicated in green for a bed room and purple for a living room.

Similar results are obtained for cost which are weighted by the solar cooling autonomy in a bed room. There, the median is 1080 $\$$ which is 62.9 % below the reference system. The best value goes even down by 76 % to 691 $\$$. There, 30 PV panels, 6 batteries, and a cold water storage with a volume of $V_{strg} = 0.080$ m^3 are the best. The price difference for this system can be until $rvn_{elect} = 0.30 * cst_{elect}$ while still being the best system. The solar cooling autonomy is increased to $SCA_{best,bed} = 0.708$. Using more batteries increases the SCA slightly, as the PV system is not capable to charge the batteries completely again. Up to 11 Batteries are worth being installed while the revenue for sold electricity is $rvn_{elect} = 0.45 * cst_{elect}$ with a resulting weighted cost of 1036 $\$$

The results for the living room point in the same direction. The median of the costs which are weighted by the solar coverage rate is with 3834 $\$$ 27.7 % smaller than of the reference system. The best system has 30 PV panels, 14 batteries and a water tank with $V_{strg} = 0.180$ m^3 and has weighted costs of 3093 $\$$. It stays the best, even with price differences of 50 % between the electricity price and revenue for local produced electric energy. The solar coverage rate is only slightly increased by 2.4 % points to $SCR_{best,liv} = 0.506$. The same system increases the solar cooling autonomy to $SCA_{best,liv} = 0.859$. This is also the best system in terms of the weighted cost of 1459 $\$$, which are weighted by the solar cooling autonomy. The system will stay the same, even with a price difference of up to 50 % between costs and revenue.

5.3. System Conclusion

The simulation results show the possibility to simplify a complex simulation problem and task of a building simulation problem. Goal is to make the simulation suitable for a parametric optimization tool to enable a user to define the best possible system based on their boundary conditions. The complex and detailed simulation model of the software *IDA-ICE* was used to cross-validate a much simpler 1D simulation model which was established with the *BuildingSystems-Library* for *Modelica*. The results showed a very good performance at a much faster simulation time. The overall performance of a standard air cooling system in the *MENA* region was evaluated. The comparison with a minimalistic PV and battery system allows the user to identify potentials to save energy or use energy more efficient. This so called reference system and its performance was then used to evaluate other possible extensions of the system, such as a system with a cold water loop and a sensible thermal storage tank.

These systems needed to be simplified further to use them in parametric optimization runs with thousands of single simulations. Therefore, a representative day of the year was selected, the initial parameter calculated and a method to penalize differences in stored energy from the beginning of a day to its end. The results of the levelized costs of electricity are confirmed by the results of a study by Hussein, et al. (2016) about the *LCOE* of various electricity costs from renewable sources for Egypt. This validated the simplification method which was used afterwards to find the best system combination to increase the solar coverage rate or solar cooling autonomy. Both values were calculated in total and the variability of the possible outcome was presented.

This thesis is a template to run optimizations for small scale, PV powered residential air cooling applications. The user can find the best needed system components based on their local boundary conditions such as the weather, capital costs, or user profiles. A code generation tool like *CoTeTo* can be used to automate the code generation for *Modelica* simulations and prepare the set up for the optimization run.

The results of one particular outcome are compared with real world behavior in the following chapter on the case study in *El Gouna, Egypt*.

6. Case study El Gouna, Egypt

In this chapter, a case study apartment is analyzed. Therefore, a particular, real existing building is modeled with the previously shown set of *Modelica* models. The apartment is located in *El Gouna*, a satellite district of *Hurghada*, 30 km north of it on the Red Sea coast of Egypt. The location in Egypt is shown in the small map in Figure 6.1. The big map in this figure shows the current map of the town, including the scheduled expansions (as of 2020). The town is chosen for a case study as the author of this thesis resided from October 2012 to May 2019 in the city and had direct access to equip one apartment with sensors and systems to analyze the solar cooling potential in the region. Thereby, the author is able to evaluate and confirm the outcome of the simulations and optimization on site and estimate the impact on the local community.

Further, the constant growth of the city allows to implement new findings directly to construction projects. This is also enabled by the close connection between the hosting university of the author, the *TU Berlin Campus El Gouna* and the cities founder and *TU Berlin* alumnus *Samih Sawiris*.



Figure 6.1.: Location of the case study location *El Gouna* at the Red Sea Coast of Egypt, 30km north of *Hurghada* (top left) and official development plan.

First of all, the chosen apartment building is described which hosts the case study apartment. The cooling energy and electricity demand is simulated according to the presented methodology. Afterwards, the results are compared with a more detailed simulation in *IDA-ICE* to account for the vaulted ceilings of the apartment. Further, these results are compared with measurements on site and analyzed with the auspices of the local conditions. Thereby the simulation results are validated and its limitations shown.

6.1. Boundary condition of El Gouna

6.1.1. Apartment building H12

The building H12 in Downtown El Gouna is monitored and simulated. The urban context of the neighborhood, in which the apartment house is located, is shown in the satellite image and the overlaid aerial plan of the so called *Downtown* area of El Gouna in Figure 6.2. There, another advantage of the case study locations becomes clear. Highlighted in yellow is the exact same building type. It is rotated and the amount of floors varies between one and three stories, also the colors are slightly varied, but the building itself can be found multiple times in the area. Hence, finding can be applied to a bigger building stock, even if the results are not transferable to other location or in case the results couldn't be generalized.



Figure 6.2.: Urban context of simulated apartment in El Gouna, Egypt and IDA-ICE simulation model of the building (top right corner).

The picture shows as well the simulation model of the observed building *H12* as a model in *IDA-ICE*. It has two stories and hosts 30 apartments of which 18 are single room apartments, so called *studios*. The rest are two room apartments, which are often rented by families. The building is originally modeled with *Sketch Up Pro 8* where the domes and vaults could be created. The case study apartment itself is modeled separately.

The construction materials are listed in Table 6.1 and are provided by the local housing authorities *Orascom Housing* or gained through own measurements as for example the density of stones and wall thicknesses. The properties of the construction material where used in the *Modelica* simulation models which where previously described. These values are used as well for the more detailed simulation model in *IDA ICE* which is used to validate the results. As climatic boundary condition, a weather data set for *El Gouna* was generated with *Meteonorm* which was used in all following simulations. It is presented in detail in Chapter 4.3.1 on page 70.

Table 6.1.: Properties of construction material being used in El Gouna, Egypt.

Constr.	Layer	λ W/mK	ρ kg/m^3	c_p J/kgK	x m	Uvalue W/m^2K
Dome/Vault	Screed	1.40	2000	1000	0.010	1.69
	Red Brick	0.58	1070	840	0.234	
	Render	0.80	1900	790	0.010	
Wall	Render	0.80	1900	790	0.010	0.94
	Red Brick	0.58	1070	840	0.505	
	Render	0.80	1900	790	0.010	
Floor/Ceiling	Tiles	1.30	2300	840	0.010	3.04
	Screed	1.40	2000	1000	0.010	
	Concrete	1.70	2300	880	0.224	
	Render	0.80	1900	790	0.010	
Ground Plate				0.254	3.10	
	Tiles	1.30	2300	840	0.010	
	Screed	1.40	2000	1000	0.010	
	Concrete	1.70	2300	880	0.234	
Door/Window frame, frame fraction window = 0.71	0.020	3.20				
	Wood	0.14	500	2300	0.020	
Single glazed window	$SHGC$	=0.85		U_{glaz}	=5.8	W/m^2K
	T_{sol}	=0.83		ϵ_{int}	=0.837	
	T_{vis}	=0.9		ϵ_{ext}	=0.837	

6.1.2. Modeling of Apartment 214

The floor plan of the building is shown in Figure 6.3. Marked in red is the outline of the considered apartment 214. This apartment was the residence of the author of this thesis during his times in *El Gouna, Egypt*. Shaded in red is the living room of the apartment. This room is modelled as a single zone. The floor area of the living room is $A_{room} = 15.96 \text{ m}^2$ and the apex of the vault is $h_{room} = 4.14 \text{ m}$ above the floor, respectively 7.64 m above ground level. The zone volume is $V_{room} = 65 \text{ m}^3$. A picture of the original building and the IDA ICE simulation model are shown as well in the following pictures in Figure 6.3. The peculiar vaults and domes, which are typical for the region, can be observed on the roof of the building. Its massive and thick walls, the relatively small windows and the vaults and domes that are integrated into the roof structure mainly influence the building performance.

The big thermal masses of the outer and inner walls have a major influence on the thermal behavior of the building. The evening peak in electric demand can be observed in all parts of Egypt. Within El Gouna, this peak demand is about one hour later (around 8 pm) than in other parts, e.g. Cairo. This can be seen by comparing the graphs in Figure 1.12 on page 11, where the load duration curve of El Gouna is shown for a specific day and the peak load profiles for Cairo in Figure 4.29 on page 97. The shift between maximum incoming radiation at noon (resp. maximum outer temperature, around 3 pm) and electric peak demand is caused by the high thermal masses of the building. On the one hand, this causes a thermally uncomfortable situation during early night hours due to the radiation asymmetry (perceived room air temperature). On the other hand, the overall annual energy demand for room air cooling is reduced, compared with common building structures in Egypt[53].

6. Case study El Gouna, Egypt



Figure 6.3.: Floor plan (left) of the building H12 in Downtown El Gouna, its appearance (top right) and a 3D simulation model of the building (lower right).

6.1.3. Reference system of Apartment H12-214

The reference system, as described in Section 2.3.2 on page 24, was designed based on a real installed system. The cooling system ($\dot{Q}_{cool} = 4kW$) was already present when the author moved into the described apartment. The electrical supply system was additionally equipped with a small scale PV system ($P_{elec} = 600W_{peak}$) and a battery storage system ($E_{bat} = 2.4kWh$).



Figure 6.4.: Photovoltaic panels on apartment H12-214 during the erection (left side) and the final set-up on top of the apartment (right side).

The solar electric system is shown in the previous figure. It was set-up in 2014 on top of the previous described apartment H12-214 with an initial peak capacity of $P_{elec} = 400W_{peak}$. This was increased to $600W_{peak}$ in 2015. The data sheets of the components were used to design, model and parametrize the used system components, e.g. the split-unit, battery system or the solar modules.

6.1.4. Simulation results of case study location

In this section, the results of the previously described living room of the apartment *H12-214* are compared with the results of a typical Egyptian apartment structure. Therefore, also the typical living room is adopted to match the appearance of the living room of the case study apartment. The floor area is slightly decreased and the outer wall, now facing eastwards, reduced in size and only contains one window. Further, the upper boundary of the room is a roof construction. Internal load and presence profiles are kept the same.

The main difference between both apartments is the building shell, as the apartment in *El Gouna* was assembled as load bearing wall construction and hosts thereby massive walls. The following results are the outcome of the system simulation with *Modelica*. Only the living room is modeled, as it was set to up to monitor the thermal performance for at least one year. Additionally, this room is equipped with multiple sensors to measure the behavior of the room to validate the results. First, the cooling energy demands are compared. Second, the resulting impact on the electric grid of the town is discussed afterwards. Following, the thermal comfort in the room and the energy storage throughput are analyzed.

Cooling demand of the living room in H12-214

As in the previous chapter, the following graphs in Figure and 6.5 show the monthly energy demands for cooling in the real existing apartment, highlighted in blue. The results of the reference system are outlined in red. Their difference to the presented results in Section 6.1.4 on page 141 are the presence of a ceiling and the rotation of the room towards the east. The annual cooling energy demand (labeled on the right y-axis) for the living room in *El Gouna, Egypt* is $Q_{cool,liv,214} = 3798 kWh/a$. This is only slightly less than the annual cooling demand of Hurgada, which is $Q_{cool,liv,HRG} = 3884 kWh/a$. This is even lower than the reference apartment of the previous chapter. The main reason is the decreased and rotated outer wall, which is not facing south anymore and only contains one small window.

The annual demand is almost equal. However, the thicker walls decrease the heat transfer and offer a big thermal storage capacity. Clearly visible is the earlier demand for cooling within a typical constructed living room in April and May. Nevertheless, the cooling demand in a load bearing construction of *El Gouna* slightly exceeds the cooling demand of a standard construction in September and October. This is due to the big thermal mass of the massive brick walls in *El Gouna*. The small cooling energy demand of the typical living room in January is due to the deep standing morning sun and the new orientation of the room towards the east. Further, the window frame fraction of a typical apartment is much less compared to the high window frame portion in *El Gouna*.

6. Case study El Gouna, Egypt

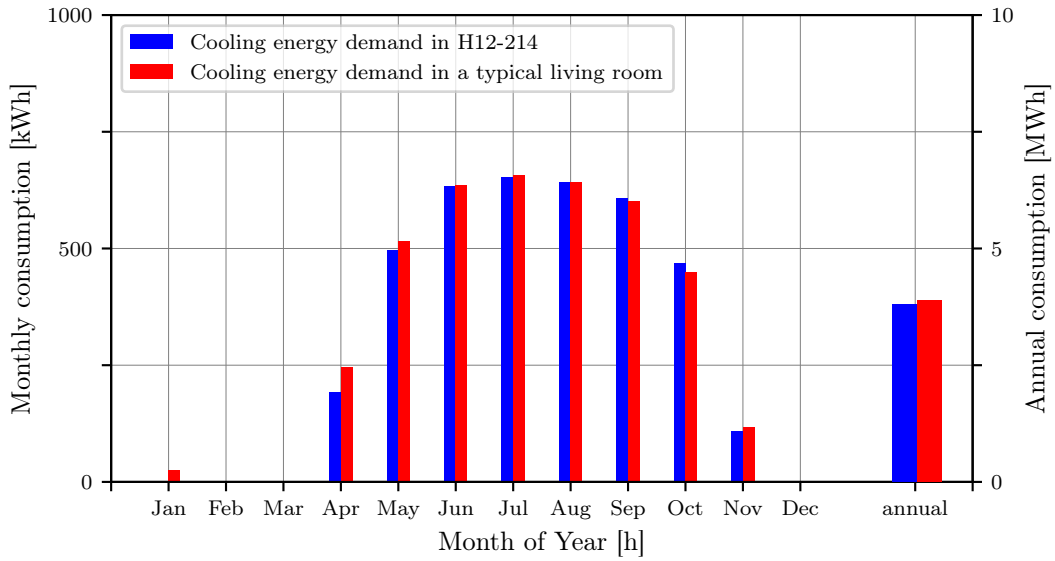


Figure 6.5.: Comparison of simulated monthly cooling energy demands in the living room of apartment H12-214 in El Gouna (red) and a typical Egyptian apartment with the same shape under the climatic conditions of Hurghada.

Impact on electrical grid

According to the used methodology, the impact on the grid is classified by the number of on- and off switches during the summer season. The monthly numbers are presented in the graph in Figure 6.6. There, the monthly sum of on and off cycles of the split-unit air conditioner are shown in red for the case study room and in blue for the reference building in Hurghada. The annual numbers are given as well on the right y-axis.

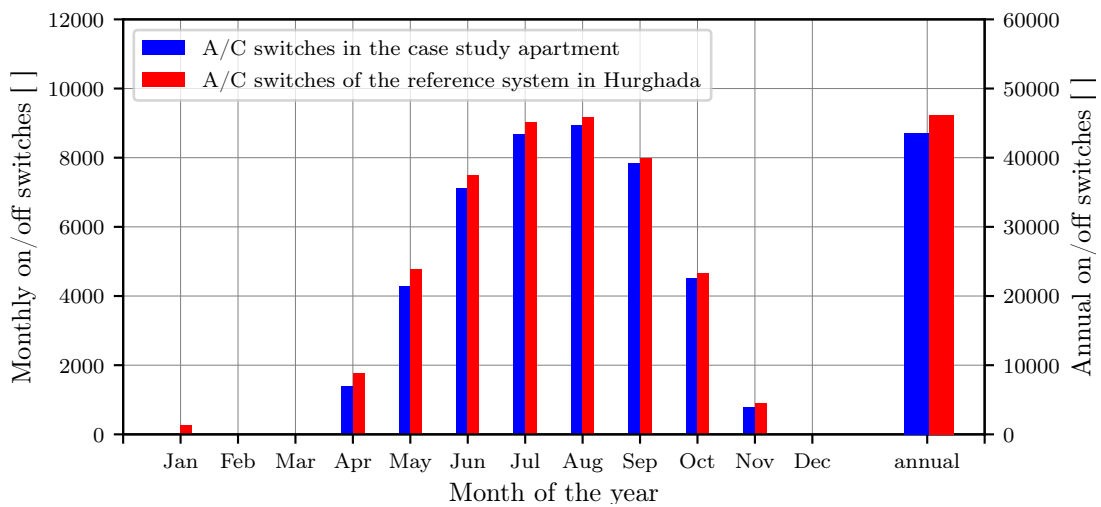


Figure 6.6.: Simulated monthly numbers of on and off switches of the living room split-unit in apartment H12-214 (red) and a comparable living room in Hurghada (blue).

Compared with the reference apartment of *Hurghada*, the number of on and off switches is reduced as the overall cooling energy demand is reduced. In *El Gouna*, the A/C is cycled about 5% less than in a typical apartment. The decrease from $n_{on-off,HRG} = 46107 /a$ to $n_{on-off,214} = 43565 /a$ can be partly explained by the better u-value of the walls and the reduced cooling demand. Thereby, the interior surface temperature is reduced and the indoor room air is not heated back up to more than $28^{\circ}C$ that fast. The overall interior temperature variation is damped and shifted.

Thermal comfort

Next, the thermal comfort is evaluated as well according to the previously described methodology. The temperature degree hours are used to evaluate the performance of the living room in terms of radiation asymmetry and as an indicator for the surface temperatures. In this case, the inner surface temperature of the ceiling is used to calculate the degree hours difference. The simulated monthly and annual sums of the apartments living room are presented in the graph in Figure 6.7. Red is used there to indicate the amount of degree hours of an exceeded surface temperature in the living room of apartment *H12-214*. The annual sum with $degH_{liv,214} = 6568^{\circ} * h$. is much lower than of the reference living room with $degH_{liv,HRG} = 8667^{\circ} * h$

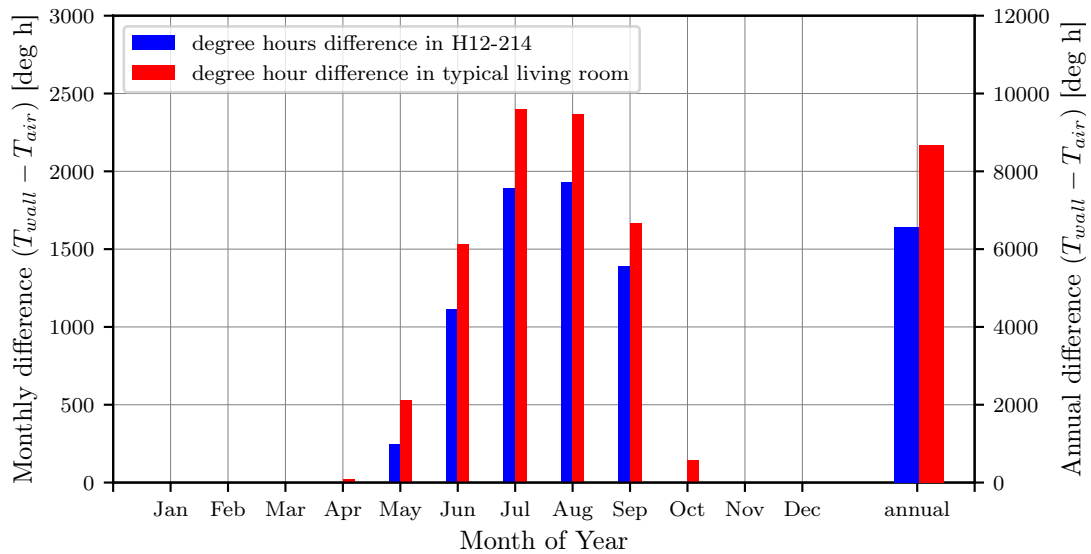


Figure 6.7.: Absolute monthly (left y-axis) and annual (right y-axis) hourly accumulated degrees difference between room air temperature and the outer wall surface temperature of the living room of *H12-214*. Only the hours where the wall surface temperature is above $28^{\circ} C$ are accounted.

The much lower surface temperatures throughout the year explain the behavior of the room in the previous two subsection. Due to the increased thermal resistance of the massive construction, the surface temperatures are drastically reduced. Thereby, the thermal comfort is increased. Further, the roof construction allows the room to be in a radiation exchange with the night sky. Constant clear sky increases this effect.

Sensible energy storage processes

The sensible energy which is stored and released from internal wall surfaces is a good indicator to evaluate the storage capacity of the building masses. The monthly sums in the living room of the apartment *H12-214* are presented in the following figure in blue. Annually, 163 *kWh/a* are stored in and released from the room surfaces of the living room. This is about 14% of the thermal energy throughput of a typically constructed apartment room which has a stored and released energy amount of 189 *kWh/a*.

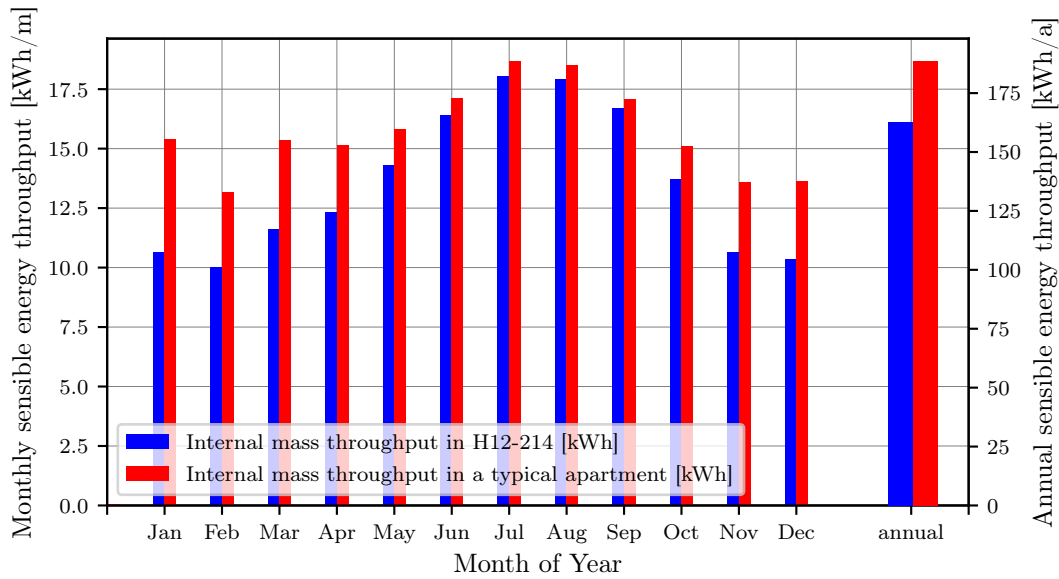


Figure 6.8.: Monthly (left y-axis) and annual (right y-axis) amount of roundtrip energy stored in the thermal masses of the living room in *H12-214* (red) and as a typical apartment in *Hurghada* (blue)

The sensible energy throughput is bigger in a typical apartment layout as the daily variation of the temperature of the entire wall mass is much higher with the thinner wall construction.

6.1.5. Supply system performance of case study system

The simulated electrical performance of the small scale photovoltaic system on top of the case study apartment is similar to the performance of the same system in *Hurghada* as the weather conditions are almost the same. Effects, like increased turbidity due to massively increased traffic in *Hurghada* are not part of the weather data set and hence, have no impact on the simulated performance of the solar electric system. The system of 6 pv modules with a peak capacity of $P_{peak,214} = 600\text{ W}$ harvest a total of $Q_{elec,214} = 890\text{ kWh/a}$ for both cases. The levelized costs for cooling are calculated for an interest period of 5 years and according to the reference case of the previous chapter. They are reduced from $LCOCHRG = 0.193\text{ \$/kWh}$ to $LCOCH12-214 = 0.134\text{ \$/kWh}$. The other key performance indicators are combined in the following Table 6.2. There, the annual needed electricity from the grid, the solar coverage rate and the solar cooling autonomy are presented additionally.

Table 6.2.: Properties of construction material being used in El Gouna, Egypt.

	Unit	Case study apartment H12-214, El Gouna	Typical constructed living room Hurghada, Egypt
$Q_{PV,annual}$	kWh/a	890.94	890.95
$E_{grid,buy}$	kWh/a	2338.61	2428.83
$LCOC$	$\$/kWh$	0.134	0.193
SCR		0.621	0.581
SCA		0.264	0.256

As shown, the simulated performance of the case study apartment is better than in all points. The lower costs for cooling are mainly the result of the reduced cooling energy demand. This also results in a lower need to buy electricity from the grid. Further, the solar coverage rate is also increased. Only the solar cooling autonomy is only slightly better in the case study location. The reason are the high internal gains during the day time, which leads to the consumption of almost all solar energy directly during the day and less energy to charge the battery system.

6.1.6. Validation of simulation results

The previous presented results are checked for validity. Therefore, the described apartment is equipped with multiple sensors and the performance of the single system components is evaluated.

First, the cooling demand simulation is analyzed. Multiple temperature sensors were installed in the apartment. This was done to get an insight to the thermal stratification in the apartment as mismatches of simulated and measured energy demand occurred.

Measurement set up

As observed in the first indoor climate simulation, the total air volume is cooled to a mean air temperature of $26^{\circ}C$. This includes the whole air volume within the vault, up to a clear inner height of 4.14 m. It is not necessary to cool the whole volume down to this point as no user is staying in the vault. The maximum height of user occupation is below a clear height of 2 m. Furthermore, a total homogenous temperature profile over the total height of the room is unrealistic. A thermal stratification is anticipated. For this reason, a temperature measurement in different height is established. The temperature performance is analyzed as free floating temperature and with activated A/C unit, set to $26^{\circ}C$. Afterwards the performances are compared by including the environmental temperature measurements of a local weather station.

Seven digital temperature sensors DHT22 are installed on each east and west walls of the observed room. They are equally distributed over the total height of the room. This is shown in the pictures in Figure 6.9. There, the sensor on the western wall of the living room of apartment 214 are shown. The data is collected with a microcontroller *Arduino Mega 2560* and directly analyzed on the *Linux* based computer *Raspberry Pi B+*. Furthermore, the radiation data and outdoor temperature are acquired through the WMO standard weather station of TU Berlin Campus El Gouna.

Further, a surface temperature monitoring system was implemented in the apartment to monitor the interior ceiling temperatures of the vault. Therefore, three *TMP006* temperature sensors are coupled to a *Raspberry Pi B+* which monitors and stores the recorded data. The naming of the surfaces and the sensor set up itself are shown in the pictures in Figure 6.10. The three sensors measure the temperature over three sections of the dome. One facing north, one upwards and one to the south.

6. Case study El Gouna, Egypt



Figure 6.9.: Temperature sensors on both side of the walls and data point names for the living room of the case study apartment H12-214.

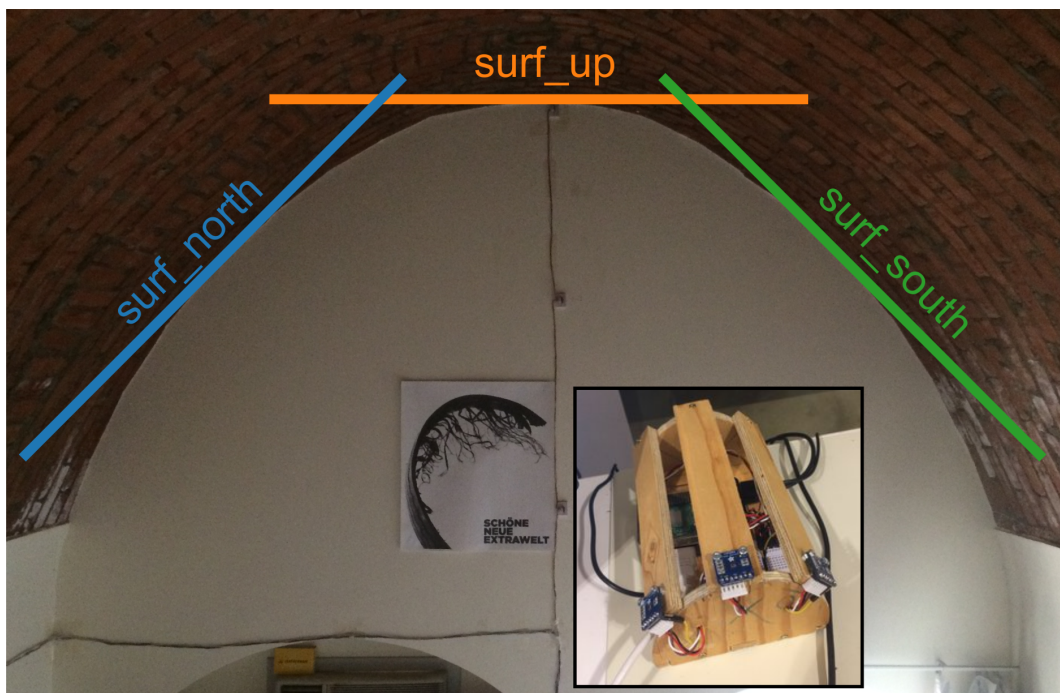


Figure 6.10.: Temperature sensors on both side of the walls and data point names for the living room of the case study apartment H12-214.

Measurement results of the free floating temperature

The graph in Figure 6.11 outlines the measured free floating temperatures. The environmental temperature, measured by TU Berlin's weather station, is presented in orange. The temperatures in the apex of the vault are drawn in blue. The temperatures near the floor of the room are given in pink. Solid lines represent temperatures at the western wall while dashed represent the eastern wall.

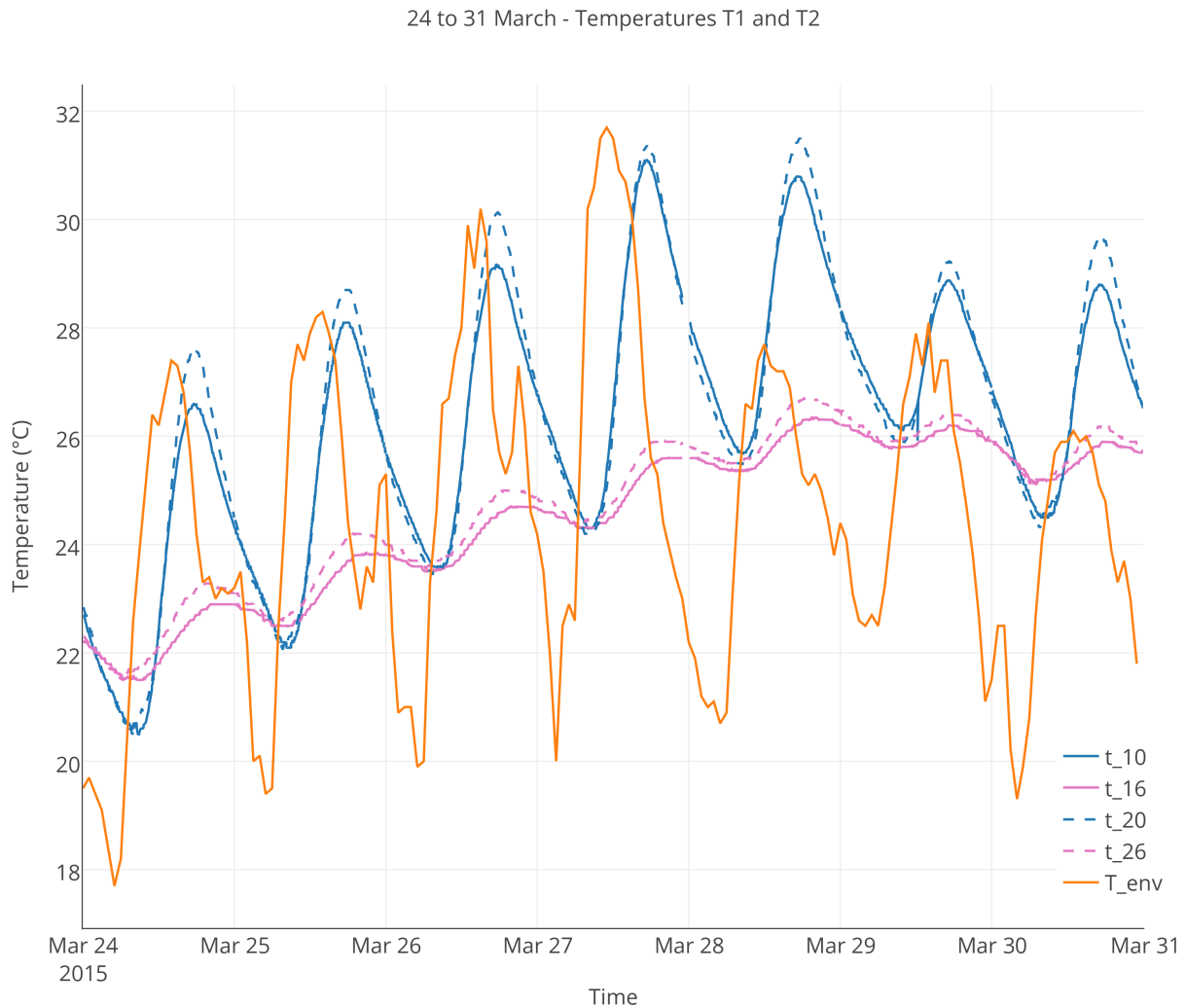


Figure 6.11.: Free floating indoor temperature in the apex of the vault (blue) and close to the floor (pink) with the measurements on the westward facing wall (solid lines) and on the eastward facing wall (dashed lines) over the environmental temperature (yellow).

Clearly visible is the temperature shift due to the thermal mass of the surrounding room surfaces. Within the observed week, the maximum outer temperature occurs on 27 March at noon (12pm) while the maximum temperature in the apex of the vault occurs at 5pm. Furthermore, it can be observed that the air temperature in the vault cools down much faster than the temperature near the floor. In the morning hours of 24 and 25 March, the vault temperature even drops below the bottom temperature. With a periodically rising environmental temperature in the period from 24 to 27 March, this effect vanishes. After a cooler period, beginning 28 March, this effect is observed again after two days in the early morning hours of 30 March. During these colder days, the temperature within the

6. Case study El Gouna, Egypt

room rises above the environmental temperature. This is due to the radiation onto the vaulted ceiling. While the temperatures within the vault have a higher amplitude and overall higher temperature, the temperature near the ground follows the outer temperatures more damped. Using the mean air temperature as cooling set-point would increase the demand for cooling energy as the A/C system needs to be activated more often and more early in the annual period.

The surface temperature measurement was only in operation for a relatively short period of time. The results for the measurements of at least one complete day of continuous measurements are presented in the following graph in Figure 6.12. The surface parts for the color code are indicated in the set up picture in Figure 6.10. The southern part of the vault is green, the upward facing part orange and the northern side blue.

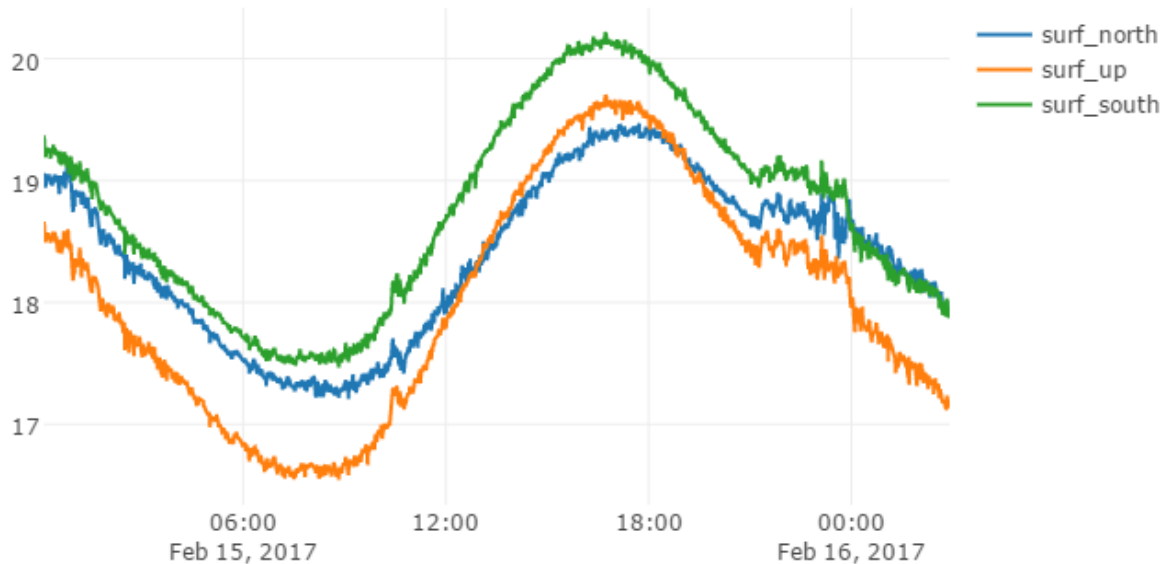


Figure 6.12.: Interior surface temperatures in a the case study apartment while the air below is free floating.

The interior temperature of the southward facing part of the dome is always higher during the day, but cools down to the temperature of the northward facing part during the night on 16 February. The upward facing section of the vault is heated up during the day beyond the temperature of the northern section but cools down much more during the nightly hours due to the radiation exchange with the nightly sky. In the time around 10 am and from 8 pm to midnight, the room was occupied by 2 people which influenced as well the temperature of the ceiling slightly.

Measurement results with the A/C set to 26°C

Next, the thermal performance is observed, when the A/C unit is set to a constant cooling set-point of 26°C. This is shown in Figure 6.13. There, the environmental temperature is drawn in yellow while the temperature in the apex of the vault, t_{10} , is drawn in blue. The color code is explained in the

right part of the figure. The single temperature sensors are marked with the corresponding color on their position on the wall. The heights h are indicated on the corresponding lines to the curves in the diagram. The analysis is done for Friday, 24 July 2015.

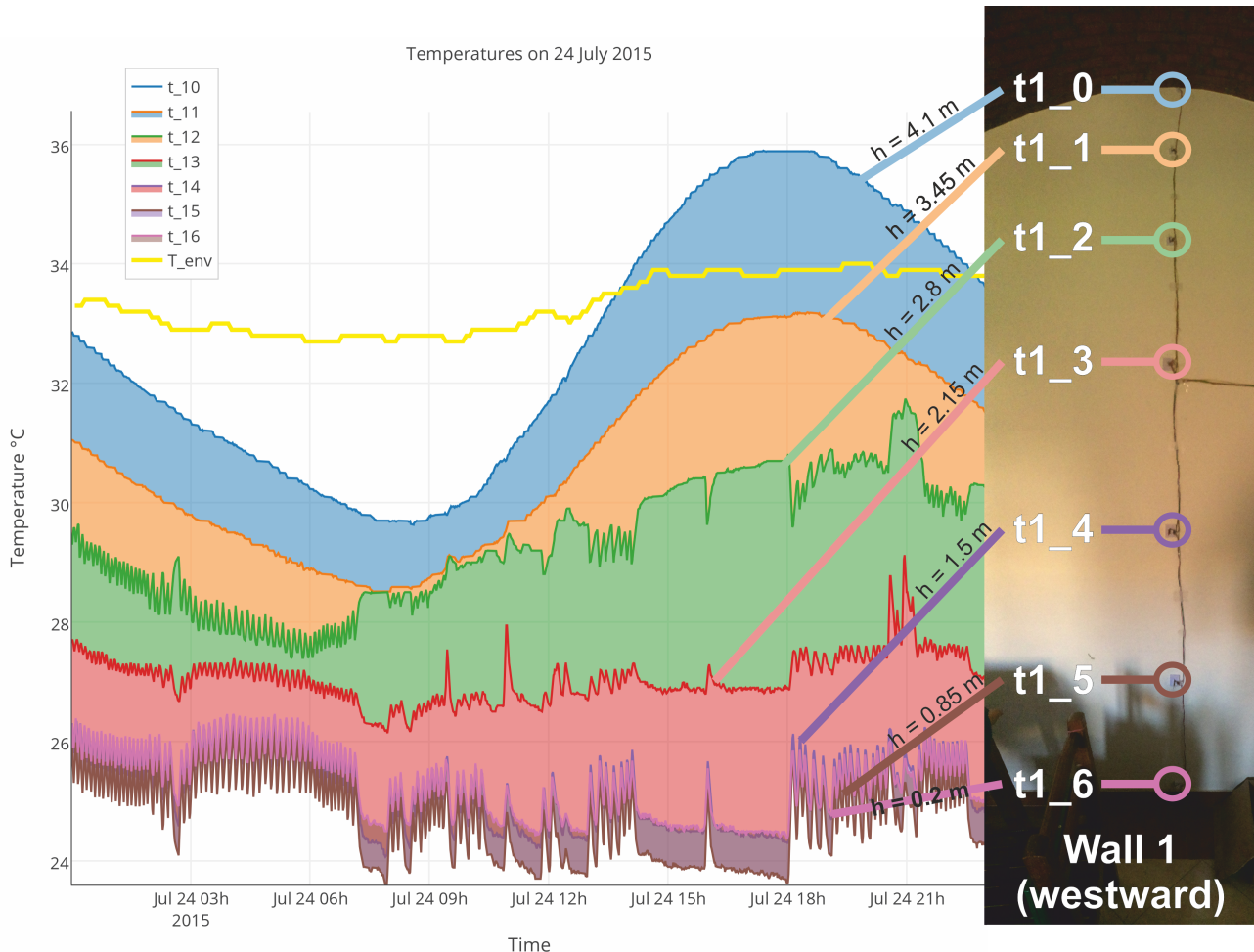


Figure 6.13.: Indoor temperature in all heights on the westward facing wall over the environmental temperature (yellow). The color and height of each sensor is indicated in the picture to the right of the graph.

Several effects are observable in the presented figure. Clearly visible is that the area of presence ($t1_3$ to $t1_6$) is highly influenced by the A/C unit. The air volume inside the vault ($t1_0$ and $t1_1$) is almost not affected. The temperature $t1_0$ in the upper vault has a daily amplitude of more than 6 K, which is equal to the daily variation in March (see Figure 6.11). It reaches a maximum temperature of almost 36°C at 6 pm. This is higher than the maximum environmental temperature t_env and is caused by the solar radiation gains onto the vault. The temperature 0.65 m below the ceiling ($t1_1$, orange) follows this amplitude slightly damped and shifted down by around 1 K. The temperatures below 2.8 m height ($t1_2$ to $t1_6$) are influenced by the A/C system. This is indicated by the peaks and drops in the profile. Within a height of 1.5 m a temperature of 27°C is achieved while it drops to around 24°C near the ground level ($t1_5$, $h = 0.85$ m). Interestingly, the temperature right at ground level ($t1_6$, $h = 0.2$ m) is higher than in $h = 0.85$ m. This might be the result of a warm floor, induced through the thermal performance of the apartment below. The short steep temperature rise around 8

6. Case study El Gouna, Egypt

pm is caused by window ventilation.

Limits of thermal stratification

This subsection aims to identify the boundaries for the mixing of the air within the room. The upper boundary was theoretically defined by Tang et al. (2005)[147]. They simulated the thermal stratification with finite element methods and calculated a difference of up to 10K between floor and apoapsis of a vaulted room. This value was observed in the previous measures as well for the temperature layering in an unused room: under free floating conditions and with an activated split-unit air cooling device. An additional research goal is to determine the lower limit. It is the resulting air mixing and thermal stratification at a maximum use of the room, e.g. with a maximum amount of people inside the room. First the experimental set up to determine the mixing and layering of such a room. Second, the measured temperatures are presented and analyzed. The resulting temperature gradient defines the lower boundary of the thermal stratification in vaulted rooms.

The goal is to determine a temperature gradient under realistic maximum mixing of the air inside a vaulted room. Presence of people is evaluated through a *netatmo* weatherstation, indicating CO₂ and sound pressure levels. The rooms was used by the author to practically measure the lower limit of thermal stratification in the previous section. The amount of present people has a high impact on the thermal gradient in the room. Often, the room is unoccupied. Hence, the air is not mixed and a thermal stratification of up to 11 K is reached as shown in Figure 6.11. This defines the upper boundary for the highest thermal stratification. A temperature gradient for the room was acquired with this measure to increase the accuracy of thermal building simulations done with the software and in cooperation with the programmers of *IDA-ICE*. This gradient is correct for minimum air mixing due to occupants and increased the accuracy of residential simulations significantly. This was shown by Banhardt et al. (2016)[148]. The other boundary for the lowest thermal stratification still remains unclear. As it shows, the temperature gradient is drastically reduced as soon as more than 2 occupants are in the room. The presence of 5 people, mainly seated, reduces the temperature difference between bottom and ceiling to 4K compared to almost 8K within an unoccupied room.

Methodology to measure the limits of thermal stratification

The upper limit for air mixing is explored within the experiment of this paper. Therefore, the observed room was filled with a maximum amount of people. One person corresponds to an approximate shape of a cylindrical heating device which are widely used in experimental facilities for room air climate analysis. The cylindrical heating device and a person can vary their sensible heating output from 60 to 600W. The participating people respond to increased sound pressure levels and acoustic patterns. The power output can be increased by increasing the sound pressure level and acoustic peaks per minute (aka beats per minute). The sound pressure level is constantly monitored with a *netatmo* indoor weather station. Additionally, in contrast to stationary cylindrical heating devices, the participating people, start to move rhythmically but unpredictable through the apartment when exposed to these acoustic inputs. Hence, a random air mixing profile is applied. The thermal power output and random movement was increased during the experiment constantly within the time frame from 9pm to 3am. The thermal stratification was observed before, during and after the experiment. This was done with seven equally distributed *DHT22* temperature sensors on the eastern and western wall surfaces of the room. Additionally, the whole experiment was recorded by a *Testo 4500* infrared camera, which was mounted in a corner of the room. The beginning of the experiment is document in the picture in Figure 2. There, three participants are shown. The maximum amount of participating heating and air mixing devices was 32 during the peak time of the experiment (around 1am).



Figure 6.14.: cylindrical heating devices ($\vartheta > 30^{\circ}\text{C}$) with smaller sources of coldness ($\vartheta < 15^{\circ}\text{C}$) at the beginning of the experiment.

The unpredictable movement and power output of the participants enables the recording of a realistic upper boundary of air mixing and hence defines the lower limit of thermal stratification within a vaulted room.

Determining the limits of thermal stratification

The following graph in Figure 6.15 highlights the thermal performance of the room during the 24 hours around the conducted experiment. It includes the time span of 3 hours before (from 5:30 to 8:30pm), 10 hours during (from 8:30pm to 6:30am), and 11 hours after (from 6:30am to 5:30pm) the experiment. Highlighted in red is the temperature in the apoapsis of the vault while blue represents the temperature close to the floor. Orange represents the outside temperature. Additionally, the sound pressure level (SPL) was monitored and is presented on the right y-axis in grey. The inside temperatures are averaged over a time period of one minute while outdoor air temperature and the sound pressure level are averaged over a five minute time period.

The preparations for the experiment started at 7 pm and the first six test subjects arrived around 9 pm. The major part of participants (approx. 20) arrived around 10 pm. At midnight, the maximum mixing experiment was conducted. Between 3 and 4 am, most of the participants left. Afterwards, the sound pressure level was reduced to around 77 dB(A), directly decreasing the air mixing capabilities of the remaining test subjects. The experiment was stopped at 6am. Due to unknown reasons, the sound pressure level and indoor temperatures were not monitored during the time period from 11:50 pm to 12:30 am.

6. Case study El Gouna, Egypt

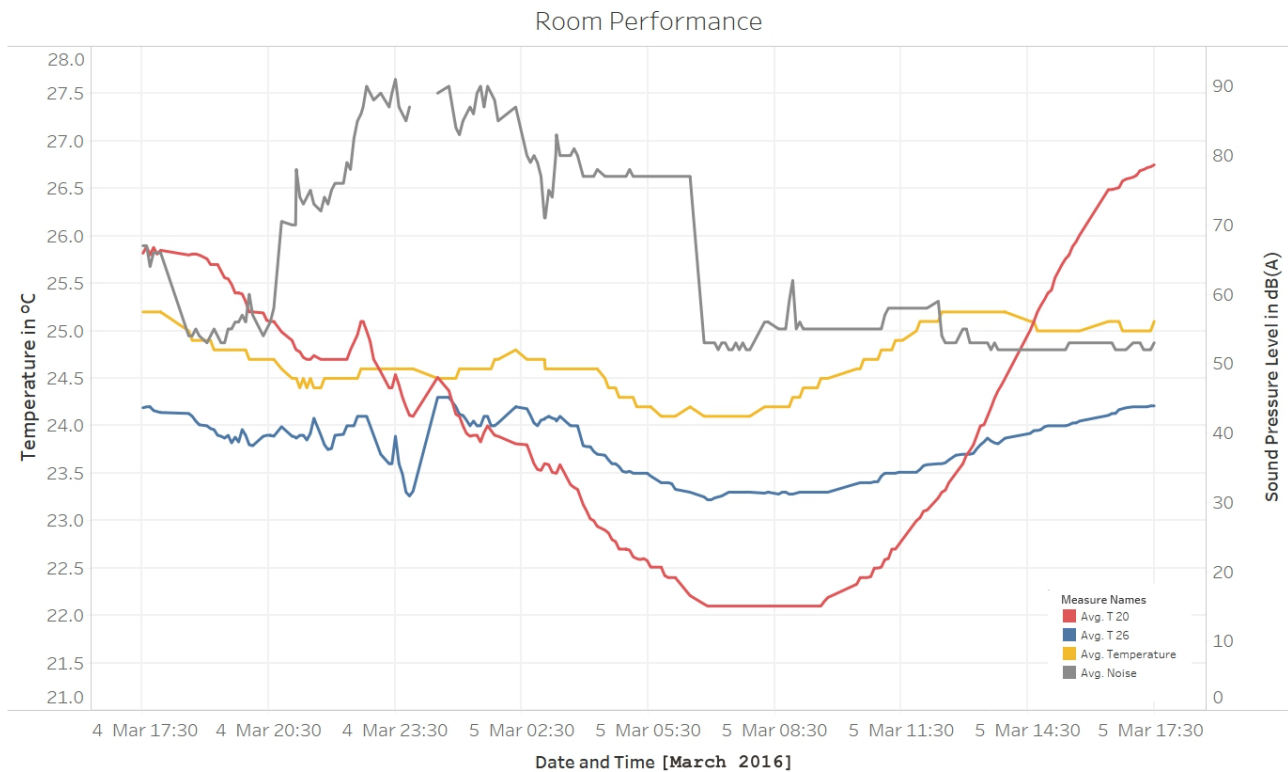


Figure 6.15.: Air temperatures in the room before, during and after the experiment in the top of the vault (red), near the ground (blue) and the outside temperature (yellow). Additionally, the sound pressure level is indicated in grey and on the right y-axis.

Discussion of the thermal stratification experiment

In Figure 6.15, the influence of people on the thermal stratification is clearly visible. Within the preface of the experiment (8:30 to 10:30pm) the air temperature in the apoapsis wasn't decreased as much as without additional internal heating sources. A group of approximately 20 people arrived at 10:30pm. This arrival of 20 internal heating sources first increased the temperature in all layers by almost 1K. In total, up to 35 subjects participated in the experiment in the test room with a total surface area of $A_{room} = 15.96 \text{ m}^2$. This results in a maximum density of 1.88 persons/m^2 .

The opening of the window decreased the temperature in all layers. The decrease below the outside temperature can only be explained by a measurement error. The outdoor sensor is located within a supply shaft of the building while the window is located in the eastward facing facade. The main air mixing experiment was started at midnight. During the whole time 20 participants (fluctuating with plus minus 10 people until 2am) were forced to increase their power output by increasing the sound pressure peaks in a low frequency spectrum (50 to 150 Hz) to 128bpm. Additionally, this increased the random movement of the subjects and thereby increasing the air mixing. The variety of different states of performance is shown in Figure 5. There four different thermographic records are presented. The pictures were taken during the experiment's climax.

The result is a minimum thermal stratification within the room. The air is homogeneously distributed from 12:30 to 2:00am. Afterwards, the internal gains were reduced by decreasing the beats per minute and dissipation of 20 internal heating sources. Immediately, the temperature difference between apex and floor level is increasing. The vault is cooled by radiation exchange with the nightly sky, decreasing the temperature well below the outside temperature. This typical behavior was shown in the previous

6.2. Measured Performance of the Case Study Apartment

subsection. The remaining presence of eight respectively four test subjects (until 4 am resp. until 6:30 am) has close to none influence on the reoccurring thermal stratification. It need to be mentioned that during this time their power output and air mixing capabilities where very limited.



Figure 6.16.: Thermographic pictures during the time from 12:30 to 2 am, showing the variety of different performance states of the internal heat sources.

6.2. Measured Performance of the Case Study Apartment

The existing room is equipped with a smart meter and the data is available for the period from March 2015 to March 2016. The daily electricity demand is shown in orange in the following graph in Figure 6.17. The data is assembled to an annual overview of the electric consumption. The overall annual electricity demand is $E_{elect} = 6379 \text{ kWh/a}$ while the demand during the cooling season (May to November) is $E_{elect,cs} = 5265 \text{ kWh}$.

The living room of the apartment was always set to 26°C and the fan for the recirculation of the air was always activated. The peak in February is caused by the use of the heating mode of the split-unit. Clearly visible is the increased demand during the summer months. During the time from mid-May to mid-July, the apartment was occupied. Within the months to end of September only the A/C system and the fridge where activated. In beginning of August and end of September, the A/C system was deactivated for maintenance for about a week. The maintenance week and the base load of the cooling season where used to estimate the overall electricity demand for cooling. It is calculated to be $E_{elect,AC,est} = 2345 \text{ kWh/a}$. With a stated COP of 2.55 (see Table 4.6, p. 100) the cooling energy demand would account $Q_{cool,est} = 5979 \text{ kWh}$.

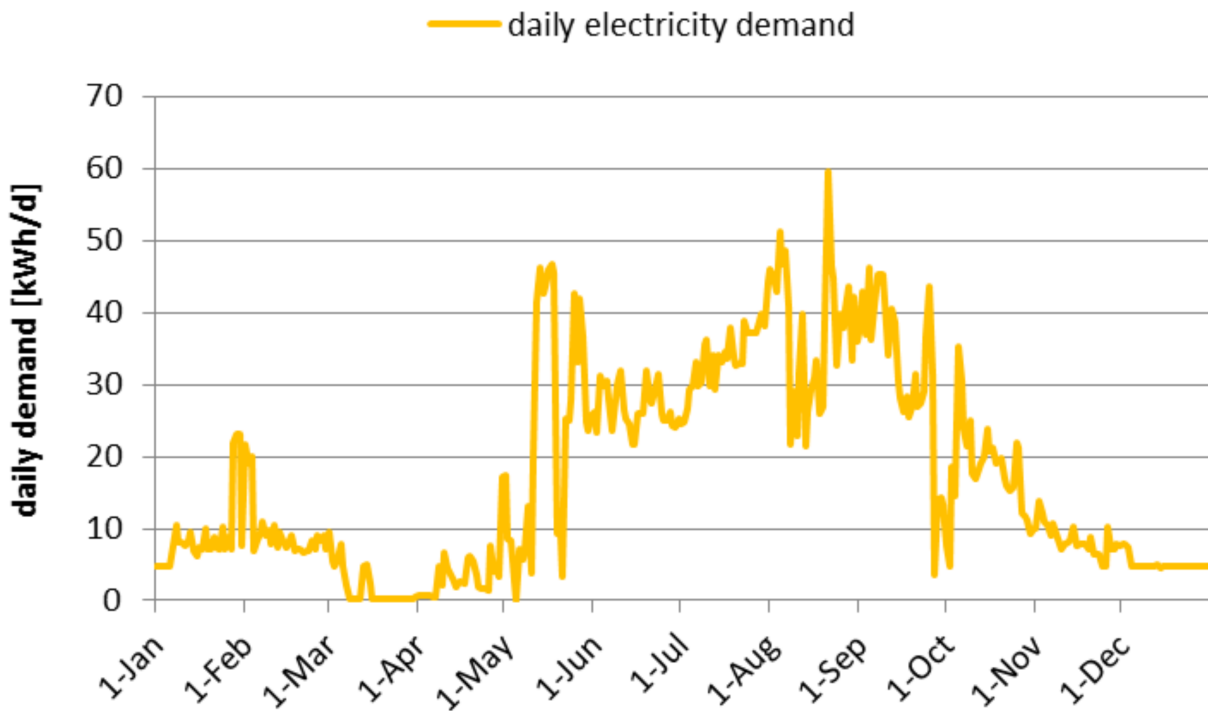


Figure 6.17.: Measured electricity profile of the apartment for the period of one year in El Gouna. The period was assembled from the time span of March 2015 to March 2016.

6.2.1. Thermal simulation of case study apartment

The real existing apartment room is modeled within the environment of *IDA-ICE 5.0 alpha*. It is a room with a vaulted ceiling ($h_{total} = 4.14 \text{ m}$), a floor area of 15.95 m^2 and a zone volume of 65 m^3 . The dimensions of the room are shown in the following figure on the left side. The right side shows the appearance in *IDA-ICE*. Here, the vaulted dome of the apartment is modeled in accordance to the real existing room. The building physics of the construction material as well as the occupant behavior are adapted to local conditions. The heat transfers to neighboring rooms (below, northwards, and southwards) is neglected. Furthermore, a constant air exchange rate of $ACR = 0.5 /h$ is set. With the given zone volume, this accounts for an outdoor air supply of $\dot{V}_{ODA} = 33 \text{ m}^3/h$.

For the simulation of the annual energy balance, the weather data of Hurghada is imported through the software integrated download interface, connecting to the *EnergyPlus* weather database. For later comparison with real measurements the months of March and July are exchanged through weather data of the meteorological weather station within El Gouna. A full annual data set is not available so far and the room is simulated as a single zone. Only a cooling set point of 26°C is introduced. Furthermore, a constant air volume, CAV, is implemented on the westward facing wall as it is done in the real existing apartment. The operation parameters are typical for a split-unit A/C systems in the MENA region which was modeled in the previous chapters.

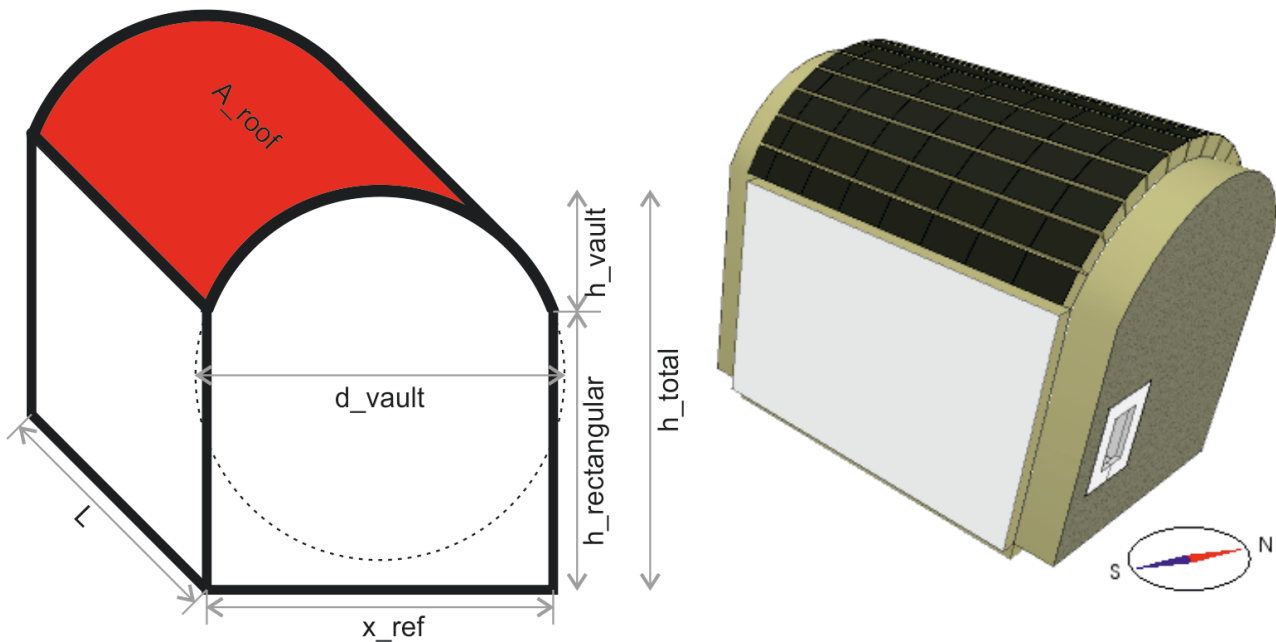


Figure 6.18.: Shape boundaries of and simulation model in *IDA-ICE 5.0 alpha*.

6.2.2. Modelling of comparative system variants

The reference system is tested against three different simulation variants. The three variants are designed to achieve a thermal stratification within the zone. At first, a rectangular model is created. It consists of seven horizontal layers, each with a height of 0.736m, except the top and bottom layer with only half the height. Horizontally, they are connected with a surface which only consists (due to modeling reasons) of an air gap. Within each layer an opening over the whole area is placed. The architectural boundaries and the simulation model in *IDA-ICE* are presented in the following Figure 6.20. The air cooling system is placed in layer 3. This layer is set to $\vartheta_{set,cool} = 26^{\circ}C$. The window is present in layer 4 and the properties match those of the reference system, except its rotated to fit into one layer only. An illustration as well as the simulation model in *IDA-ICE* are given in as well in the following Figure.

The boundaries are chosen for the room to have the same height and an as close as possible roof area and zone volume. All other boundary conditions are kept the same. The other two simulation variants are exactly the same set up within *IDA-ICE* as the reference system. The only difference is the chosen model fidelity. Both variants use the fidelity “climate” and a layered setup. The height of each layer is set to be 0.736m. This set-up will initialize the use of the new simulation algorithm of *IDA-ICE* which is currently only available in a pre-released alpha version. Within the second simulation variant, the “air flow elements” are deactivated while they are activated in the third variant.

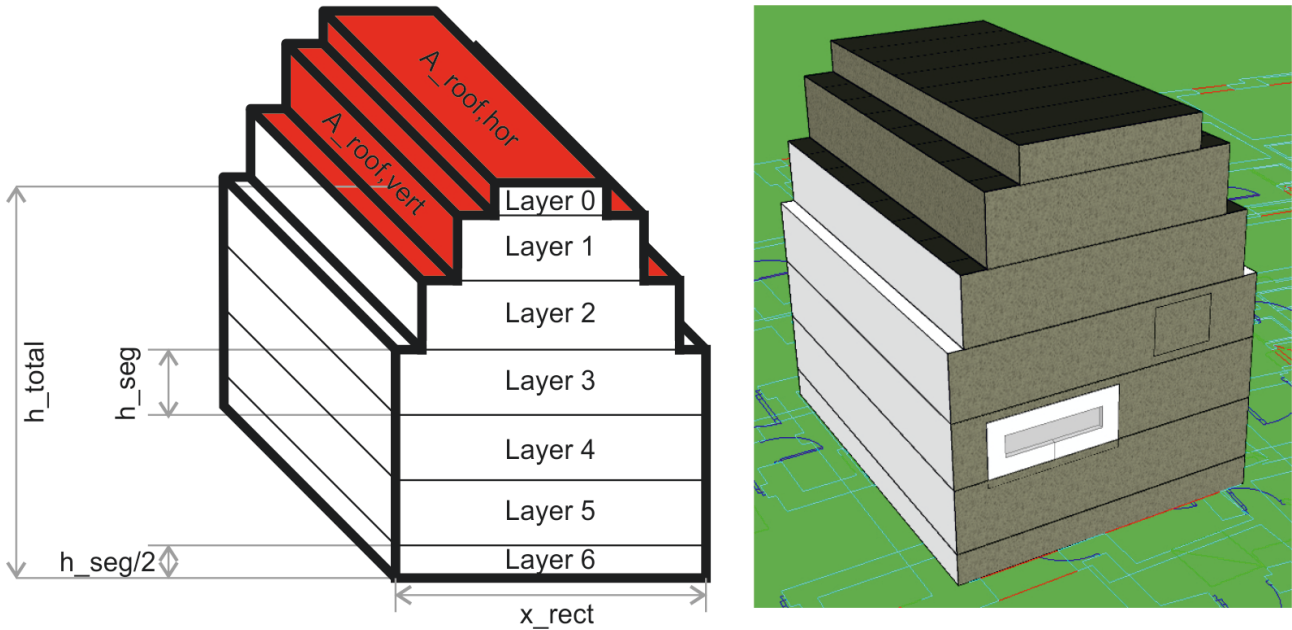


Figure 6.19.: Simplification of the complex shape of the living room in IDA-ICE 5.0 alpha.

6.2.3. Comparison of performance results

The following graph in Figure 3 compares the annual sensible cooling energy demand of the simulated variants. They are drawn in blue and indicated on the left y-axis. Furthermore, the simulation time is highlighted as red bar on the right y-axis. The reference system calculates an annual cooling demand of $Q_{ref} = 4,220kWh/a$ and takes only 30 seconds to simulate.

The first variant, the rectangular construction, takes around three minutes to simulate and evaluates an energy demand of $Q_{rect} = 2,645kWh/a$ which is 37 % lower than the reference calculation. On the other side, the vaulted zone model, without flow elements, simulates 30 seconds and concludes a total of $Q_{vault,Nf} = 3,357kWh/a$. This is 20 % less than the reference. The longest time, with more than one hour, takes the simulation with flow elements. The result is, with $Q_{vault,Wf} = 4,636kWh/a$, about 10 % higher than Q_{ref} of the reference simulation.

Additionally, all the boundaries were entered to the *Modelica* simulation model which was developed in this thesis. The electric energy demand accounts for $E_{cool} = 1,431 kWh$. In total, this electric amount satisfies the total cooling demand of $Q_{modelica,box} = 2,328kWh/a$, which is 44 % lower than the *IDA-ICE* reference simulation.

None of the results gets close to the estimated real cooling demand of $Q_{cool,est} = 5,979kWh$.

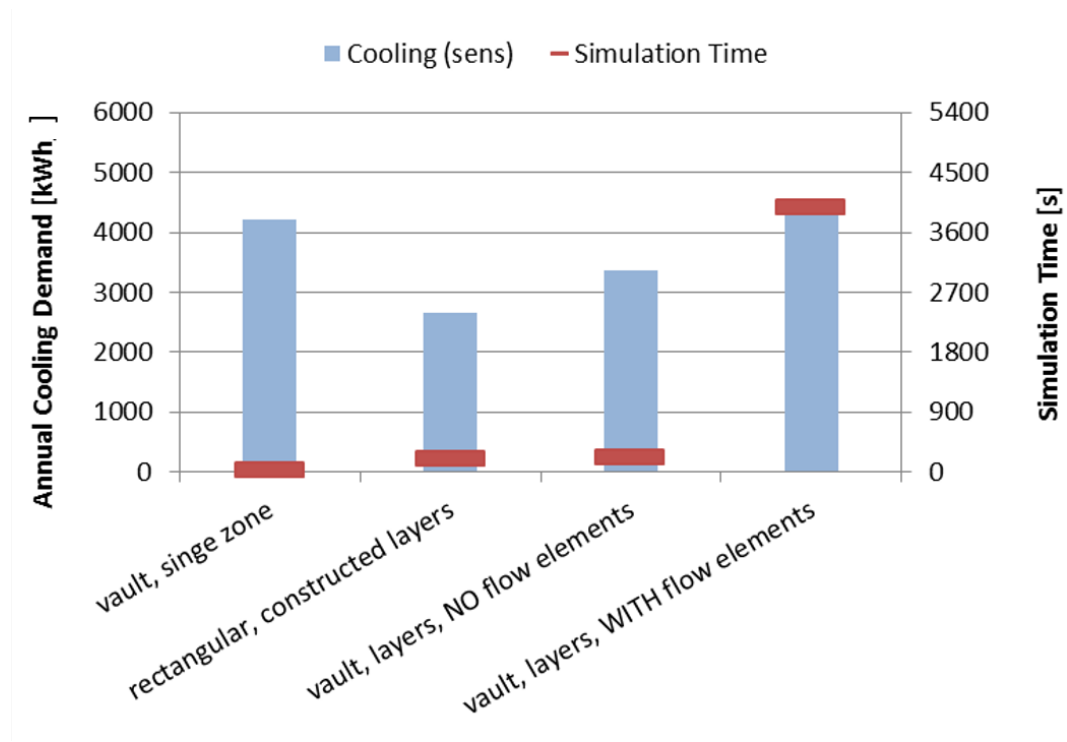


Figure 6.20.: Comparison of cooling energy demand (blue bars) and simulation time (red lines).

6.2.4. Comparison of thermal stratification

Due to the high variation in the simulation results, the different results are compared with a focus on a single day in July. There the temperature profiles are compared with each other. Figure 6.21 shows a graph with the operative (blue) and mean air (red) temperature profile of the reference simulation. As the room is set to a constant temperature, the mean air temperature is constant at $\vartheta_{air,mean} = 26^{\circ}\text{C}$ over the whole day. Only the operative temperature varies. During afternoon it reaches its maximum. This is due to the higher temperature of the ceiling which is caused by the incoming solar radiation.

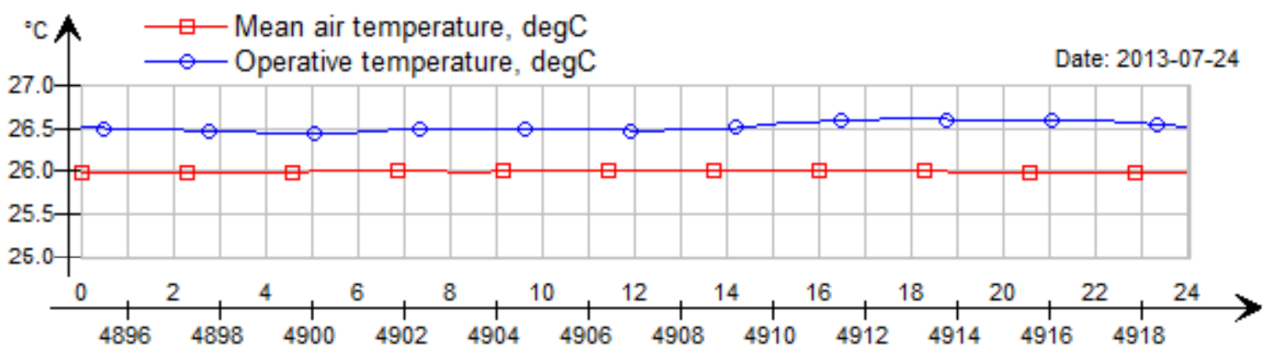


Figure 6.21.: Comparison of operative (blue) and mean air temperature (red) in the reference simulation model of the apartment.

The next graph in Figure 6.22 shows the temperatures of each layer in the rectangular, layered model. Highlighted in solid red with squares is the mean Temperature in Layer 4. This layer is set to $\vartheta_{set,cool} =$

6. Case study El Gouna, Egypt

26°C. The top layer 7 is drawn in dashed grey with a rotated square. The bottom layer 1 is indicated by a solid blue line with straight marks.

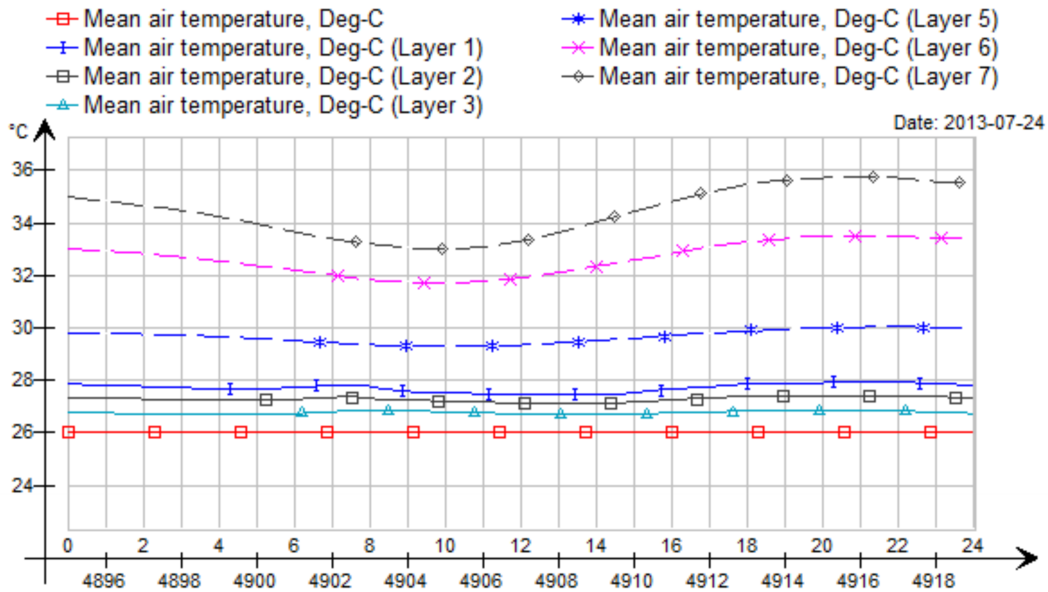


Figure 6.22.: Layer temperatures with single modeled layers with standard simulation algorithm.

The layers 5, 6, and 7 are connected to the dome and are mainly influenced by the solar radiation onto the vault and reach much higher temperatures than the others. The mean air temperature in layer 4 is kept constant at 26°C and hereby the lowest overall temperature. The air exchange to other layers happens through the openings to the upper and lower layer. This happens only due to pressure differences. Hence, the cooling effect of layer 4 to layer 1, 2, and 3 is relatively low. They are mainly heated by their small fractions of the outer walls and the relatively low air exchange.

Compared to this is the graph in Figure 6.24. It shows the temperature in each layer in a simulation with the new algorithm. The layering is done there automatically, according to the entered layer height. Within a first simulation, the “flow-elements” are not activated. The temperature T[4] within layer 4 (drawn in purple, marked with crosses) is constant at 26°C. This layer contains the intake of the split-unit. The temperature of the inlet air is the reference for the cooling set point of the room. Hereby, it is kept constant. The air outlet of the A/C unit is as well in this layer. Layer 5 and 6 are above and connected to the dome. They are mainly influenced by the solar gains of the vaulted ceilings and almost behave like free floating temperatures. They reach temperatures up to 35°C. The temperatures in the lower layers, 1, 2, and 3, is highly influenced by the A/C system as the air exchange between the layers is not only influenced by pressure differences. The empirically gained equations for mass exchange cause the temperature to drop to 2K below the set-point temperature of 26°C. The maximum temperature difference between ground and the upper layers in the dome is more than 10 K around 8 pm.

The upcoming graph in Figure 6.24 shows the temperature profile with activated flow elements. The curves behave less smooth than compared to the other simulations. All layers are influenced by the airstream of A/C outlet. The purple line, marked with crosses, indicates the temperature profile of layer 4. It is almost constant as this layer is the reference for the cooling set-point. The values in the top layer reach their maximum around 2 pm with almost 30°C. The influence of the thermal mass can be seen in the lower levels. In the morning hours, the air in all lower layer has the same temperature. After the heat has dissipated through the walls, around 2 pm, the temperatures start to

vary in different layers. The maximum temperature difference between floor and ceiling is around 8K at 5 pm.

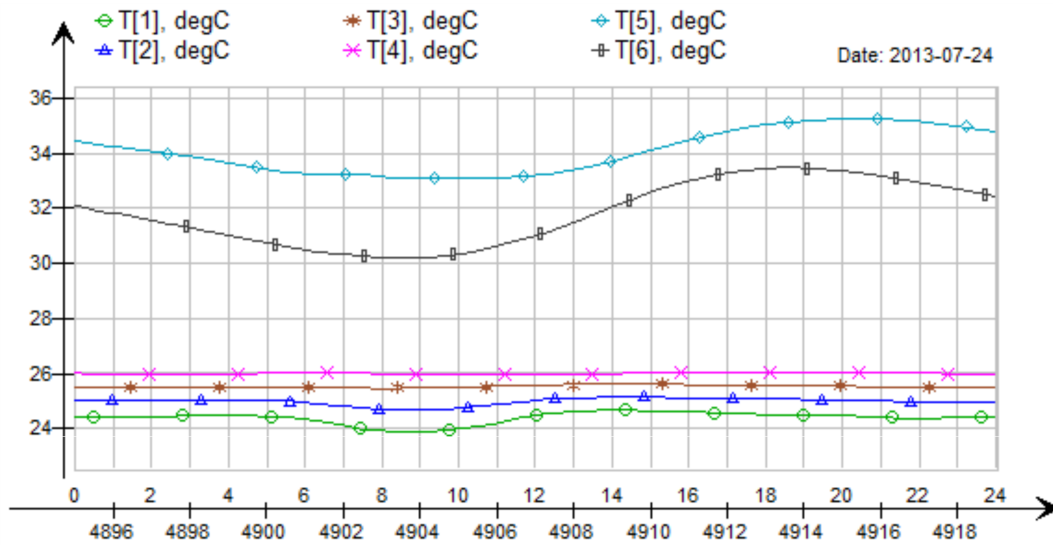


Figure 6.23.: Layer temperatures with new model and flow elements de-activated on 24 June 2016.

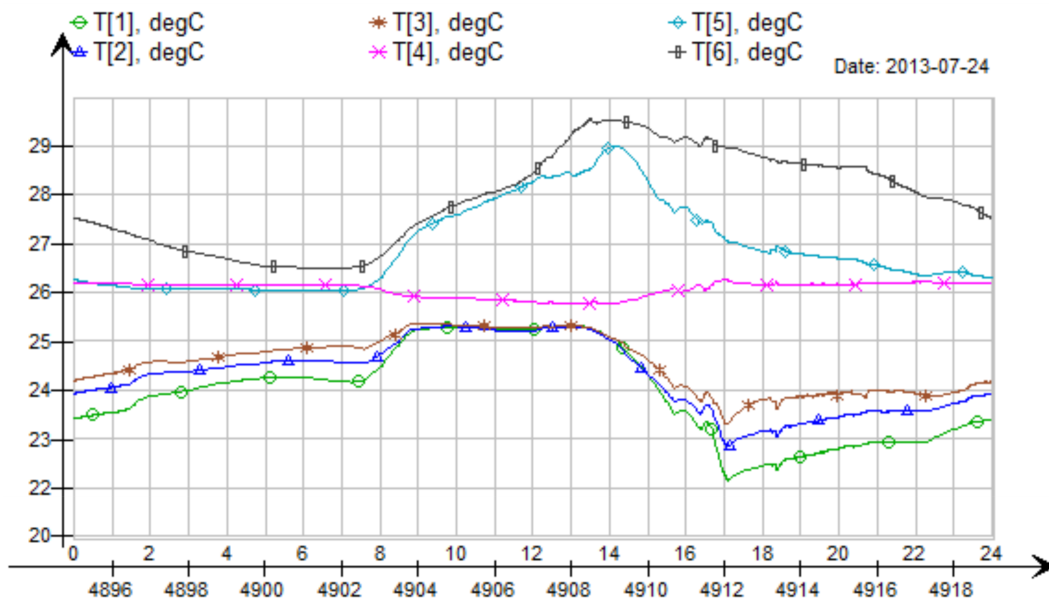


Figure 6.24.: Layer temperatures with new model and flow elements activated on 24 June 2016.

6.2.5. Comparison of simulation models

The common simulation approach with a homogenous zone delivers a higher simulation result in case of cooling energy demand than all other simulation approaches. The results show that a homogenous temperature is not realistic. Especially, the temperature within the dome is highly affected by solar gains but not by the air cooling system. This results in unnecessary cooled air space within the vault. Hence, the simulated cooling demand is too high. This is shown as well in the layered simulation model within the conventional simulation environment. There, only layer 4 is kept at 26°C. A much lower

6. Case study *El Gouna, Egypt*

air volume needs to be cooled which reduces the cooling load tremendously. Nevertheless, this results in unrealistic temperature stratification as also lower layers get hotter than layer 4.

The new simulation model, without activated flow elements show the occurring thermal stratification well. Without the activated flow elements, the impact of the room air cooling system on the air mixing is close to none, which results in an almost daily constant temperature profile with only small influences due to the outer wall. This results in a lower cooling demand as for the reference system as the vault is not cooled. Still, the cooling demand is higher than in the rectangular self-constructed layered model, as also the lower layers are now below 26°C . This result is much more realistic than the two mentioned cases with only slightly more calculation time (half a minute) than compared to the self-constructed layer model.

More realistic results, in terms of thermal behavior, are achieved with activated flow elements. A mixing of the air is now happening and a mass exchange with all layers is achieved. As the cold airstream is blown in horizontally and “falling” to the ground, the lower layers cool down much more than in the previous case without flow-elements. This causes an increased cooling demand which is almost the same as in the reference case.

The 1 dimensional *Modelica* model performs in relation much worse. The simulation time is longer (about 75 minutes) but the system model is much more complex than that of *IDA-ICE*.

6.3. Discussion on case study

The real existing building *H12* and the case study apartment *214* are modeled with the tool set which was developed in this thesis. Further, an apartment with similar boundary conditions, like floor area, orientation and surrounding surfaces are created to evaluate the performance of this specific apartment and the typical construction method of the satellite town *El Gouna* in comparison to a typical construction method of the *MENA* region as it can be found in *Hurghada* as well.

The performance of the massively constructed buildings in *El Gouna* is better due to the increased thermal resistance of the external room surfaces. Further, the cooling demand is damped and shifted towards the night times.

However, the thermal energy simulations show different results than the performance of the real existing and observed system. All simulations underestimate the cooling and electric energy demand of the building. Even, as the expectation was a much lower energy demand, as most of the vault is not influenced by the thermal stratification, the measured energy demand is much higher. The high fidelity model of *IDA-ICE* may calculate the demand quite right, when the average annual $COP_{HRG,avg} = 1.82$ of the *Modelica* simulation is taken (compare with Section 6.1.4 on page 141). Then, based on the estimated cooling demand of $E_{elect,A/C} = 2345 \text{ kWh}$ would be $Q_{cool,est} = 4268 \text{ kWh/a}$. This is only 8 % smaller than the result of the high fidelity model with $Q_{vault,Wf} = 4636 \text{ kWh/a}$.

This finding shows that complicated architecture or high rooms should not be simplified to a single knot model. The results are comparable amongst each other but have less convincing power to real life systems.

7. Conclusion and Outlook

This final chapter discusses the overall findings and shows possibilities for further investigations. At first the applicability of all findings towards the region and in term of the initial research hypothesis are concluded. The transferable findings are concluded first. Secondly, the socio-cultural acceptance of the findings are shortly discussed, based on the authors experience in the region. Thirdly, the possibility for a sub cooling strategy is concluded with a small conducted experiment which analyzed this potential.

Finally, the further investigation options are highlighted. They focus on the durability of photovoltaic systems and the underlying assumption of the module durability and degradation rates. Another focus is set on efficiency increases by maintenance. This last point concludes as well the authors own experiences in the region.

7.1. Applicability of findings

The opening chapter of this thesis concludes the overall energy demand and the energy demand for cooling in particular. Arising problems in so called developing countries are discussed and the impact of unitary air conditioners is presented for the entire *MENA* region. With the extracted necessity for new cooling concepts, which are applicable to widely spread split-unit air conditioning systems, a method to design such system was developed. However, the conducted case study showed that the simulated results can deviate tremendously to measured value as a result of architectural boundary conditions.

7.1.1. Extractable findings

In all countries of the *MENA* region, it is possible to decrease the impact of any existing room air cooling unit in terms of energy demand and operation costs, in terms of impact to a connected grid, and in terms of ecological impact by applying photovoltaic generated electricity. This is possible, without minor to none impact on the thermal comfort inside a room. The method to evaluate the performance where the levelized costs of cooling. The performance of a very general and standardized building, which can be found throughout the entire region is analyzed and its performance validated with 2 different simulation tools. The results of two room types in one flat are compared with simulation trials throughout the entire *MENA* region. The simulation model can be used for simple geometries and standardized user behavior. All boundary conditions for such a model are concluded in this dissertation. However, the case study showed that the results cannot be applied easily to all geometries. This cognizance was presented by the author in a paper [38].

Further, four system models are added to the open source *BuildinSystems* library for *Modelica*. The first is the extended kinetic battery model which also allows to calculate voltage and current and has a variable capacity which is based on the drawn current. This model was already validated through publication in a conference paper [104]. Second and third, there are two room air cooling systems implemented. They are based on existing components of the library. One is a standard split-unit air conditioning system and the other a water cooling system. Both systems are validated with example performances for the very same library. The final new model is a room transfer unit. It is based on the present radiator model but is extended with a simple control mechanism to operate a small pump to transfer water from a central cold water tank.

7. Conclusion and Outlook

Further, many smaller parts and components were added to the library. For example, the weather data of all locations was added, as well as the material properties or combination of different layers to specific constructive elements. Also, the user profiles for the different room types and seasons are added to the library.

This concludes one additional finding: a new method to create a standard load profiles for countries of the *MENA* region. The described method was already applied in a paper which will be published in 2021. The methodology section shows how the model is derived from the available occupancy rate of the case study location and calculated as a standard load profile which is not solely based on electric demand and occupation but also on the outdoor temperature.

Finally, this work confirmed the results of the Fraunhofer ISE (2016) about their calculated *LCOE* for small scale photovoltaic systems. They are financially feasible between 0.08 \$/kWh and 0.14 \$/kWh in Egypt. Additionally, a battery powered system becomes worth installing at an electricity price of 0.19 \$/kWh and at least a 10 % lower feed in tariff. Changing from an direct room air cooling system to a water cooling based system becomes worth at an electricity price of 0.22 \$/kWh. This includes the additional costs for a new chiller and a cold water storage.

7.1.2. Socio-cultural applicability of the work

The previous section concluded the prices at which the switch towards a new or additional system components becomes worth it. However, these analyses take the levelized costs of electricity into account. The investment period for this calculation is based in the *LCOE* on 25 years for the lower end of electricity generation costs (0.08 \$/kWh) and at least 5 year at the upper end of resulting electricity generation costs (0.14 \$/kWh). The cost include an assumption about the maintenance costs of about 34 \$/kW_{peak,PV}. As observed by the author, regular maintenance and service intervals are uncommon. Machines are operated until they break down. This is particular dangerous at the operation of photovoltaic panels. They require regular cleaning and careful cleaning to keep the power output high and avoid micro scratches that could blind the panels.

Also, the simulated electric power demand might be underestimated as the simulations of the case study showed. It remains unclear, if the air cooling system of the observed room in *El Gouna, Egypt* extracts less heat than expected by an average coefficient of performance, or if the simulated cooling demand is too low for such a room.

However, the rising electricity prices in the region foster the interest of citizens to rethink their energy usage. Increasing number of black outs create an additional awareness for the arising problems of air conditioners. More and more people approached the author throughout the year on how the energy demand of residential air conditioners could be lowered. This is a clear indication that the air conditioners are identified as main energy consumer in everybody's home applications. In the authors opinion, it is highly unlikely that inhabitants will buy new or more efficient cooling systems as these systems are often purchased by the landlord or included to the installed equipment when a flat is purchased (comparable to the heating systems in norther European countries). It is more likely that other methods to save energy will be applied, such as the installation of a small scale PV system.

On the first glance, battery systems might be even more unlikely to be purchased. However, battery powered back up systems are spread throughout the region in the form of uninterrupted power supplied lighting systems. These small scale systems are plugged into a socket. As soon as the power supply is interrupted, the light is seamlessly switched on. The battery is recharged as soon as the power is supplied again. These systems are sold more and more since the number of blackouts increased. Intelligent control strategies could be integrated to air conditioners and be sold by the power grid operator which is, in many *MENA* countries, the state or strictly supervised state-like entities. The increasing number of utility scale solar power plants could foster the demand for demand side management. Smart cooling systems would offer a great potential.

7.2. Methodology review

This research was primarily conducted by modeling and simulating real systems. Therefore, the simulation models were created and validated along existing physical systems, like the presented split-unit or apartment. Therefore, this subchapter is divided into three sections. First, the used simulation tools are reviewed. Second, the boundary conditions of the simulated bed and living room are evaluated. Third, the case study to validate the results is analyzed.

7.2.1. Conclusion of the simulation method

The main means of simulation was the programming language *Modelica* within the commercial software tool *Dymola*. The software offers different numerical solvers to conduct the simulations. Within this thesis, the solver *DASSL* was used. Other solvers, like *Euler*, offered much faster but sometimes unphysical results, like temperatures below -273.15°C . The *cvode* solver was as well faster but not always capable to numerically solve the problem and ended often in errors. Modifying the simulated model to work with such a faster solver while still producing valid results would offer the chance to increase the complexity of the optimization problem and increase the observed cooling period of the room or even an entire apartment or building beyond 24 hours. A further usage of the proposed simulation method should be started by a detailed investigation of the best usable solver in combination with the available simulation hard- and software. The computational limits are one of the main reasons to simplify the models and define a strategy to simulate only one representative cooling day per climate region and scale this to an annual consumption.

The used *Modelica* simulation library, the *BuildingSystems*, is in use since 2010 and under constant development. Several papers have been published about the library in general. The included models are often part of research projects such as this presented thesis. However, some models and subcomponents within the models are created for specific boundary conditions or are supposed to be used under specific circumstances. For example, the compression chiller model which is used in this simulation, was validated with data sheets of four different air cooling systems but never for a dedicated water cooling system (except the *Danfoss TurboChor* chiller). Meanwhile, there are dedicated test scenarios for the simulation of *HVAC* applications. This standardized scenarios should be used to validate the used air conditioning systems and to investigate the general usability for building supply applications.

7.2.2. Review of the simulated environment

Within building simulations annual periods are compared to evaluate the performance of a building, a supply system or other related topics. Due to the previous described constraints, the simulation was simplified. Still, a full year simulation for an optimization process with thousands of simulation runs, was not possible. Therefore, the annual energy demand was calculated by scaling the energy demand of a representative summer day. This method does not account for varying user behavior in between days and seasons. Further, the starting conditions for the 24 hours simulation run were determined for every simulated area and a warm-up phase of additional 24 hours prior to every simulation run. Especially, when simulation big thermal masses, this could lead to over or under exaggeration of the storage capabilities of the walls. However, as this method is applied to all simulations, the results are qualitatively comparable with each other.

The application of a dedicated Egyptian user behavior and inhabiting building stock is simplifying the broad cultural spectrum within the region. The suggested 3 seasons are widely spread within the

7. Conclusion and Outlook

countries of the *MENA* region but the extends of celebrating *Ramadan* is sometimes higher, as in *Saudi Arabia* or sometimes lower, as in *Jordan*. There, the impact of this third season on the cooling demand of a building can vary drastically. The main problem with the third season of *Ramadan* is that it is shifted 11 days per year as it is calculated according to the moon calendar. Countries, in which a majority of the population celebrates *Ramadan* could be simulated over a 33 year period and spreading the results evenly.

Finally, the presented models and the presented method was mainly validated with the data for an arid region. It was only used to simulate two rooms of a defined typical apartment in a standard building block structure.

7.2.3. Conclusion on the case study

As described, the case study was conducted in the social vicinity of the author of this thesis. Thereby, a lot of data was available and assumptions, like on user behavior, could be directly confirmed or adopted by on side investigations. However, thereby a critical review of usage patterns, used air-conditioning systems or other boundary conditions can be clouded or used to implement the own bias of the author. The case study revealed that the developed simulation method is limited at least to simple room structures and results for vaulted ceilings may be inaccurate.

7.3. Further investigation fields

This dissertation opened a wide field of research opportunities in terms of building supply technologies. The author was the first researcher at the *Campus El Gouna* who investigated the building and building supply system performances. Also, he was part of launching the operation of this satellite campus of the *TU Berlin* and her exploration projects in the region. Various appointments and meetings in cooperation with the German embassy in Cairo, the GIZ, the AHK or other partner institutions such as the Cairo, the German, the American, or the Heliopolis University gave the author a wide and deep insight to the current research demand and practical needs of every days building practices. The main fields of future investigation areas are concluded in this section.

7.3.1. New control strategies: sensible heat storage in walls

The topic of using the thermal mass of a building was discussed especially in the methodology and design section of this work. The rough potential of about 330 kWh annual energy throughput was evaluated in the simulations of the reference system. This would account for less than 1 kWh per day on average throughout the year. The analyses also showed that the average core temperature of the single brick layered stone walls is around 29 to 30 °C. The cooling storage potential is minimalistic. A first analysis was undertaken in the case study apartment. The results of a normal cooling process are compared with a test to sub-cool the apartment during the day and to use the stored coldness during the early evening hours. The first graph in Figure 7.1 shows the cooling process on 11 July 2016. The air conditioner is started at 3pm. This is clearly indicated by the rise in the sound pressure level which is outlined in grey and its level indicated on the right. The average interior temperature in the area of occupation is drawn in blue. Additionally, the outdoor temperature is highlighted in orange. The colors which are used in Figure 7.2 are the same.

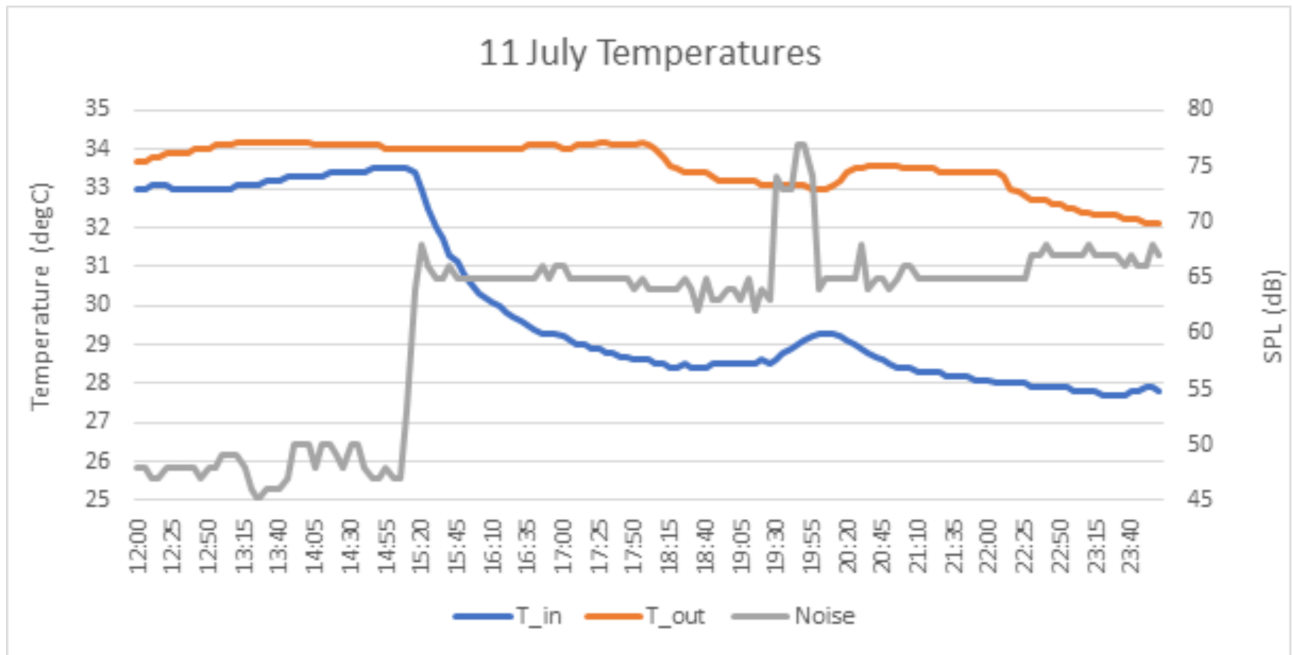


Figure 7.1.: Cooling process of apartment H12-214 in El Gouna, Egypt on 11 July 2016 with the average indoor temperature (blue), the outdoor temperature (orange) and the sound pressure level (grey).

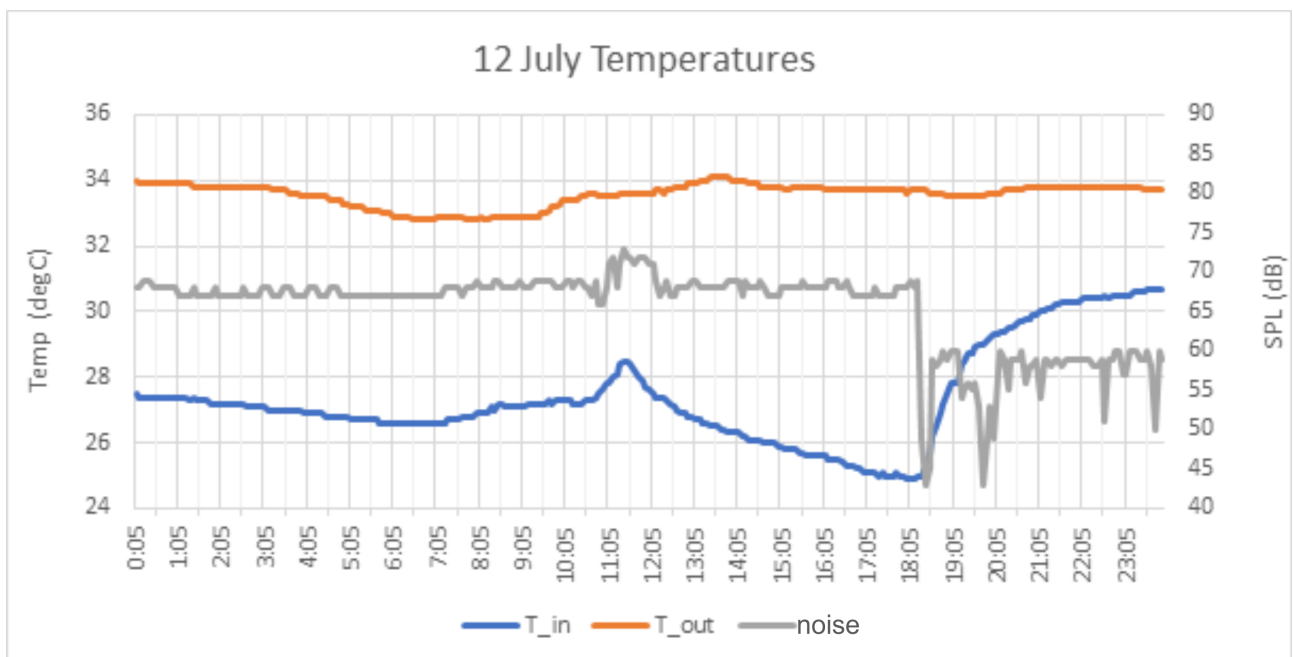


Figure 7.2.: Test to sub cool the apartment H12-214 in El Gouna, Egypt on 12 July 2016 with the average indoor temperature (blue), the outdoor temperature (orange) and the sound pressure level (grey).

The very next day, 12 July 2016, the air conditioner is switched to 16°C at 10:30 am. This is the lowest possible temperature in the settings. The system is only capable to reduce the temperature to about 25°C until 6:30 pm. The temperature rapidly rises above 26°C within 10 minutes and past 28°C within half an hour. The demand shifting potential. This behavior is indicated in the following

7. Conclusion and Outlook

picture.

Sub cooling the room to use the thermal mass on a day to day base seems ineffective. However, further investigations could be undertaken to effectively sub cool the walls. This could include an additional wall layer which is separated by an insulation layer towards the outer wall. Thereby, thermal mass could be created inside the conditioned zone of the building. Alternatively, an insulation layer on the outside might be already enough.

7.3.2. Standard load profiles

The successful development of a new standard load profile for the region offers additional investigation potential. The data base from the case study town *El Gouna, Egypt* is tremendous. Detailed load profiles for a vast variety of application could be created with this data solely. The residential building stock could be analyzed in terms of their energy consumption and surveys for the building stock and its inhabitants undertaken. Touristic and residential users could be separated. The influence on the building orientation, color use or user behavior could be analyzed on a big scale as the building architecture is repeated throughout every building planning and expansion phase.

Also, the variety of domes and vaults could be used to analyze their impact on the building energy demand. For example, the impact of the orientation of a vault could be compared. Further experiments with a variable volume or similar rooms with and without a dome could be investigated. The results could be used to increase the accuracy of building simulation tools in these special cases.

7.3.3. Degradation of PV modules in desert environments

Irregularities in the performance of a small scale PV system was observed during its operation. Besides the increased demand for cleaning, the author noticed a significant power drop in the performance of the PV modules. A picture of the system set up is shown in Figure 7.3. There, the freshly cleaned modules are shown on top of the apartment H12-214. The numbers indicate the data point columns in the done I-V curve measurements with the displayed appearance of the *HT Solar I-V* measurement system which is shown on the right. The module, which is highlighted with a red lighting arrow was already broken.

The measurements were undertaken after three years of continuous operation. The results are shown in the following table. The modules were bought with a peak power of 100 W under standard test conditions *STC*. The used *HT Solar I-V* device automatically calculates these values and shows as well the maximum power point under operation conditions *OPC*.

All modules have a massive power reduction. The maximum power point is even reduced by 15 % in the first module, besides the one which is even not working any more. The following picture shows the resulting I-V and I-P curves which were measured with the *HT Solar I-V* system. The blue line is the I-V curve which a perfectly healthy module would have under *STC* and its values are indicated on the left y-axis. The red line is the I-P curve under *STC* and with perfect health. These values are indicated on the right y-axis.

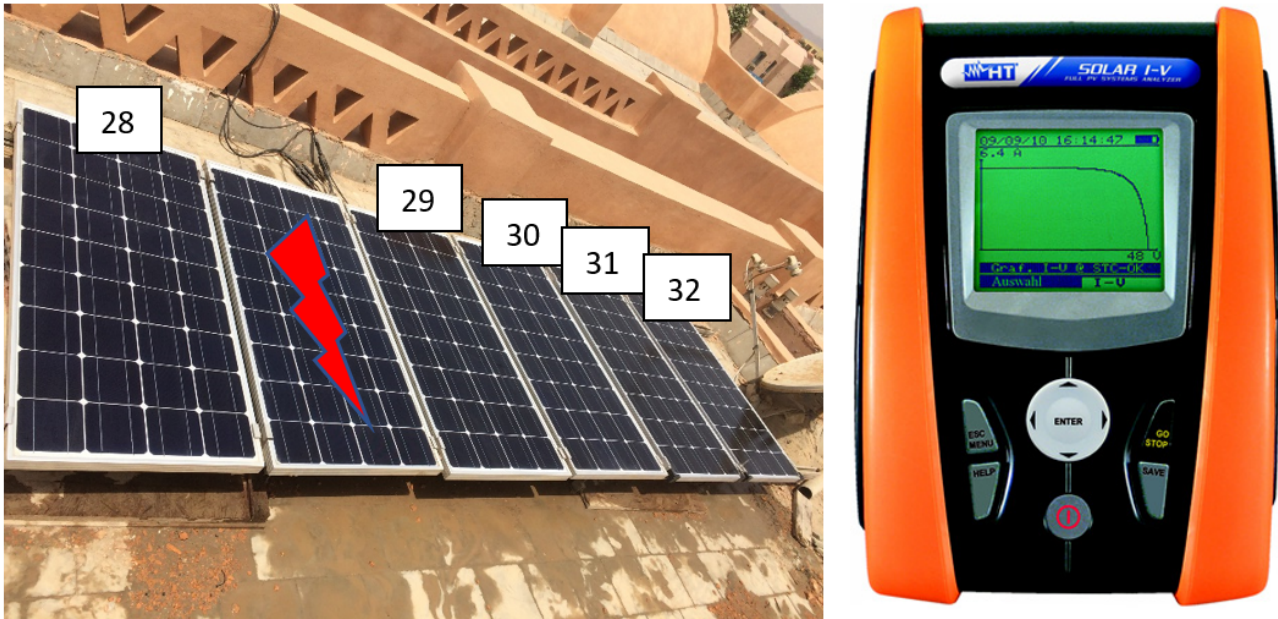


Figure 7.3.: System set up of the real small scale PV plant (left) and the numbering of the recorded I-V-curves with the HT Solar I-V measurement system (right).

Table 7.1.: Measured data points of the previously shown PV panels in El Gouna, Egypt

Datapoint	28	29	30	31	32
Modul	1	3	4	5	6
String	1	1	1	1	1
System	30	30	30	30	30
Irradiation	987.4	971.7	987.1	986.4	988.4
Modul temperature	55	55	55	55	55
Nmod	1	1	1	1	1
Alpha	0.0299	0.0299	0.0299	0.0299	0.0299
Beta	-0.31	-0.31	-0.31	-0.31	-0.31
Pmax at OPC	74.98	77.06	76.99	80.28	78.88
Pmax under STC	85.4	89.33	87.64	91.22	89.64

Clearly visible is the steep current drop at high voltages. This results in a rapid declining of the power curve way before the maximum power point. The modules are further analyzed for this reasons. A clear indication was found on the cells. Multiple cells showed thermal cracks which look like burning patterns within them. One of this cracks is shown on the right side in Figure 7.5. This results in an increased resistance in the strings which lowers the power output as the maximum current through a string is dependent on its weakest cell. The thermal images of the entire field (left) and the modules in detail (middle row) are shown in the following figure as well.

7. Conclusion and Outlook

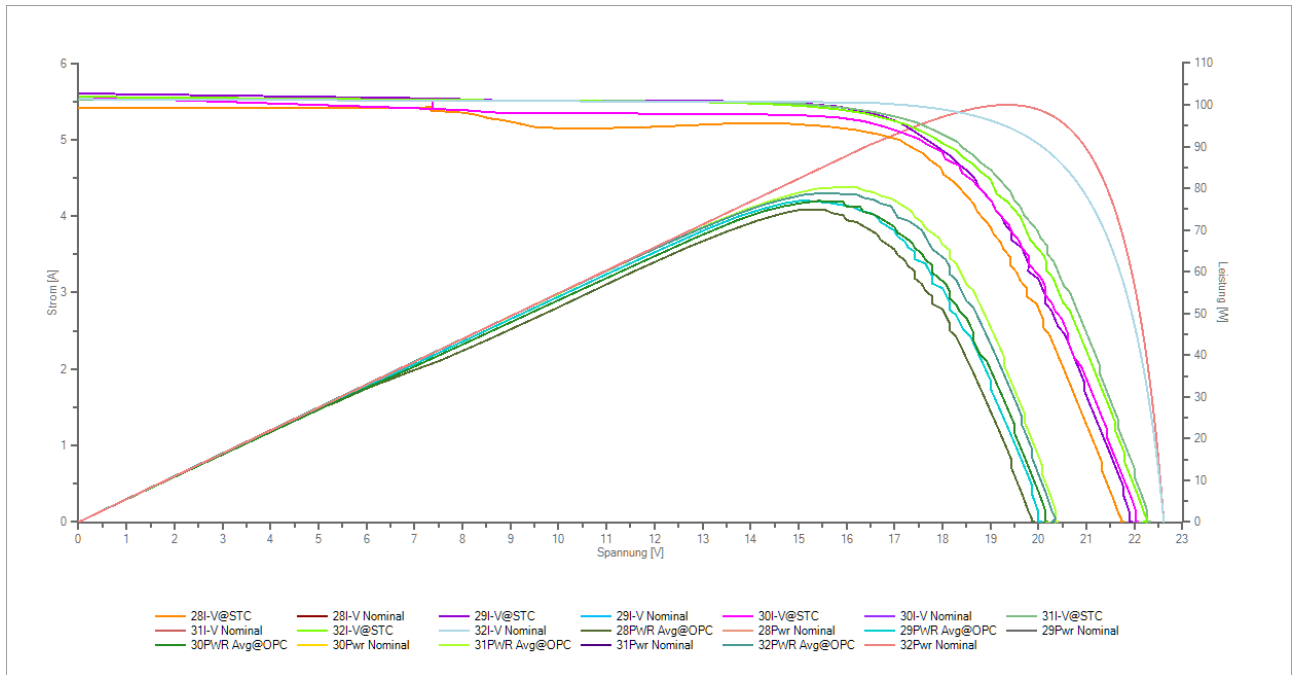


Figure 7.4.: Results of the measured I - V -curves (left y -axis) and I - P -curves (right y -axis). The nominal curves are shown in blue and red. The measured curve fall drastically below this lines.

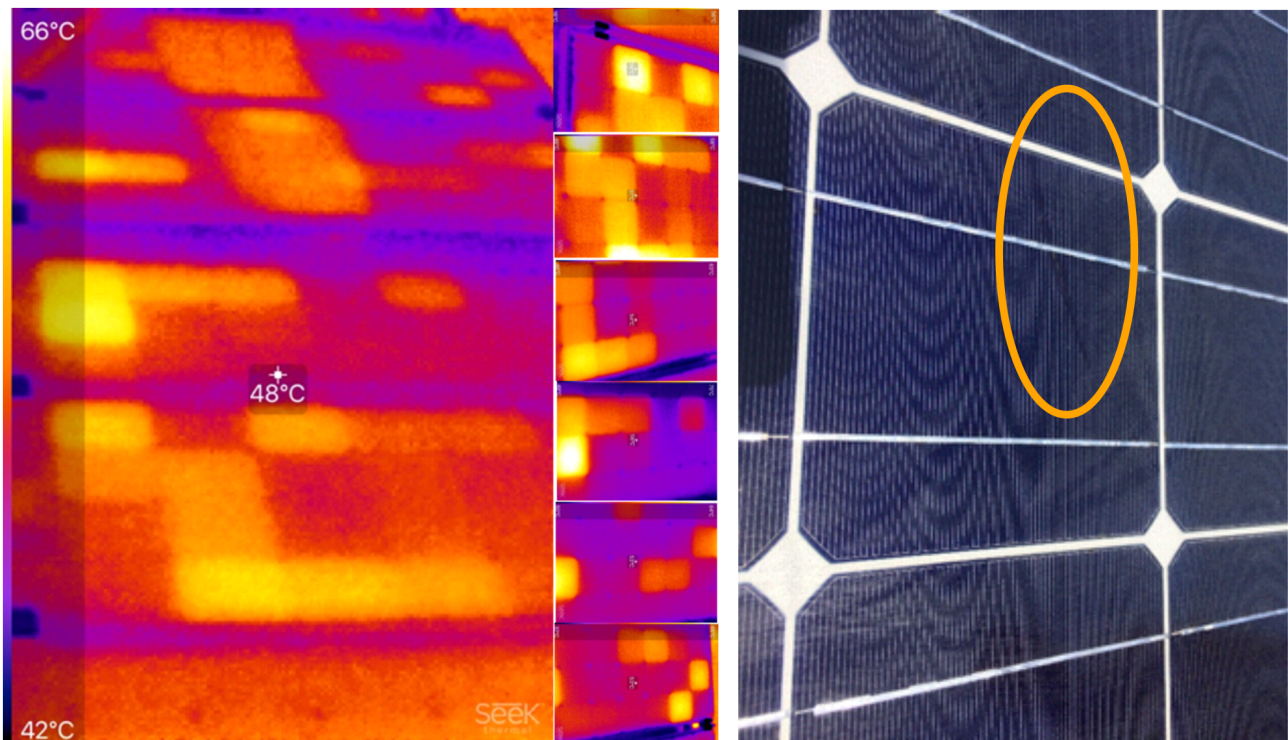


Figure 7.5.: Thermal image of all used PV modules (left), single pictures of each module (middle) and a clearly visible thermal crack in a single cell (right).

Clearly visible are the increased temperature of damaged cells. Further investigations have to be undertaken regarding the long term stability of current photovoltaic systems. Especially, the performance

of cheap small scale systems is under question. The financial feasibility would not be given, when all kind of modules have the same rate of degradation. These investigations should be done as soon as possible. Utility scale photovoltaic systems are erected throughout the region and their long term stability and continuous power output will decide about the fate of renewable energies within the region.

7.3.4. Maintenance

Another big topic which the author noticed during their travel in the region is the lack of maintenance. Machines and devices are used until they brake. Further, they are used until they fail completely. Then, their still somehow working parts are used to repair other broken systems. On the one hand, it is most environmental friendly when a system is used as long as possible. But on the other hand, their operational energy demand can increase exorbitantly. The picture below in Figure 7.6 shows a poorly maintained unitary air conditioning system.

The thick layer of dust reduces the heat transfer and air movement induced by the blades which further decreases the live time of the system. Leaking refrigerant is a common picture amongst Egyptian split-unit systems. Often, this is even the harmful *R22* which is used in the A/Cs. Education to deepen the understanding of the performance of such systems must be fostered throughout the region. The connection between poor maintenance and increased facility bill must be clear to any operator of an air conditioner. This way, the power demand in the peak load hours could be reduced without any additional systems with unclear long term durability.



Figure 7.6.: Outdoor unit of a multi-split-unit at the road crossing of Ismail Mohamed and Yousif Kamel street on Zamalek, Cairo, Egypt, taken by the author on 10 November 2017.

7.4. Contribution to the UN development goals

A briefly discussed topic is the socio-cultural acceptance. How could users and/or investors be convinced to invest in energy saving measures? Throughout the entire existence of the Campus El Gouna of the TU Berlin, local authorities were approached to bring results and knowledge from science to practice. However, non of the projects could be successfully implemented. Still, buildings are build

7. Conclusion and Outlook

with horrible properties and a bad performances in terms of building supplies. Still, no small scale solar panels are used. Still, no alternative ways to cool the building are applied. Still, not a single measure to reduce the energy footprint of any building is applied. This is especially frightening as the town of *El Gouna* is privately operated, the access to local authorities very direct and changes and impacts could be easily implemented.

One of the first guest lecturers at the campus told the author, when visiting the lax and well equipped laboratories and facilities of the campus "*You have such great opportunities and possibilities at this campus! This is amazing! If nothing useful comes out of all this, it is your fault.*" (freely quoted by the author from their memory). So far, the contribution of this thesis to the *UN development goals* is minor. Especially, when the carbon footprint of the author is put to scale. Frequent flying from Germany to Egypt (3 times a year over an ongoing period of 7 years) increased the carbon footprint of the author by more than $3 \text{ tCO}_{2,\text{equiv}}/\text{a}$ which alone is almost three times of the annual carbon budget every human has. The students, which are educated by the author every year need to reduce the electric energy demand within the region by $4,560 \text{ kWh}_{\text{elect}}/\text{a}$ to justify the ongoing travels for education. These savings have to be done for every lecturer who is participating in the education program of *TU Berlin*, including their own made travels. With a total number of maximum 240 students (each travelling twice per year) in 5 master degree courses and around 30 employees (travelling three times per year) this accounts for $570 \text{ tCO}_{2,\text{equiv}}/\text{a}$. This are more than 5 % of *El Gounas* emissions due to air cooling.

However, the author is optimistic that their research helped to increase the understanding of energy usage throughout the region and especially to increase the awareness in terms of building energy demand amongst local authorities and future engineers. May their knowledge be with them.

A. List of Abbreviations and Subscripts

Table A.1.: *List of abbreviations and subscripts in alphabetical order*

Abbreviation	Meaning
A/C	Air conditioner
AC	Alternating current
ACH	Air changes, hourly (room ventilation rate)
apt	Apartment
ava	Available
BA	Badescu model of isotropic sky
bat	Electric storage (battery)
bed	Bed room
bou	Bound
bulb	Lightbulbs
buy	Amount being bought
carnot	Carnot
cntr	Controller
comp	Compressor
con	Condenser
cond	Conduction
conv	Convection
cool	Cooling
COP	Coefficient of performance
DC	Direct current
dif	Diffuse
dir	Direct
dmd	Demand
DWD	German Meteorological Service
dwn	Lower sensor position
EHA	Exhaust air (air, released from building)
el	Electricity
elect	Electri
env	Environment
ETA	Extract air (room air exhaust)
eva	Evaporator
ext	External
GHG	Greenhouse gases
GWP	Global warming potential
grid	Electrical grid
grnd	Ground
HVAC	Heating, ventilation and air conditioning
hyst	Hysteresis
i	Specific number of an element

A. List of Abbreviations and Subscripts

Abbreviation	Meaning
IDA	Indoor air
IEA	International Energy Agency
in	Inlet
int	Internal
inv	Investment
KiBaM	Kinetic battery model
KO	Koronakis isotropic sky
lat	Latent heat
location	General form for a specific location
LI	Liu and Jordan model of isotropic sky
liv	Living room
mach	Machines
mass	Thermal mass
mat	Material
max	Maximum
MENA	Middle East and North Africa
min	Minimum
misc	Miscellaneous
MPP	Maximum power point
Mtoe	Mega tons of oil equivalent
n	Total number of elements
nom	Nominal
occ	Occupants
ODA	Outdoor air
ODP	Ozone depleting potential
off	Off signal
OM	Operation and maintenance
on	On signal
op	Operation
out	Outlet
pers	Persons
PL	Part load
PV	Photovoltaic
R	Refrigerant
rad	Radiation
RCA	Recirculation air (reused room air)
ref	Reference
RoI	Return on investment
room	Neighboring rooms
sb	Stand by
SCA	Solar cooling autonomy
SCR	Solar coverage rate
sell	Amount being sold
sens	Sensible heat
set	User defined set value
SOC	State of charge
split	Instance of a split unit air conditioner
STC	Standard test conditions

Abbreviation	Meaning
store	Thermal storage
strg	Storage
surf	Envelope
sys	System
tot	Total
trans	Transmission
TRY	Test Reference Year
UAC	Unitary air conditioner
UN	United Nations
up	Upper sensor position
vent	Ventilation
WMO	World Meteorological Organization

B. List of Symbols and Units

Table B.1.: *List of symbols and units*

Symbol	Unit	Name
α	$\frac{W}{m^2K}$	Convective heat transport coefficient
β	$^\circ$	Tilt angle
δ	$^\circ$	Declination angle
$\Delta T_{wall-air}$	$deg\ h$	Annual sum of temperature difference between wall and air
\dot{H}	W	Enthalpy stream
\dot{m}	$\frac{kg}{s}$	Mass flow rate
\dot{Q}	W	Energy flow
\dot{q}	$\frac{W}{m^2}$	Specific energy flow
η		Efficiency
λ	$\frac{W}{mK}$	Heat conductivity
ω		Hour angle
ϕ		Relative humidity
ϕ	$^\circ$	Latitude
ρ	$\frac{kg}{m^3}$	Density
σ	$\frac{W}{m^2K^4}$	Stefan Boltzmann constant
θ	$^\circ$	Angle of incidence
ϑ	$^\circ C$	Temperature
a_n		Polynomial factor for efficiency curve
A	m^2	Area
A_t	USD	Annual total costs in year t
A_{ZS}	$^\circ$	Solar azimuth angle
ACH	h^{-1}	Air change rate per hour
C	<i>Currency</i>	Costs
Cst	<i>Currency/a</i>	Annual costs
d	$\%$	Annual degradation factor
DNI	$\frac{W}{m^2}$	Direct normal irradiation
e		Emissivity
E	kWh	Amount of energy
Em	$\frac{kgCO_2,equiv}{kWh}$	Equivalent carbon emissions
em	$\frac{kgCO_2,equiv}{kWh}$	Specific GHG emissions
F		View factor
FF	$^\circ$	Wind direction
g		Solar heat gain coefficient
h	$\frac{J}{kg}$	Enthalpy
H	kJ	Enthalpy
h	$\frac{kJ}{kg}$	Specific enthalpy
HoY	h	Hour of year
I	A	Electric current
i	$\%$	Annual capital interest rate

B. List of Symbols and Units

Symbol	Unit	Name
I_0	<i>USD</i>	Initial investment costs
I_{rr}	$\frac{W}{m^2}$	Specific radiation on a surface
<i>LCOC</i>	<i>Currency/kWh</i>	Levelized costs of cooling
<i>LCOE</i>	<i>Currency/kWh</i>	Levelized costs of electricity
$M_{t,el}$	<i>kWh/a</i>	Produced quantity of electricity in year t
n	<i>a</i>	System life time
n_{XX}		Amount of XX
p	<i>hpa</i>	Pressure
P	<i>W</i>	Power
<i>PEF</i>	$\frac{kgCO_2.equiv}{kWh_{elect}}$	Prime energy factor
Q	<i>kWh</i>	Amount of thermal energy
\dot{Q}	<i>W</i>	Thermal energy flow
<i>Rvn</i>	<i>Currency/a</i>	Annual revenue
S/V	$\frac{m^2}{m^3}$	Surface to volume ratio
<i>SPL</i>	<i>dB(A)</i>	Sound pressure level
<i>ST</i>		Solar transmittance
T	<i>K</i>	Absolute temperature
<i>thk</i>	<i>m</i>	Thickness
u	$\frac{W}{m^2K}$	Heat transfer coefficient
U	<i>V</i>	Voltage
V	m^3	Volume
W	<i>kWh</i>	Amount of mechanical work
w	$\frac{m}{s}$	Wind speed
x	$\frac{g}{kg}$	Absolute humidity
y_0	<i>a</i>	Initial year of a system

C. List of parameters and variables

Table C.1.: *List of parameters and variables*

Parameter/Variable	Unit	Name
A		Factor for battery voltage calculation
a_mcr	$\frac{W}{J}$	Maximum charge rate parameter
c		Capacity relation available to bound energy
C		Factor for battery voltage calculation
c1	$\frac{m^2}{V}$	1st coefficient IPho
c2	$\frac{m^2}{(kV \cdot K)}$	2nd coefficient IPho
CF		Discharge factor for battery
cs1	$\frac{A}{K^3}$	1st coefficient ISat1
cs2	$\frac{A}{K^5}$	2nd coefficient ISat2
D		Factor for battery voltage calculation
E_nominal	J	Nominal capacity
EAva	Wh	Available energy
EBat	Wh	Energy in battery
EBou	Wh	Bound energy
Eg	eV	Band gap
ENom	Wh	Nominal battery capacity
etaCharge		Charge efficiency
etaLoad		Load efficiency
fDis	$\frac{\%}{d}$	Self discharge
h1	J	Potential of EAva
h2	J	Potential of EBou
height	m	Height
ICharge_eff	A	Current stored inside a battery
ICur	A	Actual current
Ik0	A	Short circuit current under STC
ILoad_eff	A	Current taken from a battery
INet	A	Resulting current from/to battery
ITot	$\frac{W}{m^2}$	Effective total solar irradiation on cell during STC
k	s^{-1}	Constriction between available and bound energy
nCelPar		Number of parallel connected cells
nCelSer		Number of serial connected cells
p		Peukert coefficient
PCharge_max	W	Maximal charging power
PEl_nominal	W	Module power under standard conditions
PLoad_max	W	Maximal discharging power
RPar	Ω	Parallel resistance
RSer	Ω	Serial resistance
SOC_min		Minimal accepted charge level
TCel	$^{\circ}C$	Cell temperature at STC

C. List of parameters and variables

Parameter/Variable	Unit	Name
t_{Ik0}	$\frac{mA}{K}$	Temperature coefficient for the shor circuit current
t_{U10}	$\frac{V}{K}$	Temperature coefficient for the open circuit voltage
$U_{nominal}$	V	Nominal voltage
UI	$[V; I]$	PV module characteristic curve between 0 and U_{10}
width	m	Width
x		Factor for battery voltage calculation

D. Additional information

Table D.8.: *Energy balances for the bed and the living room for all 26 locations and the calculated solar coverage rate and solar autonomy rate.*

Bed room: annual electric energy balances for a small scale split unit air conditioning system and calculated solar coverage and solar autonomy rate

Location	E split	E PV	E sell	E buy	SCR	SCA
A Morocco Casablanca	1078	1824	767	-1513	1.69	0.17
B Algeria Algiers	1184	1672	858	-1347	1.41	0.19
C Iran Tabriz	980	1993	672	-1685	2.03	0.15
D Israel Jerusalem	1189	1836	833	-1480	1.54	0.19
E Tunisia Tunis	1591	1616	1192	-1216	1.02	0.25
F Egypt Alexandria	1678	1990	1199	-1511	1.19	0.24
G Lebanon Bayrouth	1802	1646	1362	-1206	0.91	0.27
H Syria Damascus	1382	1951	970	-1538	1.41	0.21
I Iran Teheran	1734	1564	1353	-1183	0.90	0.24
J Jordan Safawi	1832	1987	1347	-1502	1.08	0.24
K Algeria Tamanrasset	2134	2511	1555	-1933	1.18	0.23
L Lybia Tripoli	1835	2034	1347	-1545	1.11	0.24
M Egypt Asyut	2067	1961	1568	-1463	0.95	0.25
N Oman Masira	3234	1467	2627	-860	0.45	0.41
O Jordan Aqaba	2700	2163	2048	-1511	0.80	0.30
P Egypt Hurguada	2578	2381	1896	-1698	0.92	0.29
Q Israel Eilat	2849	2018	2216	-1385	0.71	0.31
R Iraq Baghdad	1885	1716	1464	-1294	0.91	0.25
S Iran BandarAbass	3148	1403	2636	-891	0.45	0.37
T Bahrain Manama	3178	1476	2646	-944	0.46	0.36
U KSA Riyadh	2830	1849	2281	-1300	0.65	0.30
V UAE AbuDhabi	3405	1564	2810	-969	0.46	0.38
W Qatar Doha	3379	1430	2858	-909	0.42	0.36
X Kuwait KuwaitCity	3016	1639	2479	-1102	0.54	0.33
Y KSA Sharura	3455	1926	2777	-1249	0.56	0.35
Z Jemen AlHudaydah	4252	1736	3481	-966	0.41	0.44

Living room: annual electric energy balances for a small scale split unit air conditioning system and calculated solar coverage and solar autonomy rate

Location	E split	E PV	E sell	E buy	SCR	SAR
A Morocco Casablanca	1747	1802	1192	-1246	1.03	0.31
B Algeria Algiers	1737	1657	1212	-1132	0.95	0.32
C Iran Tabriz	1462	1988	913	-1439	1.36	0.28
D Israel Jerusalem	1736	1811	1189	-1264	1.04	0.30
E Tunisia Tunis	2008	1603	1459	-1054	0.80	0.34
F Egypt Alexandria	2180	1971	1497	-1288	0.90	0.35
G Lebanon Bayrouth	2278	1633	1683	-1037	0.72	0.36

D. Additional information

H Syria Damascus	1815	1933	1235	-1353	1.07	0.30
I Iran Teheran	2034	1556	1545	-1068	0.77	0.31
J Jordan Safawi	2198	1971	1564	-1337	0.90	0.32
K Algeria Tamanrasset	2527	2504	1716	-1694	0.99	0.32
L Lybia Tripoli	2260	2022	1600	-1363	0.90	0.33
M Egypt Asyut	2477	1951	1818	-1292	0.79	0.34
N Oman Masira	3587	1473	2884	-770	0.41	0.48
O Jordan Aqaba	3101	2162	2266	-1328	0.70	0.39
P Egypt Hurguada	3088	2375	2160	-1447	0.77	0.39
Q Israel Eilat	3276	2012	2469	-1205	0.61	0.40
R Iraq Baghdad	2211	1706	1673	-1169	0.77	0.32
S Iran BandarAbass	3561	1396	2955	-790	0.39	0.43
T Bahrain Manama	3580	1471	2944	-835	0.41	0.43
U KSA Riyadh	3226	1848	2549	-1171	0.57	0.37
V UAE Abu Dhabi	3850	1560	3131	-841	0.41	0.46
W Qatar Doha	3808	1424	3189	-805	0.37	0.43
X Kuwait KuwaitCity	3391	1638	2765	-1012	0.48	0.38
Y KSA Sharura	3861	1929	3016	-1084	0.50	0.44
Z Jemen AlHudaydah	4473	1743	3637	-908	0.39	0.48

Table D.1.: Overview of simulation results of IDA-ICE for the specific heating and cooling energy demands and capacities

Location	Annual heating demand $kWh/(m^2a)$	Annual cooling demand $kWh/(m^2a)$	Installed heating capacity kW	Installed cooling capacity kW
Casablanca, Morocco	6.6	-16.2	19.5	-15.8
Algiers, Algeria	16.5	-24.9	25.5	-22.5
Tabriz, Iran	72.3	-19.8	44.7	-23.4
Jerusalem, Israel	10.7	-34.3	18.8	-24.8
Tunis, Tunisia	11.8	-34.3	19.5	-27.5
Alexandria, Egypt	4.9	-34.7	16.0	-20.6
Beirut, Lebanon	2.5	-41.3	11.3	-22.2
Damascus, Syria	34.8	-28.6	35.4	-24.6
Tehran, Iran	41.6	-40.0	34.7	-25.9
Safawi, Jordan	21.4	-42.0	26.1	-29.7
Tamarasset, Algeria	6.8	-48.8	19.2	-24.7
Tripoli, Libya	10.4	-47.4	20.4	-37.8
Asyut, Egypt	8.4	-52.9	18.9	-28.2
Masirah, Oman	0.0	-99.8	0.0	-31.7
Aqaba, Jordan	2.3	-76.5	15.4	-43.2
Hurghuada, Egypt	0.5	-69.6	6.7	-28.9
Eilat, Israel	1.4	-75.8	11.8	-31.8
Baghdad, Iraq	19.6	-65.1	29.4	-37.0
Bandar Abass, Iran	0.1	-117.2	2.9	-38.8
Manama, Bahrain	0.1	-108.9	1.3	-37.9
Riyadh, Saudi Arabia	3.2	-92.8	17.0	-35.7
Abu Dhabi, UAE	0.0	-114.0	0.6	-39.1
Doha, Qatar	0.0	-114.4	1.4	-38.1
Kuwait City, Kuwait	5.5	-100.3	19.6	-39.7
Sharurah, Yemen	0.0	-128.2	0.5	-37.5
Al Hudaydah, Yemen	0.0	-143.8	0.0	-34.5
Average values	10.8	-68.1	16.0	-30.8
Standard deviation	16.2	37.0	12.0	7.1

D. Additional information

Table D.2.: *IDA-ICE simulation results of ideal calculated annual cooling energy demands*

Location Name	Bed room: cooling demand kWh/a	Living room: cooling demand kWh/a
Casablanca, Morocco	77.73	163.32
Algiers, Algeria	146.51	319.40
Tabriz, Iran	142.41	313.50
Jerusalem, Israel	207.60	439.96
Tunis, Tunisia	217.06	444.41
Alexandria, Egypt	202.74	408.87
Beirut, Lebanon	249.04	476.95
Damascus, Syria	187.19	455.95
Tehran, Iran	302.27	607.10
Safawi, Jordan	295.51	635.60
Tamarasset, Algeria	348.59	726.40
Tripoli, Libya	305.44	639.88
Asyut, Egypt	381.12	806.07
Masirah, Oman	584.45	1096.73
Aqaba, Jordan	548.01	1084.18
Hurghuada, Egypt	503.83	981.50
Eilat, Israel	566.86	1121.56
Baghdad, Iraq	482.50	968.74
Bandar Abass, Iran	712.03	1360.38
Manama, Bahrain	687.30	1288.17
Riyadh, Saudi Arabia	709.75	1390.03
Abu Dhabi, UAE	739.99	1437.22
Doha, Qatar	757.85	1441.84
Kuwait City, Kuwait	765.06	1497.55
Sharurah, Yemen	1041.80	1908.92
Al Hudaydah, Yemen	1048.78	1723.76
Average values	469.7	913.0
Standard deviation	270.7	476.0

Table D.3.: *Specific costs for electricity and greenhouse gas emissions for a kWh of electricity*

Country	Residential electricity tariff (USD/kWh) [12]	Prime Energy Factor (kgCO ₂ equiv/kWh) [32]
Algeria	0.04	0.576
Bahrain**	0.04	0.636
Egypt	0.02	0.466
Iran	0.03	0.661
Iraq**	0.03	0.636
Israel	0.16	0.661
Jordan	0.09	0.581
Kuwait	0.03	0.870
Lebanon*	0.13	0.717
Libya*	0.21	0.872
Morocco	0.11	0.638
Oman*	0.26	0.842
Qatar	0.03	0.494
Saudi Arabia	0.05	0.757
Syria*	0.01	0.641
Tunisia	0.07	0.538
UA Emirates	0.08	0.631
Yemen*	0.07	0.630

* electricity prices for 2012 or 2015 (see [141] to [145] and [146])

** emissions are the regions average

D. Additional information

Table D.4.: *Impact on grid stability: share of electricity demand for peak load hours in total cooling energy and number of on/off switches*

Location	Share in bed room peak demand	Share in living room peak demand	On/off switches in bed room	On/off switches in living room
A Morocco Casablanca	0.295	0.295	764	1420
B Algeria Algiers	0.281	0.291	805	1327
C Iran Tabriz	0.282	0.293	616	1063
D Israel Jerusalem	0.279	0.287	809	1310
E Tunisia Tunis	0.248	0.272	1144	1544
F Egypt Alexandria	0.249	0.270	1235	1707
G Lebanon Bayrouth	0.242	0.263	1339	1795
H Syria Damascus	0.263	0.278	944	1330
I Iran Teheran	0.233	0.257	1209	1489
J Jordan Safawi	0.238	0.258	1300	1628
K Algeria Tamanrasset	0.245	0.265	1552	1903
L Lybia Tripoli	0.241	0.261	1318	1704
M Egypt Asyut	0.238	0.259	1473	1831
N Oman Masira	0.235	0.248	2529	2839
O Jordan Aqaba	0.226	0.234	1947	2309
P Egypt Hurguada	0.225	0.237	1890	2349
Q Israel Eilat	0.221	0.230	2042	2424
R Iraq Baghdad	0.236	0.256	1281	1566
S Iran BandarAbass	0.216	0.222	2288	2656
T Bahrain Manama	0.217	0.222	2308	2677
U KSA Riyadh	0.222	0.228	1968	2314
V UAE AbuDhabi	0.221	0.225	2481	2880
W Qatar Doha	0.215	0.219	2431	2817
X Kuwait KuwaitCity	0.218	0.220	2063	2390
Y KSA Sharura	0.221	0.227	2485	2826
Z Jemen AlHudaydah	0.218	0.223	3171	3361

Table D.5.: *Thermal comfort and Latent energy storage throughput in bed and living rooms*

Location	Hours with wall temperatures above 28°C in <i>deg * h</i>		Roundtrip energy stored in the internal masses of a bed room and living room in kWh	
	Bed room	Living room	Bed room	Living room
A Morocco Casablanca	341.2	290.5	181.3	331.6
B Algeria Algiers	1156.9	1250.3	193.7	335.9
C Iran Tabriz	1063.4	1195.1	193.9	333.5
D Israel Jerusalem	735.4	767.1	195.9	338.7
E Tunisia Tunis	2774.5	3314.8	218.2	340.7
F Egypt Alexandria	2052.5	2504.2	228.0	354.0
G Lebanon Bayrouth	3291.6	4023.5	233.8	352.6
H Syria Damascus	1947.4	2192.3	214.5	346.8
I Iran Teheran	4719.5	5679.5	239.9	347.4
J Jordan Safawi	4916.1	5915.5	245.4	359.7
K Algeria Tamanrasset	4250.0	5115.2	266.5	375.1
L Lybia Tripoli	4426.7	5387.0	242.8	361.5
M Egypt Asyut	5208.2	6400.1	260.1	373.6
N Oman Masira	7280.0	9034.5	344.9	424.7
O Jordan Aqaba	11233.2	13833.8	299.5	403.9
P Egypt Hurguada	8745.9	10609.5	291.1	402.6
Q Israel Eilat	12131.5	14864.0	304.8	410.7
R Iraq Baghdad	5771.9	6856.8	245.4	359.8
S Iran BandarAbass	14609.8	17776.1	325.0	427.4
T Bahrain Manama	15309.8	18606.3	323.7	426.6
U KSA Riyadh	13218.7	16171.4	303.4	412.8
V UAE AbuDhabi	15693.2	19272.2	341.8	442.1
W Qatar Doha	17778.9	21716.8	336.7	440.9
X Kuwait KuwaitCity	16439.3	20297.8	308.7	417.2
Y KSA Sharura	15716.0	19294.0	347.6	443.5
Z Jemen AlHudaydah	22589.1	27843.2	406.4	482.8

Table D.6.: *Monthly cooling and electric energy demands in kWh of the reference location of Hurghada, Egypt.*

Month	Cooling energy (kWh) demand bed room	Electric energy (kWh) demand bed room	Cooling energy (kWh) demand bed room	Electric energy (kWh) demand bed room
January	0	22	0	22
February	0	20	29	32
March	0	22	304	155
April	170	100	469	235
May	512	279	614	327
June	715	392	665	371
July	809	463	775	449
August	815	467	782	452
September	714	392	737	403
October	523	281	619	325
November	213	117	413	204
December	0	22	215	112

D. Additional information

Table D.7.: *Simulation results for the reference location Hurghada, Egypt for the number of on/off switching cycles for the air conditioner system, the cooling degree hours and the energy throughput to and from the internal walls in a bed and a living room.*

Month	Monthly number of on/off switching cycles		Monthly sum of degree hours difference between surface and air temperature while the surface is at least 28°C		Monthly energy throughput to and from internal room surfaces	
	On/off bed room	On/off living room	degH bed room	degH living room	qInt bed room	qInt living room
January	0	0	0	0	11.5	23.2
February	0	162	0	0	9.9	20.1
March	0	1668	0	0	10.7	28.2
April	856	3714	26	43	13.1	31.0
May	3751	6579	383	492	22.1	32.1
June	5637	8833	1006	1350	28.5	31.8
July	7579	10769	2029	2570	32.0	36.2
August	7576	10790	2145	2693	32.1	36.5
September	5997	8982	1486	2029	28.2	35.5
October	3936	6396	682	901	21.9	31.2
November	1201	3035	123	160	14.2	28.2
December	3	1103	0	0	10.5	24.1

E. Modelica code sources

Listing E.1: *BaseClass of battery model*

```
1 partial model Battery "partial model of a battery"
2 equation
3   EAva = h1*c;
4   EBou = h2*(1-c);
5   E = EAva + EBou;
6   SOC = E / E_nominal;
7   PNet = PCharge - PLoad;
8   PChargeEff = BuildingSystems.Utilities.Math.Functions.smoothLimit (
9     0.5*(1.0-Modelica.Math.tanh(100000.0*(SOC-1.0)))*PNet*etaCharge,
10    0.0,
11    BuildingSystems.Utilities.Math.Functions.smoothLimit (a_mcr*(E_nominal-E)
12      ,
13      0.0,
14      PCharge_max,
15      0.001),
16    0.001);
17   PGrid = 0.5*(1.0-Modelica.Math.tanh(100000.0*(PNet)))*(PNet + PLoadEff*etaLoad) +
18     0.5*(1.0+Modelica.Math.tanh(100000.0*(PNet)))*(PNet - PChargeEff/etaCharge);
19   der(E_charged) = PChargeEff;
20   der(E_discharged) = PLoadEff;
21 end Battery;
```

Listing E.2: *Extended battery model of base class battery*

```
1 model BatteryComplex
2   extends BaseClasses.Battery;
3   equation
4     der(EAva) = PChargeEff - E_nominal/E_current * PLoadAva + k*(h2 - h1);
5     der(EBou) = -k*(h2 - h1) - E_nominal/E_current * PLoadBou;
6     E_current = BuildingSystems.Utilities.Math.Functions.smoothLimit (
7       t_loadNominal*(E_nominal/t_loadNominal/PLoadEff)^p*PLoadEff,
8       0.0,
9       E_max,
10      0.001);
11    PLoadBou = BuildingSystems.Utilities.Math.Functions.smoothLimit (
12      0.5*(1.0-Modelica.Math.tanh(100000.0*(SOC_min-SOC)))*(-PNet/etaLoad -
13        PLoadAva)+fDis*E,
14      0.0,
15      PLoad_max,
16      0.001);
17    PLoadAva = 0.5*(1.0-Modelica.Math.tanh(100000.0*(SOC_min-SOC)))*
18      BuildingSystems.Utilities.Math.Functions.smoothLimit (
19        -0.5*(1.0+Modelica.Math.tanh(100000.0*(EAva)))*PNet/etaLoad,
20        0.0,
21        PLoad_max,
22        0.001);
23    PLoadEff = BuildingSystems.Utilities.Math.Functions.smoothLimit (
24      PLoadBou + PLoadAva,
25      0.0,
26      PLoad_max,
27      0.001);
28 end BatteryComplex;
```

E. Modelica code sources

Listing E.3: Equation section of source code for the modeled transformer

```
1 model DCACTransformer
2 equation
3   loadFactor = abs((P1/P_nom))*100+0.001;
4   eta_dcac = BuildingSystems.Utilities.Math.Functions.smoothMax(
5     eta_max + (0.009*log(loadFactor/0.6))/loadFactor,
6     0.02,
7     0.001);
8   P2 = BuildingSystems.Utilities.Math.Functions.smoothMax(
9     (P_out / eta_dcac)*100,
10    0.5 * (1 - Modelica.Math.tanh(100000 * (0.01-P_out))) * P_nom * (1-
11      eta_max),
12    0.001);
13 der(E_in) = P2;
14 der(E_out) = P1;
```

Listing E.4: Equation section of source code for the extended transformer model to use from and discharge to a connected grid

```
1 model DCACTransformer
2 equation
3   loadFactor = abs((P1/P_nom))*100+0.001;
4   eta_dcac = if gridConnection == true
5     then
6     0.5*(1.0 - Modelica.Math.tanh(100000.0*(P1)))*1 + 0.5*(1.0 +
7     Modelica.Math.tanh(100000.0*(P1)))*
8     BuildingSystems.Utilities.Math.Functions.smoothMax(
9     eta_max + (0.009*log(loadFactor/0.6))/loadFactor,
10    0.3,
11    0.001)
12   else
13     BuildingSystems.Utilities.Math.Functions.smoothMax(
14     eta_max + (0.009*log(loadFactor/0.6))/loadFactor,
15     0.3,
16     0.001);
17
18   P2 = if gridConnection == true
19     then
20     P1*eta_dcac
21   else
22     BuildingSystems.Utilities.Math.Functions.smoothMax(
23     (P1/eta_dcac),
24     0.5*(1 - Modelica.Math.tanh(100000*(0.01 - P1)))*P_nom*(1 - eta_max),
25     0.001);
26 der(E2) = P2;
27 der(E1) = P1;
```

Bibliography

- [1] User DanPMK. Mena.jpg - based on "africa in the world (grey).svg" by tubs, 2011.
- [2] United Nations. Transforming our world: the 2030 agenda for sustainable development.
- [3] International Energy Agency. Statistical country info - energy balances, 2016.
- [4] Hassan Fathy. *Architecture for the poor: An experiment in rural Egypt*. Univ. Press, Chicago, 2000.
- [5] DigitalGlobe. 8th district, cairo, egypt, 2019.
- [6] Shady Attia, Arnaud Evrard, and Elisabeth Gratia. Development of benchmark models for the egyptian residential buildings sector. *Applied Energy*, 94:270–284, 2012.
- [7] Green Cooling Initiative. Number of appliances in use of unitary air conditioning: Appliances in use - unitary air conditioning - absolute, 2016.
- [8] International Energy Agency. *World Energy Outlook 2018: Gold standard of long-term energy analysis*. OECD/IEA, Paris, 2018.
- [9] Energy Dubai. How to save on energy consumption. *Energy Dubai Blog*, 2019.
- [10] IEA International Energy Agency, editor. *The Future of Cooling - Opportunities for energy-efficient air conditioning*. IEA International Energy Agency, online, 2018.
- [11] n.d. El gouna annual electricity load profile.
- [12] N. Valev. Global electricity prices - collected from globalpetrolprices.com, 2018.
- [13] N. S. H. Hussein, M. Abokersh, C. Kost, and T. Schlegl. Electricity cost from renewable energy technologies in egypt. 2016.
- [14] The Trustees of Columbia University in the City of New York. National aggregates of geospatial data collection: Population, landscape, and climate estimates, version 3 (place iii), 2012.
- [15] Krasilshchikov Yegor. R22-t-s-diagram-a2, 2021.
- [16] Carrier. Comfort window units: Vg100c-2, 2013.
- [17] Ekaterina Vinogradova. *Economizers in Chiller Systems: Bachelor's Thesis*. PhD thesis, Mikkeli University of Applied Sciences, Mikkeli, Finland, 2012.
- [18] Lauris Bisenieks, Andrejs Stepanovs, and Ilja Galkin, editors. *Comparison of a traditional diode photovoltaic model and simplified I-V curve based model*, online, 2008.
- [19] Nahla Mohamed Abd Alrahim Shannan, Nor Zaihar Yahaya, and Balbir Singh. Single-diode model and two-diode model of pv modules: A comparison. pages 210–214, 2013.

Bibliography

- [20] Vandana Khanna, B. K. Das, Dinesh Bisht, Vandana, and P. K. Singh. A three diode model for industrial solar cells and estimation of solar cell parameters using pso algorithm. *Renewable Energy*, 78:105–113, 2015.
- [21] James F. Manwell and Jon G. McGowan. Lead acid battery storage model for hybrid energy systems. *Solar Energy*, 50(5):399–405, 1993.
- [22] Festo Didactics. Transformer losses, efficiency, and regulation: Excercise 3, n.d. [2018].
- [23] Corel Corporation. Coreldraw graphis suite 2018, 2018.
- [24] Jan Honke. Weather station data dump from kbc el gouna.
- [25] METEOTEST Genossenschaft. Software meteonorm v7.1.11.24422, 2019.
- [26] C. Nytsch-Geusen, C. Banhardt, A. Inderfurth., K. Mucha, Jens Möckel, Jörg R., and Thorade, M. and Tugores, C., editors. *BuildingSystems – Eine modular hierarchische Modell-Bibliothek zur energetischen Gebäude- und Anlagensimulation*, Conference Proceedings, 2016.
- [27] BizEE Software Limited. Software degree days.net desktop v1.1.10, 2012 - 2019.
- [28] Ministry of Electricity and Renewable Energy, Egypt. Annual report 2014/2015.
- [29] World Meterological Organisation WMO. Wmo presence on undata: a data access system to un databases, 2019.
- [30] Hassan Baig. Working principle of a.c: Air conditioner compressor, 2015.
- [31] Thermopompes N&R SOL inc. Ameristar ductless heat pump, 2019.
- [32] Guy El Khoury. Carbon footprint of electricity in the middle east. *Carboun Middle East Sustainable Cities*, 2009.
- [33] Daniel W. O’Neill, Andrew L. Fanning, William F. Lamb, and Julia K. Steinberger. A good life for all within planetary boundaries. *Nature Sustainability*, 1(2):88–95, 2018.
- [34] C. Banhardt and C. Nytsch-Geusen. Simulation based design of a test rig for developing solar cooling concepts for the mena region. *Proceedings of Egyptian IBPSA 2013*, Egypt(1):165–174, 2013.
- [35] Systemair Airwell SAS. Ductable split-system air conditioners - models 125 to 905, 2014.
- [36] R. K. Pachauri and Leo Mayer, editors. *Climate change 2014: Synthesis report*. Intergovernmental Panel on Climate Change, Geneva, Switzerland, 2015.
- [37] Sahar Sodoudi. Adapting urban planning to local climate change in el gouna: A case study in ancient sands and el kafr, 10/14/2017.
- [38] C. Banhardt, G. Grozman, and C. Nytsch-Geusen. Simulation and validation of thermal air stratification in living spaces. *Proceedings of BauSIM 2016*, 1:605–611, 2016.
- [39] Daisy Lorenzi. Yazd, an earthern town of wind-catchers: Yazd, the mystical city of windcatchers.
- [40] Wei Chen, Shuqiong Zhang, and Yunsong Zhang. Analysis on the cooling and soaking-up performance of wet porous wall for building. *Renewable Energy*, 115:1249–1259, 2018.

- [41] GEO. "masdar city": Die null-emissions-stadt in der wüste. *GEO*, 11/08, 11/2008.
- [42] Hans Rosling, Anna Rosling Rönnlund, and Ola Rosling. *Factfulness: Wie wir lernen, die Welt so zu sehen, wie sie wirklich ist*. Ullstein, Berlin, 4. edition, 2018.
- [43] Johanna Gloel, Dietram Oppelt, Claudia Becker, and Jonathan Heubes. Green cooling technologies: Market trends in selected refrigeration and air conditioning subsectors.
- [44] United Nations, Department of Economic and Social Affairs, and Population Division. World population prospects: The 2017 revision, dvd edition.
- [45] Padu S. Padmanaban. Opening speech of ibpsa 2015 conference, india: Key note lecture, 5.12.2015.
- [46] Arwa Ibrahim. Egypt's power outages continue to intensify, 09/05/2014.
- [47] Ministry of Electricity and Renewable Energy, Egypt. Annual report 2008/2009.
- [48] Ministry of Electricity and Renewable Energy, Egypt. Annual report 2009/2010.
- [49] Ministry of Electricity and Renewable Energy, Egypt. Annual report 2010/2011.
- [50] Ministry of Electricity and Renewable Energy, Egypt. Annual report 2011/2012.
- [51] Ministry of Electricity and Renewable Energy, Egypt. Annual report 2013/2014.
- [52] Ministry of Electricity and Renewable Energy, Egypt. Annual report 2015/2016.
- [53] Mohamed Sabry Abdalla. *Developing of a decision matrix for optimizing the energy efficiency and the life cycle costs for new planned residential buildings in Egypt*. Master's dissertation, Technische Universität Berlin, El Gouna, Egypt, 2015.
- [54] Abdul Ghafoor and Anjum Munir. Worldwide overview of solar thermal cooling technologies. *Renewable and Sustainable Energy Reviews*, 43:763–774, 2015.
- [55] Research and Markets. Evaporative cooling market - growth, trends and forecast (2019 - 2024).
- [56] MK Solar. Acdc hybrid solar air conditioner.
- [57] HANGNING. Off grid solar air conditioner, 2019.
- [58] Jing-Chien Hsu. *Comparison of Decentralized and Centralized Photovoltaic Powered Air Conditioning Systems for Hotels in Hot and Dry Climates*. Master's dissertation, Technische Universität Berlin, El Gouna, Egypt, 2015.
- [59] Johannes Wellmann and Tatiana Morosuk. Renewable energy supply and demand for the city of el gouna, egypt. *Sustainability*, 8(4):314, 2016.
- [60] Haresh Khemani. What is hermetically sealed compressors. refrigeration & air conditioning compressors, 2018.
- [61] S. F. Y. Motta and P. A. Domanski, editors. *Performance of R-22 and Its Alternatives Working at High Outdoor Temperatures*, online, 2000. Purdue e-Pubs.
- [62] VDI Verein Deutscher Ingenieure e.V. Calculation of thermal loads and room temperatures: design cooling load and annual simulation, 2015.

Bibliography

- [63] Egyptian Organization for Standards & Quality. standardsearch for air conditioners, 2019.
- [64] Jeffrey D. Spitler. *Load calculation applications manual*. ASHRAE, Atlanta, second edition, si edition edition, 2014.
- [65] Daniel Mugnier. Solar cooling potential in the mena region, 31.10.2017.
- [66] Y. Y. A. Badran. *Analytical and Comparative Study for Solar Thermal Cooling and Photovoltaic Solar Cooling in the MENA Region*. Master's dissertation, Cairo University, Cairo, Egypt, 2012.
- [67] Hans-Martin Henning. Solar assisted air conditioning of buildings – an overview. *Applied Thermal Engineering*, 27(10):1734–1749, 2007.
- [68] H. Wirth, editor. *Aktuelle Fakten zur Photovoltaik in Deutschland*. pv-fakten, online, fassung vom 7.5.2019 edition, 2019.
- [69] I. Rutschmann. Solaranlage und batteriespeicher günstig finanzieren, 2019.
- [70] H.-S. Finke. Die vergütung für eingespeisten solarstrom 2019, 2019.
- [71] M. El Sobki. Doing business between euromed and egypt - investment and cooperation opportunities in the re sector, 08.12.2015.
- [72] Bassam Fattouh and Laura El-Katiri. Energy subsidies in the middle east and north africa. *Energy Strategy Reviews*, 2(1):108–115, 2013.
- [73] Ferdinand Eibl. The political economy of energy the political economy of energy subsidies in egypt and tunisia: the untold story. *Oxford Energy Comment*, 2017.
- [74] The World Bank. Overview of middle east and north africa: Growth has picked up across the region and is projected to strengthen over the next few years. and almost all mena countries have moved to reduce or eliminate energy subsidies, identify new sources of non-oil revenues, and expand social safety nets to shield the poor from adverse effects of change., 2018.
- [75] Todd Otanicar, Robert A. Taylor, and Patrick E. Phelan. Prospects for solar cooling – an economic and environmental assessment. *Solar Energy*, 86(5):1287–1299, 2012.
- [76] Best Directory. : Software listings, 2019.
- [77] Joana Sousa, editor. *Energy Simulation Software for Buildings: Review and Comparison*, online, 2012.
- [78] Bob Fassbender. Energy modeling software comparison as cars, 2018.
- [79] Targo Kalamees, editor. *IDA ICE: the simulation tool for making the whole building energy- and HAM analysis.*, online, 2004.
- [80] Donghum Kim, Wangda Zuo, James E. Braun, and Michael Wetter, editors. *Comparisons of building system modeling approaches for control system design*, online, 2013.
- [81] Christoph Nytsch-Geusen, Jörg Huber, Manuel Ljubijankic, and Jörg Rädler, editors. *Modelica BuildingSystems - eine Modellbibliothek zur Simulation komplexer energietechnischer Gebäudesysteme*, volume 35, 2014.
- [82] IBPSA. Ibpsa project 1 - bim/gis and modelica framework for building and community energy system design and operation, 2016.

- [83] Hotspot Energy. Dc air conditioner: 12,000 btu dc air conditioner for off-grid solar & telecom applications, 2014.
- [84] Deutsches Institut für Normung e.V. DIN. Energy efficiency of buildings – calculation of the net, final and primary energy demand for heating, cooling, ventilation, domestic hot water and lighting – part 10: Boundary conditions of use, climatic data, 2018.
- [85] World Meteorological Organisation WMO. The role of climatological normals in a changing climate. *WMO/TD- No. 1377; WCDMP- No. 61*, 2007.
- [86] Deutscher Wetterdienst. Ortsgenaue testreferenzjahre von deutschland für mittlere, extreme und zukünftige witterungserhältnisse: Handbuch, 06.2017.
- [87] Jan Remund. Accuracy of meteonorm - a detailed look at the model steps and uncertainties: v. 7.1.6.14035, 22.10.2015.
- [88] K. N. Shukla, Saroj Rangnekar, and K. Sudhakar. Comparative study of isotropic and anisotropic sky models to estimate solar radiation incident on tilted surface: A case study for bhopal, india. *Energy Reports*, 1:96–103, 2015.
- [89] Oguejiofor M. Mbah, Chigbo A. Mgbemene, Samuel O. Enibe, Paul A. Ozor, and Mbohwa Charles, editors. *Comparison of Experimental Data and Isotropic Sky Models for Global Solar Radiation Estimation in Eastern Nigeria: Conference period and venue: Imperial College London.*, Lecture notes in engineering and computer science, Hong Kong, 2018. Newswood Limited International Association of Engineers.
- [90] M. Mesri, A. Choucha, and L. Chaib, editors. *Evaluation of Global Solar Radiation Models for Inclined Surfaces*. Atlantis Press, 2015.
- [91] Nikolaj V. Charčenko, editor. *Thermische Solaranlagen: Grundlagen, Planung und Auslegung ; mit 80 Tabellen*. Springer, Berlin, 1995.
- [92] Deutsches Institut für Normung e.V. DIN. Din 4108 - wärmeschutz und energie-einsparung in gebäuden, 2013.
- [93] P. O. Fanger. Thermal comfort: analysis and applications in environmental engineering, by p. o. fanger. 244 pp. danish technical press. copenhagen, denmark, 1970. danish kr. 76, 50. *Royal Society of Health Journal*, 92(3):164, 1972.
- [94] K. C. Parsons. The effects of gender, acclimation state, the opportunity to adjust clothing and physical disability on requirements for thermal comfort. *Energy and Buildings*, 34(6):593–599, 2002.
- [95] American National Standard Institute ANSI. Ventilation for acceptable indoor air quality, 2016.
- [96] Da Yan, William O’Brien, Tianzhen Hong, Xiaohang Feng, H. Burak Gunay, Farhang Tahmasebi, and Ardeshir Mahdavi. Occupant behavior modeling for building performance simulation: Current state and future challenges. *Energy and Buildings*, 107:264–278, 2015.
- [97] Lars Junghans and Nuri Bae. Influence of the uncertainties of occupant behavior on computer-based optimization processes. *Energy and Buildings*, 116:478–497, 2016.
- [98] Jie Zhao, Khee Poh Lam, B. Erik Ydstie, and Vivian Loftness. Occupant-oriented mixed-mode energyplus predictive control simulation. *Energy and Buildings*, 117:362–371, 2016.

Bibliography

- [99] Elisabeth Rosenthal and Andrew Lehren. Relief in every window, but global worry too. *New York Times*, 2012.
- [100] ASHRAE, editor. *2016 ASHRAE handbook: Heating, ventilating, and air-conditioning systems and equipment, SI edition*. ASHRAE, Atlanta, Georgia, si edition edition, 2016.
- [101] C. A. Balaras. The role of thermal mass on the cooling load of buildings. an overview of computational methods. *Energy and Buildings*, 24(1):1–10, 1996.
- [102] Energy Informative. Which solar panel type is best? mono- vs. polycrystalline vs. thin film, 2012.
- [103] Pruthviraj Balekai. *Energy performance analysis of single axis tracking PV system for the Rooftop Building based on Modelica and openHAB*. Master’s dissertation, Technische Universität Berlin, Berlin, 2018.
- [104] *Simplifying the Parametrization of the Extended Kinetic Battery Model to Calculate Voltage, Current, and a Variable Load Dependent Capacity*, volume 1, Rome, Italy, 2019.
- [105] Marijn Jongerden and B. R. Haverkort. Battery modeling. 2008.
- [106] Wolf Daniel. Energy storage modelling: Integrated laboratory course, 14/01/2018.
- [107] J. F. Manwell and J. G. McGowan, editors. *Extension of the kinetic battery model for wind/hybrid power systems*, 1994.
- [108] vela solaris. Polysun: Simulation software.
- [109] Wilhelm Peukert. Über die abhängigkeit der kapazität von der entladestromstärke bei bleiakkulatoren. *Elektrotechnische Zeitschrift*, 18:287–288, 1897.
- [110] Joseph Huwaldt. Plot digitizer, 2001.
- [111] EBC Energy in Buildings and Communities Programme. Iea-ebc annex 66 - definition and simulation of occupant behavior in buildings, 2017.
- [112] IEA Energy in Buildings and Communities. Ebc annex 79 - occupant-centric building design and operation, 2018.
- [113] Yixing Chen, Xuan Luo, and Tianzhen Hong, editors. *An Agent-Based Occupancy Simulator for Building Performance Simulation*, 2016.
- [114] Siemens Aktiengesellschaft. Siemens power engineering guide · transmission and distribution: Technical data distribution transformers tunorma and tumetic.
- [115] Daniel Chiras. *The Solar House: Passive Heating and Cooling*. Chelsea Green Publishing Company, 2002.
- [116] P. M. Heathcote, editor. *’A’ level computing*. Payne-Gallway Publishers, Ipswich, 4th ed. edition, repr. 2001, 2000.
- [117] A. Urkiaga, L. de las Fuentes, B. Bis, E. Chiru, B. Bodo, F. Hernández, and T. Wintgens. Methodologies for feasibility studies related to wastewater reclamation and reuse projects. *Desalination*, 187(1-3):263–269, 2006.

- [118] Christina Lotz and Karin Schneider, editors. *Fraunhofer ISE - Jahresbericht 2018/19*. Fraunhofer-Institut für Solare Energiesysteme, Freiburg, Germany, 2018.
- [119] Raphael Hollinger, Bernhard Wille-Hausmann, Thomas Erge, Thies Stillahn, Niklas Kreifels, and Christof Wittwer, editors. *Chancen und Risiken dezentraler Solarstromspeicher für das elektrische Energiesystem*, Offenbach, 2013. VDE Verlag GmbH.
- [120] John P. Rafferty. Tropical and subtropical desert climate. In *Encyclopaedia Britannica*.
- [121] European Environment Agency. Heating and cooling degree days: Indicator assessment, 2016.
- [122] Lucas W. Davis and Paul J. Gertler. Contribution of air conditioning adoption to future energy use under global warming. *Proceedings of the National Academy of Sciences of the United States of America*, 112(19):5962–5967, 2015.
- [123] ANSI. Thermal environmental conditions for human occupancy: Ansi/ashrae standard 55-2010, 2010.
- [124] Kate E. Charles. Fanger’s thermal comfort and draught models: Irc research report rr-162.
- [125] Oluwafemi K. Akande and Micheal A. Adebamowo, editors. *Indoor Thermal Comfort for Residential Buildings in Hot-Dry Climate of Nigeria*, Network for Comfort and Energy Use in Buildings, London, 2010.
- [126] Christina Hoffmann, Marc Hanisch, Jana B. Heinsohn, Vanessa Dostal, Melissa Jehn, Uta Liebers, Wulf Pankow, Gavin C. Donaldson, and Christian Witt. Increased vulnerability of copd patient groups to urban climate in view of global warming. *International journal of chronic obstructive pulmonary disease*, 13:3493–3501, 2018.
- [127] N. Abdrabou, C. Banhardt, and F. Hartenstein. Reducing carbon emissions in egypt’s building sector: The ecological case for bearing walls. *Proceedings of SBE2016*, 1, 2016.
- [128] Fayçal El Fgaier, Zoubeir Lafhaj, Franck Brachelet, Emmanuel Antczak, and Christophe Chapiseau. Thermal performance of unfired clay bricks used in construction in the north of france: Case study. *Case Studies in Construction Materials*, 3:102–111, 2015.
- [129] Trina Solar Limited. Tsm-pc05 - the universal solution.
- [130] Spectra Volt. Spv-100m36 - spectra volt.
- [131] Long Batteries. Wp7.2-12: 12volt 7.2ah rechargeble sealed lead acid battery: Datasheet.
- [132] n.d. Clh 12-200 12v 200ah rechargable lead acid battery: Chloride - the energy solution, 2018.
- [133] Jörg Rädler. Smooth transition between functions with tanh(), 2010.
- [134] Verband der Elektrizitätswirtschaft VDEW. Repräsentative vdew-lastprofile, 1999.
- [135] Verband der Elektrizitätswirtschaft VDEW. Anwendung der repräsentativen vdew-lastprofile: step-by-step, 31.01.2000.
- [136] Thomas Gobmaier and Serafin von Roon. Standardlastprofile für kunden mit elektrostraßenfahrzeugen, 2010.
- [137] n.d. Daily occupancy rate for 2014 from the three corners ocean view hotel, provided by grübel, jürgen.

Bibliography

- [138] n.d. Odh annual report 2014: Back on track.
- [139] Haresh Khemani. R22 phase out timeline. freon 22 bans timeline, 2010.
- [140] Michael Wetter. *GenOpt(R) - Generic Optimization Program User Manual Version 3.1.1*. Software documentation, Lawrence Berkeley National Laboratory, Berkeley, California, USA, 2016.
- [141] dynamic Energy & Water Solutions. Lebanon electricity tariffs 2012.
- [142] dynamic Energy & Water Solutions. Oman electricity tariffs.
- [143] dynamic Energy & Water Solutions. Libya electricity tariffs.
- [144] dynamic Energy & Water Solutions. Kuwait electricity tariffs.
- [145] dynamic Energy & Water Solutions. Yemen electricity tariffs.
- [146] U4E United for Efficiency. Country specific data and input assumptions for syrian arab republic.
- [147] Runsheng Tang, I. A. Meir, and Tong Wu. Thermal performance of non air-conditioned buildings with vaulted roofs in comparison with flat roofs. *Building and Environment*, 41(3):268–276, 2006.
- [148] Christoph Banhardt and Felix Hartenstein. A makeshift approach to carbon accounting in egyptian towns. *Procedia Environmental Sciences*, 34:152–163, 2016.